



# Holocene climate and vegetation change in the Asian monsoon region

Anne F. Dallmeyer



## Hinweis

Die Berichte zur Erdsystemforschung werden vom Max-Planck-Institut für Meteorologie in Hamburg in unregelmäßiger Abfolge herausgegeben.

Sie enthalten wissenschaftliche und technische Beiträge, inklusive Dissertationen.

Die Beiträge geben nicht notwendigerweise die Auffassung des Instituts wieder.

Die "Berichte zur Erdsystemforschung" führen die vorherigen Reihen "Reports" und "Examensarbeiten" weiter.



## Notice

*The Reports on Earth System Science are published by the Max Planck Institute for Meteorology in Hamburg. They appear in irregular intervals.*

*They contain scientific and technical contributions, including Ph. D. theses.*

*The Reports do not necessarily reflect the opinion of the Institute.*

*The "Reports on Earth System Science" continue the former "Reports" and "Examensarbeiten" of the Max Planck Institute.*

## Anschrift / Address

Max-Planck-Institut für Meteorologie  
Bundesstrasse 53  
20146 Hamburg  
Deutschland

Tel.: +49-(0)40-4 11 73-0  
Fax: +49-(0)40-4 11 73-298  
Web: [www.mpimet.mpg.de](http://www.mpimet.mpg.de)

## Layout:

Bettina Diallo, PR & Grafik

Titelfotos:

vorne:

Christian Klepp - Jochem Marotzke - Christian Klepp

hinten:

Clotilde Dubois - Christian Klepp - Katsumasa Tanaka

Holocene climate and  
vegetation change in the Asian  
monsoon region

Anne F. Dallmeyer

aus Kappeln

Hamburg 2011

Anne F. Dallmeyer  
Max-Planck-Institut für Meteorologie  
Bundesstrasse 53  
20146 Hamburg  
Germany

Als Dissertation angenommen  
vom Department Geowissenschaften der Universität Hamburg

auf Grund der Gutachten von  
Prof. Dr. Martin Claussen  
und  
Dr. Victor Brovkin

Hamburg, den 2. November 2011  
Prof. Dr. Jürgen Oßenbrügge  
Leiter des Departments für Geowissenschaften

# Holocene climate and vegetation change in the Asian monsoon region

---



Anne F. Dallmeyer

Hamburg 2011

*Overleaf*

Sutlej Valley, Kalpa (31°32'N, 78°15'E)

Himachal Pradesh, NW-Himalaya, India

In the background: Kinnaur Kailash mountain

Photo: S. Polanski, Sept. 2009.

## Abstract

The mid- to late-Holocene climate and vegetation change in the Asian monsoon domain is investigated by using different simulations performed with the general-circulation model ECHAM5/JSBACH(-MPIOM). The study includes a detailed evaluation of the model with respect to the present-day climate as well as a comparison of the simulated results with mid-Holocene climate reconstructions and reconstructed vegetation trends. Our analysis identifies differences in the response of the East Asian and Indian monsoon systems to mid-Holocene insolation forcing and reveals the importance of including the pre- and post-monsoon seasons in climate analysis covering the Asian monsoon domain. During the mid-Holocene, most parts of the Indian subcontinent receive more annual mean precipitation due to a strengthening of the Indian summer monsoon. The East Asian monsoon region exhibits local inhomogeneities in the annual precipitation signal with sign depending on the balance of decreased pre-monsoon and increased monsoon precipitation during the mid-Holocene. The reconstructions confirm the regional dissimilarities in the Holocene precipitation change and agree well with the model results when using a high numerical resolution.

Most of the mid- to late-Holocene temperature and precipitation change can be attributed to the direct response of the atmosphere to the insolation forcing. The ocean-atmosphere interaction modifies the signal and leads, on average, to an amplification of the precipitation response. Regionally, differences exist between the East Asian and the Indian monsoon where the ocean-atmosphere interaction contributes with a decrease and increase of rainfall to the total Holocene climate change, respectively. The ocean-atmosphere interaction furthermore induces a lag in the temperature response to the insolation forcing by having a warming effect in autumn and winter and a cooling effect in spring and summer. The vegetation-atmosphere interaction plays a minor role in the large-scale Holocene climate change, but the simulated large-scale vegetation changes are also small and probably underestimated by the model. When prescribing large-scale forest cover changes in the entire Asian monsoon domain, the local climate and also the climate in remote areas is substantially altered. An idealised numerical experiment shows that the loss of forest from an entirely forested Asian monsoon domain to present-day potential land cover causes a decrease of precipitation with regional magnitudes half as large as the simulated orbitally-induced precipitation decline from mid-Holocene to present-day. Such a region is the Yellow River basin which was the settlement area of major prehistoric Asian cultures. Thus, large-scale Holocene land cover changes could have amplified the decreasing Asian monsoon precipitation during the Holocene known from reconstructions and could also have strongly affected the prehistoric cultures living in the monsoon domain.

To further assess the performance of the model with respect to Holocene vegetation changes, results of a transient simulation are compared to pollen-based vegetation reconstructions on the Tibetan Plateau. The reconstructed and simulated land cover trends are qualitatively in good agreement and reveal a strong degradation of vegetation on the Plateau including a large decrease of forests. The model primarily suggests temperature changes as the responsible mechanism for the land cover change. This factor, so far, has been underestimated as possible explanation for vegetation changes in monsoon influenced regions in previous studies.

## Zusammenfassung

Mittels verschiedener in dem Zirkulationsmodell ECHAM5/JSBACH-MPIOM durchgeführter Simulationen werden die Klima- und Vegetationsänderungen seit dem Mittleren Holozän im Asiatischen Monsungebiet untersucht. Dabei werden die Modellergebnisse in Bezug auf das gegenwärtige Klima evaluiert und auch mit Rekonstruktionsdaten für das Klima des mittleren Holozän und den Vegetationstrend verglichen. Unsere Ergebnisse lassen Unterschiede in der Reaktion des Ostasiatischen und Indischen Monsunsystems auf den Antrieb, die solare Einstrahlung des mittleren Holozäns, erkennen und verdeutlichen die Notwendigkeit, auch die Vor- und Nachmonsunsaision in Klimastudien für das Asiatische Monsungebiet zu integrieren. Während des mittleren Holozäns fällt in den meisten Gebieten Indiens mehr Niederschlag, da der Indische Sommermonsun stärker ausfällt. Das Ostasiatische Monsungebiet weist lokale Ungleichmäßigkeiten bezüglich des Niederschlagssignals auf, dessen Vorzeichen von der Differenz der Niederschlagsabnahme in der Vormonsunsaision und Niederschlagszunahme in der Monsunsaision abhängt. Die Rekonstruktionen bestätigen die regionalen Unterschiede im Niederschlagssignal und stimmen gut mit den Modellergebnissen überein, jedoch nur in den Simulationen mit hoher numerischer Auflösung.

Der größte Anteil der Temperatur- und Niederschlagsänderung seit dem Mittleren Holozän wird durch die direkte Antwort der Atmosphäre auf den Einstrahlungs-Antrieb getragen. Die Ozean-Atmosphären-Wechselwirkung modifiziert das Signal und führt im Gebietsmittel zu einer Verstärkung der Niederschlagsänderung. Regional existieren jedoch Unterschiede zwischen dem Ostasiatischen und dem Indischen Monsungebiet, in denen die Atmosphären-Ozean Interaktion eine Abnahme beziehungsweise Zunahme des lokalen Niederschlags bewirkt. Sie verursacht zudem eine Verschiebung des Temperatursignals zum Einstrahlungsantrieb, denn sie führt im Mittleren Holozän zu einer Erhöhung der Temperaturen im Herbst und im Winter und einer Abnahme der Temperaturen im Frühling und Sommer. Wechselwirkungen zwischen Vegetation und Atmosphäre spielen großskalig nur eine untergeordnete Rolle bei der holozänen Klimaveränderung, jedoch simuliert das Modell nur geringe Vegetationsänderungen und unterschätzt diese wahrscheinlich. Werden dem Modell großflächig Änderungen in der asiatischen Waldbedeckung vorgeschrieben, wird das Klima lokal wie auch in fernen Gebieten substantiell verändert. In einem idealisierten numerischen Experiment wird gezeigt, dass der Waldverlust von einem gänzlich beforsteten Asiatischen Monsungebiet zu der gegenwärtigen potentiellen Landbedeckung eine Abnahme des Niederschlags hervorruft, die regional halb so groß ausfallen kann wie die orbital induzierte Niederschlagsänderung. Eine solche Region ist das Einzugsgebiet des Gelben Flusses, das auch die Siedlungsregion bedeutender prähistorischer Kulturen war. Großflächige Landbedeckungsänderungen seit dem Mittleren Holozän könnten folglich die in Rekonstruktionen vielerorts nachgewiesene Abnahme im Asiatischen Monsunniederschlag verstärkt und damit das Leben der prähistorischen Kulturen in diesem Gebiet beeinflusst haben.

Um die Fähigkeit des Modells bei der Simulation der Vegetationsänderung seit dem Mittleren Holozän abzuschätzen, werden Ergebnisse einer transienten Simulation mit pollen-basierten Rekonstruktionen für das Tibet Plateau verglichen. Der rekonstruierte und simulierte Trend stimmen qualitativ gut überein und offenbaren eine starke Degradierung der Vegetation und eine starke Waldabnahme auf dem Plateau. Laut Modell sind vornehmlich Temperaturänderungen dafür verantwortlich. Diese wurden in bisherigen Studien als mögliche Erklärung für Vegetationsänderungen in Monsun-beeinflussten Regionen unterschätzt.

# Contents

<b>List of Figures .....</b>	<b>IV</b>
<b>List of Tables.....</b>	<b>IX</b>
<b>1. Introduction .....</b>	<b>1</b>
<b>2. Simulated present-day Asian monsoon climate.....</b>	<b>7</b>
2.1 Introduction.....	7
2.2 Methods .....	9
2.2.1 Model and experiments .....	9
2.2.2 Calculation of the monsoon onset and withdrawal period.....	10
2.3 Model evaluation .....	11
2.3.1 Annual precipitation.....	11
2.3.2 Monsoon onset and withdrawal .....	15
2.3.3 Near-surface air temperature.....	15
2.3.4 Mean sea level pressure and atmospheric circulation in 850hPa.....	17
2.4 The effect of prescribing SST/sea-ice and changing resolution .....	18
2.4.1 Precipitation .....	19
2.4.2 Near-surface air temperature.....	21
2.5 Summary and discussion of Chapter 2 .....	23
2.6 Conclusion of Chapter 2 .....	26
<b>3. Simulated mid-Holocene Asian monsoon climate .....</b>	<b>27</b>
3.1 Introduction.....	27
3.2 Methods .....	28
3.3 Results.....	29
3.3.1 General precipitation pattern and monsoon season.....	29
3.3.2 Comparison with moisture-reconstructions .....	31
3.3.3 Near-surface air temperature.....	32
3.4 Discussion of Chapter 3 .....	34
3.4.1 Possible Mechanisms causing the precipitation change.....	34
3.4.2 Comparison with other modelling studies .....	40

3.5 Summary and conclusion of Chapter 3 .....	45
<b>4. Contribution of the atmosphere-ocean and atmosphere-vegetation interaction to the Holocene climate change.....</b>	<b>47</b>
4.1 Introduction .....	47
4.2 Methods .....	48
4.2.1 Model & experiments .....	48
4.2.2 Analysis methods.....	50
4.3 Main characteristics of Central and East Asian climate and land cover changes.....	52
4.3.1 Climate change from 6k to present-day .....	52
4.3.2 Land cover change from 6k to present-day .....	56
4.4 The impact of dynamic vegetation and ocean on the climate change between 6k and present-day .....	58
4.4.1 Near-surface air temperature .....	58
4.4.2 Precipitation.....	64
4.5 Summary and discussion of Chapter 4 .....	70
<b>5. Comparison of the simulated Holocene vegetation change with pollen-based vegetation reconstructions.....</b>	<b>77</b>
5.1 Introduction .....	77
5.2 Study area .....	80
5.2.1 The Tibetan Plateau .....	80
5.2.2 Study sites for pollen-based vegetation reconstructions.....	81
5.3 Methods .....	82
5.3.1 General model setup and experimental design .....	82
5.3.2 Dynamic vegetation module .....	84
5.3.3 Vegetation reconstruction (written by U. Herzschuh).....	86
5.4 Results .....	87
5.5 Discussion of Chapter 5.....	90
5.5.1 Potential reasons for disagreements in the simulated and reconstructed vegetation cover.....	90
5.5.2 Site-specific discussion of the vegetation change.....	93
5.5.3 Simulated total vegetation and biomass changes on the Tibetan Plateau.....	98
5.6 Summary and conclusion of Chapter 5 .....	100

<b>6. Sensitivity of the Asian monsoon climate to large-scale forest cover change .....</b>	<b>103</b>
6.1 Introduction.....	103
6.2 Model and experiments.....	105
6.3 Results.....	109
6.3.1 Effect of land cover change on precipitation .....	109
6.3.2 Effect of land cover change on near-surface air temperature .....	111
6.4 Discussion of Chapter 6.....	112
6.4.1 Change of circulation and water balance .....	113
6.4.2 Change of albedo and turbulent heat fluxes.....	117
6.4.3 Comparison to other model studies.....	119
6.4.4 Remote effect on precipitation in North Africa and the Middle East .....	120
6.4.5 Effect of idealised forest-cover change on mid-Holocene climate .....	122
6.5 Summary and conclusion of Chapter 6.....	124
<b>7. Summary and Conclusion.....</b>	<b>127</b>
7.1 Summary and Conclusion.....	127
7.2 Outlook .....	130
<b>Bibliography .....</b>	<b>133</b>
<b>Appendix A: Additional figures .....</b>	<b>149</b>
<b>Appendix B: Additional tables.....</b>	<b>155</b>
<b>Appendix C: Summary of the simulated climate and land cover change on the Tibetan Plateau .....</b>	<b>157</b>
<b>Acknowledgements .....</b>	<b>163</b>

## List of Figures

Figure 2.1: Simulated present-day annual mean precipitation compared to the observational datasets of GPCP and CMAP. ....	11
Figure 2.2: Hovmöller diagrams, simulated and observed seasonal precipitation cycle in an East Asian and Indian monsoon sector .....	13
Figure 2.3: Simulated onset and withdrawal period of the Asian monsoon, monsoon season length and related precipitation in comparison to CMAP observations .....	14
Figure 2.4: Simulated present-day near-surface air temperature of the wet season (May-October) compared to CRU TS2.1 and ERA40 reanalysis data .....	16
Figure 2.5: Simulated present-day near-surface air temperature of the dry/cold season (November-April) compared to CRU TS2.1 and ERA40 reanalysis data .....	16
Figure 2.6: Simulated mean sea level pressure and 850hPa wind circulation compared to ERA40 reanalysis data averaged over the winter and summer season .....	18
Figure 2.7: Simulated present-day annual mean precipitation in all model-setups used in this study .....	19
Figure 2.8: Differences in annual mean precipitation between the different model simulations and between the model simulations and GPCP .....	20
Figure 2.9: Simulated dry/cold season temperatures compared to CRU TS 2.1 .....	22
Figure 2.10: Simulated wet season temperatures compared to CRU TS 2.1 .....	23
Figure 2.11: Taylor diagram of simulated precipitation in the different model setups for the entire Asian region (30-170°E, 10°S-60°N), Reference dataset: GPCP .....	24
Figure 2.12: Taylor diagram of simulated temperature in the different model setups for the entire Asian region (30-170°E, 10°S-60°N), Reference: ERA40 and CRU TS 2.1 .....	26
Figure 3.1: Insolation difference between mid-Holocene and present-day .....	28
Figure 3.2: Significant difference in annual mean precipitation between the mid-Holocene and present-day simulation. ....	29
Figure 3.3: Simulated difference in onset and withdrawal time, length of the Asian summer monsoon and the related precipitation between mid-Holocene and present-day .....	30
Figure 3.4: Hovmöller diagram, differences in the the seasonal precipitation cycle in an East Asian and Indian monsoon sector between mid-Holocene and present-day. ....	31
Figure 3.5: Reconstructed moisture difference (Wang et al. 2010) and simulated annual mean precipitation difference (6k-0k/0k) between mid-Holocene and present-day .....	32
Figure 3.6: Simulated difference in dry/cold season and wet season near-surface air temperature between the mid-Holocene and present-day .....	33

Figure 3.7: Reconstructed warmth difference (Wang et al. 2010) and simulated annual mean near-surface air temperature difference between mid-Holocene and present-day ..	34
Figure 3.8: Annual cycle of precipitation change between mid-Holocene and present-day for different regions in the Asian monsoon domain.....	35
Figure 3.9: Simulated precipitation averaged over the present-day pre-monsoon season (February-May) and idealised summer monsoon season (June-September), lower panel: difference between mid-Holocene and present-day .....	36
Figure 3.10: Simulated upper-tropospheric zonal wind in 200hPa and vertical velocity in 400hPa, averaged over the pre-monsoon season for 0k and 6k-0k.....	36
Figure 3.11: Simulated vertical integrated moisture flux and its convergence averaged over the pre-monsoon season and idealised summer monsoon season for 0k and 6k-0k .....	37
Figure 3.12: Simulated upper-tropospheric zonal wind in 200hPa and vertical velocity in 400hPa, averaged over the idealised summer monsoon season for 0k and 6k-0k. ....	38
Figure 3.13: Ratio of summer to spring precipitation according to the present-day simulation and change in the difference of summer and spring precipitation between mid-Holocene and present-day.....	40
Figure 3.14: Comparison of the relative annual mean precipitation change between 6k and 0k simulated in PMIP2 and T31_AOV with the reconstructed moisture index .....	42
Figure 3.15: Differences in the seasonal precipitation cycle between the mid-Holocene and present-day for Central-East Asia and northern India as simulated within PMIP2. ....	43
Figure 3.16: Comparison of the annual mean temperature change between 6k and 0k simulated in PMIP2 and T31_AOV with the reconstructed warmth index .....	44
Figure 4.1: Location of the areas we consider in our feedback study. ....	51
Figure 4.2: Seasonal and annual averaged 2m-temperature anomalies between mid-Holocene and present-day climate (T31_AOV) .....	53
Figure 4.3: Seasonal and annual averaged precipitation anomalies between mid-Holocene and present-day climate (T31_AOV).....	55
Figure 4.4: Simulated land-cover change between mid-Holocene and present-day climate, given as fraction of forest, shrubs, grass and non-vegetated area.....	56
Figure 4.5: Factors contributing to the seasonal temperature change between mid-Holocene and present-day climate for six regions in the Asian monsoon domain, i.e. direct response of atmosphere, contribution of ocean-atmosphere and vegetation-atmosphere interaction as well as their synergy .....	59
Figure 4.6: Factors contributing to the seasonal evaporation change between mid-Holocene and present-day, for details see Figure 4.5.....	60

Figure 4.7: Simulated differences in seasonal sea surface temperature between mid-Holocene and present-day climate. ....	62
Figure 4.8: Factors contributing to the seasonal precipitation change between mid-Holocene and present-day, for details see Figure 4.5 .....	65
Figure 4.9: Difference in mean sea level pressure and wind in 850hPa between mid-Holocene and present-day as simulated by the atmosphere-only run.....	66
Figure 4.10: Upper-tropospheric velocity-potential (200hPa) as simulated by the atmosphere-only model, averaged over the summer season.....	66
Figure 4.11: Difference in mean sea level pressure and wind in 850hPa between mid-Holocene and present-day attributed to the ocean-atmosphere interaction. ....	67
Figure 4.12: Difference in summertime upper-tropospheric velocity potential between mid-Holocene and present-day, attributed to the ocean-atmosphere interaction .....	68
Figure 4.13: Summertime precipitation changes attributed to the ocean-atmosphere interaction. ....	69
Figure 4.14: Factors contributing to the temperature and precipitation change between mid-Holocene and present-day climate averaged over all six regions and all periods. ....	70
Figure 4.18: Contribution of the atmosphere-ocean interaction to the mid- to late-Holocene annual precipitation and temperature change. ....	76
Figure 5.1: Sketch of the main atmospheric circulation systems affecting the Tibetan Plateau during the summer monsoon season, distribution of the main vegetation types on the Tibetan Plateau and locations of the different study sites.....	79
Figure 5.2: ECHAM5 orography, model grid (T31) and grid boxes used for determining the averaged vegetation trend in four different regions on the Tibetan Plateau .....	83
Figure 5.3: Reconstructed vegetation trend from mid-Holocene (6000yrs before present) to present-day, based on four different lake sediment cores on the Tibetan Plateau.....	87
Figure 5.4: Simulated vegetation trend from mid-Holocene to present-day, averaged over four different regions on the Tibetan Plateau. ....	88
Figure 5.5: Simulated present-day annual mean 2m-temperature and summer precipitation compared to ERA40 and GPCP .....	92
Figure 5.6: Change of the climate factors yielding the land cover change on the north-eastern Tibetan Plateau (NETP), i.e. summer near-surface air temperature and growing degree days.....	93
Figure 5.7: Change of the climate factors yielding the land cover change on the south-eastern Tibetan Plateau (SETP), i.e. winter near-surface air temperature and mean near-surface air temperature of the coldest month.....	95

Figure 5.8: Simulated change of summer (JJA) and winter (DJF) near-surface air temperature on the central Tibetan Plateau (CTP).....	97
Figure 5.9: Simulated change of annual precipitation on the central-western Tibetan Plateau (CWTP) .....	98
Figure 6.1: Extended Asian monsoon region .....	107
Figure 6.2: Differences in the land cover distribution between the potential vegetation and the land cover used in the afforestation and deforestation experiment. ....	108
Figure 6.3: Simulated precipitation change between the afforestation or deforestation experiment and the control run, averaged over the monsoon and the dry/cold season...	110
Figure 6.4: Simulated 2m air temperature change between the afforestation/deforestation experiment and the control run, averaged over the monsoon and the dry/cold season...	111
Figure 6.5: Simulated change of different parameters influencing the precipitation change between the afforestation experiment and the control run, for the monsoon season, i.e. total cloud cover, evaporation, mean sea level pressure and 850hPa wind, P-E. ....	113
Figure 6.6: Simulated change of different parameters influencing the precipitation change between the afforestation experiment and the control run, for the dry/cold season .....	114
Figure 6.7: Simulated change of different parameters influencing the precipitation change between the deforestation experiment and the control run, monsoon season. ....	115
Figure 6.8: Simulated change of different parameters influencing the precipitation change between the deforestation experiment and the control run, dry/cold season.. ....	116
Figure 6.9: Simulated change of different parameters influencing the temperature change between the afforestation experiment and the control run, averaged over the monsoon season, i.e. albedo, net surface shortwave radiation, latent and sensible heat flux.....	116
Figure 6.10: Simulated change of different parameters influencing the temperature change between the afforestation experiment and the control run, dry/cold season. ....	117
Figure 6.11: Simulated change of different parameters influencing the temperature change between the deforestation experiment and the control run, monsoon season. ....	118
Figure 6.12: Simulated change of different parameters influencing the temperature change between the deforestation experiment and the control run, dry/cold season. ....	119
Figure 6.13: Simulated relative change in monsoon season precipitation and simulated change in upper-tropospheric velocity potential, afforestation experiment - control run and deforestation experiment - control run. ....	121
Figure 6.14: Simulated summer monsoon precipitation change: mid-Holocene afforestation experiment - control run, mid-Holocene - present-day afforestation-induced climate signal, mid-Holocene - present-day control run, mid-Holocene - present-day afforestation-induced change in moisture convergence and 850hPa-winds .....	123

Figure A.1: The Asian monsoon region .....	149
Figure A.2: Land and sea-floor elevation, based on ETOPO5.....	150
Figure A.3: Sketch of the main mean sea-level pressure and circulation systems (850hPa) affecting the Asian monsoon region during winter.....	150
Figure A.4: Sketch of the main mean sea-level pressure and circulation systems (850hPa) affecting the Asian monsoon region during summer .....	151
Figure A.5: The Asian monsoon in its planetary context. Synthesis of the boreal summer divergent wind circulation, heat sinks and heat sources .....	151
Figure A.6: Factors contributing to the seasonal temperature change between mid-Holocene and present-day climate for six regions in the area of the Asian monsoon. ...	152
Figure A.7: Factors contributing to the seasonal precipitation change between mid-Holocene and present-day climate for six regions in the area of the Asian monsoon ....	153
Figure A.8: Summer mean sea-level pressure and wind in 850hPa as simulated by the atmosphere-only run for present-day orbital conditions.....	154
Figure C.1: Simulated change in summer (JJA) and winter (DJF) temperature, annual precipitation and land cover on the north-eastern Tibetan Plateau (NETP).....	157
Figure C.2: Simulated change in summer (JJA) and winter (DJF) temperature, annual precipitation and land cover on the south-eastern Tibetan Plateau (SETP).....	158
Figure C.3: Simulated change in summer (JJA) and winter (DJF) temperature, annual precipitation and land cover on the central Tibetan Plateau (CTP).....	158
Figure C.4: Simulated change in summer (JJA) and winter (DJF) temperature, annual precipitation and land cover on the central-western Tibetan Plateau (CWTP). .....	159
Figure C.5: Simulated change in bioclimatic conditions and the net primary productivity (NPP) on the north-eastern Tibetan Plateau for all simulated plant functional types.....	160
Figure C.6: Simulated change in bioclimatic conditions and the net primary productivity (NPP) on the south-eastern Tibetan Plateau for all simulated plant functional types. ...	160
Figure C.7: Simulated change in bioclimatic conditions and the net primary productivity (NPP) on the central Tibetan Plateau for all simulated plant functional types.....	161
Figure C.8: Simulated change in bioclimatic conditions and the net primary productivity (NPP) on the central-western Tibetan Plateau for all simulated plant functional types. ...	161

## List of Tables

Table 2.1: Setup of the different model simulations. ....	10
Table 3.1: Overview on the PMIP2 simulations including an atmosphere, ocean and dynamic vegetation model. ....	41
Table 4.1: Start day and length of the seasons for the mid-Holocene and present-day orbital configuration, respectively .....	50
Table 4.2: Description of the areas we consider in our feedback study. ....	51
Table 4.3: Differences between mid-Holocene and present-day climate for certain parameters characterising the energy balance of the surface. ....	61
Table 5.1: Bioclimatic limits for the 8 plant functional types (PFTs) in JSBACH.....	85
Table 5.2: Simulated present-day and observed orographic height, annual mean temperature and precipitation at each site on the Tibetan Plateau. ....	94
Table 5.3: Total vegetation and biomass change on the Tibetan Plateau between mid-Holocene and present-day .....	99
Table 6.1: Physical properties and phenology type of each plant functional type .....	106
Table B.1: Simple statistical significance test of the simulated land cover trend at each area on the Tibetan Plateau.....	155
Table B.2: Assignment of the pollen-taxa to the major vegetation types in the model. ...	156



# 1. Introduction

Like all monsoon systems, the Asian monsoon is primarily induced by the seasonal differential heating of the continents and the adjacent oceans which leads to land-sea temperature and pressure gradients (Webster et al., 1998). The inclusion of processes on land, in the atmosphere and in the oceans excites a strong sensitivity of the monsoon circulation to changes in all components of the climate system. Monsoon systems are therefore characterised by a strong temporal variability covering multi-millennial to intraseasonal timescales (e.g. Lau et al., 2000; Wang B., 2006; Ding, 2007). A unique feature of the Asian monsoon, however, is the presence of the Tibetan Plateau within the monsoon domain. Due to its large horizontal and vertical extent, it strongly affects the regional atmospheric circulation via both, thermal and hydrodynamical processes (e.g. Wu and Zhang, 1998; Ye and Wu, 1998; Liu Y. et al., 2007). This interaction of the Tibetan Plateau and the regional climate makes the Asian monsoon the strongest and most complex monsoon system of the world (Wang B., 2006).

The Asian monsoon system incorporates the East Asian and the Indian monsoon, which are independent sub-systems but can also interact (Ding and Chan, 2005). Together, they affect the life of nearly two-thirds of the global population (Clift and Plumb, 2008) that face the strong variability of the monsoons embedding long-lasting droughts and heat-waves as well as extensive rain and floods (Wang B., 2006).

The recent decades have revealed large climatic changes in the Asian monsoon domain (e.g. Sivakumar et al, 2005; Ding et al. 2007), in particular on the Tibetan Plateau. The temperature on the Plateau rises more and faster than in most parts of the globe and is accompanied by a rapid retreat of the majority of the Tibetan Plateau's glaciers (Kang et al., 2010). This strong climatic sensitivity could have dramatic consequences with regard to the future Asian water resources. The Tibetan Plateau is the source region of all major rivers in the Asian monsoon domain supplying fresh-water to billions of people and to agriculture that is still the most important economic sector in the region. Future climate changes on the Tibetan Plateau and in the entire Asian monsoon region are therefore a matter of particular social, ecological and economical interest.

To be able to give a reasonable projection of the future climate, it is necessary to understand the controlling factors in the Asian monsoon climate system and to investigate the fundamental mechanisms that determined variability and past climate changes in this region (Clift and Plumb, 2008). For this purpose, complex climate models have to be applied and validated against observations; but, the capability of representing the present-day climate reasonably cannot guarantee the capability of the model to simulate climate states different from today's (Joussaume et al. 1999). Therefore, climate models have also

to be validated against reconstructions of past climates that are substantially different from the present-day one. As reconstructions can only provide estimation of the basic past climate state, but not of the mechanisms behind, paleoclimate modelling can improve the understanding and interpretation of the reconstructed climate. A comparison of reconstructed climate states and modelling results is therefore beneficial for both, the reconstruction and the climate modelling community.

A time-slice that is often used for model comparison and validation is the mid-Holocene, 6000yrs before present (e.g. Paleoclimate Modelling Intercomparison Project, Braconnot et al. 2007a,b; Kohfeld and Harrison, 2000; Bush, 2004;). During the mid-Holocene, the surface boundary conditions such as continental ice-sheets or sea-level were comparable to present-day and the atmospheric composition, particularly the CO<sub>2</sub>-concentration, was similar to pre-industrial times. The major difference between mid-Holocene and present-day boundary conditions was the difference in the incoming solar radiation that can be attributed to a change in the Earth's orbital configuration (Berger, 1978). During summer (winter), the insolation was increased (decreased) by approx. 5% on the northern hemisphere yielding an enhancement of the seasonal cycle.

The main objective of this study is a detailed analysis of the mid- to late Holocene climate and vegetation change in the Asian monsoon domain. This includes the comparison of model results with reconstructions and the retrieval of substantiated explanations for the reconstructed climate and vegetation change. As a second objective, we want to assess the performance of the state-of-the-art general circulation model ECHAM5/JSBACH(-MPIOM) with respect to the Asian monsoon system. This thesis is organised as follows:

## CHAPTER 2

The Asian monsoon region is characterised by a very heterogeneous topography manifested particularly in the strong variations of the surface elevation (Figure A.2). Together with the complex atmospheric dynamic and the large internal variability of the monsoon system, this leads to difficulties in the simulation of the Asian monsoon climate and a rather poor reproducibility of the recent variations in the monsoon system within climate models (cf. Zhou et al., 2009 and references there). The climate models have particular problems in simulating the seasonal cycle, variability and distribution of precipitation.

To give an overview on the performance of the model ECHAM5/JSBACH concerning the present-day mean climate state in the Asian monsoon domain, we compare the simulated climate with observations and reanalysis data. Thereby, we introduce the different model setups used in this study that differ with respect to resolution or prescribed ocean surface parameters. We raise the questions:

- (I) How well is the present-day Asian monsoon climate system represented in the model?
- (II) Do the model results depend on the numerical resolution and the prescribed ocean surface parameter?

### CHAPTER 3

In the majority of cases, earlier reconstructions of the mid-Holocene climate reveal a substantial warmer and wetter climate in the Asian monsoon domain relative to the present-day climate (e.g. Shi et al., 1993). Reconstructed Holocene climate trends, however, also suggest an asynchronous precipitation change in the Indian and East Asian monsoon region indicating a complex response of the Asian monsoon system to climate forcings (An et al., 2000, Maher and Hu, 2006; Maher, 2008; Wang YB. et al., 2010). Simulating the mid-Holocene Asian monsoon climate could therefore be associated with high uncertainties. Previous simulations conducted e.g. in the Paleoclimate Modelling Intercomparison Project (PMIP) show a strengthening of the summer monsoon circulations due to an increased thermal gradient between the continents and the ocean, but they strongly differ regarding the magnitude and the pattern of the associated precipitation and temperature change (e.g. Braconnot et al., 2007a, b). To assess the performance of the different models, the model results have to be compared to reconstructions. However, the reconstructions in the Asian monsoon region often suffer from large discrepancies in the age control and the sample resolution (Wang YB. et al., 2010) that, so far, has reduced their potential of application in model validation studies.

In Chapter 3, we present the differences between the mid-Holocene and present-day monsoon climate simulated by ECHAM5/JSBACH and thereby particularly focus on precipitation. We compare for the first time results of high-resolution global climate model simulations with a synchronised dataset of reconstructions for the mid-Holocene time slice (conducted by Wang YB. et al., 2010) and quantify changes in the summer monsoon characteristics. Furthermore, we shed light on the processes leading to the reconstructed mid-Holocene moisture pattern. We raise the following questions:

- (III) Applying mid-Holocene orbital forcing, how does the simulated Asian monsoon climate change compared to present-day?
- (IV) Is the simulated mid-Holocene climate consistent with reconstructions?
- (V) Which changes in atmospheric circulation could have led to the mid- to late-Holocene moisture change in the Asian monsoon region?

## CHAPTER 4

Climate modelling studies on the Holocene climate change in the African monsoon region reveal that the strengthening of the North African monsoon system during the mid-Holocene cannot be explained by orbital forcing alone (e.g. Joussaume et al., 1999). Internal feedbacks between the atmosphere and the ocean or the land-surface (including vegetation) have probably strongly enhanced the mid- to late-Holocene monsoon change in North Africa (e.g. Claussen and Gayler, 1997; Kutzbach and Liu, 1997; Broström, et al., 1998; Braconnot et al., 2000; Levis et al., 2004; Liu Z. et al., 2004). Fewer studies exist concerning the role of interactions in the Holocene Asian monsoon climate change and these studies furthermore show contradictory results that probably contribute to the above mentioned discrepancy between the model simulations within PMIP (Braconnot et al., 2007b), for instance. In some climate models, the ocean-atmosphere interaction results in an increase of the Asian monsoon precipitation (e.g. Hewitt and Mitchell, 1998; Braconnot et al., 2000; Wei and Wang, 2004). Other climate modelling studies reveal a decrease of precipitation related to the ocean-atmosphere interaction (e.g. Voss and Mikolajewicz, 2001; Ohgaito and Abe-Ouchi, 2007; Li and Harrison, 2008; Marzin and Braconnot, 2009). Regarding the vegetation and land-surface interaction with the atmosphere, the climate model results are in better agreement and suggest an enhancement of the Asian summer monsoon due to these interactions (e.g. Claussen, 1997; Wang H.-J., 1999; Diffenbaugh and Sloan, 2002, Li and Harrison, 2009). However, fully coupled atmosphere-ocean-vegetation models have been applied only in a few studies and these studies do not follow a consistent methodology to derive the interactions of the atmosphere with the other compartments of the climate system. Therefore, none of the simulations conducted in previous studies or in PMIP are designed to derive the pure contributions of the atmosphere-ocean and the atmosphere-vegetation interactions as well as their synergy to the mid- to late-Holocene Asian monsoon climate change.

In Chapter 4, we assess the contribution of the ocean-atmosphere and vegetation atmosphere interaction as well as their synergy to the Holocene climate change. For this purpose, we analyse a set of coupled simulations conducted by Otto et al (2009a) in the comprehensive Earth system model ECHAM5/JSBACH-MPIOM. These simulations have been designed to allow the application of the factor-separation technique (Stein and Alpert, 1993) and therefore provide the opportunity to separate the pure contribution of the different interactions. The main research question of this chapter is:

(VI) How strong is the contribution of ocean-atmosphere and vegetation-atmosphere interactions as well as their synergy to the mid- to late-Holocene climate change?

This chapter has been published in *Climate of the Past* (Dallmeyer et al., *Clim. Past*, 6, 195-218, 2010).

## CHAPTER 5

The Tibetan Plateau exerts a strong influence on the regional as well as the global climate (e.g. Ye and Wu, 1998; Duan and Wu, 2005; Wu et al., 2007). It plays an important part in the Asian monsoon dynamics as it, for instance, forms an elevated heat source for the atmosphere in spring and summer and thus modifies and enhances the thermal contrast between the land and the ocean (e.g. Liu Y. et al., 2007). Due to its height, the Tibetan Plateau furthermore transfers this contrast to the upper troposphere where it can strongly influence the atmospheric large-scale circulation. The strong convective activity on the Plateau induces a huge air-pump and a strong vertical circulation leading to subsidence north and west of the Plateau and even in the Sahara (e.g. Rodwell and Hoskins, 1996). As the energy balance at the surface and the transfer of energy and momentum between the atmosphere and the land depends to a large part on the land cover, land cover changes on the Tibetan Plateau may have strongly affected the Holocene climate change in the Asian monsoon domain. The Tibetan Plateau is very sensitive to climate change and reconstructions have reported strong natural land cover changes on the Plateau since the early and mid-Holocene (Gasse et al, 1991, Shen et al., 2005 and 2006, Herzschuh 2010a).

In Chapter 5, we compare simulated vegetation trends for different regions on the Tibetan Plateau with pollen-based vegetation reconstructions. For this purpose, we analyse the transient mid-to late-Holocene simulation performed with the comprehensive Earth system model ECHAM5/JSBACH-MPIOM by Fischer and Jungclaus (2011) that was forced with orbital forcing alone. We raise the question:

- (VII) Is the model able to capture the reconstructed mid- to late-Holocene vegetation trend?
- (VIII) Which climatic mechanisms have caused the vegetation change on the Tibetan Plateau?

This Chapter is a joint work of our group and U. Herzschuh from the Alfred-Wegener-Institute in Potsdam, Germany, and has been published in *Climate of the Past* (Dallmeyer et al., *Clim. Past*, 7, 881-901, 2011). The parts of the text that have been written by U. Herzschuh are marked.

## CHAPTER 6

Land cover changes are accompanied by a modification of the physical surface properties such as roughness length or surface albedo and therefore have a direct effect on the surface energy, momentum and water balance (biogeophysical effects). Land cover changes may, thus, exert a strong influence on the monsoon dynamics (Yasunari, 2007). According to reconstructions, the Holocene was characterised by large-scale natural land cover changes that are often related to the decreasing summer monsoon strength entailing shifts in the

precipitation distribution. During the mid-Holocene, forest cover in the Asian monsoon domain was strongly increased and the vegetated and forested areas extended further inland compared to present-day (e.g. Yu et al. 2000; Ren, 2007; Zhao et al., 2009).

So far, idealised experiments on the climate impact of large-scale forest cover changes has only been conducted for the entire tropics or extratropics (e.g. Henderson-Sellers, 1993; Claussen et al., 2001; Snyder, 2010; Bathiany et al., 2010) or single continents e.g. Africa (e.g. Werth and Avissar, 2005b), but not for the Asian monsoon region. As the Asian monsoon domain incorporates tropical and extratropical regions, one can not simply draw conclusions from these studies for the climatic impact of large-scale forest cover changes in the Asian monsoon region. Studies on recent anthropogenic land cover changes reveal that the degradation of the land cover in the Asian monsoon domain has led to significant changes in the regional climate. However, these studies do not agree with respect to the sign and magnitude of the associated climate change.

The Asian monsoon domain was the homeland of some of the oldest human civilisations which had already had a highly-developed agriculture and infrastructure (Clift and Plumb, 2008). The linkage between the development and collapse of these cultures and the monsoon variability as well as the role early human societies could have played in the Holocene climate and vegetation change is often discussed (e.g. Ren, 2000; Fu, 2003; Clift and Plumb, 2008).

In Chapter 6, we present results of an idealised sensitivity study conducted with the general circulation model ECHAM5-JSBACH and investigate the biogeophysical effect of large scale forest cover changes in the Asian monsoon domain on present-day and mid-Holocene climate. We thereby address the following research questions:

- (IX) How does the Asian monsoon climate respond to large-scale forest cover changes?
- (X) Could large-scale forest cover changes have amplified the insolation-induced Holocene climate change?
- (XI) What is the implication of our results concerning the relation of mid-Holocene climate, vegetation and neolithic cultures in the Asian monsoon domain?

This chapter has been published in *Biogeosciences* (Dallmeyer and Claussen, *Biogeosciences*, 8, 1499-1519, 2011).

## CHAPTER 7

In Chapter 7, we conclude this thesis by summarising the main results and suggesting possible directions for future research.

## 2. Simulated present-day Asian monsoon climate

### 2.1 Introduction

Monsoon systems are mainly confined to tropical and subtropical regions and primarily form in consequence of seasonal and latitudinal differences in incoming solar radiation. The different heat capacities of the continent and ocean lead to strong land-sea thermal contrasts (Webster et al., 1998). As consequence, large-scale pressure gradients are generated inducing strong low-level atmospheric wind circulations that reverse seasonally according to the change in insolation. During winter, cold highs form above the continents and the main monsoon circulation is directed from the continents towards the warmer ocean leaving the continents in a dry climate. During summer, monsoon troughs develop above the warm (tropical) land-mass and the low-level atmospheric wind changes the direction by more than  $120^\circ$ . As monsoon systems are large-scale atmospheric phenomena, the flow direction of monsoon circulations is strongly modified by the Coriolis force. Another important driving force of monsoons are the involved moist processes (Webster et al. 1998, He et al., 2007). The summer monsoon transports moisture towards the continents and thereby redistributes solar energy and enhances the energy gradient between the land and the oceans. The release of latent heat in the middle troposphere above the continent invigorates the strong vertical uplift and the deep convection associated with summer monsoons and contributes to the maintenance of the monsoon circulation. Summer monsoons are accompanied by intensive precipitation that usually accounts for most of the annual total in the affected regions. Related to the seasonal changes of the low-level monsoon circulation are modifications in the upper-tropospheric wind circulation including large latitudinal shifts of the upper-tropospheric jet streams. The divergence of the upper tropospheric wind circulation strongly determines the precipitation distribution (e.g. Sato, 2009).

The major features of the Asian monsoon system are summarised in Figure A.1-A.5. The Asian monsoon system is divided into three subsystems: the Indian Monsoon (IM), the East Asian monsoon (EAM) and the western North Pacific monsoon (WNPM) that is mainly not affecting the continental regions (e.g. Ding, 2007). These monsoon systems strongly interact but differ with respect to their major characteristics and their variability (e.g. Wang B. et al., 2001). The Indian summer monsoon is related to the monsoon trough in North India and the Mascarene high causing an interhemispheric circulation that intensifies close to the east coast of Africa in the so called Somali Jet or Findlater Jet (e.g. Lau et al., 2000). The Indian monsoon is, thus, characterised by a meridional pressure-gradient and represents a classical monsoon embedded in the Hadley cell circulation. The seasonal march of the monsoon rainband is strongly connected with the movement of the

Intertropical Convergence Zone (ITCZ). In contrast, the East Asian summer monsoon is controlled by the monsoon trough on the Asian continent and the western Pacific subtropical high. It is, therefore, characterised by a zonal pressure-gradient and has to be seen in association with the Walker Circulation (Webster et al., 1998). As a result of the east-west thermal contrast, a planetary subtropical front is formed (Meiyu-Baiu frontal system) whose seasonal march determines the propagation of the East Asian summer monsoon rainbelt (e.g. Ding, 2007). The subtropical front is separated from the ITCZ, which forms a second rainband in East Asia (tropical rainbelt) affecting mainly the western North Pacific monsoon.

According to Ding and Chang (2005), Ding (2007) and He et al. (2007), the summer monsoon season first starts in the equatorial East Indian Ocean and Sumatra in late April. In a second stage beginning early to mid of May, the monsoon expands to the Bay of Bengal, southern Indochina and the South China Sea. From these regions, two branches move north-west- and north-eastward to South China (mid and late May) and the Indian subcontinent (early to mid June) establishing the onset of the East Asian and the Indian summer monsoon, respectively. The Indian monsoon then penetrates further inland arriving in Northwest India in the mid of July. The East Asian monsoon moves northward in a stepwise manner that is characterised by abrupt jumps from one region to another. In early June, it arrives in the Yangtze River valley and Japan bringing the so called Meiyu and Baiu rain, respectively. It then jumps to Northeast China and the Korean Peninsula (Changma rainy season) in early and mid-July where it stays until the end of August or early September before it starts to continuously move back to the South China Sea. The Indian monsoon terminates not until late September.

The East Asian monsoon system differs from the Indian monsoon also in other respects. The interplay of the mid-latitude westerlies, the subtropical circulation around the western Pacific subtropical high and the tropical circulation including the Indian monsoon flow makes the East Asian monsoon domain unique and enables the occurrence of many significant weather and climate phenomena (Ding, 2007). In contrast to other monsoon regions, the precipitation in the East Asian monsoon domain is not temporally confined to the summer monsoon season. The wintertime pressure-gradient between the Siberian high and the Aleutian low induces cold northerly winds embedding regularly cold-air outbreaks (Wang B., 2006) in the entire East Asian monsoon region. Therefore, the East Asian monsoon domain is not characterised by the alternation of wet and dry seasons but rather by the alternation of particularly wet and cold seasons.

Recent studies have shown that climate models reveal large deficits in representing the mean precipitation distribution, the season cycle and the interannual variability of the Asian monsoon system (Kang et al. 2002; Zhou et al., 2009; Boo et al., 2011). In contrast, the temperature distribution and monsoon circulation can be captured by the models.

In this study, we assess the performance of the general circulation model ECHAM5/JSBACH with respect to the precipitation and near-surface air temperature distribution in the Asian monsoon domain as well as the monsoon circulation in the lower troposphere. As the outcome of this evaluation may depend on the model setup, we test the dependence of the simulated results on the numerical resolution and the prescribed ocean surface parameters. We thereby introduce the model setups used in the next chapters of this thesis.

## 2.2 Methods

### 2.2.1 Model and experiments

The first part of this study aims to give a short evaluation on the representation of the Asian monsoon system in the model ECHAM5/JSBACH. This model consists of the general circulation model for the atmosphere ECHAM5 (Roeckner et al., 2003) that is coupled to the land surface scheme JSBACH (Raddatz et al. 2007). JSBACH includes the dynamic vegetation module of Brovkin et al. (2009). The models ran with the spectral resolution T106L31, corresponding to a latitudinal distance of approx.  $1.125^\circ$  and 31 levels in the vertical. Atmospheric composition was fixed at pre-industrial values with  $\text{CO}_2$ -concentration set to 280ppm. Sea surface temperature and sea-ice were prescribed according to their pre-industrial distributions. Values were taken from a coarse resolution simulation conducted with the comprehensive Earth System Model ECHAM5/JSBACH-MPIOM (Fischer and Junglaus, 2011) that included the dynamic ocean model MPIOM (Marsland et al. 2003). ECHAM5/JSBACH was brought to quasi-equilibrium climate state (spin-up of approx. 200years) before it ran for additional 30 years (analysis period). This simulation is referred to as T106\_AV<sub>0k</sub> in the following.

In the second part of this study, we assess how the method of prescribing SSTs/sea-ice affects the representation of the monsoon system in the model and how the results depend on the numerical resolution. For this purpose, we compare the simulation T106\_AV<sub>0k</sub> with simulations conducted with the same model, but with a varying setup regarding the following aspects:

- Resolution: T106L31, T63L31 or T31L19
- SST/sea-ice: pre-industrial (0k, prescribed), observed (AMIP, prescribed) or dynamically simulated (AOV)
- Vegetation: fixed (A) or dynamically simulated (AV)

These simulations have been performed in several projects at the Max-Planck-Institute for Meteorology. The coarse resolution experiments (T31L19) with prescribed SSTs and sea-ice following the SSTs and sea-ice distributions of the Atmospheric Model

Intercomparison Project (AMIP, Gates 1992) have been undertaken by Vamborg (2011). The other coarse resolution experiments have been conducted by Otto et al. (2009b, 2011). The medium resolution experiment (T63L31) has been performed by Dallmeyer and Claussen (2011). Details on the setup of the experiments are summarised in Table 2.1.

Experiment	Resolution	SST/sea-ice	vegetation	analyses period	reference
T106_AV <sub>0k</sub>	T106L31	prescribed, 0k	dynamic	30 years	new
T63_A <sub>0k</sub>	T63L31	prescribed, 0k	fixed	100 years	Dallmeyer and Claussen, 2011
T31_A <sub>0k</sub>	T31L19	prescribed, 0k	fixed	240 years	Otto et al., 2011
T31_A <sub>AMIP</sub>	T31L19	prescribed, AMIP	fixed	135 years	Vamborg, 2011
T31_AOV <sup>*)</sup>	T31L19	dynamic	dynamic	600 years	Otto et al, 2009b
T31_AV <sub>0k</sub>	T31L19	prescribed, 0k	dynamic	240 years	Otto et al, 2011
T31_AV <sub>AMIP</sub>	T31L19	prescribed, AMIP	dynamic	135 years	Vamborg, 2011

Table 2.1: Setup of the different model simulations. <sup>\*)</sup> T31\_AOV ran with a different model version of ECHAM5/JSBACH-MPIOM.

## 2.2.2 Calculation of the monsoon onset and withdrawal period

Following the definition of Wang and Linho (2002), we calculate the onset and withdrawal of the rainy season based on the relative pentad mean rainfall rate ( $rp_i$ ) defined as difference between the pentad mean rainfall rate ( $p_i$ ) and the January mean rainfall rate ( $p_{jan}$ ):

$$rp_i = p_i - p_{jan} \quad i = 1, 2, \dots, 73 \quad (2.1)$$

The period in which  $rp_i$  reaches values above 5mm/day represents the monsoon season. Accordingly, the onset (withdrawal) is defined as the pentad in which  $rp_i$  exceeds (falls below) 5mm/day. This method is a good approximation of the observed monsoon propagation.

This definition of the onset and withdrawal is designed to reflect the mayor characteristics of monsoon rainy seasons, i.e. the total amount of summer precipitation and its intensity, strong seasonal differences in precipitation and the temporal concentration of precipitation

in the local summer season. This last point is accounted for by the additional criterion that the above defined onset pentad has to occur between May and September (Wang B. and Linho, 2002). This criterion is not included in our calculations of the monsoon onset, as ECHAM5/JSBACH overestimates the pre-monsoon precipitation in Eastern China. An application of this criterion would lead to a constant onset period in the model (i.e. 1st pentad of May) and would disregard regional differences.

## 2.3 Model evaluation

### 2.3.1 Annual precipitation

Figure 2.1 shows the annual mean precipitation of the simulation T106\_AV<sub>0k</sub> compared to the observed climatology derived by the Global Precipitation Climatology Project (GPCP, version 2.1, 1979-2006, Adler et al., 2003) and the Climate Prediction Centre (CMAP, 1979-2008, Xie and Arkin, 1997). Overall, the model captures the major annual precipitation pattern. The contrast between the arid/semi-arid regions of central Asia and the wet monsoon region is well represented. The highest precipitation rates are simulated in the equatorial region at the Maritime Continent, the Bay of Bengal, in the Intertropical Convergence Zone and in the Subtropical Front which is related to the strong moisture

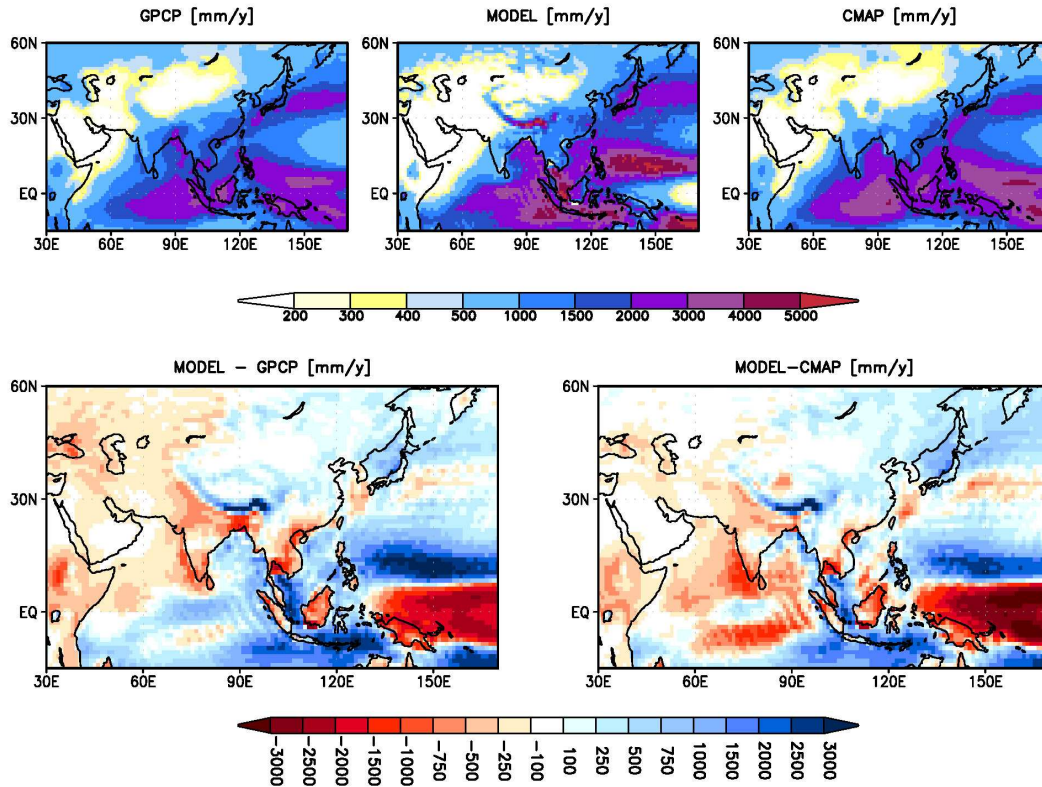


Figure 2.1: Simulated present-day annual mean precipitation [mm/year] compared to the observational datasets of GPCP (Adler et al., 2003) and CMAP (Xie and Arkin, 1997).

convergence in the northern flank of the Western Pacific Subtropical High. For the region approx. 30-170°E, 10°S-60°N, the pattern correlation coefficient of the simulated annual precipitation and observations is 0.66 (GPCP) and 0.7 (CMAP), respectively. However, the magnitude of the simulated and observed annual mean precipitation rates differ. The comparison exhibits strong rainfall deficits in large parts of the Southern and Western Asian continent. The simulated annual mean precipitation is underestimated by up to 750mm/year in India and 1400mm/year in Indochina compared to GPCP. This strong rainfall deficit is also a problem in the African monsoon region. In contrast, the model overestimates the annual precipitation on the Southern Himalaya by up to 4500mm/year. This could be related to an inappropriate parameterisation of convective precipitation at steep mountain slopes (Cui et al., 2006). Regarding precipitation over the ocean, the two observational data-sets do not agree. The major difference of the T106\_AV<sub>0k</sub> to both datasets is a poleward shift of the Pacific Intertropical Convergence Zones which is accompanied by a strong rainfall deficit in a 10° of latitude wide region along the equator. Furthermore, the simulated annual mean precipitation rate exceeds the observed values in the oceanic part of the Maritime Continent by up to 3000mm/year. The precipitation rate in the northern Indian Ocean is underestimated by the model (up to 900 mm/year).

Figure 2.2 shows a latitude-time transect through the East Asian monsoon region (110-120°E) and the Indian monsoon region (70-80°E) based on pentad-mean precipitation rates. Compared to CMAP, many features of the East Asian annual precipitation cycle are well represented in the model. This includes, for instance, the simulation of spring precipitation at ca. 30°N and the seasonal march of the monsoon rainband, i.e. its northward jump in late spring and its slow retreat in autumn. The major difference in the simulated and observed cycle is the occurrence of a second rainband directly south of the equator. During the monsoon season, the model calculates too little precipitation (ca. 4-6mm/day) in the central East Asian monsoon region which is associated with a 5°-northward displacement of the major monsoon front. The simulated spring precipitation period in Eastern China starts too early and the rainband is located too far in the north (ca. 4°). In addition, the magnitude of spring precipitation is overestimated by the model.

The comparison of the Indian transects exhibits a strong rainfall deficit in the monsoon region nearly all over the year. Particularly in the summer season, the mean pentad rainfall rate is too small by up to 6mm/day. The general march of the Indian monsoon is well represented by the model, but the northward advance of the major rainband begins nearly one month too late.

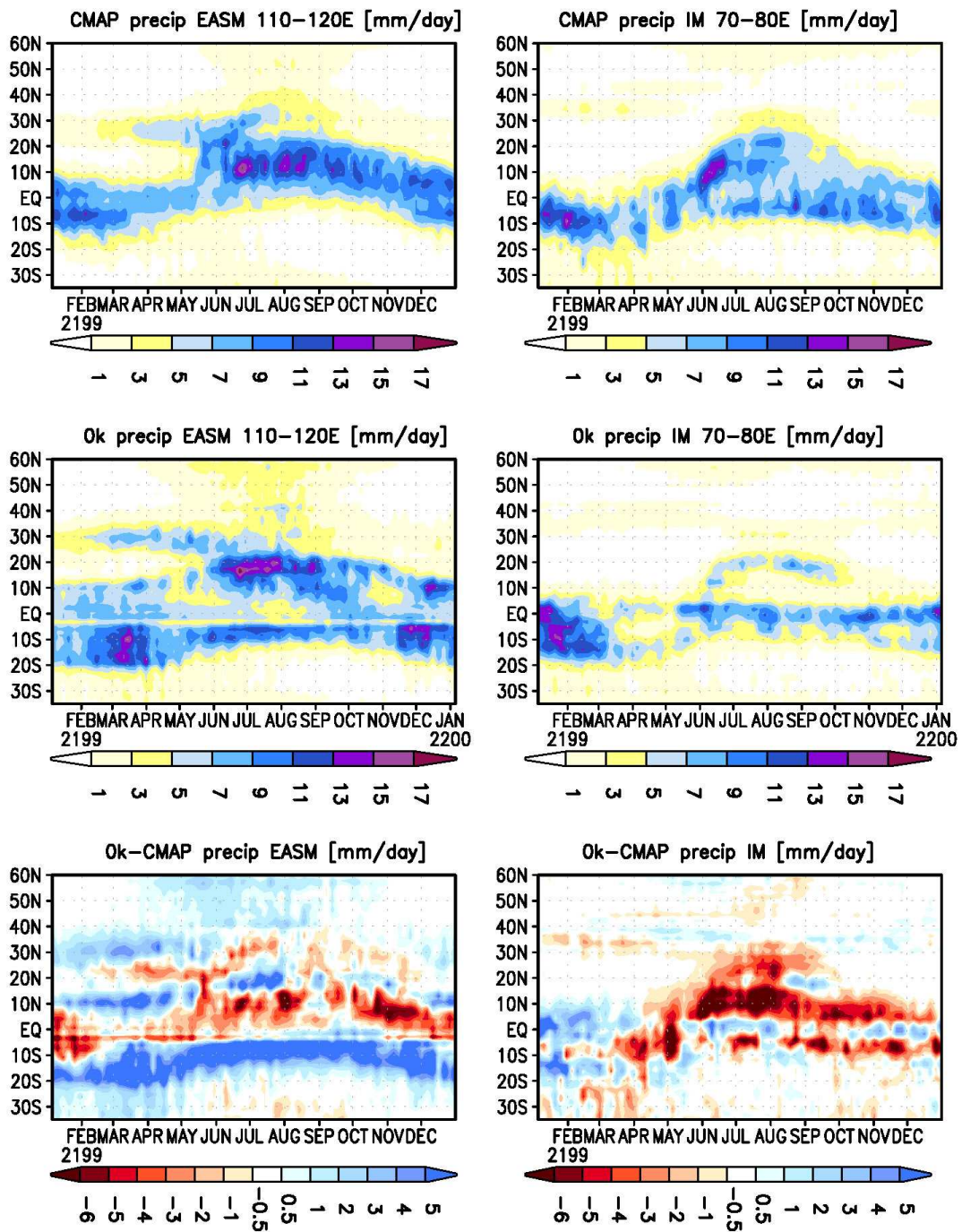


Figure 2.2: Hovmöller diagram showing the difference in the latitudinal structure of the seasonal precipitation cycle in an East Asian (110–120°E, left panel) and Indian monsoon sector (70–80°E, right panel) between the model (based on T106\_AV0k) and the observational dataset CMAP (Xie and Arkin, 1997). Shown are pentad-mean precipitation rates in mm/day.

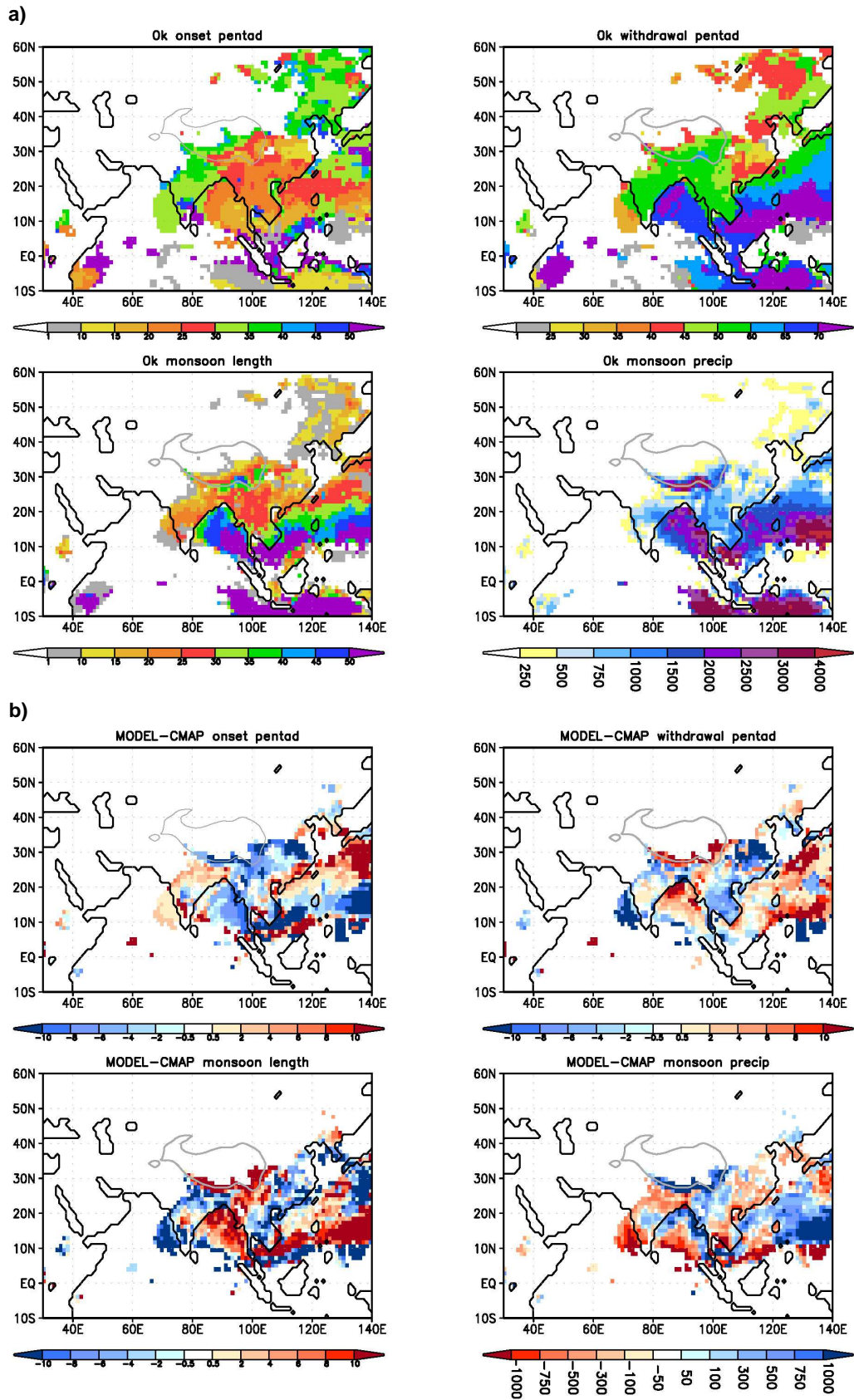


Figure 2.3: Simulated onset and withdrawal period of the Asian monsoon as well as monsoon season length and related precipitation [mm/monsoon season], based on the definition of Wang B. and Linho, 2003. a) present-day simulation (T106\_AV0k), b) difference between the present-day simulation and CMAP observations.

### **2.3.2 Monsoon onset and withdrawal**

The onset and withdrawal time of the Asian summer monsoon is calculated via the simulated and observed (CMAP) relative pentad mean rainfall rates. The seasonal advance of the monsoon can only partly be represented by the model. In observations, the monsoon season first starts in the Bay of Bengal and the South China Sea. It, then, moves onto the East Asian continent and India. This typical track is depicted by the model in the Indian monsoon region, but not in the East Asian monsoon region (Figure 2.3a). Nevertheless, the monsoon season in north India starts later in the model than in observation (2-8 pentads, Figure 2.3b). In Eastern China, the simulated summer monsoon begins 2-10 pentads too early. This is partly related to the overestimated spring precipitation rate in Central Eastern China that already reaches values fulfilling the applied monsoon season criterion.

The simulated monsoon retreats on most parts of the continent up to 10 pentads earlier compared to the observations. Therefore, the monsoon season length is shorter in these regions. Exceptions are the Himalaya mountain range and the area between the southeastern Tibetan Plateau and the Bay of Bengal. The differences in simulated and observed monsoon season length are reflected in the monsoon season precipitation pattern, i.e. the precipitation falling in the monsoon season. In most parts of the continental monsoon domain, monsoon related precipitation is underestimated in the model by up to 750mm. This strongly contributes to the annual rainfall deficit in India mentioned above.

### **2.3.3 Near-surface air temperature**

The near-surface air temperature in 2m height is compared with the observational dataset of the Climate Research Unit CRU TS 2.1 (1960-2000; Mitchell and Jones, 2005) and the reanalysis data ERA40 of the European Centre for Medium-Range Weather Forecasts (ECMWF, Simmons and Gibsons, 2000). The CRU data does not include temperatures over the oceans. Temperatures are examined for two seasons. These are the wet season lasting from May to October (Figure 2.4) and the cold/dry season lasting from November to April (Figure 2.5). In both seasons, the observed/reanalysed temperature distribution is well represented in the model. The lowest near-surface temperatures are located on the elevated Tibetan Plateau and in North Eastern Asia. The highest temperatures are calculated for the equatorial regions during the cold/dry season and in the monsoon trough (i.e. North India) and the desertic regions of Africa and the Middle East during the wet season. The pattern correlation coefficient for the continental region ca. 30-170°E, 10°S-60°N of the simulated and the observed temperature is 0.99 for the cold/dry season and 0.97 for the wet season, respectively. Biases between the model and both, observational and reanalysis data, exist regarding the absolute temperature. In the wet season, simulated climate is up to 7-9K too warm in North India, East Africa and the Middle East compared

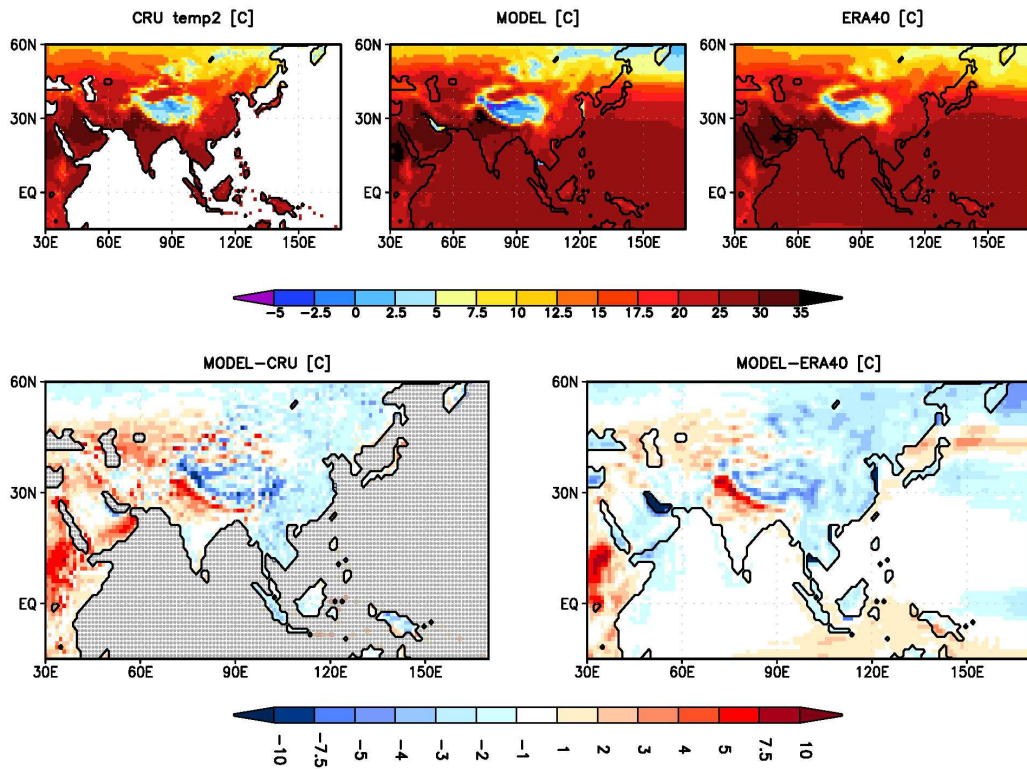


Figure 2.4: Simulated present-day near-surface air temperature of the wet season (May-October, in °C) compared to the observational dataset CRU TS2.1 (Mitchell and Jones, 2005) and ERA40 reanalysis data (Simmons and Gibson, 2000). CRU TS2.1 does not include oceanic regions.

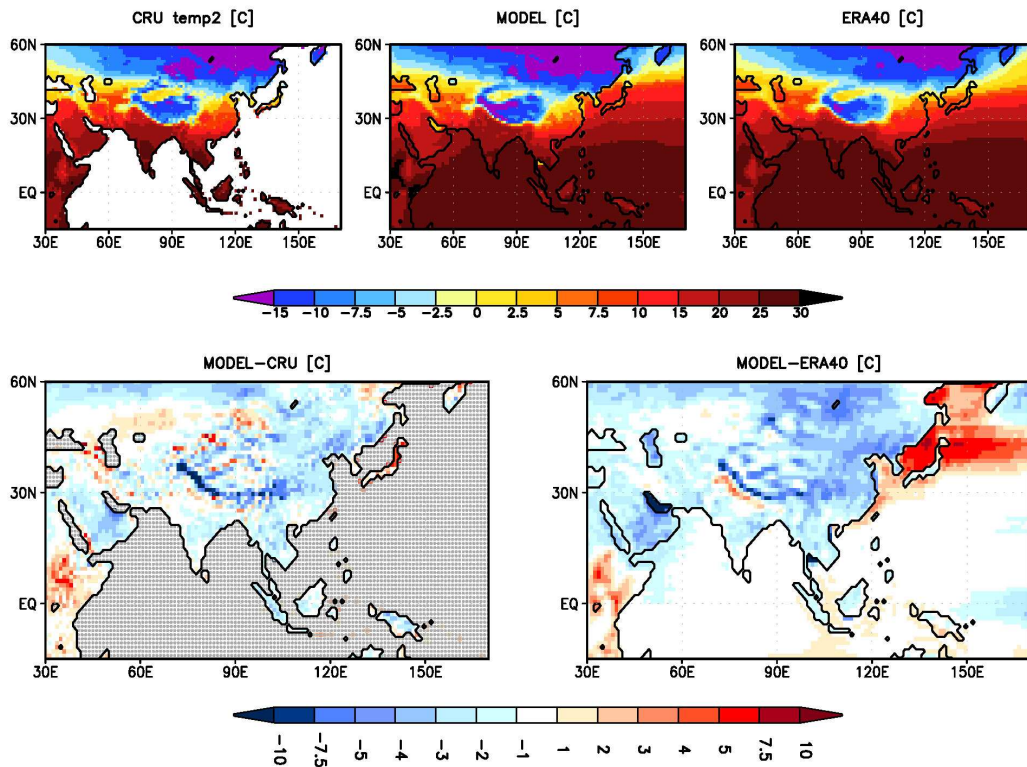


Figure 2.5: Same as Fig. 2.4, but for the dry/cold season (November-April).

to observations and reanalysis data. Part of this warm bias may be related to the rainfall deficit in the model. In contrast, wet season temperatures are lower than observed on the Tibetan Plateau (up to 12K) and at the continental region east of 90°E (up to 4K). In Southern Arabia, CRU and ERA40 deviate, so that the model simulated up to 5K too high temperatures compared to CRU and up to 3K too low temperatures compared to ERA40. In the cold/dry season, the model strongly underestimates the temperatures on the Asian continent (up to ca. 10K). The bias to observations is smaller than to ERA40. Simulated near-surface air temperatures above the West Pacific are up to 8K too high compared to ERA40. Part of the differences in simulated and observed/reanalysed temperatures is caused by the lower CO<sub>2</sub>-concentration prescribed in the model (pre-industrial instead of present-day).

#### **2.3.4 Mean sea level pressure and atmospheric circulation in 850hPa**

Figure 2.6 shows the winter and summer mean sea level pressure distribution as well as the wind field in 850hPa based on the model simulation T106\_AV<sub>0k</sub> and ERA40 reanalysis data. Overall, the circulation systems are well represented in the model. The simulated and reanalysed position of the controlling pressure systems such as the Siberian high and the Aleutian low in winter or the western Pacific subtropical high and the monsoon trough in summer agree well. The strength of the pressure systems partly differ in the model and ERA40. In winter, the Aleutian low is underestimated in the model (up to 8hPa). The mean sea level pressure in North East China is overestimated by up to 4hPa in the model. Therefore, the East Asian winter monsoon is slightly weaker in the model than in the reanalysis data. The model simulates an up to 10hPa too high mean sea level pressure north of 55°N showing a positive north-south gradient. This leads to a weakening of the westerly wind circulation by up to 4m/s. The winter mean sea level pressure above the Indian Ocean, India, the Tibetan Plateau and Indochina is underestimated by the model.

During summer, the model simulation exhibits a low pressure anomaly of up to 3hPa in the Eastern Chinese Sea. Combined with a slight overestimation of the mean sea level pressure in Eastern China and Indochina, this results in a cyclonic wind anomaly in the Eastern Chinese Sea and a weakening of the East Asian summer monsoon. The western Pacific subtropical high is slightly too strong in the model (up to 2hPa). A high pressure anomaly in the northern Arabian Sea leads to a decreased Indian monsoon strength in South India. In North India, the summer monsoon is enhanced by up to 4m/s in the model. Above the equatorial Indian Ocean, the model simulates anomalous westerlies which are probably associated with a low pressure anomaly centred south of Indonesia. These westerly winds converge above the Maritime Continent and may contribute to the overestimation of precipitation there.

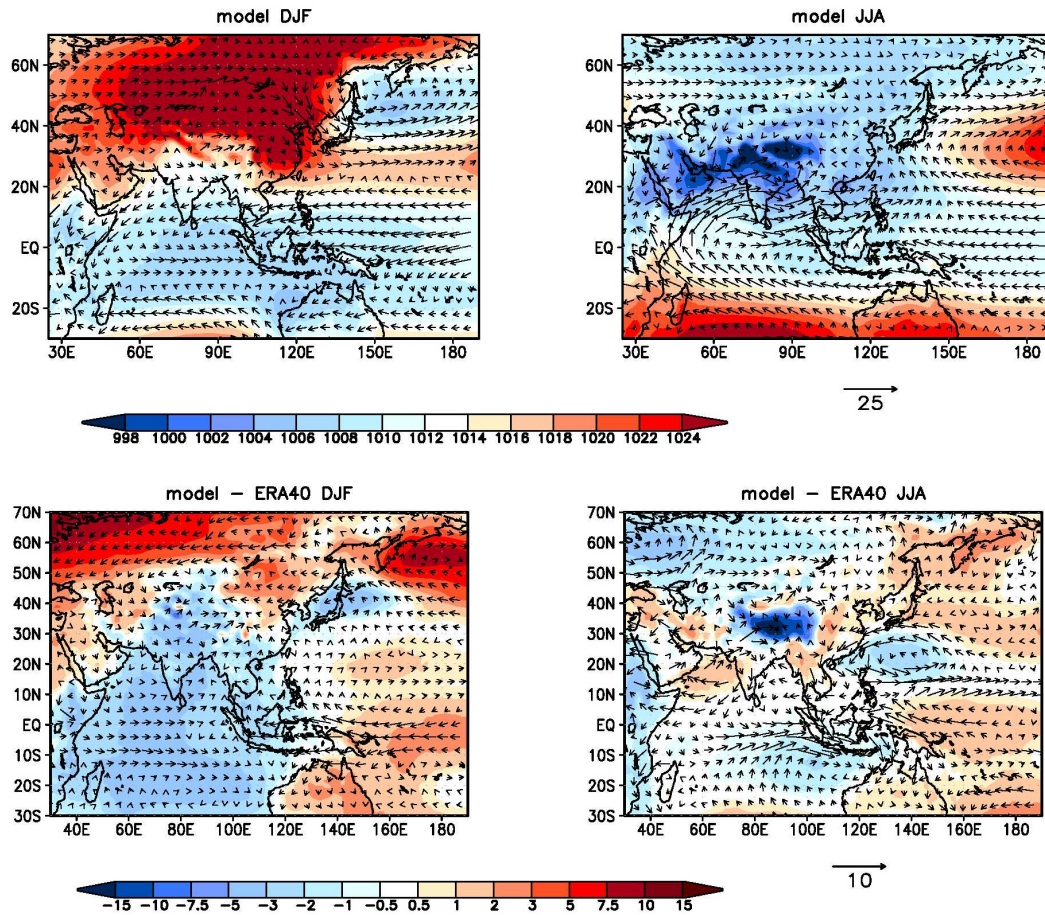


Figure 2.6: Simulated mean sea level pressure in hPa, shaded, and 850hPa wind circulation in m/s, vector, compared to ERA40 reanalysis data (Simmons and Gibson, 2000), averaged over the winter (left) and summer season (right).

## 2.4 The effect of prescribing SST/sea-ice and changing resolution

In the simulation T106\_AV<sub>0k</sub>, the sea surface temperatures and sea-ice distribution have been prescribed according to results of a pre-industrial simulation performed in a coupled atmosphere-ocean-vegetation model. Using this method could lead to additional biases in the simulation. To test whether the differences between T106\_AV<sub>0k</sub> and observations are caused by this method, we compare results of simulations using model derived SSTs and sea-ice with simulations that ran with prescribed AMIP SSTs and sea-ice. Furthermore, we investigate how the representation of the Asian monsoon climate in the model depends on the chosen numerical resolution. The effect of coupling vegetation dynamically instead of prescribing land cover is investigated to complete the picture of the sensitivity of the simulated results to differences in the model setup. In the following, the names of the different simulations consist of the respective resolution (T31, T63 or T106), the used models (A: atmosphere and land-surface model only, V: including dynamic vegetation)

and as indices the method of prescribing the ocean (AMIP: using observations; 0k: using model derived SSTs and sea-ice). To calculate the pattern correlation coefficient of the different simulations, the simulated values are bilinearly interpolated to a uniform grid (equivalent to the grid of T106\_AV<sub>0k</sub>).

### 2.4.1 Precipitation

Figure 2.7 shows the annual mean precipitation distribution for all simulations used in this study. The difference between these simulations as well as the differences between the observation (GPCP) and these simulations are displayed in Figure 2.8. The coarse resolution simulation with prescribed AMIP SSTs (T31\_A<sub>AMIP</sub>) reveals a positive precipitation bias in large parts of eastern China and the Tibetan Plateau (up to ca. 800mm/year, Figure 2.8d). Parts of Northern India, Bangladesh and Indochina receive less precipitation compared to GPCP (up to ca. 1000mm/year). With the exception of the East China Sea and the Pacific east of Japan, annual precipitation above the ocean is overestimated by the model.

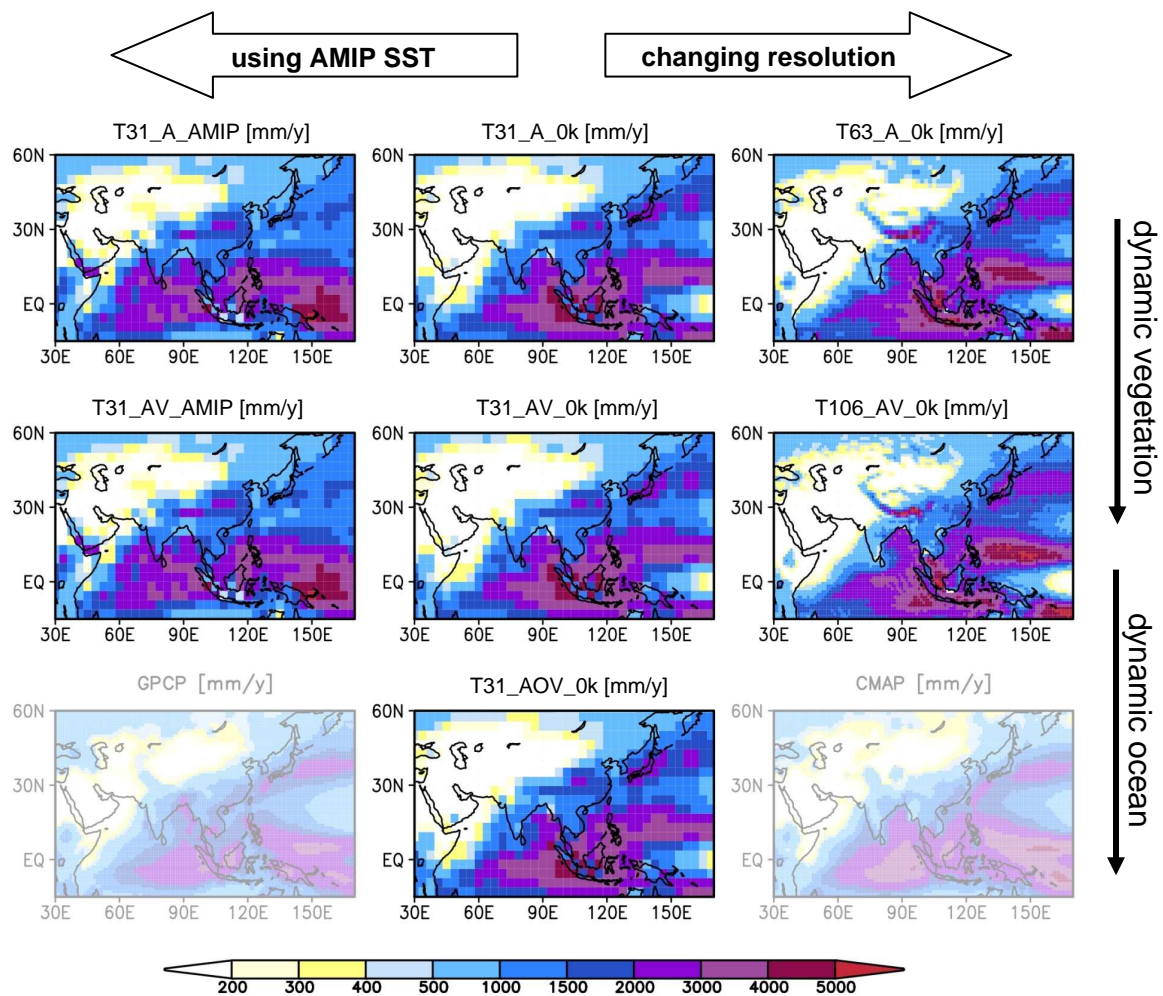


Figure 2.7: Simulated present-day annual mean precipitation [mm/year] in all model-setups used in this study that differ with respect to resolution, coupling and prescribed sea surface temperature and sea-ice distribution.

Overall, this simulation is in better agreement with the observations than T106\_AV<sub>0k</sub>. The pattern correlation to GPCP and CMAP is 0.83 and 0.87, respectively. An improvement of the simulated precipitation pattern is received particularly over the ocean. The technique of prescribing pre-industrial (0k) SSTs and sea-ice from a coupled model affects the continental precipitation pattern only slightly (Figure 2.8a). Nevertheless, part of the precipitation bias (up to ca. 350mm/year) in the Indian monsoon region can be attributed to the application of this method. The simulated precipitation pattern in the East Asian monsoon region remains unaffected by this method. Over the oceans, prescribing 0k SSTs induces strong precipitation biases. Annual mean precipitation at the western Indian Ocean is reduced by ca. 1500-2000mm/year in the simulations with 0k SSTs. The poleward shift of the ITCZ exhibited in T106\_AV<sub>0k</sub> can also be related to the application of this technique.

The second important factor influencing the precipitation pattern in the Asian monsoon region is the numerical resolution used in the model. The effect of different resolutions is

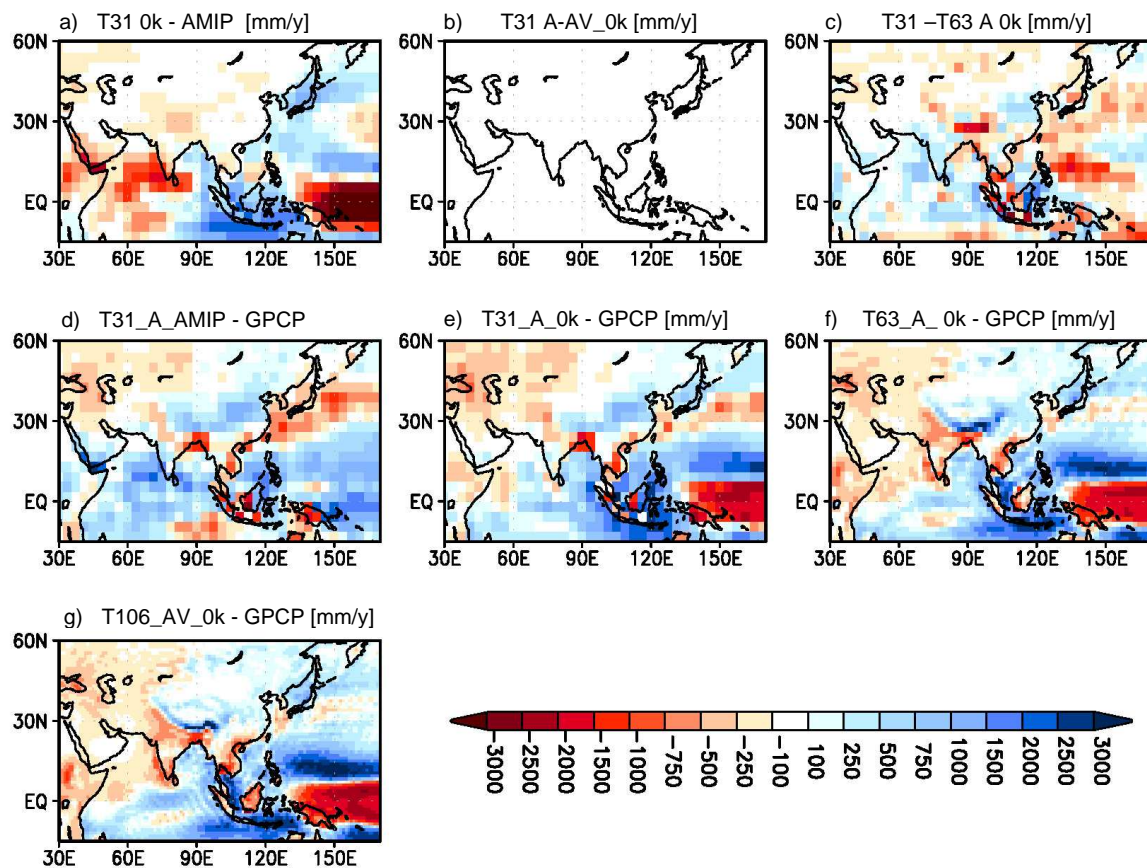


Figure 2.8: Differences in annual mean precipitation [mm/year] between the different model simulations (partly interpolated to same grid) and between the model simulations and the observational dataset GPCP (Adler et al., 2003). It shows: a) Effect of prescribing SSTs and sea-ice from a coupled simulation instead of AMIP SSTs; b) Effect of including dynamic vegetation; c) Effect of increasing numerical resolution.

investigated by comparing atmosphere-only simulations in T31L19 (T31\_A<sub>0k</sub>) and T63L31 (T63\_A<sub>0k</sub>). Increasing the numerical resolution enhances the negative precipitation bias in India by up to 700mm/year and diminishes the positive precipitation bias in East China by up to 600mm/year (Figure 2.8c). Thus, the model bias to observations is increased in India and decreased in the East Asian monsoon region when using higher resolutions. The problems of ECHAM5 to calculate too large precipitation rates at steep mountain slopes and to simulate a shifted ITCZ worsen with higher resolutions. The differences between T63\_A<sub>0k</sub> and T31\_A<sub>0k</sub> mainly result from the difference in the vertical resolution. A further increase in horizontal resolution from T63 to T106 changes the simulated precipitation distribution only slightly.

Including dynamic vegetation has a weak effect on the simulated precipitation pattern. The precipitation differences between the atmosphere-only simulation and the coupled atmosphere-vegetation simulation are less than 100mm/year. This is, of course, related to the fact that the dynamic vegetation module calculates an only slightly different land cover distribution compared to the prescribed one in the simulation with fixed vegetation.

#### **2.4.2 Near-surface air temperature**

Compared to the CRU TS 2.1 derived dry/cold season temperature, the model with prescribed AMIP SSTs calculates a too warm climate in Central Asia (up to 8K) and a too cold climate in the eastern (coastal) parts of the continent (up to 5K, Figure 2.9d). Prescribing 0k-SSTs reduces the temperature north of ca. 40°N and in East China by up to 3K. Thus, using this method leads to a reduction of the temperature bias in the former region and an enhancement of the temperature bias in the latter region, respectively (Figure 2.9a). The Tibetan Plateau, South India and Indochina experience a warmer dry season climate in T31\_A<sub>0k</sub>. Above the ocean, prescribing SSTs leads to warmer near-surface air temperatures in large parts of the Indian Ocean and in the North Pacific (east of Japan, up to 6K).

Increasing the resolution results in a cooler climate on the continent by up to 8K (Figure 2.9c). The warm bias in the coarse resolution simulations is overcompensated in most parts of Asia. Above the ocean, temperature is nearly unaffected by the chosen resolution. The general representation of the near-surface temperature improves with higher resolution. In particular, regional details in the temperature field are better resolved. The pattern correlation coefficient increases from 0.98 in T31\_A<sub>0k</sub> to 0.99 in T106\_AV<sub>0k</sub>.

In the wet season, the temperature bias in T31\_A<sub>AMIP</sub> looks similar to the bias in the dry/cold season (Figure 2.10). Prescribing 0k-SSTs has only a weak effect on continental temperatures. It mainly leads to a warming in India due to less precipitation. Like in the dry/cold season, increasing resolution cools the climate in large parts of Asia and leads to a

better representation of the near-surface air temperature distribution. The pattern correlation increases from 0.92 in T31\_A<sub>0k</sub> to 0.97 in T106\_AV<sub>0k</sub>.

Including dynamic vegetation has no influence on the climate in both seasons (less than +/- 0.5K).

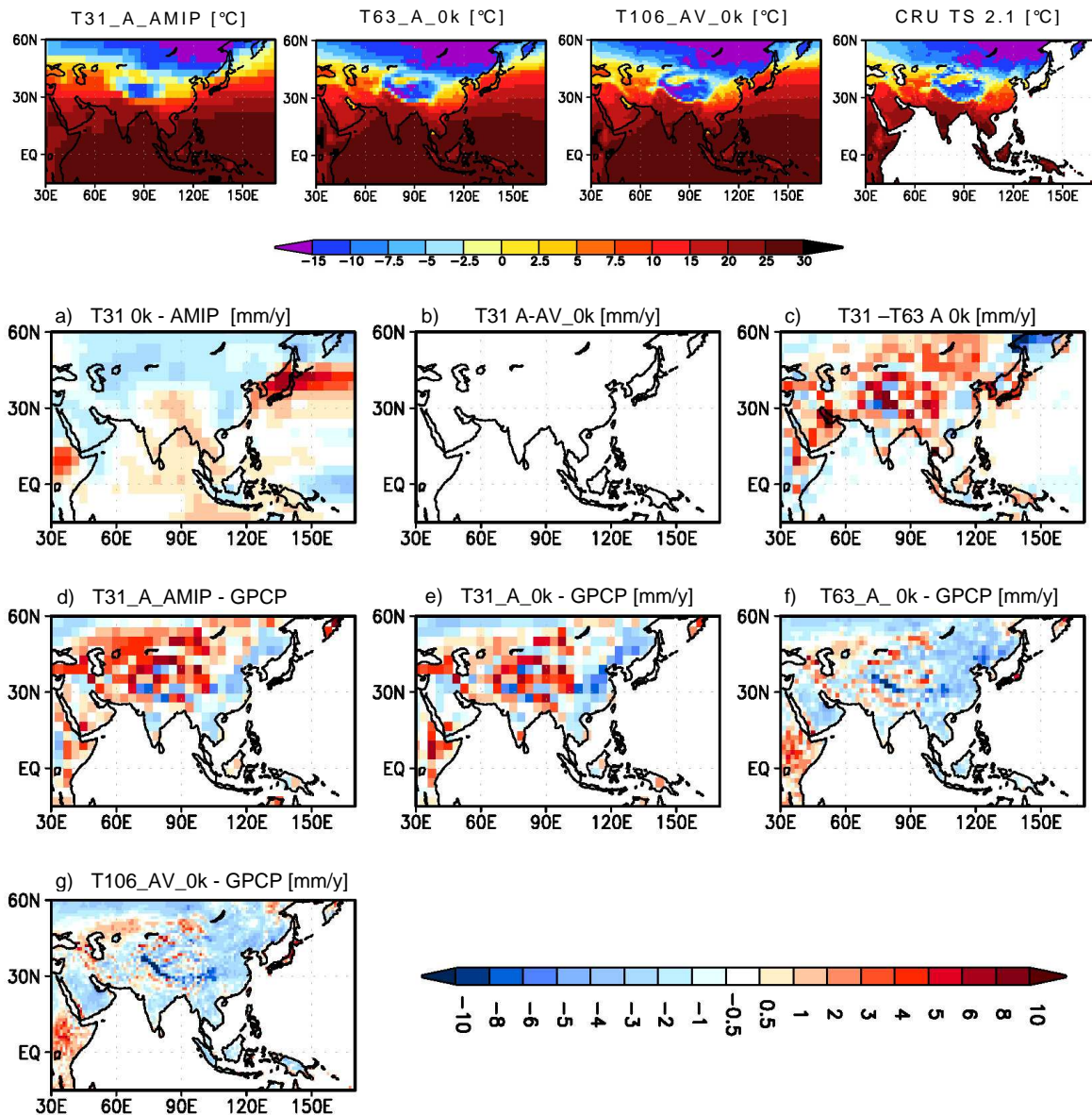


Figure 2.9: Simulated and observed dry/cold season temperatures (November-April, in °C, upper panel). Lower panels: Same as Fig. 2.8, but for dry/cold season temperature (partly interpolated to same grid) compared to CRU TS 2.1 observation (Mitchell and Jones, 2005).

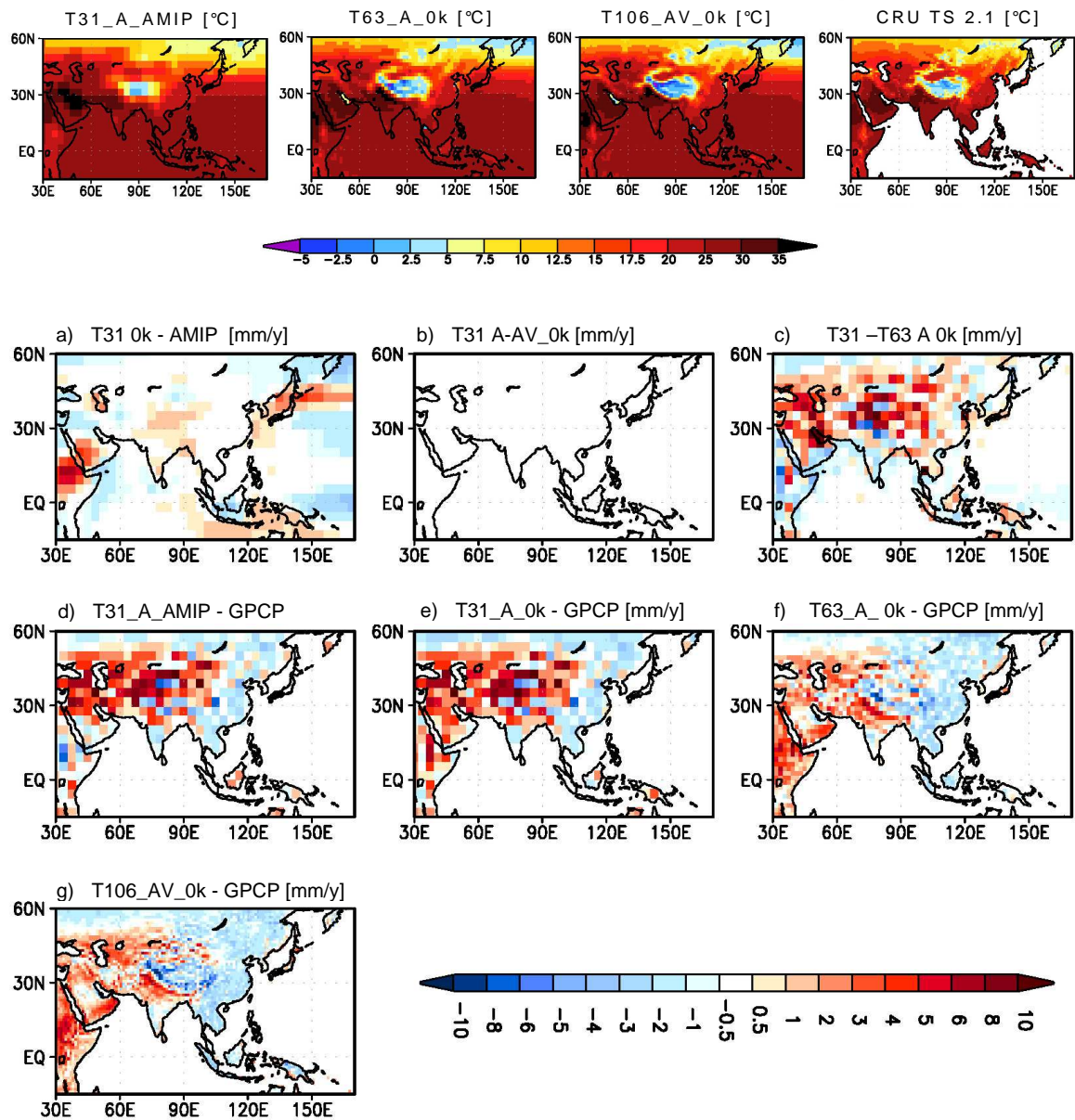


Figure 2.10: Same as Fig. 2.9, but for the wet season (May-October).

## 2.5 Summary and discussion of Chapter 2

This study provides an overview of the performance of the general circulation model ECHAM5/JSBACH with respect to the simulation of the Asian monsoon climate. Precipitation, near-surface air temperatures and the low level atmospheric dynamics have been compared to observations and reanalysis data using a high-resolution simulation with prescribed simulated SSTs and sea-ice. In a second step, the sensitivity to changes in the model setup (e.g. resolution) has been investigated.

The performance of the model regarding the precipitation in the continental and entire Asian domain (here: 30-170°E, -10-60°N), respectively, is summarised in Figure 2.11 for all considered model setups. The spatial distributions of the model results have been interpolated bilinearly to a uniform grid (equivalent to the grid of T106\_AV<sub>0k</sub>). The Taylor diagram quantifies how closely the simulated precipitation patterns match the observations (here: GPCP) by combining the pattern correlation coefficient, centred root-mean square error (RMSE) and the standard deviation of the model results and the reference data-set. The closer these statistical parameters of the individual model simulations are to the reference point (black circle on the x-axis), the larger is the similarity of the simulated model results to the observations. Overall, the plot reveals the following tendencies:

- The performance of the model is better for the continental regions than for the oceanic regions.
- The simulations in the different model setups deviate less on land than over the oceans, i.e. the precipitation distribution on land is less affected by the resolution and, in particular, by the prescribed oceanic surface boundary conditions.
- The simulations performed with a coarse numerical resolution generally match the observed pattern better than the high-resolution runs. The high-resolution simulation, however, shows the best fit with regard to the spatial and temporal variability for the continental regions.
- Including dynamic vegetation has no effect on the simulated precipitation distribution which can be explained by the only minor deviations of the simulated vegetation pattern in the coupled simulations from the prescribed vegetation distribution in the uncoupled simulations.

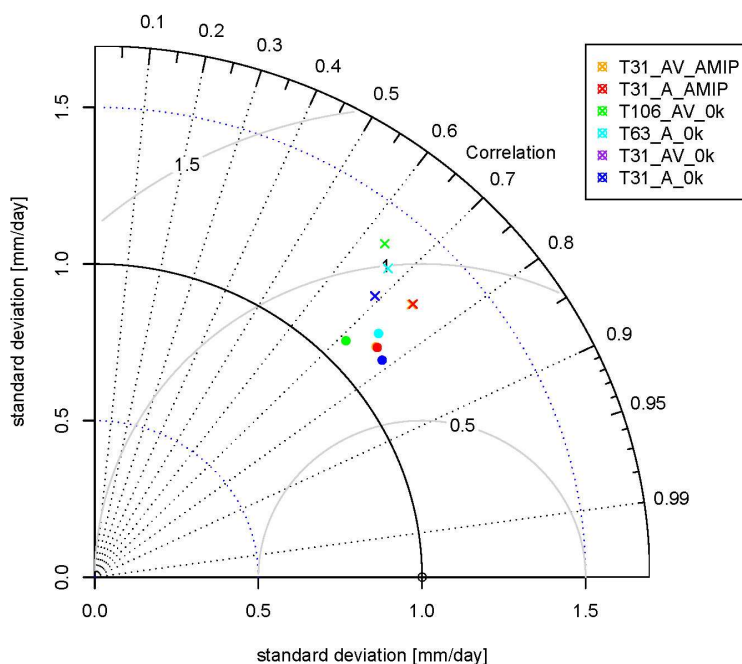


Figure 2.11: Taylor diagram showing the pattern correlation, normalised standard deviation and normalised root-mean-square error (grey circles) of the simulated precipitation in the different model setups for the entire Asian region (30-170°E, 10°S-60°N) with (crosses) and without (dots) oceans, based on monthly mean values. Reference dataset: GPCP (black dot).

- Overall, the simulation T31AV<sub>0k</sub> agrees best with the observed precipitation pattern on land. For the entire region, the AMIP experiments show the best results with regard to the correlation and RMSE, but reveal a slightly worse representation of the variability than the coarse resolution runs with prescribed simulated SSTs and sea-ice.

The model is able to capture the observed precipitation pattern well, regardless of which model setup is used. However, our analysis reveals large differences with respect to the magnitude of the precipitation. In the high-resolution simulation (T106AV<sub>0k</sub>), the model calculates slightly too much precipitation in East Asia. In large parts of southern and western Asia, in contrast, total precipitation is underestimated by the model. Particularly during the monsoon season, the Indian continent receives much less precipitation than observed. This rainfall deficit can partly be related to the method of prescribing sea surface temperatures and sea-ice distributions derived from a coupled model simulation as the bias is slightly reduced in the AMIP simulations. Nevertheless, using this method only accounts for approx. 30% of the simulated bias. The rest has to be attributed to other sources. Since the rainfall deficit is also present in the North African monsoon domain, the source of error has to be related to deficiencies in the large-scale circulation or in the model physics. In this respect, one source of error could be the cloud parameterisation that might not be able to represent the complex convective cloud physics in the tropical monsoon regions. This should be tested in separate sensitivity studies.

Like in previous studies regarding the performance of ECHAM5 in different numerical resolutions, our results reveal more Asian monsoon precipitation in the coarse resolution simulations than with higher resolutions (Roeckner et al., 2006). This is at least partly related to numerical diffusion in the advection scheme of water vapour in the model. In course vertical resolutions, the vertical transport of humidity may be enhanced due to a stronger artificial diffusion (Pope et al., 2001; Roeckner et al., 2006). Therefore, increasing the numerical resolution improves the magnitude of the mean precipitation rate in East China (overestimated in the coarse resolution) and worsens it in the Indian monsoon region, but for the wrong reason.

Figure 2.12 illustrates how well the near-surface air temperature is represented in the different model setups. Overall the following conclusions can be drawn:

- In all considered model setups, the simulated temperature pattern shows a very high correlation (>0.96) to the observational dataset CRU TS2.1 as well as to the reanalysis data ERA40.
- The temperature pattern is slightly better represented in the high-resolution simulations (T63 and T106) than in the coarse-resolution simulations (T31).

- Regarding the variability, the simulations with prescribed AMIP SSTs match the observed variability best, but the variability is also well represented in the other simulations.
- The model reveals higher correlation to the reanalysis data than to observations.
- Including dynamic vegetation has no effect on the representation of the 2m air temperature field.

In the simulations with higher horizontal resolution, the near-surface air temperature is represented in more detail than in the coarse resolution runs, not least because of a better representation of the complex orography in the region. This probably leads also to a better agreement between the simulated and observed sea level pressure and monsoon circulation (not shown).

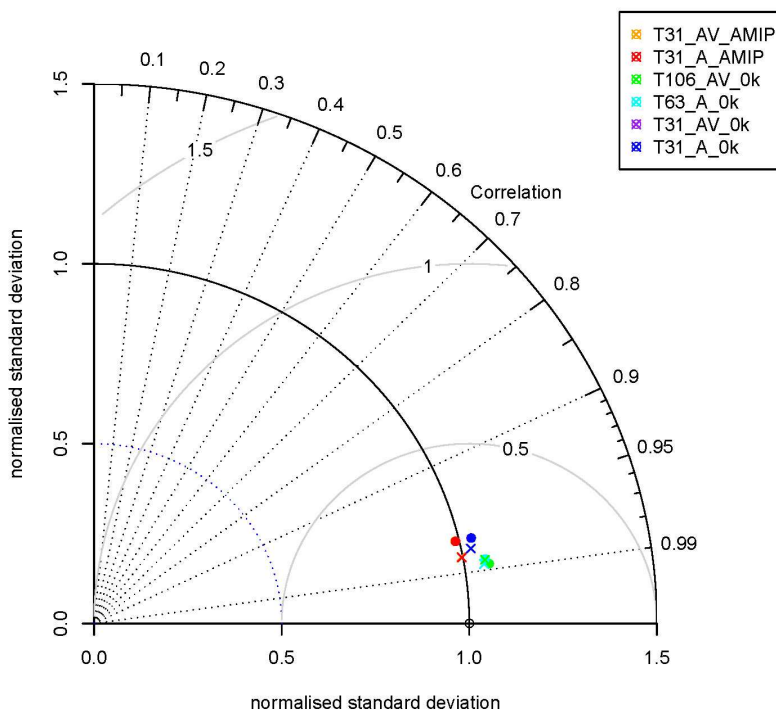


Figure 2.12: Same as Fig. 2.12, but for temperature on land., based on monthly mean values. Reference dataset: ERA40 (crosses) and CRU TS 2.1(dots).

## 2.6 Conclusion of Chapter 2

Overall, ECHAM5/JSBACH is able to reproduce the mean climate state in the Asian monsoon domain in all considered model setups. In the high resolution simulation, regional atmospheric dynamics are particularly well represented. Nevertheless, the model has a rainfall deficit in the tropical monsoon regions. Details in the seasonal cycle of precipitation can only partly be simulated by the model. The observed propagation of the monsoon systems, their onset and withdrawal, for instance, can not fully be reproduced.

## 3. Simulated mid-Holocene Asian monsoon climate

### 3.1 Introduction

The assessment of the capability of climate models to give reasonable projections of future climate change requires the validation of model simulations to past climate states that are substantially different from the present-day one (Joussaume et al., 1999). In contrast to present-day observational records, the comparison of paleoclimate modelling results with paleoclimate reconstructions provides the opportunity to test the sensitivity of the model to strong external forcings (Kohfeld and Harrison, 2000).

The mid-Holocene, 6000 years before present, is a time-slice that is often used for model comparison and validation (e.g. Paleoclimate Modelling Intercomparison Project, Braconnot et al. 2007a,b; Kohfeld and Harrison, 2000; Bush, 2004). As the surface boundary conditions such as the continental ice-sheet distribution and the sea-level were comparable to present-day and the atmospheric greenhouse gas concentration was similar to pre-industrial times, the major forcing to the climate system arose from differences in the incoming solar radiation that can be attributed to changes in the Earth's orbital configuration (Berger, 1978). Mainly due to the precession related shift of the timing of the equinoxes on the Earth's orbit and the associated shift of the Perihelion from January (present-day) to September (mid-Holocene), the insolation on the northern hemisphere was, on average, increased and decreased by 5% during summer and winter, respectively (Figure 3.1). This led to an enhancement of the seasonal cycle in the northern hemisphere.

Climate modelling studies suggest a general strengthening of the Asian summer monsoon circulation as response to this insolation forcing that can mainly be explained by an intensification of the land-sea thermal gradient (e.g. Braconnot et al, 2007a, 2008; Marzin et al., 2009a; Wang T. et al., 2010). Monsoon related precipitation is stated to be increased in most parts of the continental monsoon domain during the mid-Holocene. Internal feedbacks in the climate system such as interactions of the atmosphere and the ocean or the vegetation have been shown to modify the initial response to the insolation forcing. The strength of these interactions reveals regional dissimilarities in the Asian monsoon domain as well as contradictory contributions to the Holocene climate change in different climate models (see Dallmeyer et al. 2010 and references therein). This induces also dissimilarities in the regional precipitation signal.

For monsoonal central Asia, a large number of paleoclimate records of different nature exists that, in general, confirm the intensification of the Asian monsoon system and the enhanced precipitation in most regions of the Asian monsoon domain during early and mid-Holocene (e.g. Fleitmann et al, 2003; Wang YJ. et al., 2005; Maher, 2008). These

records often serve as proof for the simulated increase in monsoon precipitation at the mid-Holocene, but they reveal a large disparity in sample resolution and age control that can influence the interpretation and the applicability of these records (Wang YB. et al., 2010).

Recently, Wang et al. (2010) have provided a synthetic review of the spatial and temporal pattern of temperature and moisture evolution in monsoonal central Asia that is based on more than 90 synchronised proxy records. In this study, we compare results of high-resolution global climate model simulations with an extended version of these synchronised reconstructions for the mid-Holocene time-slice. Using the climate model results, we quantify changes in the summer monsoon characteristics and assess the possible atmospheric mechanisms leading to the reconstructed moisture pattern. With this study, we provide for the first time a comprehensive and consistent comparison of reconstructions and climate model results for the mid-Holocene Asian monsoon climate.

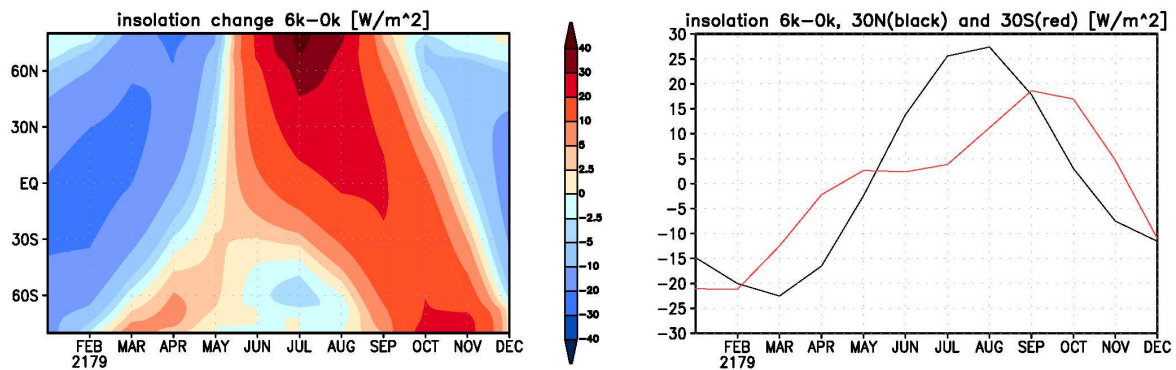


Figure 3.1: Insolation difference between mid-Holocene (6k) and present-day (0k); right panel: zonal mean change per month in the model; left panel: insolation difference in 30°N (black) and 30°S (red). Shifts in calendar are not accounted for, i.e. the model calendar is used.

### 3.2 Methods

To analyse differences in climate between the mid-Holocene and present-day, we performed time-slice experiments with the model ECHAM5/JSBACH. This model consisted of the general circulation model for the atmosphere ECHAM5 (Roeckner et al., 2003) and the land surface scheme JSBACH (Raddatz et al. 2007) that also included a dynamic vegetation module (Brovkin et al., 2009). The models ran with the spectral resolution T106L31. This corresponds to a latitudinal distance of approx.  $1.125^\circ$  and 31 levels in the vertical. We conducted two experiments, one with mid-Holocene orbital configuration (T106\_AV<sub>6k</sub>), one with present-day orbital configuration (T106\_AV<sub>0k</sub>) prescribed. In T106\_AV<sub>6k</sub> and T106\_AV<sub>0k</sub>, sea surface temperature and sea-ice were prescribed according to their mid-Holocene and pre-industrial distributions, respectively.

Values were taken from a course resolution simulation performed with the comprehensive Earth System Model ECHAM5/JSBACH-MPIOM (Fischer and Jungclaus, 2011) which included the general circulation model for the ocean MPIOM (Marsland et al., 2003). During both simulations, atmospheric composition was fixed at pre-industrial values, i.e. CO<sub>2</sub>-concentration was set to 280ppm. ECHAM5/JSBACH was brought to quasi-equilibrium climate state (spin-up of approx. 200years) before it ran for additional 30 years (analysis period).

In this study, we focus on differences in precipitation and near-surface air temperature between mid-Holocene (6k) and present-day (0k) as these are the most important parameters characterising monsoonal climate.

In all other respects, we applied the same methods as in Chapter 2.

### 3.3 Results

#### 3.3.1 General precipitation pattern and monsoon season

Figure 3.2 shows the annual mean precipitation difference between the mid-Holocene (6k) and the present-day simulation (0k). Most of the continental Asian monsoon region experiences a wetter climate during mid-Holocene. Precipitation is increased by up to 250mm/year in North East China and North India, up to 350mm/year in South China and up to 1000mm/year at the Himalaya mountain range. Precipitation is decreased in southern Indochina (up to 200mm/year), on the south eastern Tibetan Plateau (up to 350mm/year) and in the Yangtze-Huanghe-plain (up to 150mm/year). As the summer monsoon is responsible for most of the annual precipitation, the Holocene precipitation change is closely related to changes in the monsoon season, but cannot be explained fully by the summer monsoon signal. Due to the reduced solar radiation on the northern hemisphere

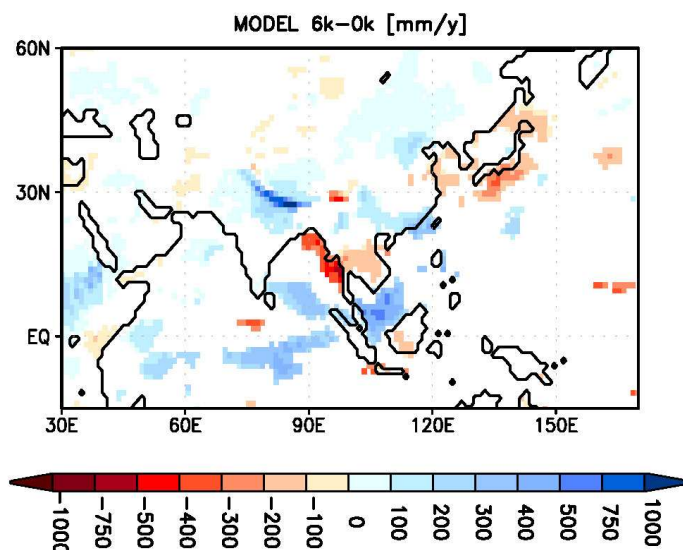


Figure 3.2: Significant (T-test, 95%) difference in annual mean precipitation [mm/year] between the mid-Holocene (6k) and present-day (0k) simulation.

during spring and the accompanied weaker temperature gradient between ocean and land in the pre-monsoon season, the summer monsoon starts approx. 2-8 pentads later at 6k than at 0k (Figure 3.3). Only at the margin area of the present-day monsoon domain and in North East China, the monsoon season begins approx. 1 month earlier in the mid-Holocene simulation. This probably indicates a faster advance of the summer monsoon onto the continent at 6k compared to 0k. The withdrawal of the summer monsoon is postponed by 0.5 pentads in South India and Indochina to 10 pentads in East China and begins earlier at the Bay of Bengal and the South China Sea (approx. 4-6 pentads). This may also indicate a faster retreat of the monsoon.

Related to the shifts in the onset and withdrawal period, the summer monsoon season length is different at 6k and at 0k (Figure 3.3). In large parts of the continent, the monsoon season is prolonged and the monsoon related precipitation is enhanced during the mid-Holocene. Exceptions are parts of Middle and North East India, Indochina and Bangladesh which experience a shorter monsoon season and less monsoonal precipitation in 6k. These are by and large also the areas showing less annual mean precipitation in the mid-Holocene simulation than in the present-day one.

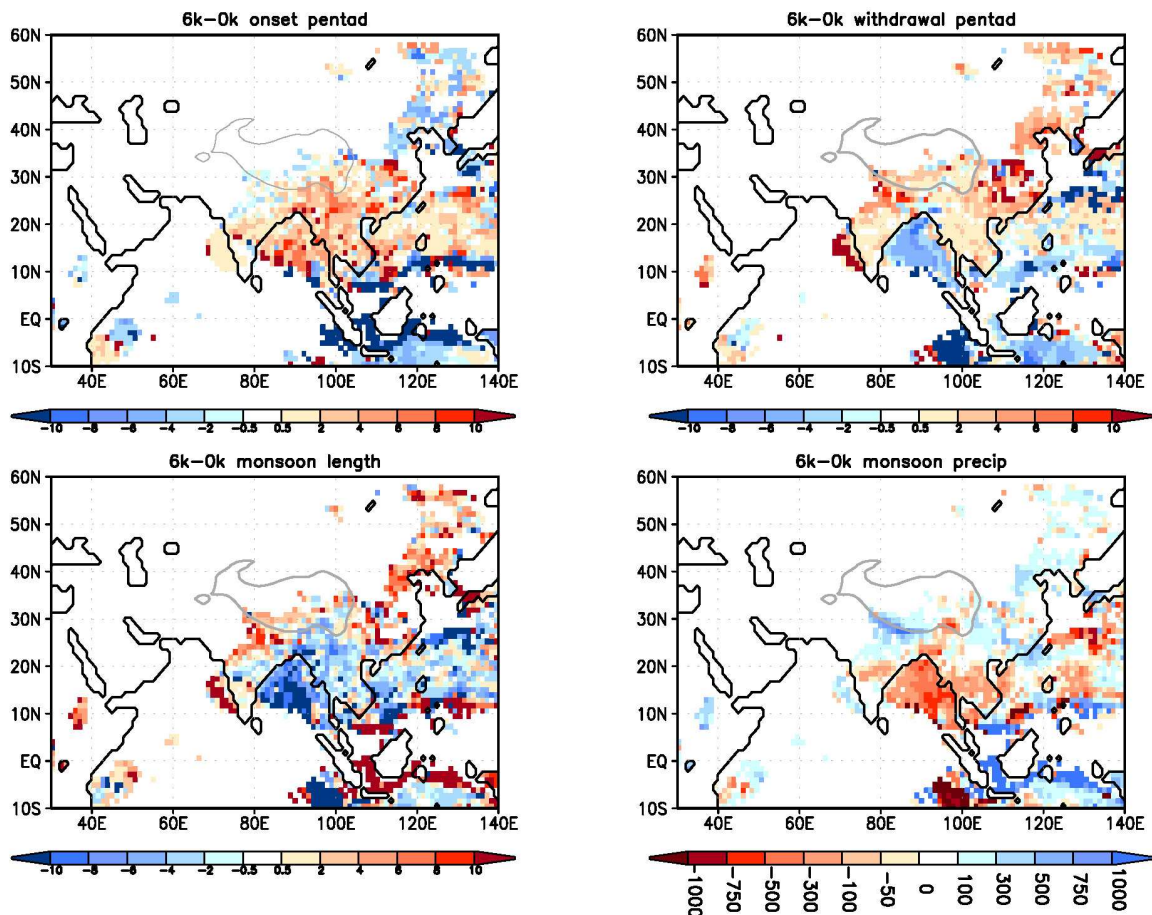


Figure 3.3: Simulated difference in onset time, withdrawal time and length of the Asian summer monsoon as well as differences in monsoon related precipitation between mid-Holocene (6k) and present-day (0k).

To further analyse the differences in the precipitation pattern between mid-Holocene and present-day, Hovmöller diagrams are provided (Figure 3.4) showing the latitudinal structure of the seasonal precipitation cycle in an East Asian (110-120°E) and Indian monsoon sector (70-80°E). These diagrams reveal a similar picture: East China receives less spring precipitation during mid-Holocene. In summer, the major East Asian summer monsoon rainband is slightly shifted northward. Therefore, precipitation is decreased in the region between 5°N and 20°N and increased north of it. During autumn, East Asian monsoon precipitation is enhanced at 6k compared to 0k. The Indian summer monsoon onset is postponed providing less precipitation in May and June. The major summer rainband is slightly shifted northward which leads to an increase of summer precipitation at ca. 30°N. In the post-monsoon season, the Indian continent experiences more precipitation during mid-Holocene.

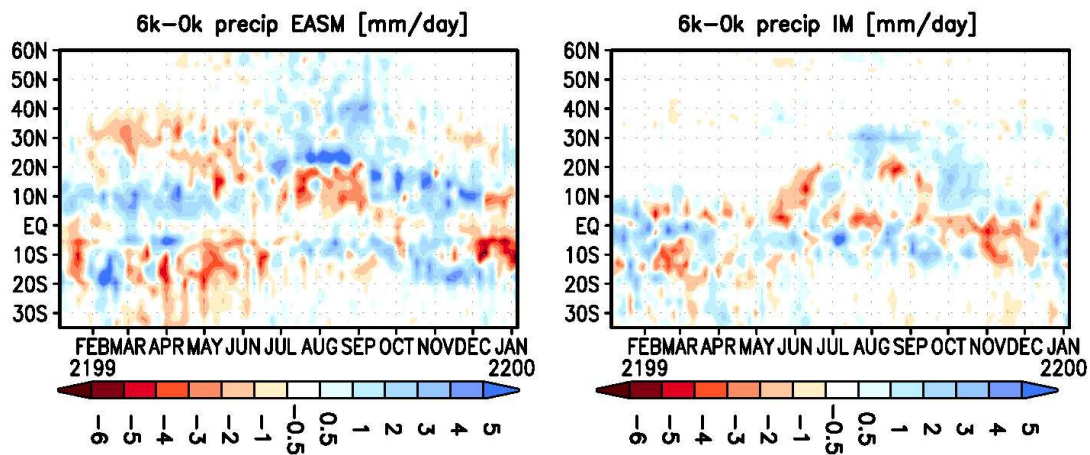


Figure 3.4: Hovmöller diagram showing the difference in the latitudinal structure of the seasonal precipitation cycle in an East Asian (110-120°E) and Indian monsoon sector (70-80°E) between mid-Holocene and present-day.

### 3.3.2 Comparison with moisture-reconstructions

The simulated precipitation difference between mid-Holocene and present-day is compared with a new version of the moisture index of Wang et al. (2010). This index is based on diverse reconstructions and describes the moisture change only qualitatively. It categorises the mid-Holocene climate as ‘wetter’, ‘similar’, or ‘drier than present-day’. Overall, the model and reconstructions show a similar pattern of moisture change with wetter conditions in North India and large parts of the Tibetan Plateau as well as in south-western China (Figure 3.5). In north-western China, the model and reconstructions suggest drier conditions during mid-Holocene. In the East Asian monsoon region, they partly disagree, particularly in Central China. The model calculates less annual mean precipitation in a broad region between ca. 25°N-35°N and 95°E-120°E at 6k. This signal is mostly not

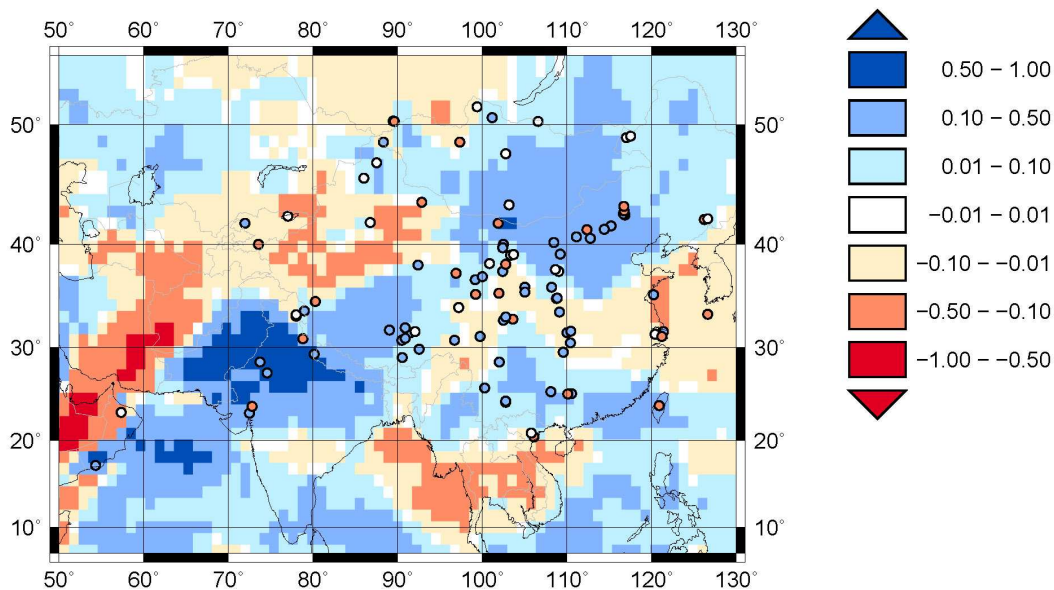


Figure 3.5: Reconstructed moisture difference (dots, Wang et al. 2010) and simulated relative annual mean precipitation difference (6k-0k/0k, shaded) between mid-Holocene and present-day (blue = wetter, red = drier conditions at mid-Holocene than at present-day, white= no change).

significant on a 95% significance level, which reveals a high interannual variability in the model. The reconstructions suggest predominantly a wetter climate in Central China during mid-Holocene, but the reconstructed pattern is very diffuse and not well-defined.

Reconstructions and the model show a more chessboard like, patchy and non-systematic moisture change in the Asian monsoon region. This patchiness underlines the complexity of the Asian monsoon system consisting of several interacting monsoon sub-systems and it exposes the complexity of the response of this system to the Holocene insolation change. The good resemblance of model results and reconstructions allows us to assess the mechanism leading to the reconstructed moisture change and can help to understand the patchy signal in the reconstructions. This aspect is discussed in section 3.4.1.

### 3.3.3 Near-surface air temperature

The difference in near-surface air temperature between mid-Holocene and present-day reflects the seasonal insolation change. During the cold/dry season (November-April) the Asian continent experiences a cooler climate (Figure 3.6). Maximal differences appear in West India (ca. 2.7K) and in Northeast China (ca. 2.1K). The temperature on the southern Himalaya is slightly increased by up to 0.5K at mid-Holocene compared to present-day. The near-surface air temperature above the adjacent oceans is not affected by the insolation forcing except in regions that are covered by sea-ice (North-Pacific). This is related to the fact that the response of the ocean lags the insolation forcing due to its large heat capacity.

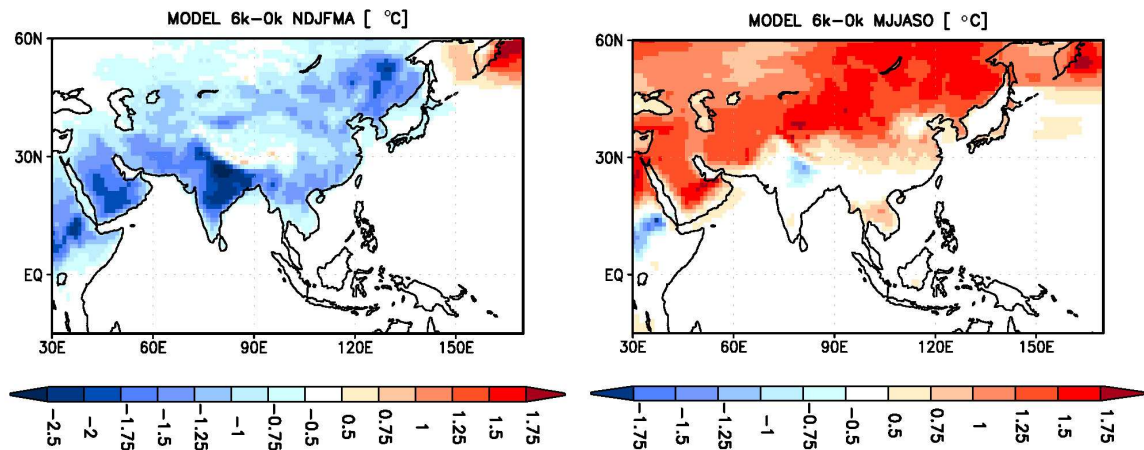


Figure 3.6: Simulated difference in dry/cold season (left) and wet season near-surface air temperature (right) between the mid-Holocene and present-day in °C.

Therefore, the surface temperature of the oceans is higher (lower) than at present-day in the first (last) months of this period with magnitudes cancelling each other out.

During the warm season, near-surface air temperatures in North and Central Asia are higher at mid-Holocene than at present-day (Figure 3.6). The magnitude of the signal roughly increases with increasing latitudes reaching values of up to 1.75K in southern Russia and North China. North India and South China experienced a cooler or similar mid-Holocene climate (up to 1.2K). This is probably related to more clouds and a higher evaporative cooling accompanying the precipitation increase in these regions that overcompensates the orbitally-induced signal.

Averaged over the year, the differences in near-surface air temperature between mid-Holocene and present-day are small. Simulated mid-Holocene temperatures are lower in East China and in the region south of 30°N at mid-Holocene compared to present-day (Figure 3.7). The region north of 30°N exhibits a warmer climate. The reconstructed warmth index by and large agrees with this signal, but reveals a warmer mid-Holocene climate also south of 30°N. This discrepancy between the model and the reconstructions could indicate a too strong evaporation in the model and therewith too strong evaporative cooling. At some sites in North China and Inner Mongolia, the reconstructions suggest a cooler mid-Holocene climate, which also deviates from the model results. Like the moisture-index, the temperature reconstructions reveal a patchy, not well-defined signal on the eastern slopes and foothills of the Tibetan Plateau. However, the reconstructed warmth-index is less reliable than the moisture index since most proxies depend on moisture and thus indicate a mixture of temperature and precipitation signals (Wang YB. et al. 2010).

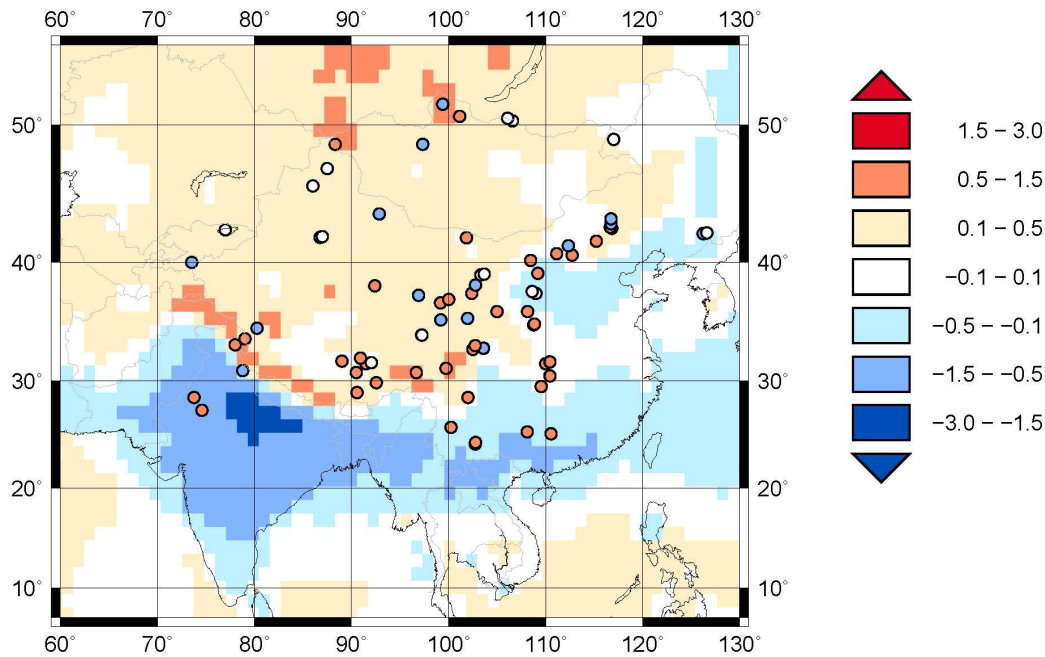


Figure 3.7: Reconstructed warmth difference (dots, Wang et al., 2010) and simulated annual mean near-surface air temperature difference (shaded) between mid-Holocene and present-day (blue = colder, red = warmer conditions at mid-Holocene than at present-day, white= no change).

### 3.4 Discussion of Chapter 3

#### 3.4.1 Possible Mechanisms causing the precipitation change

Figure 3.8 illustrates the simulated seasonal precipitation cycle in different areas of Asia representing zones with a characteristic mid- to late-Holocene annual precipitation signal. The difference in the seasonal cycle between mid-Holocene (6k) and present-day (0k) reveals only few regions where the change in annual mean precipitation is completely determined by the change in summer monsoon rainfall. Large parts of the monsoon domain also experience a precipitation change in other seasons. Four different modes of the precipitation signal can be identified compared to present-day:

- I decreased and increased mid-Holocene precipitation in spring and summer, respectively (e.g. CE China, CE China II, SE China)
- II increased mid-Holocene precipitation during summer (e.g. N India, NE China)
- III decreased mid-Holocene precipitation predominantly during spring, but with high variability also in the other seasons (C Asia)
- IV decreased mid-Holocene precipitation in spring and summer (e.g. Indochina)

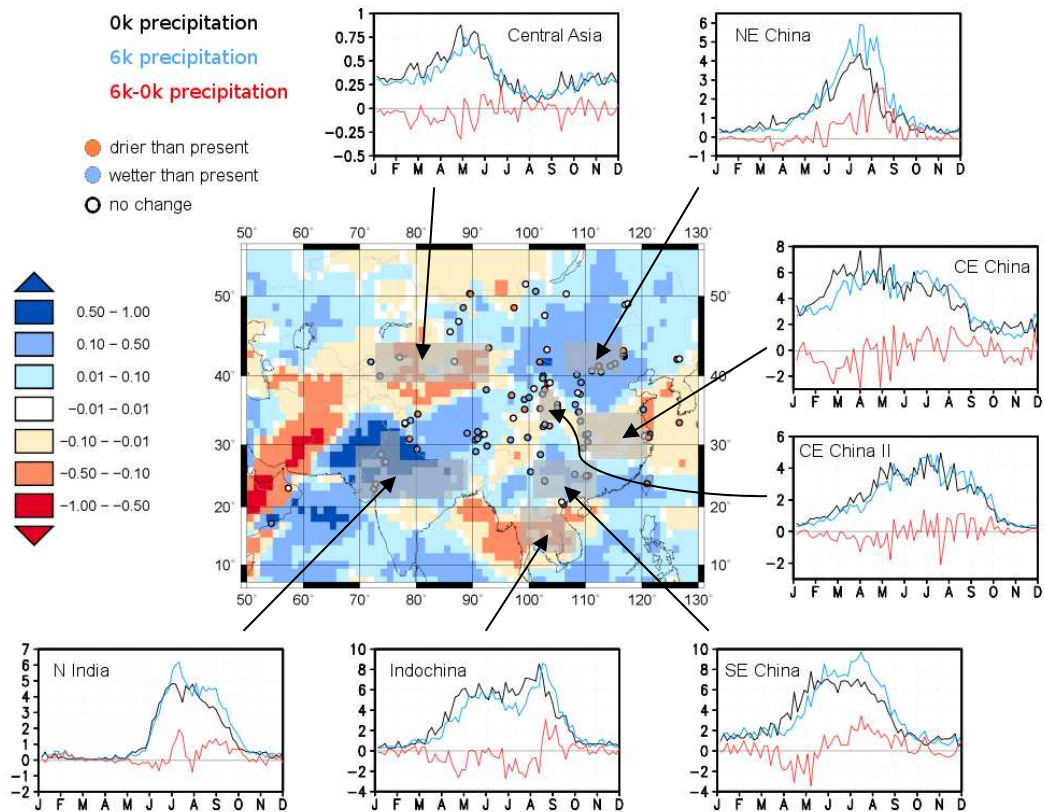


Figure 3.8: Annual cycle of precipitation change between mid-Holocene (blue curve) and present-day (black curve) for different regions in the Asian monsoon domain, in mm/day. Differences: red curve.

The annual mean precipitation change is, thus, determined by changes in spring and summer precipitation. In the following, the precipitation change in these two seasons is discussed in detail.

### 3.4.1.1 Mechanisms causing differences in spring (FMAM) precipitation

Figure 3.9 displays the spatial precipitation distribution averaged over the pre-monsoon season and the monsoon season. Compared to other parts of the continental monsoon regions, Southeast Asia (e.g. Indochina, central- and south-eastern China) receives already a large amount of precipitation during the pre-monsoon season. In central- and south-eastern China, the simulated mean precipitation rates in FMAM reach values of up to 8mm/day and even exceeds the precipitation rates in the monsoon season (only up to 6mm/day) at present-day. The amount of FMAM precipitation is strongly overestimated and the monsoon rainfall is underestimated by the model. Nevertheless, also in observations, the spring precipitation account for 32% of the annual total (Yihui and Zunya, 2008). This pre-monsoon precipitation is mainly related to the mid-latitude baroclinic zone (Boo et al., 2011). The interaction of the subtropical westerly jet and the Tibetan Plateau leads to subsidence in Northeast China and South Asia (Broccoli and Manabe, 1992; Sato, 2009) and to the suppression of convective precipitation

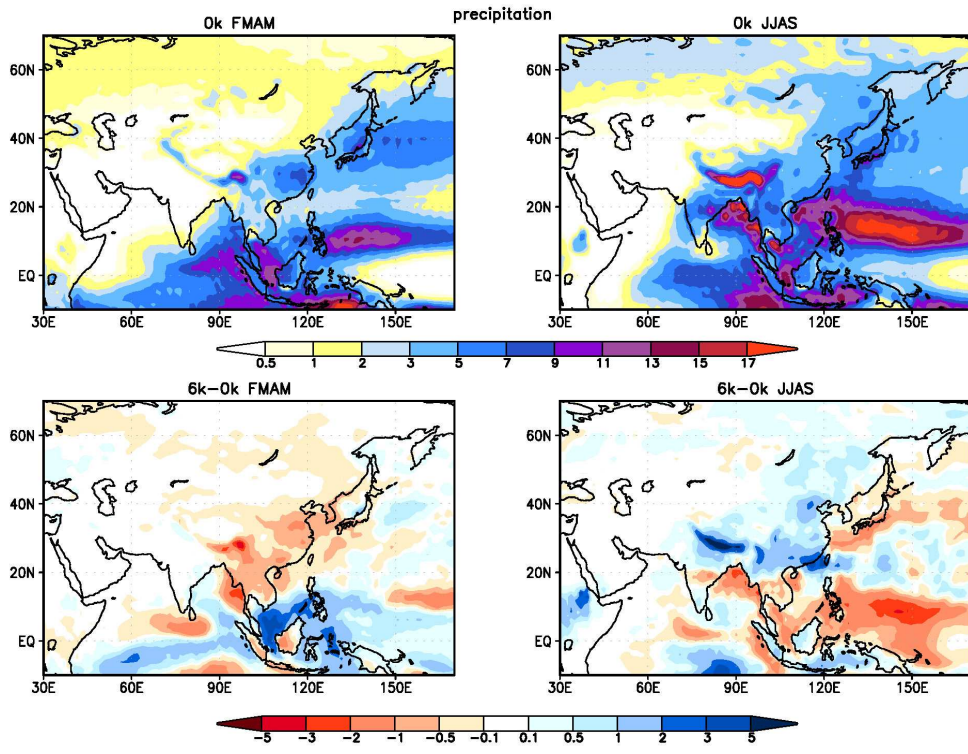


Figure 3.9: Simulated precipitation averaged over the present-day pre-monsoon season (February-May) and idealised summer monsoon season (June-September), lower panel: difference between mid-Holocene and present-day.

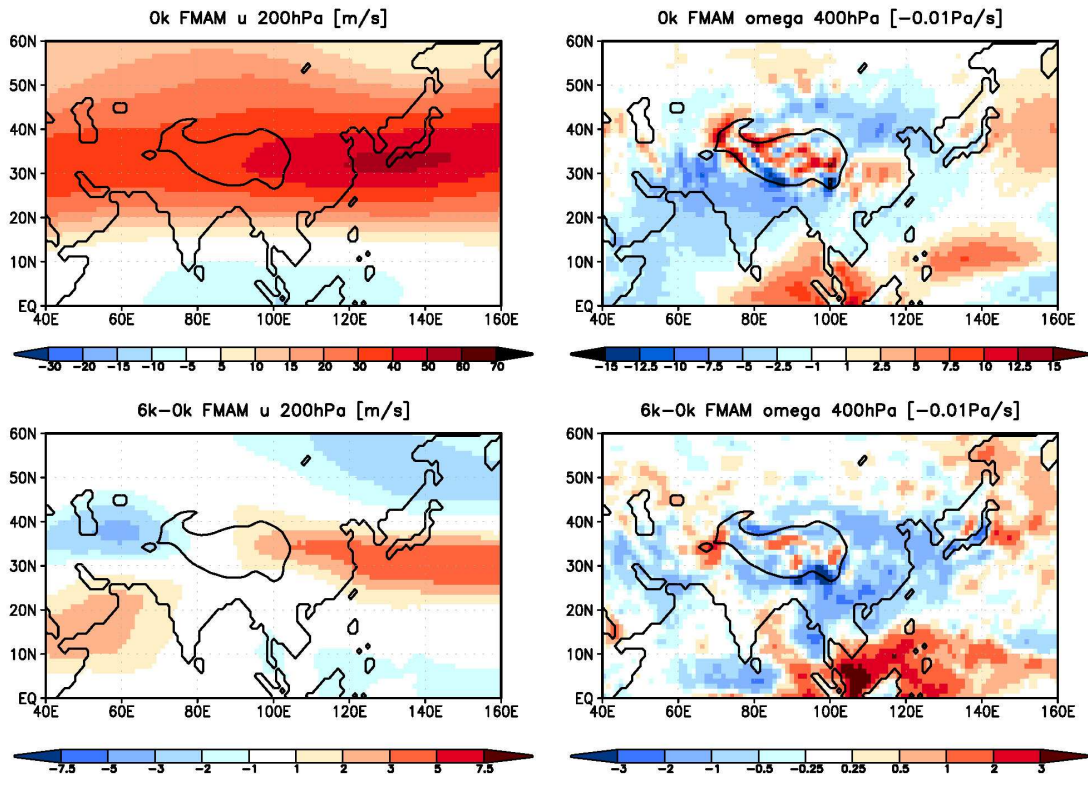


Figure 3.10: Simulated upper-tropospheric zonal wind in 200hPa (left) and vertical velocity in 400hPa (uplift: red, sinking: blue), averaged over the pre-monsoon season for 0k and 6k-0k.

in these regions during the pre-monsoon season. However, due to the upper-tropospheric wind divergence at the right entrance of the jet core, a zone of vertical ascent is established in central and south-eastern China (Figure 3.10) favouring convective precipitation. In this region, the vertically integrated moisture-flux converges (Figure 3.11). The major circulation systems transporting moisture to this area are the southern branch of the middle- and upper-tropospheric westerlies and a south-westerly circulation related to the West Pacific subtropical high. These moisture channels are confirmed by present-day observations (e.g. Yihui and Zunya, 2008). The reduced incoming solar radiation on the northern hemisphere during mid-Holocene winter and early spring leads to a cooler climate and a higher mean sea level pressure over the continental Asian monsoon region compared to present-day. Above the adjacent ocean (particularly the Pacific), the temperature decrease in the lower atmosphere is less pronounced due to the larger heat capacity of the ocean compared to the land. The mean sea level pressure is lower at mid-Holocene than at present-day. This leads to a north-easterly-wind anomaly in the lower troposphere in central- and south-eastern China. In the upper troposphere, an anticyclonic circulation is established with a core at approx. 20°N, 100°E that leads to north-easterly winds south of 20°N. Both anomalies contribute to the decreased transport of moisture to Southeast Asia and the reduced moisture convergence in this area during mid-Holocene (Figure 3.11).

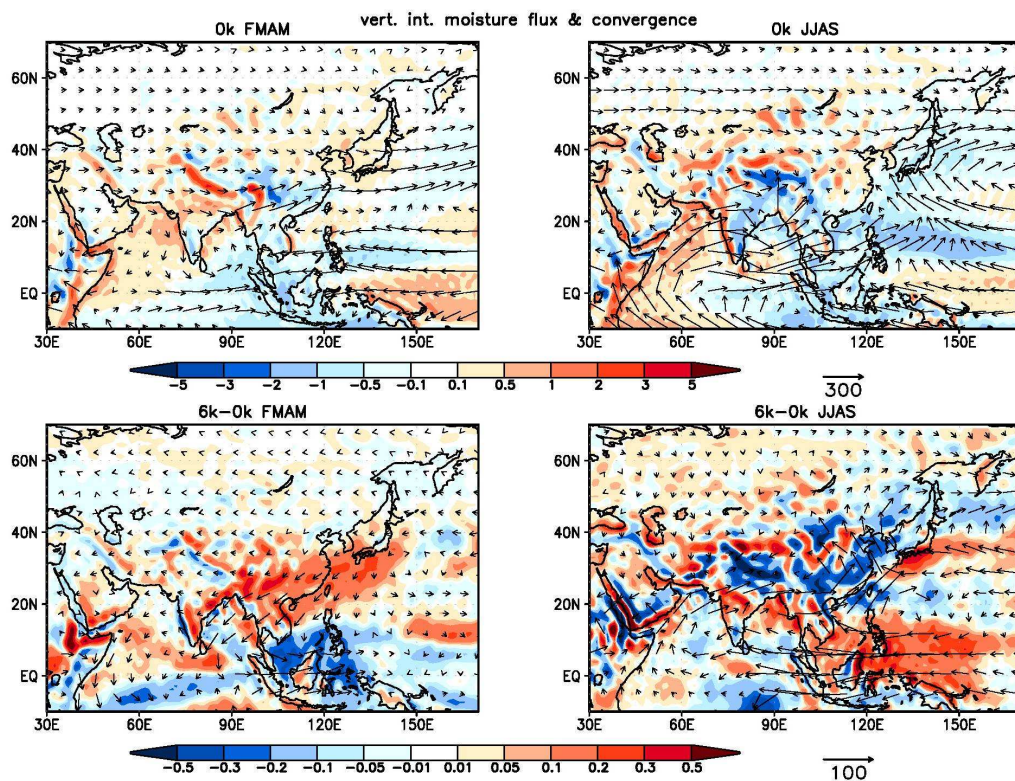


Figure 3.11: Simulated vertical integrated moisture flux and its convergence (convergence (blue) = moisture sink), divergence (red) = moisture source) averaged over the pre-monsoon season (left) and idealised summer monsoon season (right), for 0k and 6k-0k.

Furthermore, the cooler lower and middle troposphere at mid-Holocene compared to present-day induces subsidence in Southeast Asia. Therefore, the pre-monsoonal precipitation is reduced by up to 3.5mm/day on the south-eastern Tibetan Plateau and 1mm/day in Indochina and central and south-eastern China at mid-Holocene (Figure 3.9).

The decreased spring precipitation in Central Asia during the mid-Holocene can probably be attributed to changes in the Westerly wind circulation and could result from changes in storm-tracks and/or the strength and frequency of disturbances. As this area is located outside the Asian monsoon region, mode III will not be discussed further in this study.

### 3.4.1.2 Mechanisms causing differences in summer (JJAS) precipitation

The summer (JJAS) precipitation in South and East Asia is related to the Asian summer monsoon transporting moisture from the adjacent ocean to the continents (Figure 3.11). As a consequence of the increased solar insolation to the northern hemisphere during mid-Holocene and the different heat capacity of land and water, the Asian continent warms up more strongly than the oceans and the temperature and pressure gradients between the continent and adjacent ocean are enhanced. This leads to an intensification of the Asian monsoon circulation and a strengthening of the moisture flux onto the continent (Figure 3.11). The divergence of the vertically integrated moisture flux shows a negative anomaly (more convergent) in North India, the southern Tibetan Plateau and South China, and a

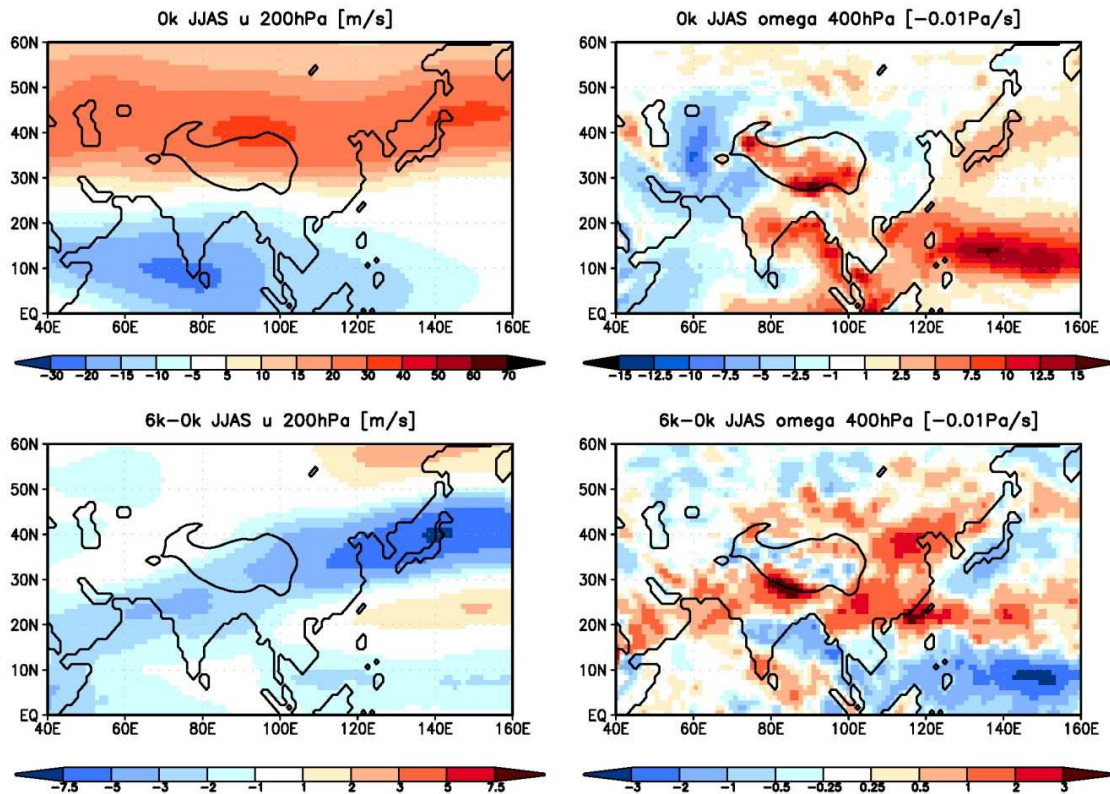


Figure 3.12: Simulated upper-tropospheric zonal wind in 200hPa (left) and vertical velocity in the middle of the troposphere (uplift: red, sinking: blue), averaged over the summer monsoon season for 0k and 6k-0k.

positive anomaly (more divergent) in Indochina and Central India between 6k and 0k. In large parts of the continental Asian monsoon domain, the vertical ascent in the mid-troposphere is enhanced at mid-Holocene (Figure 3.12). This is probably related to shifts in the upper-tropospheric wind circulation above the Asian continent being more divergent during mid-Holocene compared to present-day. The general heating of the lower and middle troposphere above the continent may also contribute to the enhanced uplift. The reduced mid-tropospheric vertical motion at Central India, Indochina and the western Pacific in the same latitude probably indicates a northward shift of the Intertropical Convergence Zone. The decreased moisture flux convergence and vertical uplift in Middle India and Indochina leads to a reduction of summertime precipitation by up to 1.2mm/day and 0.8mm/day, respectively (Fig. 3.10). In both regions, the monsoon season is shortened (cf. sec. 3.3.1). In contrast, the enhanced moisture transport and moisture flux convergence combined with the enhanced vertical uplift lead to an increased summertime precipitation in the rest of the Asian monsoon domain during mid-Holocene. Precipitation is increased by 3mm/day in South China, up to 2.5mm/day in Northeast China, up to 1.5mm/day in North India and more than 5mm/day at the Himalaya.

#### **3.4.1.3 Implications for the moisture reconstruction**

The appearance of several modes in the precipitation signal reveals that the change in moisture/precipitation can not simply be attributed to summer monsoon dynamics. Other seasons, particularly the pre-monsoon season, have also to be taken into account. The response to the Holocene insolation change is different in the individual sub-regions of the Asian monsoon domain. The cause of this different behaviour can be found in the different nature of the monsoon systems. The Indian monsoon is determined by meridional temperature and pressure gradients. Therefore the Holocene insolation change, which is zonally uniform but reveals meridional variations, has a different effect on the Indian monsoon than on the East Asian monsoon that is formed by zonal temperature and pressure gradients. Furthermore, the two monsoon systems reveal strong differences in the seasonal precipitation distribution. Figure 3.13 shows the ratio of summer to spring precipitation and point out the difference between the Indian monsoon domain and the East Asian monsoon domain. India and the southern Tibetan Plateau (mode II) are strongly characterised by summer precipitation. The strengthening of the Indian summer monsoon in the mid-Holocene simulation is, thus, responsible for the annual total precipitation change in the model. This clear signal can probably be represented easily in model and reconstructions. In contrast, the core region of the East Asian monsoon receives a large amount of precipitation outside the monsoon season. The difference in the simulated seasonal precipitation cycle between mid-Holocene and present-day is predominantly characterised by a reduction of precipitation in the months February to May (FMAM) and an increased precipitation during the months June to September (JJAS). The regions

exhibiting this precipitation signal (mode I) are the regions in which the reconstructions show the patchiest moisture change and also the major disagreement to the model results. At least in the model, the sign of the annual mean precipitation change in these regions depends on the balance of the precipitation decrease in the pre-monsoon season and the precipitation increase in the monsoon season. This ratio is probably not only determined by changes in the large- and regional-scale atmospheric dynamics between mid-Holocene and present-day, but also strongly affected by the local environment, particularly the orography. The region with the strongest disagreement between the model and the reconstructions (100-110°E, 30-40°N) is located at the eastern slopes and foothills of the Tibetan Plateau and the adjacent regions where altitudes vary strongly. Thus, the patchiness of the moisture reconstruction may simply be an imprint of the local topography.

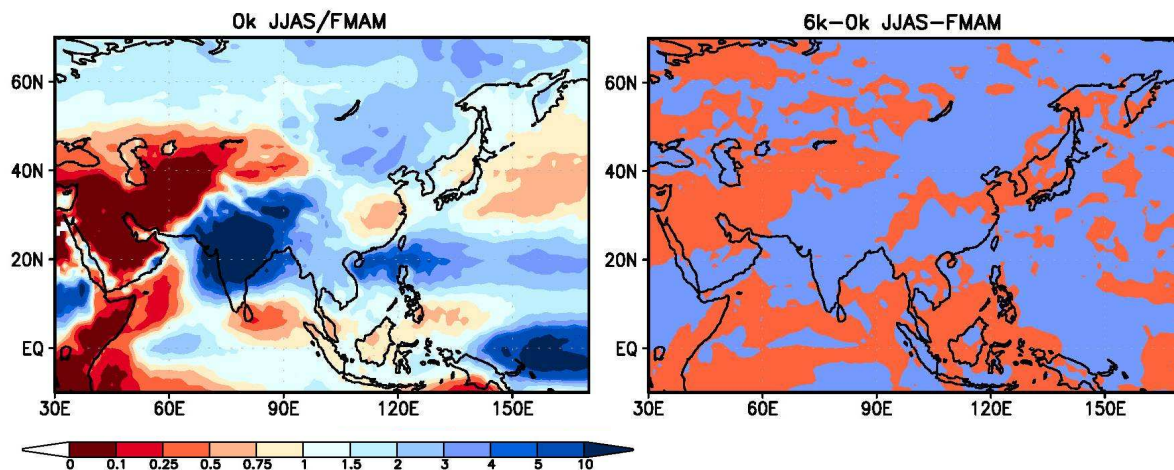


Figure 3.13: Ratio of summer to spring precipitation according to the present-day simulation (left) and change in the difference of summer and spring precipitation between mid-Holocene and present-day, red: negative (i.e. decrease in FMAS > increase in JJAS); blue: positive.

### 3.4.2 Comparison with other modelling studies

The model used in this study does not include a dynamically coupled ocean model. Therefore, important feedback mechanisms between ocean and atmosphere (e.g. sea-ice albedo feedback, or feedbacks within the water cycle) are neglected that may have an influence on the simulated climate change. The advantage of this model setup, however, is the possibility to conduct simulations in a high numerical resolution (T106L31) without spending excessive computational power and time. Albeit the only slight improvements of the simulated present-day climate that are mainly confined to the monsoon dynamics and do not include the precipitation distribution (see Chap. 2), we expect the simulated climate response to be more manifold in high resolution simulations. To assess the robustness of

our results, we compare the reconstructed moisture and warmth index with results from coupled atmosphere-ocean-vegetation-model simulations performed within the Paleoclimate Modelling Intercomparison Project Phase II (PMIP2, Braconnot et al., 2007a) and coarse-resolution simulations (referred to as T31\_AOV) conducted with the comprehensive Earth system model ECHAM5/JSBACH-MPIOM (Figure 3.14, Figure 3.16). The individual simulations are listed in Table 3.1. They have all been undertaken using similar boundary conditions and the same orbital forcing as in T106\_AV<sub>6k</sub> and T106\_AV<sub>0k</sub>.

Model	resolution
MRI CGCM2.3.4nfa	T42L30
MRI CGCM2.3.4fa	T42L30
ECBILT CLIO VECODE	T21L3
FOAM-LPJ	R15L18
UBRIS HADCM3	2.5°x3.75°, L19

Table 3.1: Overview on the PMIP2 simulations including an atmosphere, ocean and dynamic vegetation model. For further information see: <http://pmip2.lsce.ipsl.fr/>

Compared to the high resolution simulation, T31\_AOV show a much clearer annual precipitation change in the Asian monsoon domain with drier mid-Holocene conditions in central- and south-eastern China and a wetter climate elsewhere. This uniform precipitation signal cannot represented the complex signal seen in reconstructions and points out the added value of the high resolution in T106\_AV. In the course resolution, the model is probably able to capture the large-scale response of the climate to the insolation forcing, but can not represent the regional dynamics.

The individual model simulations of PMIP2 reveal large discrepancy regarding the sign, magnitude and pattern of the mid- to late- Holocene annual total precipitation change. Relatively robust signals are:

- the wetter mid-Holocene climate in Northern India (3 of 5 models). The other two models (FOAM-LPJ and ECBILT-CLIO-VECODE) also show regions with drier climate in mid-Holocene compared to present-day.
- the increased precipitation on the central southern Tibetan Plateau (around 90°E, 30°N), this is shown by all 5 models.
- the existence of regions in eastern China receiving less precipitation during mid-Holocene; only UBRIS-HADCM3M2 suggests increased precipitation in the entire eastern China.
- the wetter climate in Northeast China (ca. 110-120°E, 38-42°N).

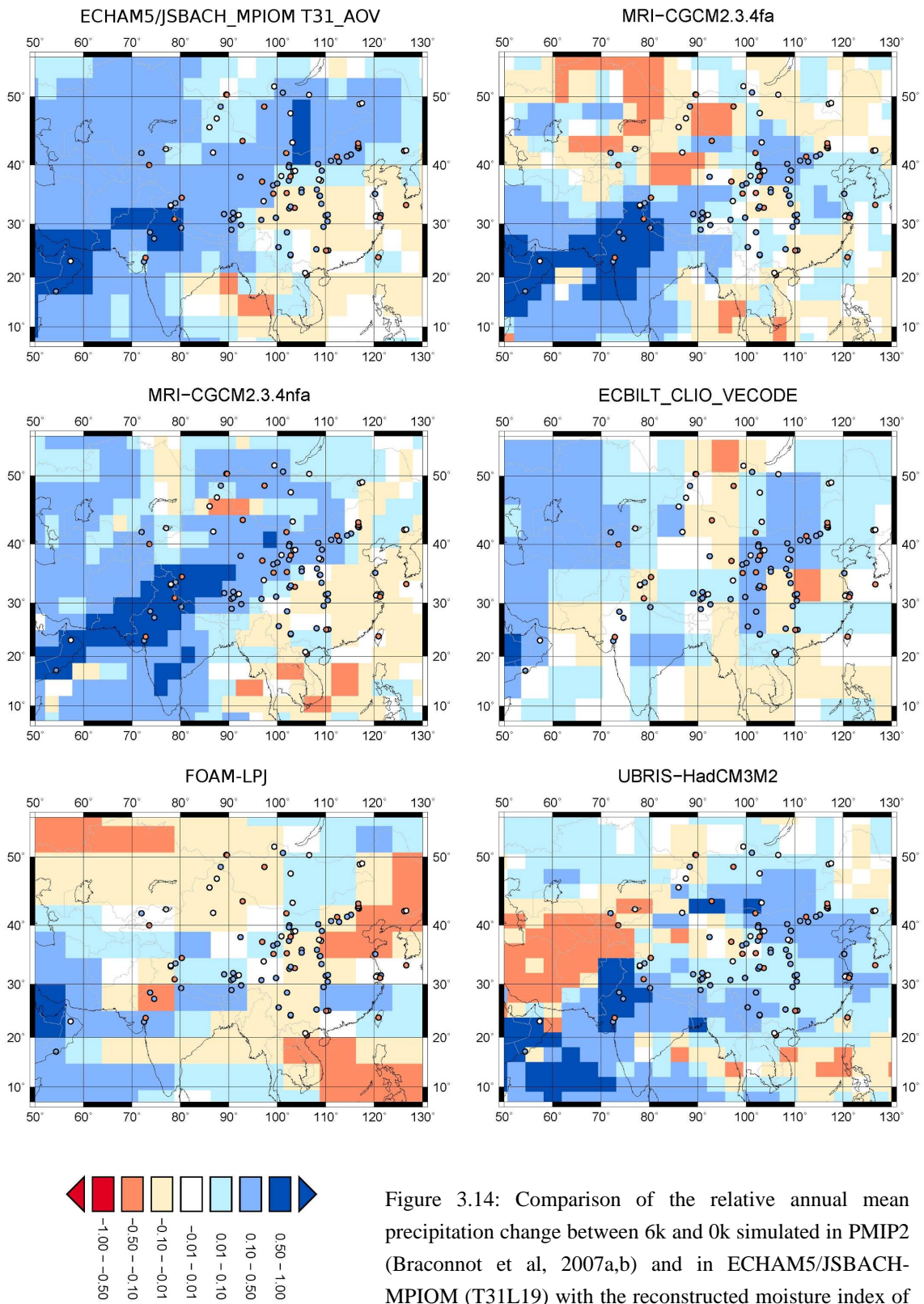


Figure 3.14: Comparison of the relative annual mean precipitation change between 6k and 0k simulated in PMIP2 (Braconnot et al, 2007a,b) and in ECHAM5/JSBACH-MPIOM (T31L19) with the reconstructed moisture index of Wang et al. (2010).

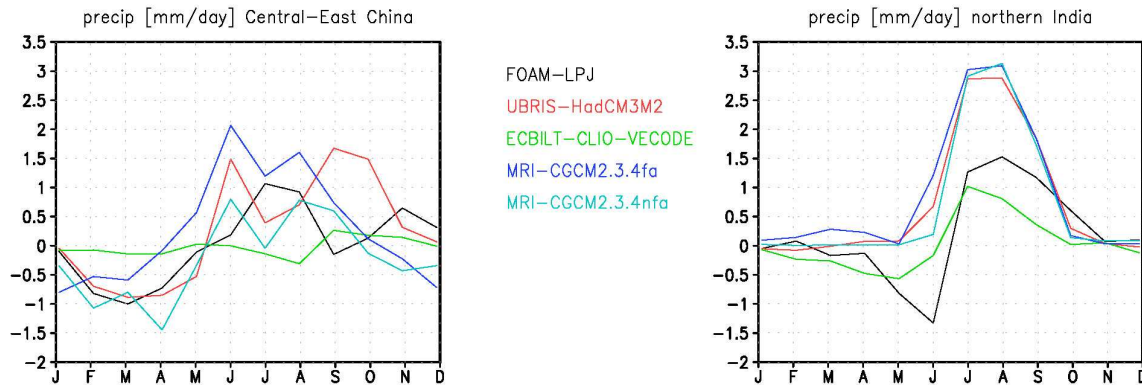


Figure 3.15: Differences in the seasonal precipitation cycle between the mid-Holocene and present-day for the regions Central-East Asia and northern India as simulated within PMIP2.

Figure 3.15 shows the difference in the seasonal precipitation cycle between mid-Holocene and present-day climate as simulated within PMIP2 for an area in central-eastern China (110-120°E,30-35°N) and northern India (70-80°E, 25-30°N). These simulations confirm the different character of the East Asian and the Indian monsoon region and the different response of the monsoon systems to the insolation forcing. In most models, the seasonal signal referred to as mode I in our study, i.e. decreased precipitation in mid-Holocene spring and increased precipitation in mid-Holocene summer, can be found in central eastern China. In this region, UBRIS-HADCM3M2 and MRI-CGCM2.3.4fa show wetter conditions during mid-Holocene that can be related to a stronger increase of precipitation in summer overcompensating the decrease of precipitation in spring. The drier mid-Holocene climate simulated by MRI-CGCM2.3.4nfa and FOAM-LPJ is associated with strongly decreased precipitation during mid-Holocene spring that overcompensates the increased precipitation during summer. In northern India, three out of five models simulate the seasonal signal referred to as mode II in our study, showing a strong increased precipitation during mid-Holocene summer and no response in the other seasons. ECBILT-CLIO-VECODE and FOAM-LPJ simulated decreased spring precipitation also for northern India during the mid-Holocene compared to present-day.

Figure 3.16 shows the annual mean near-surface air temperature difference between the mid-Holocene and the present-day simulations conducted within PMIP2 and in T31\_AOV. Regarding temperature, T106\_AV and T31\_AOV show a similar signal, however, the region revealing a warmer mid-Holocene climate extends further southward in T106\_AV which is in better agreement with the reconstructions. The PMIP2 simulations reveal large discrepancies with respect to the temperature response to the insolation forcing. Four out of five models suggest a mostly cooler mid-Holocene climate south of 30°N which is not in line with the reconstructions. North of 30°N three models calculate lower temperatures during mid-Holocene compared to present-day. MRI-CGCM2.3.4nfa suggests a warmer

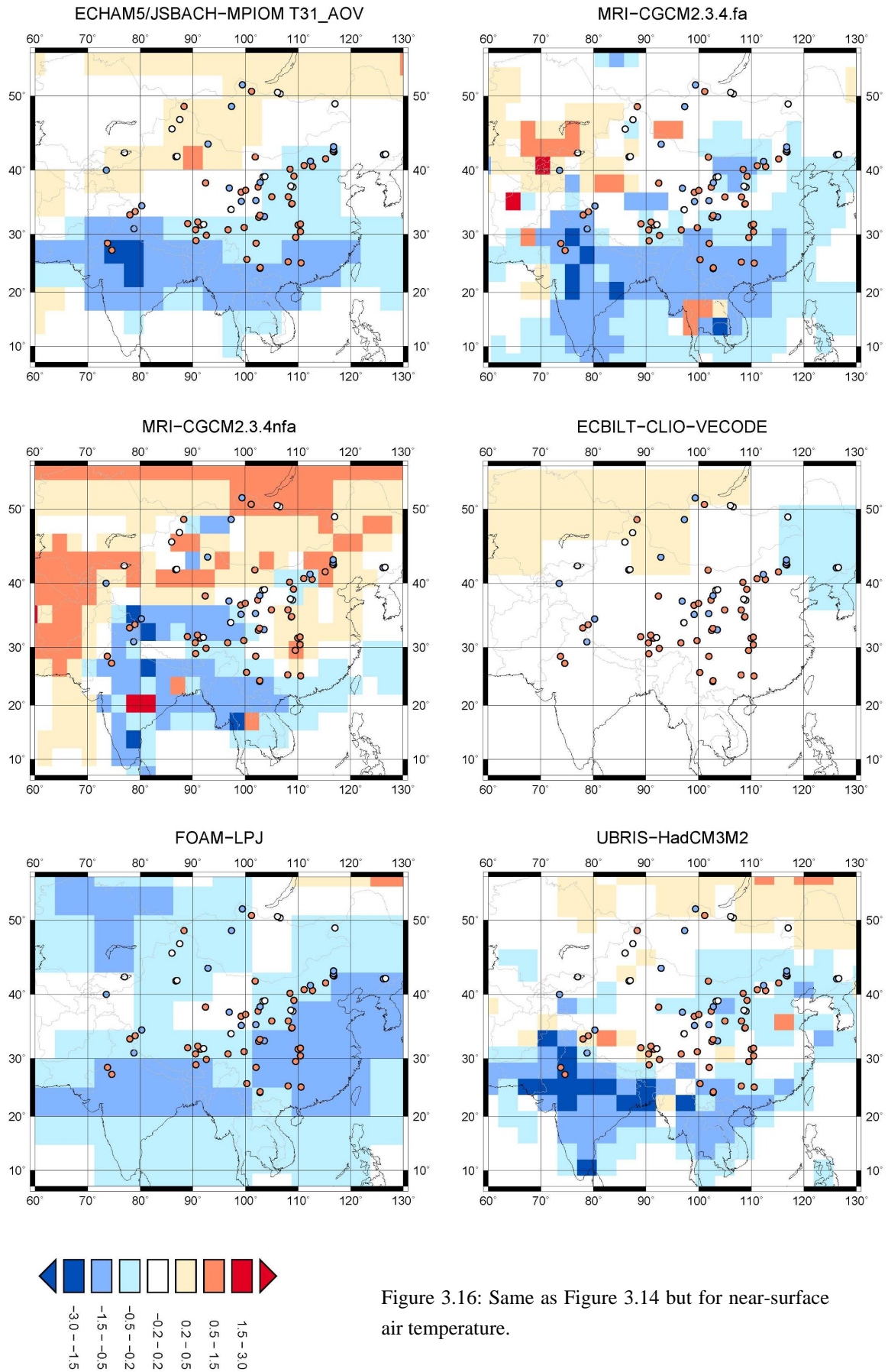


Figure 3.16: Same as Figure 3.14 but for near-surface air temperature.

mid-Holocene climate north of 40°N. ECBILT-CLIO-VECODE shows only slight differences in annual mean temperatures between the mid- and late-Holocene.

Overall, the high resolution simulation T106\_AV<sub>6k</sub> matches the reconstructions best despite of the missing ocean-atmosphere interactions. The effect of ocean-atmosphere interaction on Holocene climate change is discussed in the next Chapter.

### **3.5 Summary and conclusion of Chapter 3**

A high resolution numerical experiment conducted with the general circulation model ECHAM5/JSBACH by applying mid-Holocene insolation forcing has been compared to synchronised climate reconstructions for the Asian monsoon region. Overall the model results and the reconstructions are in good agreement. They both show wetter conditions in large parts of the Indian monsoon region and a partly drier and partly wetter climate in East Asia. Especially in central-eastern China, reconstructions suggest a very inhomogeneous mid- to late-Holocene annual total precipitation signal which indicates the complexity of the Asian monsoon dynamics. The model is able to capture this patchy signal and attributes the inhomogeneity to the different responses of the East Asian and Indian monsoon system to the insolation forcing. In large parts of Eastern China, present-day precipitation is not confined to the summer monsoon season as it is the case in India, but also falls during spring. Therefore, the Holocene moisture change also depends on the response of the spring precipitation to the seasonal insolation forcing. The sign of the annual total precipitation difference between mid-Holocene and present-day is determined by the balance of decreasing spring and increasing summer precipitation as response to the mid-Holocene insolation forcing. This may also explain the inhomogeneity in the reconstructions, since the ratio of spring to summer precipitation change could be less affected by the regional circulation but rather be sensitive to the local environment such as the orography that is very complex in the Asian monsoon region. The coupled atmosphere-ocean-vegetation model simulations performed within the Paleoclimate Modelling Intercomparison Project Phase II (PMIP2) show large discrepancies among each other and all agree less with the reconstructions than the high resolution simulation considered here. They cannot represent the inhomogeneity of the signal which might be a problem of the numerical resolution used in the PMIP2 simulations. However, the PMIP2 simulations confirm the conclusion that the sign of the annual total precipitation change depends on the balance of the spring and summer signals.

Regarding the temperature, the reconstructions suggest a mostly warmer climate in Asia during the mid-Holocene. North of 30°N, this signal is confirmed by the results of the high resolution model simulation. South of 30°N neither the high resolution simulation nor any of the presented simulations performed within PMIP2 agree with the reconstructed signal

as they show a cooler climate in this area. Among the different model simulations large discrepancies can be found. However, the temperature reconstructions are less reliable than the moisture reconstructions. The high resolution simulation matches the reconstructions best.

The simulated differences in precipitation and temperature between mid-Holocene and present-day are smaller than the differences between the simulated present-day climate and the observations (cf. Chap.2). Since the systematic model biases are probably similar in the mid-Holocene and present-day simulations, this fact does not affect the general credibility of the inferred results as long as only differences between the two time-slices are analysed.

## **4. Contribution of the atmosphere-ocean and atmosphere-vegetation interaction to the Holocene climate change**

### **4.1 Introduction**

The Asian monsoon is the most complex and strongest monsoon system of the world, affecting human life since the first settlement in that region (Clift and Plumb, 2008). It consists of two nearly independent but also interacting monsoon systems, namely the East Asian and the Indian monsoon, and includes processes in the tropics as well as in the mid-latitudes (Lau et al., 2000). Monsoon systems are primarily driven by the seasonal differential heating between continents and oceans and the related land-sea temperature and pressure gradients. Their strength and the location of major monsoon precipitation, however, are also largely influenced by moist processes (Webster et al., 1998). Thus, each modification that has an impact on the hydrological cycle, energy storage or exchange between land, ocean and atmosphere affects the monsoon circulation, its onset and duration (Yasunari et al., 2006). This includes external forcings, such as changes in insolation, as well as interactions between the different components of the climate system, which might also have a strong influence on the regional climate and impose a large intraseasonal to multi-centennial variability on the system.

Paleoreconstructions reveal significant changes of the monsoon intensity during the Holocene. Around 6000 years before present (6k) the African as well as the Asian monsoon likely penetrated further inland, implying a wetter climate (e.g. Winkler and Wang, 1993; Kohfeld and Harrison, 2000; Ge et al. 2007; Maher, 2008) and a change in the vegetation distribution (e.g. Jolly et al., 1998; Yu et al., 2000). Early modelling studies related this enhancement of the monsoons to the impact of changing insolation on climate (e.g. Kutzbach and Otto-Bliesner, 1982; Harrison et al., 1998). Due to the variations in the Earth's orbit (mainly the precessional cycle), perihelion was reached in September (6k) instead of January at present time, yielding an increase of summer and decrease of winter insolation in the Northern Hemisphere relative to today (Berger, 1978). The seasonal cycle was enhanced in the Northern and reduced in the Southern Hemisphere, affecting the cross-equatorial ocean-land temperature gradient and thereby the monsoon flows. However, modelling studies just focusing on the direct response to orbital forcing tend to underestimate the monsoon expansion and associated increase of rainfall, at least over North Africa (Joussaume et al., 1999). More recently, research studies also consider ocean and/or vegetation interactions by performing coupled model simulations. Ocean-atmosphere interaction seems to further enhance the North African monsoon (Kutzbach

and Liu, 1997; Braconnot et al., 2000; Liu et al., 2004). Regarding the Asian monsoon ambiguous results can be found. Several climate modelling studies report an increase of precipitation to be attributed to the ocean coupling (Hewitt and Mitchell, 1998; Braconnot et al. 2000, Wei and Wang, 2004). Other model results suggest an attenuation of Asian monsoon precipitation due to interactive ocean (Voss and Mikolajewicz, 2001; Liu et al., 2004 (for 11k); Ohgaito and Abe-Ouchi, 2007; Li and Harrison, 2008, Marzin and Braconnot, 2009b).

Feedback studies concerning the role of the vegetation in Holocene climate change have mostly been applied to the African monsoon region (e.g. Claussen and Gayler, 1997; Broström et al., 1998; Irizarry-Ortiz et al., 2003; Levis et al. 2004; Hales et al., 2006). Nevertheless, some studies include or even focus on the Asian monsoon (e.g. Claussen, 1997; Texier et al., 2000, Wang H.-J., 1999; Diffenbaugh and Sloan, 2002; Li and Harrison, 2009). All model results agree that vegetation and land-surface feedbacks with the atmosphere could have enhanced the orbital-induced monsoon change during the Holocene.

To determine the contribution of the land-atmosphere and ocean-atmosphere interactions as well as their synergy to the climate change between the mid-Holocene (6k) and present-day (pre-industrial climate), we analyse a set of numerical experiments, performed by Otto et al. (2009a and 2009b). They used a coupled atmosphere-ocean-vegetation model and applied a factor-separation technique (Stein and Alpert, 1993) to isolate the impact of different feedbacks on Holocene climate change in the northern latitudes. Following the methods of Otto et al. (2009a) we repeat their study for the Asian monsoon Region. Furthermore, we analyse all seasons separately.

After a short description of the model and the analysis methods in section 4.2, we discuss the simulated climate and land-cover differences between mid-Holocene and present-day (section 4.3). The contributions of land-atmosphere and ocean-atmosphere interactions as well as their synergy are further examined in section 4.4.

## **4.2 Methods**

### **4.2.1 Model & experiments**

The results of this study are based on numerical experiments, performed by Otto et al. (2009b) with the comprehensive Earth system model ECHAM5-JSBACH/MPIOM, developed at the Max-Planck-Institute for Meteorology. In this model, the atmosphere is represented by ECHAM5 (Roeckner et al., 2003), extended with the land-surface scheme JSBACH (Raddatz et al., 2007). The model was run with the spectral resolution T31 (approx.  $3.75^\circ$ ) and 19 vertical levels, following a hybrid sigma-pressure system. JSBACH

includes the dynamic vegetation module of Brovkin et al. (2009). For the ocean, MPIOM (JungCLAUS et al., 2006) is used at a horizontal resolution of approximately 3° and 40 vertical levels.

The models have been tested against observation and reanalysis data (cf. Chap.2). They capture the major structure of global and regional climate. A detailed comparison of ECHAM5 model output (resolution T63L31) and observations for the Central and East Asian region is also presented by Cui et al. (2006). The simulated climate in our coupled control run does not substantially differ.

The experimental set-up was designed to separate the contribution of the ocean-atmosphere interaction, the vegetation-atmosphere interaction and their synergy from the total climate change between mid-Holocene (6k) and present-day (0k) by applying the factor-separation technique (Stein and Alpert, 1993). Altogether, eight experiments were undertaken: four with present-day orbital configuration (set 0k), four with mid-Holocene orbit (set 6k). Each set contains a fully-coupled run, performed with the atmosphere-ocean-vegetation model (AOV), two simulations with the atmosphere either coupled to the vegetation or the ocean (AV and AO, respectively) and an atmosphere-only run (A). In these experiments, the non-interactive components were prescribed as boundary conditions from the present-day runs. Thereby, the ocean (in the experiments AV<sub>6k</sub>, AV<sub>0k</sub>, A<sub>6k</sub> and A<sub>0k</sub>) was prescribed as monthly mean values of sea surface temperature (SST) and sea-ice, taken from the present-day run AOV<sub>0k</sub>. The vegetation (in AO<sub>6k</sub>, AO<sub>0k</sub>, A<sub>6k</sub> and A<sub>0k</sub>) was prescribed as fraction of land cover type per grid-box. Values were taken from AOV<sub>0k</sub> for the experiments AO and from AV<sub>0k</sub> for the atmosphere-only runs. Atmospheric composition was fixed at pre-industrial values in all simulations, e.g. CO<sub>2</sub>-concentration was set to 280ppm. All simulations were brought to equilibrium before they were continued for another 600 years in total. To assess the robustness of our results, the entire simulation period of the final 600 years was subdivided into five subsequent periods of 120 years (Otto et al., 2009b). For each 120-year sub-period the sea surface conditions (for simulations AV and A) and the global vegetation pattern (for AO and A) were prescribed from the corresponding 120-year period of the respective run. For example, for the first 120-year period of run A<sub>0k</sub>, sea surface conditions and global vegetation pattern of the first 120-year period of run AOV<sub>0k</sub> were taken, and so on. Thereby, individual members of each ensemble of five 120-year simulations do not have exactly the same boundary conditions. For example, the individual members of the ensemble of five 120-year runs A<sub>0k</sub> do not have exactly the same ocean and land boundary conditions.

The results of this study are based on seasonal means of all periods (i.e. 600yrs-mean). Further information on the setup of experiments is given in Otto et al. (2009a and 2009b).

## 4.2.2 Analysis methods

Following the factor-separation technique (Stein and Alpert, 1993), the contribution of vegetation-atmosphere and ocean-atmosphere interactions, or feedbacks, and the synergy between these feedbacks to the difference between mid-Holocene and present-day (pre-industrial) climate are determined as:

$$\begin{aligned}
 \text{Total climate change:} & \quad \Delta\text{AOV} = \text{AOV}_{6k} - \text{AOV}_{0k} \\
 \text{Response of the atmosphere:} & \quad \Delta\text{A} = \text{A}_{6k} - \text{A}_{0k} \\
 \text{Contribution of vegetation-atmosphere feedback:} & \quad \Delta\text{V} = (\text{AV}_{6k} - \text{AV}_{0k}) - (\text{A}_{6k} - \text{A}_{0k}) \\
 \text{Contribution of ocean-atmosphere feedback:} & \quad \Delta\text{O} = (\text{AO}_{6k} - \text{AO}_{0k}) - (\text{A}_{6k} - \text{A}_{0k}) \\
 \text{Contribution of synergy:} & \quad \Delta\text{S} = \Delta\text{AOV} - \Delta\text{A} - \Delta\text{O} - \Delta\text{V}
 \end{aligned}$$

In this study, we restrict our analysis to two climate parameters, the near-surface air temperature (2m above ground) and precipitation. Time and spatial averaging is explained in section 2.2.1 and 2.2.2, respectively.

### 4.2.2.1 Calendar

Joussaume and Braconnot (1997) show that paleo-climate model results and their interpretation strongly depend on the chosen calendar. Due to the precession of the earth, not just the seasonal insolation but also the length of the seasons changes in time. Comparing seasons of the mid-Holocene with present-day's, thus, requires an absolute time reference. Joussaume and Braconnot (1997) suggest the definition of seasons based on astronomical positions, i.e. vernal equinox, summer solstice, autumnal equinox and winter solstice. In accordance with the respective astronomical dates, we calculate the seasonal averages for 6k and 0k from daily model output. To facilitate the comparison of our results with previous studies, which are usually based on present-day model (meteorological) calendar (e.g. summer = JJA), we shifted the seasons by three weeks. The day, each season starts at, as well as the length of the seasons is summarized in Table 4.1.

season	6k		0k	
	start (day)	length [days]	start (day)	length [days]
winter	334	93	336	88
spring	62	94	59	93
summer	156	89	152	94
autumn	245	89	246	90

Table 4.1: Start day and length of the seasons for the mid-Holocene and present-day orbital configuration, respectively. The seasons are defined on astronomical calendar, based on the time of vernal and autumn equinox as well as summer and winter solstice. The beginning of the seasons is shifted backwards by three weeks.

Region	Approximate longitude (°E)	Approximate latitude (°N)	Description
IND	71.25 - 78.75	12.99 - 24.12	Indian subcontinent (land only), core region Indian monsoon
INCPIN	93.75 - 108.75	12.99 - 20.41	Indochina Peninsula (land only), tropical region, influenced by East Asian monsoon
PAK	56.25 - 75	27.83 - 31.55	includes parts of Pakistan, Afghanistan and Iran, affected by the Indian monsoon
TP	75 - 101.25	27.83 - 38.97	Tibetan Plateau (model orography higher than 2500m), affected by Indian and East Asian monsoon
YANG	105 - 120	31.54 - 38.97	Yangtze and Huanghe plain, represents core region of the East Asian monsoon
NECH	116.25 - 135	46.39 - 53.81	North-eastern China, lower reaches of the Amur river, affected by East Asian monsoon, to some extent

Table 4.2: Description of the areas we consider in our feedback study. Listed are the abbreviation, geographic position (latitude and longitude of grid-box centres) as well as a short characterization. For location and shape of the regions see also Figure 4.1.

#### 4.2.2.2 Regions

Asia is a continent with strong climatic and orographic contrasts. Affected by different circulation systems (Indian and East Asian monsoon, mid-latitude westerlies), deserts are located next to dense vegetated area, and tropical climate can be found as well as regions covered by snow for half of the year. Huge mountains and high-elevated plateaus as well as wet plains around

large rivers form the landscape. Due to this heterogeneity it can be assumed that the atmospheric response to the orbital forcing and the strength of the feedbacks differ for different regions. This hypothesis is corroborated by reconstructions, revealing an asynchronous precipitation maximum in various parts of the Asian monsoon region (An et al., 2000), which indicates large spatial differences in the climatic change between the mid-

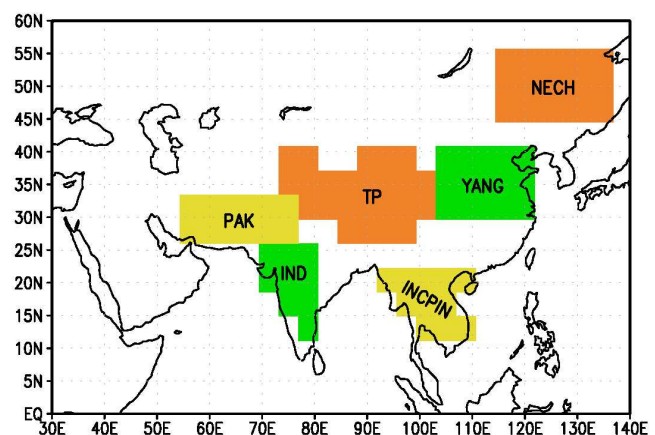


Figure 4.1: Location of the areas we consider in our feedback study.

Holocene and today. Our analyses show that even in regions influenced by only one of the above mentioned circulation systems the response of the different climate components locally varies. Therefore, we divided the Asian monsoon region into sub-areas, which differ with respect to orography and vegetation changes. Ad hoc, we define the following regions of interest: In the region of the large plain in East China, (referred to as YANG in the following) and in North-East China (NECH) we expect a clear signal of the East Asian monsoon, whereas in the regions PAK and IND of the Indian subcontinent, the Indian monsoon is likely to dominate climate dynamics. The areas roughly identified with the Tibetan Plateau and the Indochina Peninsula (INCPIN) are presumably affected by both monsoon systems. A detailed definition of the sub-areas is given in Table 4.2 and Figure 4.1. Although these sub-regions cover only nine grid boxes in some cases, the differences between the areas, we used for the allocation, consistently stay the same regarding orography and vegetation change.

### **4.3 Main characteristics of Central and East Asian climate and land cover changes**

#### **4.3.1 Climate change from 6k to present-day**

The climate in Central and Eastern Asia is influenced by three different circulation systems: the East Asian monsoon, the Indian monsoon and the mid-latitude westerlies. These systems are all strongly affected by the Tibetan Plateau. They in turn originate from different climate factors and are characterized by distinct seasonal cycles. Therefore, the regional climate is very heterogeneous, with arid and desert like conditions in the northwest, a general wet southern and eastern part and an alpine climate on the elevated Tibetan Plateau.

Before discussing the climatic impact of the dynamic ocean and vegetation (next section), we describe the main characteristics of the climate and land cover changes in the Asian monsoon and surrounding regions (60-140°E, 10-55°N). These results are based on the coupled experiments  $AOV_{6k}$  and  $AOV_{0k}$ , averaged over all five periods (i.e. 600yrs-mean). The long duration increases the significance and reliability.

In our analysis we focus on near-surface air temperature (temperature 2m above ground) and precipitation as the basic parameter characterizing monsoonal influenced climates. Both variables strongly determine the vegetation distribution. In order to estimate the quality of our model results, we compare them with reconstructions. Since paleoclimate reconstructions are sparse and often derived from pollen assemblies, we confine the comparison to the vegetation change, assuming that the land cover reflects climate conditions.

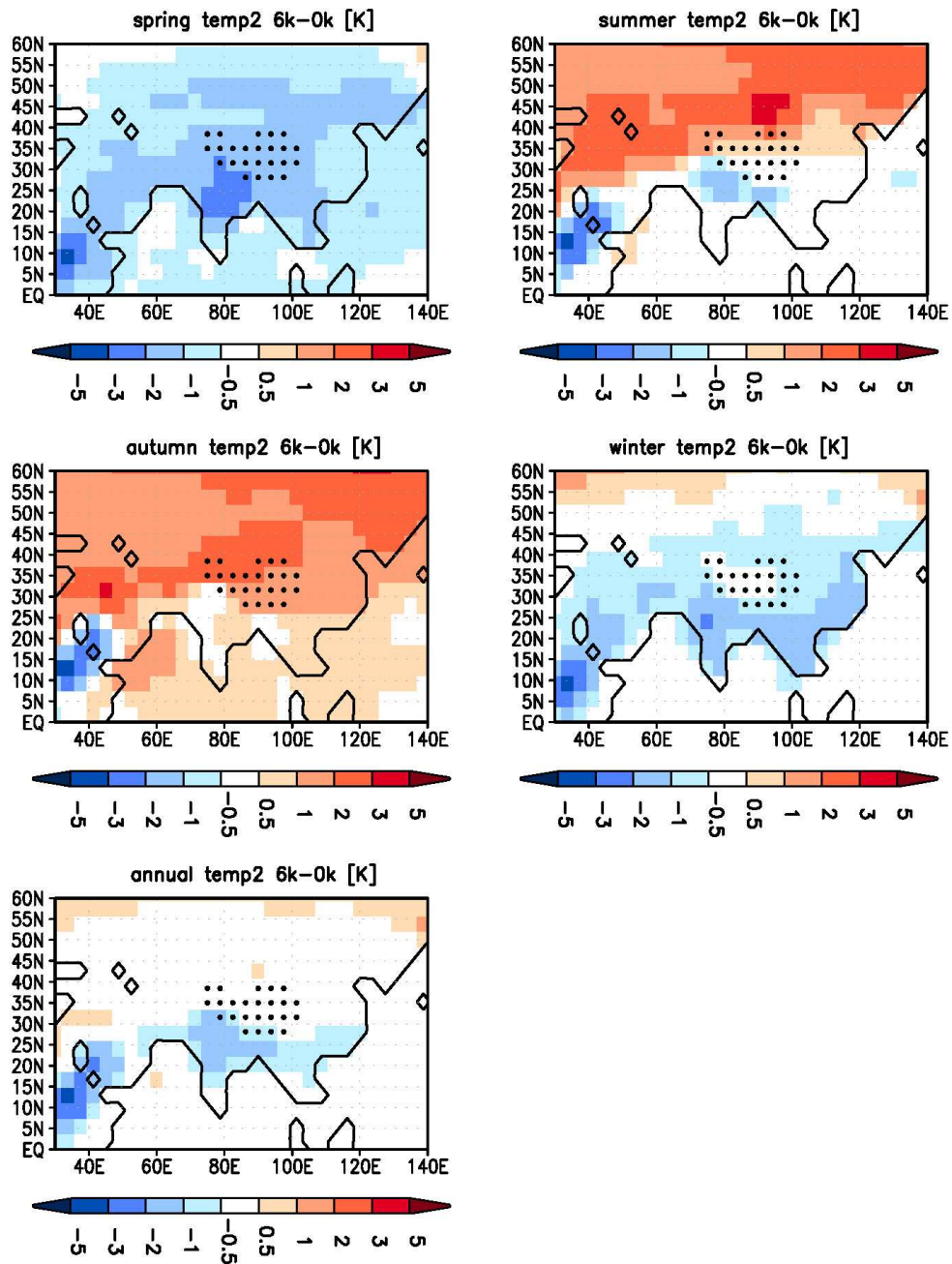


Figure 4.2: Seasonal and annual averaged 2m-temperature anomalies [K] between mid-Holocene and present-day climate resulting from the coupled experiment AOV. Seasons are defined on astronomical calendar, based on the time of vernal and autumn equinox and summer and winter solstice. The annual temperature anomaly is calculated on daily model output. Due to the different length of the respective seasons in mid-Holocene and present-day climate, the annual mean value is not the arithmetic average of the seasons. Stippled area indicates the Tibetan Plateau (orography in the model higher than 2500m).

#### **4.3.1.1 Near-surface air temperature**

Figure 4.2 shows the geographic pattern of temperature changes between 6k and 0k for each season and as annual mean. For mid-Holocene spring, the model simulates lower near-surface air temperatures over the whole region (60-140°E, 10-55°N) compared to present day. Strongest cooling occurs in the northern part of India (up to -2.8K) and on the Tibetan Plateau (-1.5 to -2K). Whereas summer temperature is increased in the regions north of 30°N with maximum amplitude of 3K, the western Pacific as well as the region between 20°N and 30°N, particularly northern India and the southern rim of the Tibetan Plateau, experience a cooler near-surface climate under 6k orbital conditions (up to -1.6K). The slightly higher temperatures over South India, Indochina and the adjacent Indian Ocean are negligible (<0.5K). With the exception of some grid-boxes south west of the Tibetan Plateau, an up to 3K temperature rise occurs in all parts of the considered region in autumn (up to 2.2K). For the winter season, the model results reveal lower near-surface temperatures over the continental area south of 55°N and slightly higher temperatures above the adjacent oceans. The strongest change occurs in the coastal areas and in the region south west of the Tibetan Plateau.

Averaged over the year, the Asian monsoon region experiences a cooling of up to 1.5K (northern India). Near-surface air temperatures in the other regions are slightly (<0.5K) higher in 6k than in 0k. The warming becomes more pronounced in the northern latitudes.

#### **4.3.1.2 Precipitation**

The seasonal precipitation changes between mid-Holocene and present-day are illustrated in Figure 4.3. One has to be careful with the interpretation of precipitation changes. Due to the differences in the length of the respective seasons between 6k and 0k, a higher mean precipitation-rate per day (mm/day) does not necessarily imply a higher seasonal sum (mm/season). On average, the region, affected by the Asian monsoon in spring, and adjacent oceans receive less spring precipitation (up to -1mm/day) under 6k orbital conditions, likely indicating a later onset of the summer monsoons. In all other parts of the region, precipitation is slightly enhanced, in particular on the Tibetan Plateau, where snowfall is increased by nearly 0.5mm/day.

The mid-Holocene summer climate is characterized by more precipitation (per day) than today in most parts of Central and Eastern Asia, but the difference is often smaller than 1mm/day. The strongest change occurs at the southern rim of the Tibetan Plateau, where the steep slope of the Himalaya induces an increase in precipitation of 3-4mm/day for 6k. In contrast, rainfall decreases in the north eastern Bay of Bengal and the East and South China Sea (up to 2mm/day). In autumn, the area gaining more precipitation in 6k is expanded to the adjacent oceans. Averaged daily precipitation is especially enhanced in the Indian monsoon region (up to 2mm/day). A reduction of rainfall rate is only apparent at

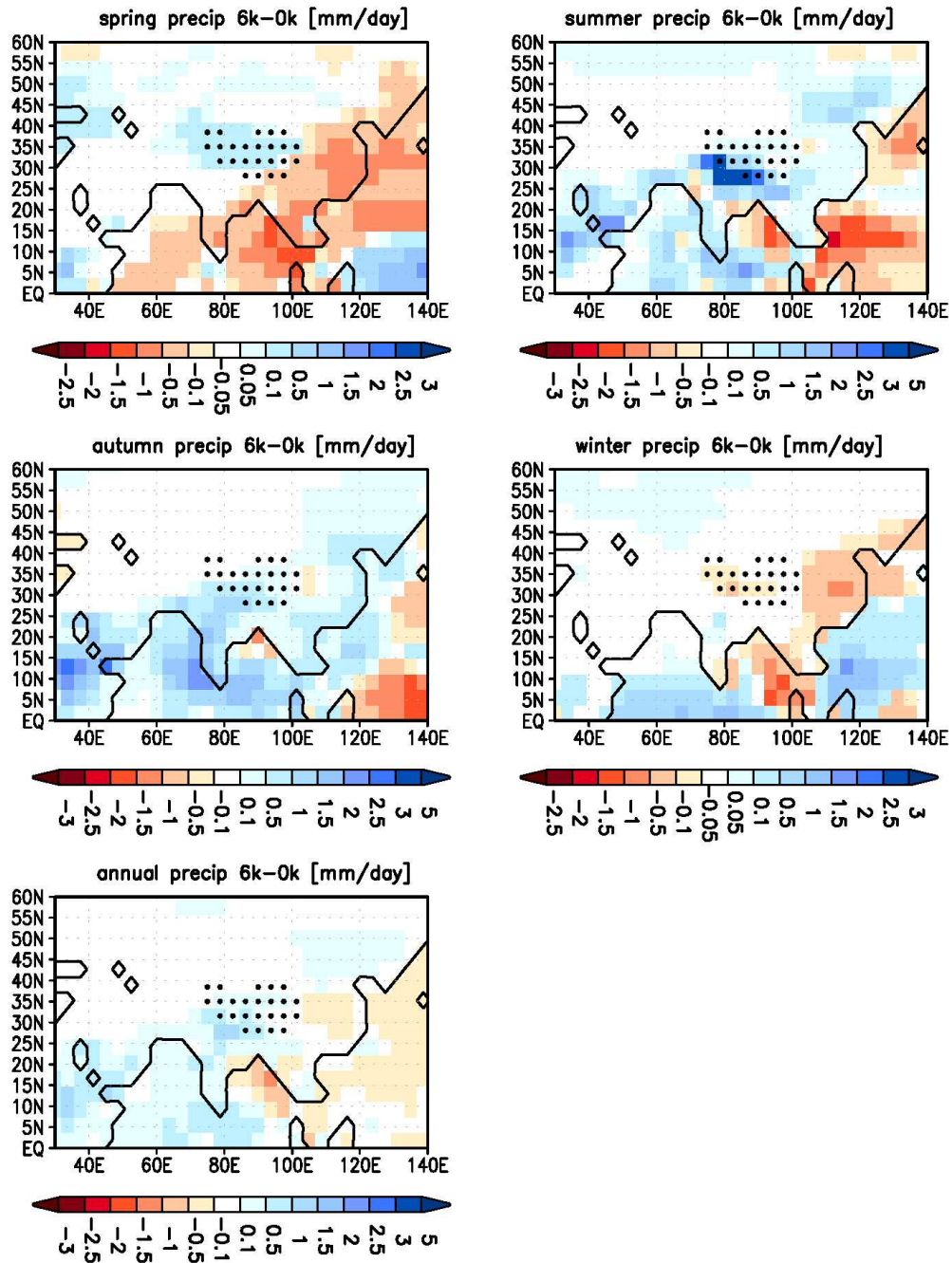


Figure 4.3: Same as Figure 4.2, but for seasonal and annual averaged precipitation anomalies [mm/day]. It has to be emphasized that, due to the differences in the length of the respective seasons between mid-Holocene (6k) and present-day (0k) climate, a higher precipitation rate per day does not necessarily indicate a higher seasonal sum, i.e. a higher amount of precipitation per season. Please note differences in colour scales.

some grid boxes east of the Tibetan Plateau, the northern Bay of Bengal and in the non-coastal western Pacific. In most parts of East China wintertime precipitation is decreased in 6k compared to present-day. The largest change on the continent occurs in the Yangtze-Plain (up to  $-0.7\text{mm/day}$ ). The northern regions and India receive slightly more

precipitation. Except for the Bay of Bengal (up to -1,5mm/day) all adjacent oceans experience an enhancement of precipitation rate (up to 1.5 mm/day).

On average, the annual precipitation rate is increased over land in 6k (up to 1mm/day), except for the Yangtze-Huanghe-Plain.

### 4.3.2 Land cover change from 6k to present-day

The differences in climatic conditions for 6k and 0k induce large-scale land cover changes (Figure 4.4). The simulated vegetation changes are assigned to four categories, namely forest, shrub, grass and non-vegetated fraction of a grid box (in the following referred to as desert fraction). Overall, Central Asia is covered by more vegetation in 6k, although the decrease in desert fraction is mostly small, not reaching changes higher than 10%. Only the region south west of the Tibetan Plateau (ca. 60°E-75°E, 27°N-33°N) and the margin area of the East Asian summer monsoon (108°E-111°E, 40°N-48°N) experience a larger increase of vegetated area (up to 40%). On the contrary, the desert in North Africa and Arabia is strongly reduced. In the transition zone between monsoon-influenced area and

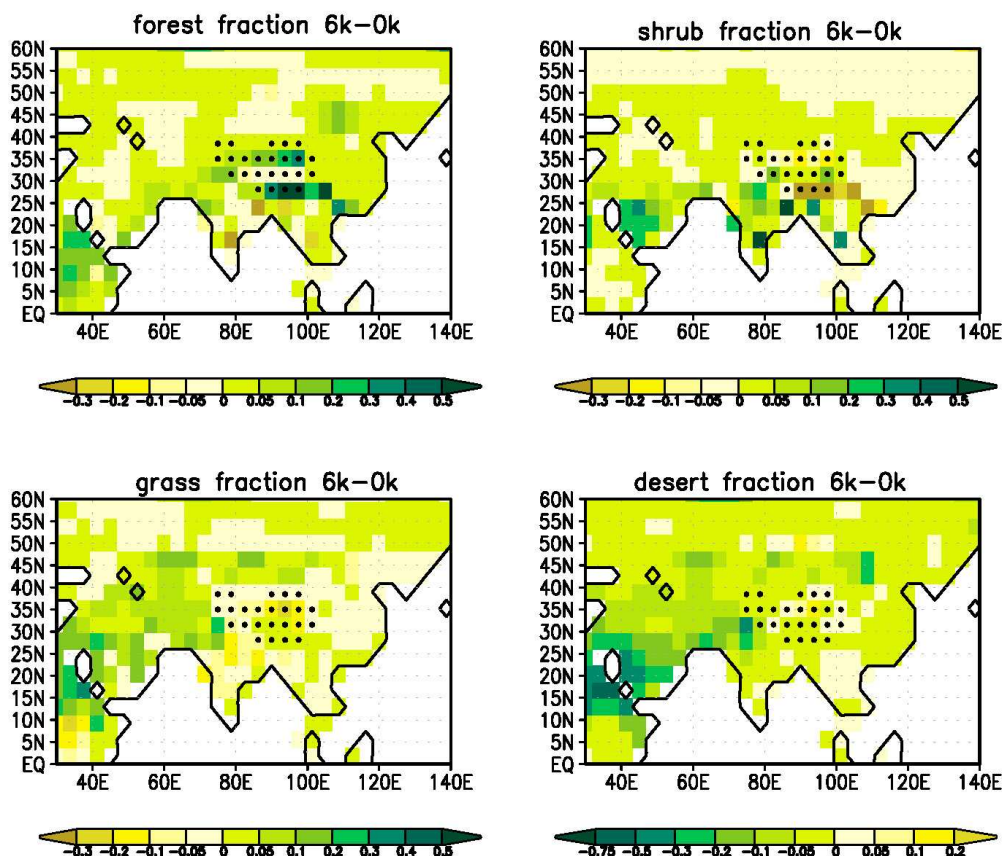


Figure 4.4: Simulated land-cover change between mid-Holocene and present-day climate, given as fraction of forest, shrubs, grass and non-vegetated area (referred to as desert) per grid-box. Stippled area indicates the Tibetan Plateau (orography in the model higher than 2500m). Please note the change in colour scales.

nearby desert or sparsely vegetated area, the fraction covered by any type of vegetation is controlled by rainfall. The Tibetan Plateau is a large orographic barrier, preventing a further inland penetration of the Indian (northward) and East Asia summer monsoon (westward), whereas the African monsoon is able to expand northward. Since most of the total precipitation in those regions can be attributed to the summer monsoons, changes in the amount of rain at the lee side of the Tibetan Plateau and thereby the reduction of the desert fraction must be small. Thereby, the Tibetan Plateau limits the expansion of vegetation north of the Plateau.

For the monsoon regions, where the moisture supply is sufficient, the model only simulates a change in the type of vegetation. In 6k, more area is covered by forest instead of shrubs and grass, particularly in the region south of and on the Tibetan Plateau as well as Eastern China. In the Indian monsoon region, part of the grass is replaced by shrubs.

Pollen analyses reveal a generally increased forest cover in the central and eastern parts of China (e.g. Ren and Beug, 2002; Ren, 2007) and a northwestward shift of the steppe-forest boundary of up to 500km (Ren, 2007; Yu et al., 2000) for mid-Holocene climate. The model indicates a significant shift of forest to the west. However, in the low resolution of the model this shift is expressed by one single grid-box. A northward displacement cannot be detected. Ren (2007) reports a decline of arboreal pollen in Northeast China (123-133°E, 40-52°N) from 6k to 0k. Although the regions do not exactly coincide, the tendency of less forest in the northeastern part of China is also apparent in our model. Pollen reconstructions from the Tibetan Plateau indicate a spatial heterogeneous vegetation trend. Many records collected on the Eastern and Southern Tibetan Plateau reveal a reduction of moisture availability and forest cover since 6k (e.g. Herzsuh et al. 2006, Shen et al. 2006, Tang et al. 1999), which are proposed to be associated with a gradual weakening of the Asian summer monsoon. However, some records also show comparably dry and even drier conditions in the mid-Holocene affecting the local vegetation composition (Zhao et al. 2009, Herzsuh et al. 2009). This inhomogeneous land cover trend is also obvious in the model results.

Given the coarse resolution of the model, the spatial distribution of the simulated vegetation changes between Mid-Holocene and present-day qualitatively agrees with reconstructions. However, the magnitude of changes differs. Whereas reconstructions suggest a decrease in forest cover of up to 90% (Ren, 2007; middle and lower reaches of the Yellow River and Huaihe River basin) our model reveals differences of less than 50%, everywhere. However, no other reconstruction studies report such large vegetation change.

## **4.4 The impact of dynamic vegetation and ocean on the climate change between 6k and present-day**

The impact of vegetation-atmosphere interaction, ocean-atmosphere interaction and of their synergy on the difference between mid-Holocene and present-day climate is calculated for each region and for each 120-year sub-period as well as for the whole 600-year simulation period. Even though the prescribed boundary conditions only slightly differ between each sub-period, the magnitude of the factor-contributions strongly varies, even with respect to the sign of factors, particularly for the vegetation contribution and the synergy. To assess the robustness of the factors over the entire simulation period, we conducted a standard student's t-test. Therefore, we define the five 120-year sub-periods of each 600-year run as an individual realisation of an ensemble. The contribution of the respective factor is supposed to be robust if the t-value exceeds the 95%-significance level. Please note that because of differing boundary conditions within each ensemble (see Section 4.2.1) this test does not exclusively tests the significance of a pure contribution and synergy, but also includes effects from – albeit small – changes in boundary conditions.

The summarizing figures in this section depict mean values of the whole 600-year simulation period. Only significant, or robust, factors are shown. All factors for all sub-regions and seasons are presented in the Appendix (Figure A.6, Figure A.7). The detailed presentation of results reveals strong variations in magnitude as well as in sign for some cases. Hence a small, or even missing, factor for the entire simulation period does not necessarily imply that the factor under consideration is always small.

### **4.4.1 Near-surface air temperature**

#### **4.4.1.1 Direct response of the atmosphere to the orbital forcing**

Figure 4.5 illustrates the robust contributions of the ocean-atmosphere and vegetation-atmosphere interactions to the temperature change as well as their synergy and the direct response of the atmosphere to the orbital forcing as seasonal means for each defined area. Following the orbital-induced insolation change between 6k and 0k, the direct reaction of the atmosphere causes an overall cooling in winter and spring and a warming in summer and autumn. Depending on region and season different mechanism influence this temperature change by affecting the local energy balance. Important parameters characterising the energy balance are summarized in Table 4.3 for the atmosphere-only run. As the change in evaporation between mid-Holocene and present-day climate has a strong effect on the surface temperature, the robust contributions of the different factors to the evaporation differences are additionally shown in Figure 4.6.

In spring, less insolation is received at the top of the atmosphere in 6k (10°N: ca.  $-10.5 \text{ W/m}^2$ ; 55°N: ca.  $-3.5 \text{ W/m}^2$ ). Nevertheless, the areas along the western Pacific (YANG,

## Temperature [K]

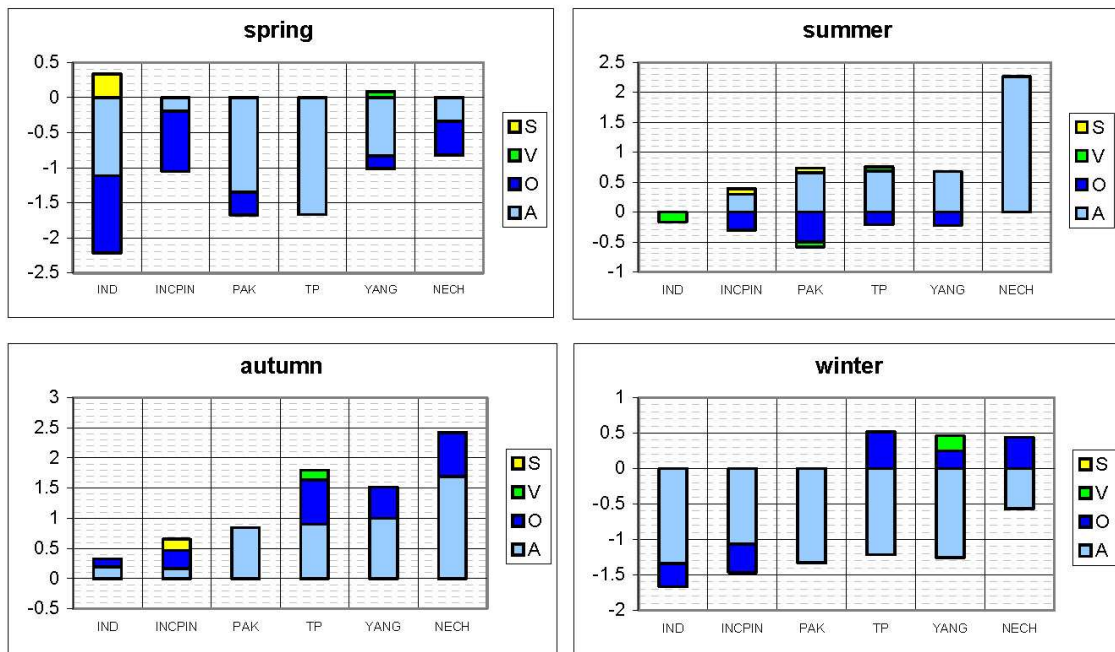


Figure 4.5: Factors contributing to the seasonal temperature change between mid-Holocene (6k) and present-day (0k) climate for six regions in the area of the Asian monsoon. Only robust contributions are shown. Seasons are defined on astronomical calendar, based on the time of vernal and autumn equinox as well as summer and winter solstice. Light blue colours show the results of the atmosphere-only run, i.e. the direct response of atmospheric dynamics (A) to changes in insolation. Dark blue colours represent the contribution of ocean-atmosphere-interaction (O), including sea-ice dynamics. Green colours indicate the contribution of vegetation-atmosphere interaction (V). Yellow colours reveal the contribution of the synergy (S) between atmosphere - ocean and atmosphere - vegetation feedbacks. Please note the change in scales.

INCPIN) experience a relatively small cooling ( $-0.83\text{K}$  and  $-0.2\text{K}$ , respectively). This can be attributed to a reduced cloudiness and surface evaporative cooling (warming effect, cf. Figure 4.6) due to a later onset of the East Asian summer monsoon, which can partly compensates the temperature decline expected from the insolation change. In contrast, the latent heat flux in IND, TP and PAK is increased at the expense of the sensible heat flux (Table 4.3). This leads to a more effective surface cooling and contributes to the temperature change induced by the general smaller insolation. Altogether, mid-Holocene climate in IND and PAK is colder than present-day climate by  $-1.12\text{K}$  and  $-1.34\text{K}$ , respectively. The temperature difference is most pronounced on the Tibetan Plateau (TP:  $-1.67\text{K}$ ). Due to the orbital-induced temperature decline, the snowfall rate is enhanced on the Plateau, leading to a higher surface albedo (0.01), a reduction of absorbed solar energy and an amplification of the near-surface cooling. The snow-albedo feedback acting on TP, thus, likely creates the contrast to the surrounding areas. Less insolation results in an approx.  $-0.34\text{K}$  colder climate in NECH.

## Evaporation [mm/day]

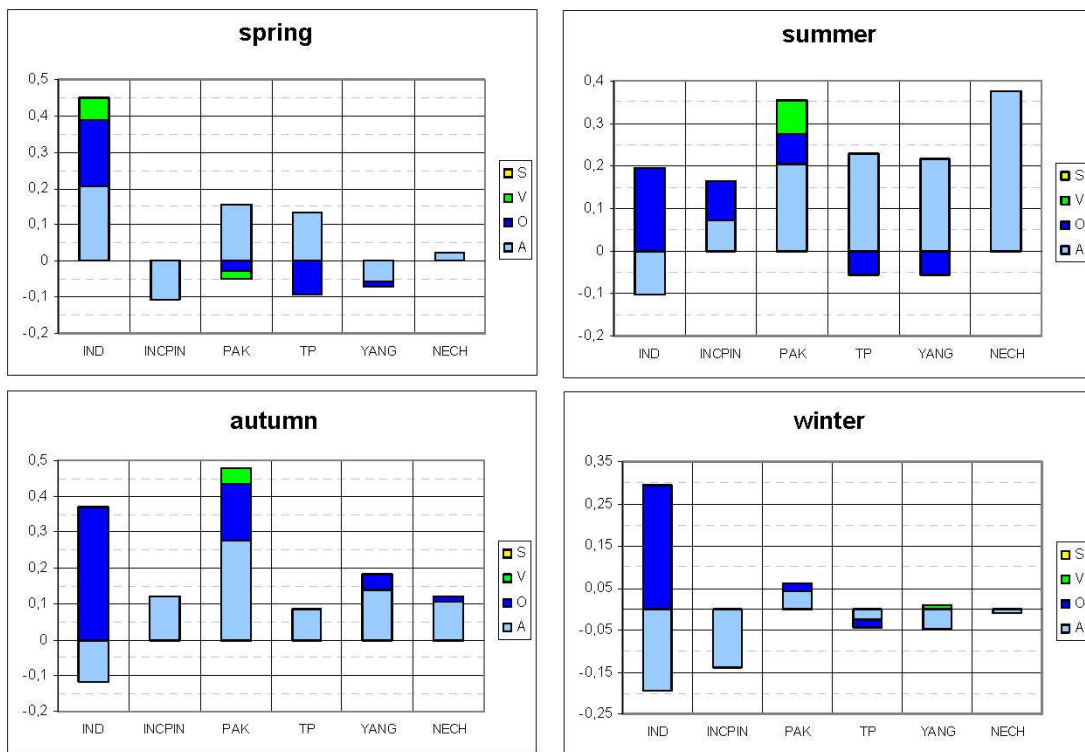


Figure 4.6: Same as Figure 4.5, but for evaporation anomalies [mm/day]. Please note the different scales.

The near-surface temperature difference between 6k and 0k in summer is strongly determined by the direct response of the atmosphere to the orbital forcing, yielding more solar incoming radiation at the top of the atmosphere ( $10^{\circ}\text{N}$ :  $+18.5\text{W/m}^2$ ;  $55^{\circ}\text{N}$ :  $+26.5\text{W/m}^2$ ). In line with the latitudinal gradient of the insolation change, higher temperatures of up to 2.26K in the northern region (NECH) and slightly higher temperatures in the other regions (0.29K in INCPIN to 0.68K in TP) are obtained (Figure 4.5). Besides, more cloudiness and higher evaporation rates associated with a stronger summer monsoon (except IND) cool the surface and diminish the temperature rise, particularly in YANG, PAK and TP. In IND, the contribution of the direct effect is not robust.

The enhancement and later retreat of the Asian summer monsoon (see section 4.2) also affects the temperature differences between mid-Holocene and present-day climate in the atmosphere-only simulations: Despite the negative latitudinal gradient of solar incoming radiation difference between mid-Holocene and present-day ( $+9.5\text{W/m}^2$  at  $10^{\circ}\text{N}$ ;  $+4\text{W/m}^2$  at  $55^{\circ}\text{N}$ ) the strongest temperature rise (1.69K) occurs in the northern region (NECH) and not near the equator. Near-surface temperature in IND and INCPIN increases only by 0.2K and 0.17K, respectively. The later retreat of the Asian summer monsoon is accompanied by an enhanced cloudiness, resulting in a reduced net solar radiation at the surface in IND.

	spring	summer	autumn	winter		spring	summer	autumn	winter
	IND					INC			
SW <sub>in</sub> TOA [W/m <sup>2</sup> ]	-9,34	20,85	8,67	-15,55		-9,67	20,27	8,96	-16,07
Sens. heat flux [W/m <sup>2</sup> ]	-6,26	1,99	2,19	0,32		0,54	1,87	-0,82	-2,08
Lat. heat flux [W/m <sup>2</sup> ]	5,84	-2,84	-3,42	-5,74		-3,15	2,11	3,53	-4,14
Cloud Cover	-0,02	0,02	0,04	0,05		-0,04	0,01	0,02	0,02
SW <sub>net</sub> surface [W/m <sup>2</sup> ]	-4,22	-3,02	-5,56	-12,26		0,08	2,76	1,77	-9,56
LW <sub>net</sub> surface [W/m <sup>2</sup> ]	4,13	2,10	4,51	5,57		-2,49	0,82	1,40	2,26
Temperature 2m [K]	-1,12	-0,05	0,20	-1,33		-0,20	0,29	0,17	-1,07
	PAK					TP			
SW <sub>in</sub> TOA [W/m <sup>2</sup> ]	-8,00	22,82	7,56	-13,36		-7,37	23,48	7,06	-12,33
Sens. heat flux [W/m <sup>2</sup> ]	-4,56	2,83	-0,27	-3,30		-7,80	-4,50	-1,69	-3,07
Lat. heat flux [W/m <sup>2</sup> ]	4,53	5,94	8,02	1,27		4,31	6,45	2,50	-0,75
Cloud Cover	0,03	0,09	0,06	0,02		0,04	0,05	0,06	0,02
SW <sub>net</sub> surface [W/m <sup>2</sup> ]	-7,31	-0,49	-1,92	-8,24		-11,08	-2,71	-5,93	-8,26
LW <sub>net</sub> surface [W/m <sup>2</sup> ]	7,36	10,43	10,05	5,38		8,08	6,24	6,97	3,67
Temperature 2m [K]	-1,34	0,66	0,85	-1,33		-1,67	0,68	0,90	-1,21
	YANG					NECH			
SW <sub>in</sub> TOA [W/m <sup>2</sup> ]	-7,13	23,74	6,87	-11,90		-4,36	25,78	4,89	-7,52
Sens. heat flux [W/m <sup>2</sup> ]	-0,80	-0,30	-0,65	-0,89		-1,79	-0,84	-1,50	-1,25
Lat. heat flux [W/m <sup>2</sup> ]	-1,63	6,30	4,05	-1,33		0,62	10,87	3,07	-0,31
Cloud Cover	-0,01	0,03	0,03	0,00		0,00	0,02	0,02	0,00
SW <sub>net</sub> surface [W/m <sup>2</sup> ]	-2,51	4,67	0,15	-3,97		-1,69	9,90	-1,67	-2,06
LW <sub>net</sub> surface [W/m <sup>2</sup> ]	0,80	2,61	3,68	0,62		0,49	2,92	2,69	-0,19
Temperature 2m [K]	-0,83	0,68	1,00	-1,26		-0,34	2,26	1,69	-0,57

Table 4.3: Differences between mid-Holocene and present-day climate for certain parameters characterising the energy balance of the surface. Differences are calculated for each sub-region, based on results of the atmosphere-only run. Listed are incoming shortwave radiation at the top of the atmosphere (SW<sub>in</sub> TOA), sensible and latent heat flux (positive values indicate a higher flux from the surface to the atmosphere in 6k compared to 0k), total cloud cover, net shortwave radiation at the surface (SW<sub>net</sub> surface [W/m<sup>2</sup>]), net longwave radiation at the surface (LW<sub>net</sub> surface [W/m<sup>2</sup>]), and near-surface temperature.

In winter, 2m-temperature is reduced in all regions due to less insolation (-17.5W/m<sup>2</sup> at 10°N; -6W/m<sup>2</sup> at 55°N). The largest cooling occurs in IND (-1.33K), the weakest in NECH (-0.57K). Since the cold temperatures enhance snow-fall rate in YANG and TP, these regions might experience an additional cooling caused by the snow-albedo feedback.

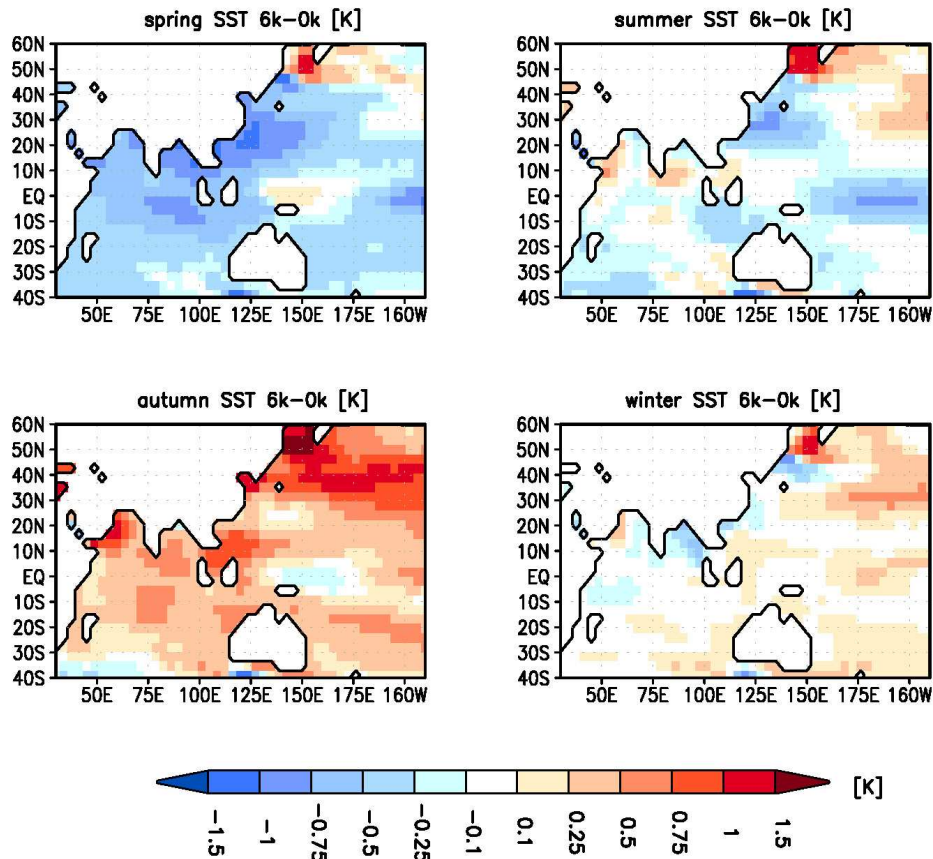


Figure 4.7: Simulated differences in seasonal sea surface temperature [K] between mid-Holocene and present-day climate.

#### 4.4.1.2 Contribution of the dynamic ocean

The simulated differences in sea surface temperature between mid-Holocene and present-day are depicted in Figure 4.7. Due to the large thermal inertia of the water mass, differences in sea surface temperatures lag differences in insolation by about one month.

This causes a shift in the seasonal cycle of the oceanic contribution compared to the atmospheric response. Thus, the ocean-atmosphere feedback exerts a cooling in all considered parts of Asia in spring and summer (Figure 4.5), thereby amplifying the atmospheric signal in the former and counteracting the direct response in the latter of these seasons. However, the magnitude of the ocean-induced cooling is generally small in summer as well as in spring (less than  $-0.5\text{K}$  in most areas). Only in India (IND) and on the Indochina Peninsula (INCPIN) the springtime temperature decrease associated with the atmosphere-ocean interaction reaches larger values of  $-1.1\text{K}$  and  $-0.85\text{K}$ , respectively. In IND, this pronounced cooling is associated with a higher evaporation (ca.  $0.2\text{mm/day}$ , Figure 4.6) and hence, evaporative cooling. The temperature change is neither robust for TP in spring nor for IND and NECH in summer.

In autumn, the contribution of the interactive ocean amplifies the direct effect and shows a warming in the same order of magnitude as the atmospheric response in most of the regions (Figure 4.5). It ranges from 0.13K in IND to 0.73K in NECH and TP. No robust autumnal temperature change can be attributed to the ocean in PAK.

The ocean-atmosphere interaction leads to a cooling of the tropical regions (IND: -0.33K, INCPIN: -0.4K) in boreal winter, which intensifies the direct response of the atmosphere to the insolation change. Enhanced cloudiness and therewith less net solar energy at the surface (ca.  $-5\text{W/m}^2$ ) causes the temperature decline in INCPIN. In the sub-region IND, a pronounced ocean-induced increase in evaporation (ca. 0.38mm/day) is found (Figure 4.6).

In the other regions, the ocean-atmosphere interaction counteracts the direct effect and leads to a reduction of the temperature difference given by the atmosphere-only run (Figure 4.5, TP: 0.52K; YANG: 0.25K; NECH: 0.44K). The temperature change in PAK is not robust.

#### **4.4.1.3 Contribution of the dynamic vegetation**

As seen in Sec. 4.3.2, the vegetation change in the Asian monsoon region is small. Thus, one does not expect pronounced vegetation-atmosphere interactions in that area. Compared to the oceanic and atmospheric response, the averaged contribution of the dynamic vegetation to the Holocene temperature change is mostly negligible, reaching at most 0.22K in YANG (winter). With few exceptions it reveals a warming in higher latitudes and a cooling in the tropical regions (IND, INCPIN) during the whole year. However, since the signal strongly varies between the different periods (see Figure A.6), in both, magnitude and sign, the dynamic vegetation-induced temperature change is robust only in a few cases (Figure 4.5).

In spring, only YANG experienced a robust warming (+0.04K). The slight increase in higher vegetation (more forest instead of shrubs) is accompanied by a reduction of surface albedo and a potential warming of the near-surface air, due to more absorbed shortwave radiation at the surface ( $0.5\text{W/m}^2$ ).

The slight (but robust) temperature decrease in the Indian monsoon region in summer (IND: -0.17K; PAK: -0.09K), is likely related to an increase of cloudiness and evapo-transpirational cooling of the surface due to an enlargement of the area covered by higher vegetation (shrubs instead of grass and desert). Interestingly, vegetation is the only factor yielding a robust signal for IND in summer. The Tibetan Plateau (TP) experiences a slight summer warming (0.07K) attributed to dynamic vegetation.

This warming is still robust in autumn (0.16K) and probably reflects an increase of net solar energy at the surface due to more forests and the associated decrease of surface albedo.

In winter, the temperature change attributed to the dynamic vegetation is only robust in YANG (+0.22K). YANG is a region covered by snow in winter, so that the increase in forest fraction probably leads to a higher snow-masking effect and a reduction of the surface albedo (-0.01). Apart from the effect on the local energy balance the interactive vegetation leads to slight changes in local atmospheric dynamics. The increase in forest and vegetation cover northeast of the Tibetan Plateau (cf. Figure 4.4, 103°E-117°E, 40°N-48°N) warms the surface and regionally weakens the anticyclone, which develops in autumn over the cold land masses of the extratropical Asian continent (not shown). Total cloud cover as well as snow fall decrease in YANG, yielding an additional warming of the near-surface atmosphere.

#### **4.4.1.4 Contribution of the synergy**

The synergy between the ocean-atmosphere and vegetation-atmosphere feedback is small, but on average positive in nearly all regions and seasons. Its contribution to the temperature change tends to be larger in the southern regions (IND, PAK, INCPIN) than in the northern regions (YANG, NECH). Like the signal of the vegetation-induced temperature change, the synergy strongly varies between different 120-year periods. Thus, it is robust only in a few regions and seasons.

In spring, IND experiences a robust warming associated with the synergy (on average: 0.34K). The synergy contribution is also robust in INCPIN (summer and autumn) and in PAK (summer). No robust temperature change can be attributed to the synergy in winter.

## **4.4.2 Precipitation**

### **4.4.2.1 Direct response of the atmosphere to the orbital forcing**

The contributions of the dynamic ocean and vegetation to the precipitation change as well as their synergy and the direct response of the atmosphere to the orbital forcing are depicted in Figure 4.8 as seasonal means for each defined area.

The dominant mechanism forming the monsoons is the thermal contrast between the land and the ocean. Thus, the seasonal cycle of monsoons is primarily determined by the distribution of incoming solar radiation, which depends on the Earth's orbit around the sun (Webster et al., 1998; He et al. 2007). As expected, the change of the orbital parameter from 0k to 6k affects the simulated annual cycle of precipitation in the Asian monsoon region. The reduced solar energy input in spring postpones the East Asian summer and Bay of Bengal monsoon onset. Therefore, less spring precipitation is received in IND (-0.06mm/day), INCPIN (-0.4mm/day) and YANG (-0.33mm/day). The East Asian monsoon region is strongly affected, since less insolation weakens and shifts the western Pacific subtropical high southwards, reducing the East Asian monsoon flow onto the continent (Figure 4.9). The regions PAK and TP experience an increase in precipitation by

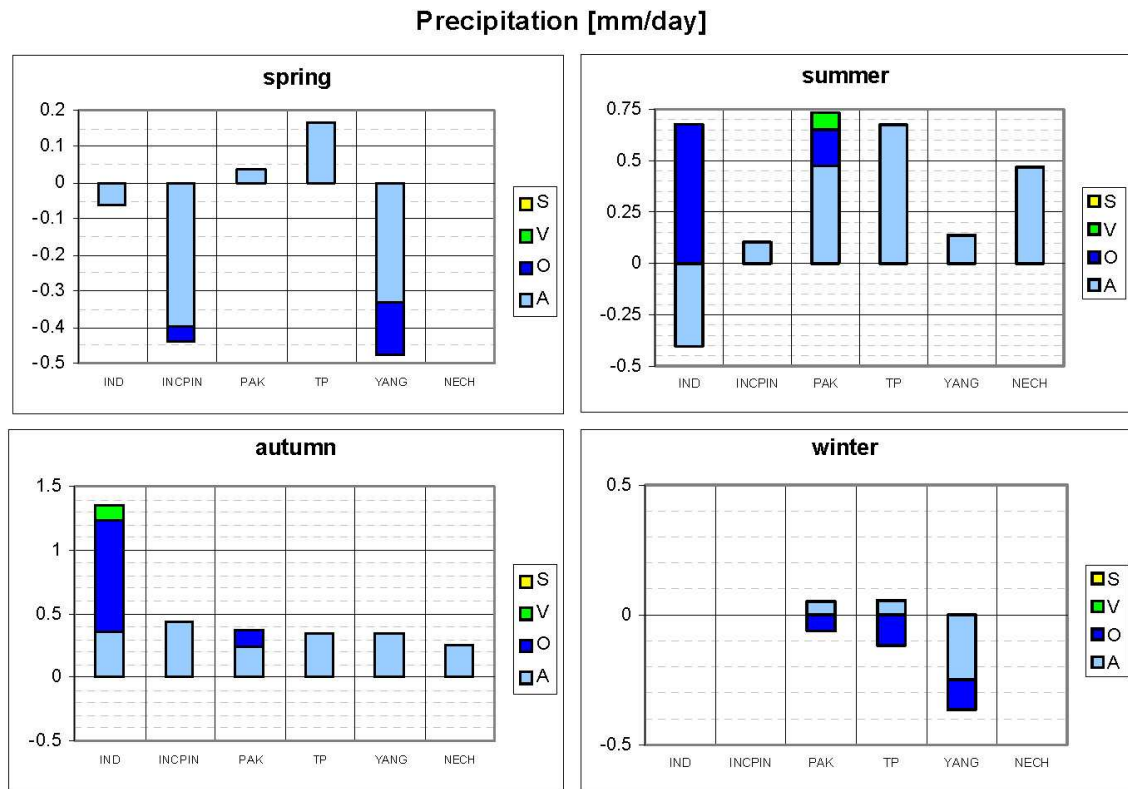


Figure 4.8: Same as Figure 4.5 but for precipitation anomalies [mm/day]. Please note the change in scales.

0.04mm/day and 0.17mm/day, respectively, due to the orbital forcing. On the Tibetan Plateau (TP), the snow fall-rate is enhanced, reflecting the colder mid-Holocene climate in spring (Figure 4.8).

As a consequence of the strong continental warming in summer, the large-scale circulation is modified. The upper tropospheric flow over Africa and the Central Asian continent is much more divergent in summer, except over South India and some parts of Indonesia (Figure 4.10). This is related to an enhanced vertical uplift of moist air, more clouds and higher precipitation-rates in all considered regions except IND. Whereas the East Asian monsoon is intensified and penetrates further inland (Figure 4.8; YANG: +0.14mm/day; NECH: +0.47mm/day), the atmosphere-only run suggests less precipitation (weaker monsoon) in India (-0.4mm/day). Due to a low-level pressure anomaly in the area between Kazakhstan and the Arabian Sea (approx. 3hPa, Figure 4.9), the low level Indian monsoon flow is slightly shifted in 6k compared to present-day, strengthening the monsoon branch directed to the north Arabian Sea. Over Pakistan, this branch turns towards and streams along the Tibetan Plateau, resulting in more precipitation in PAK (+0.47mm/day) and on the southern Plateau (TP: +0.67mm/day). By contrast, the monsoon flow in South India and the southern Bay of Bengal is attenuated. The changes in precipitation as well as outgoing longwave radiation (not shown) suggest a northward shift of the ITCZ in summer.

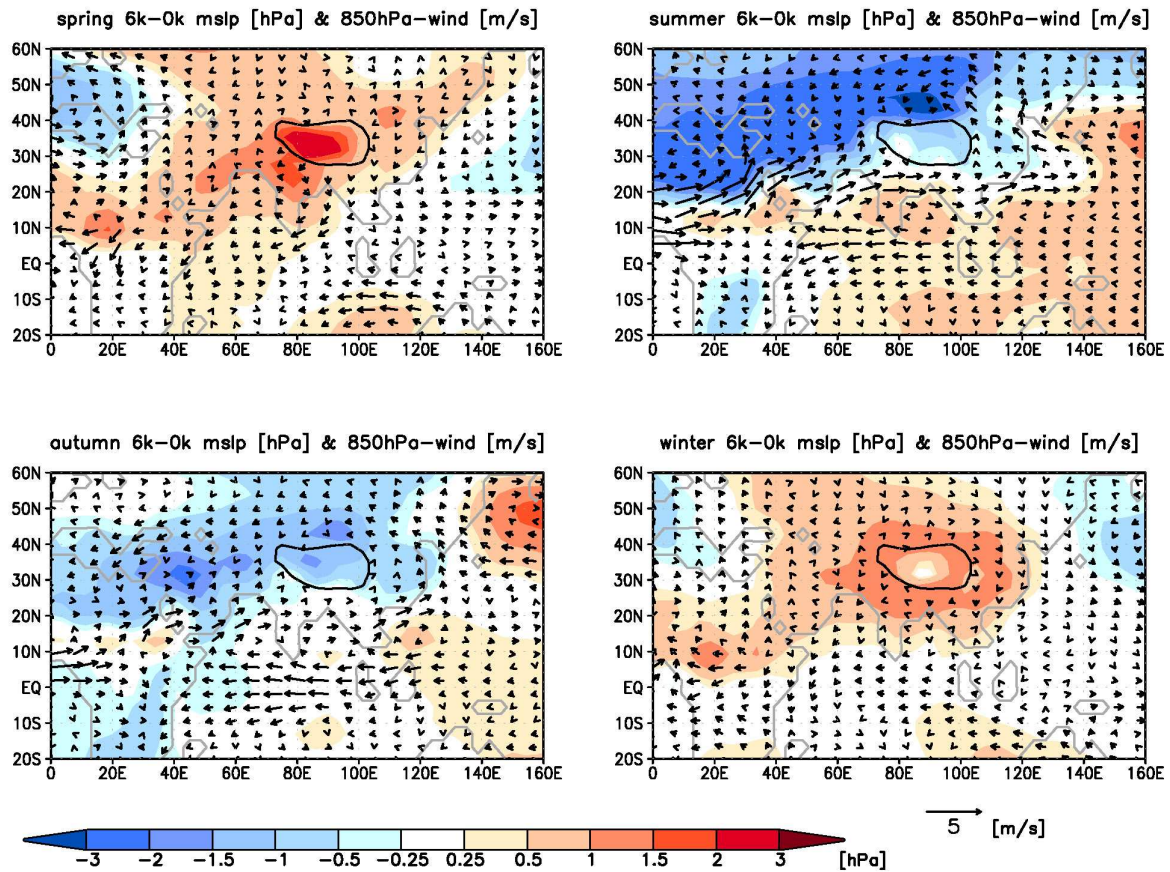


Figure 4.9: Mean sea level pressure (shaded, [hPa]) and wind in 850hPa (vector, [m/s]) as simulated by the atmosphere-only run. Presented are anomalies between mid-Holocene and present-day climate on average over each season. Simulated present-day summer monsoon wind field can be seen in the Figure A.8). The black solid line marks the Tibetan Plateau (orography in the model higher than 2500m). No wind vectors are shown, where the orography in the model exceeds 1500m (approx. corresponding to the 850hPa-Niveau).

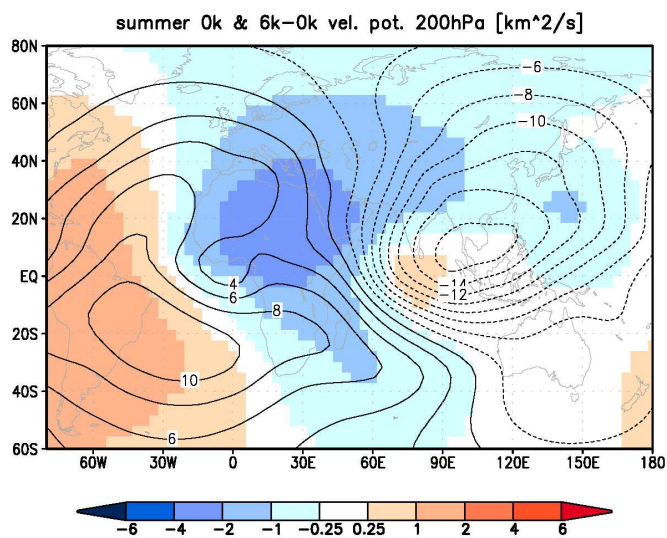


Figure 4.10: Upper-tropospheric velocity-potential (200hPa, [km<sup>2</sup>/s]) as simulated by the atmosphere-only model, averaged over the summer season. Contour lines illustrate the velocity-potential under present-day orbital configuration. Shaded areas show the velocity-potential anomalies between 6k and 0k. Negative values represent divergence, positive values convergence.

The atmospheric response to the orbital forcing leads to more autumn precipitation in the continental Asian monsoon region, especially in the coastal areas. On the contrary, less precipitation is received over the adjacent oceans, suggesting a later retreat of the summer monsoon system. The precipitation-rate is increased by about 0.25mm/day in PAK to 0.44mm/day in INCPIN (Figure 4.8).

The change of wintertime precipitation is small compared to the other seasons and not robust in all regions. However, YANG is the only sub-region receiving appreciable precipitation in present-days winter monsoon. Whereas the direct effect yields an increase of precipitation in PAK (0.05mm/day) and TP (0.06mm/day) as a reaction to the orbital forcing, YANG experiences a pronounced reduction of precipitation by -0.25mm/day.

#### 4.4.2.2 Contribution of the dynamic ocean

The oceanic impact on the seasonal precipitation distribution is mainly manifested in the change of evaporation and the modification of the large-scale and local circulation due to changed sea surface temperatures (SSTs). Thus, lower SSTs in spring reduce evaporation and results in several high-pressure anomalies above the East and South China Sea as well as the northern Indian Ocean (Figure 4.11). The accompanied decrease of the moist-air

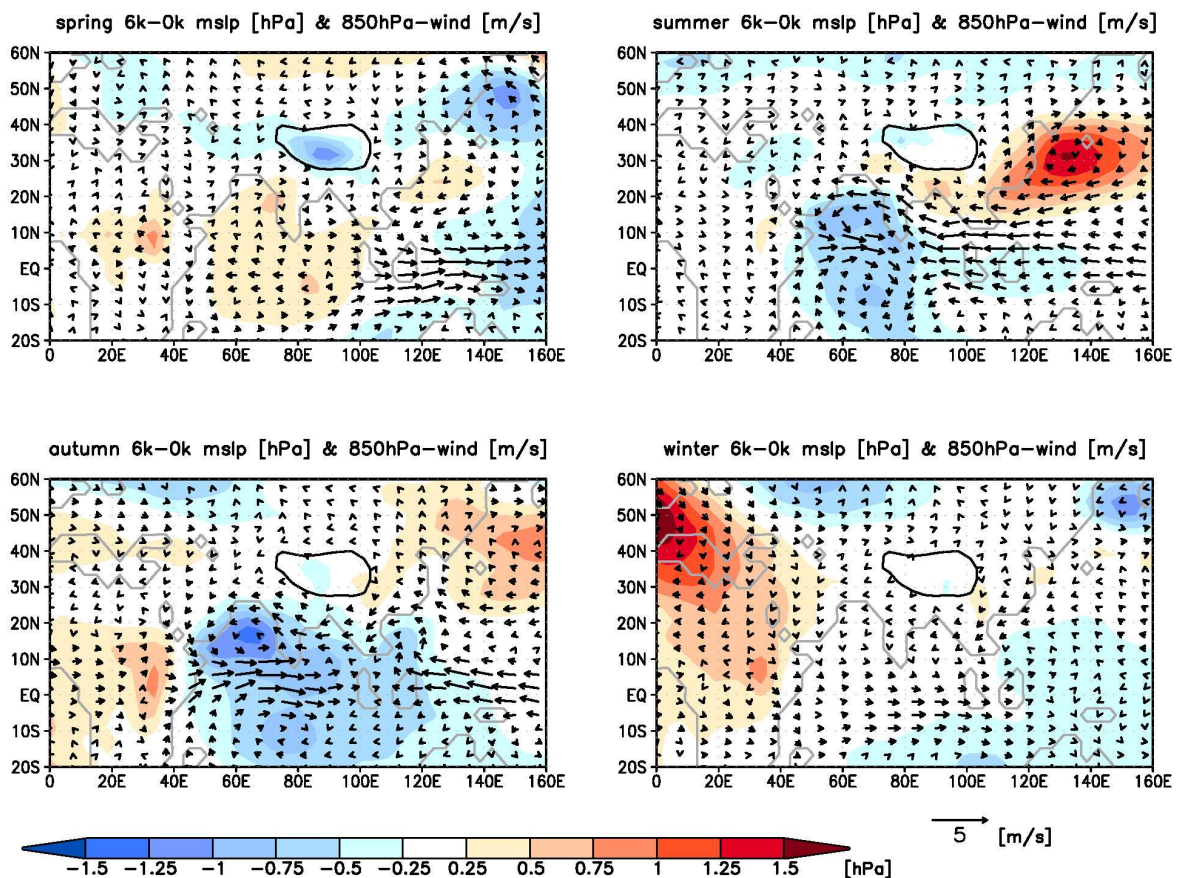


Figure 4.11: Same as Figure 4.9, but for the differences in wind and pressure field attributed to the ocean-atmosphere interaction.

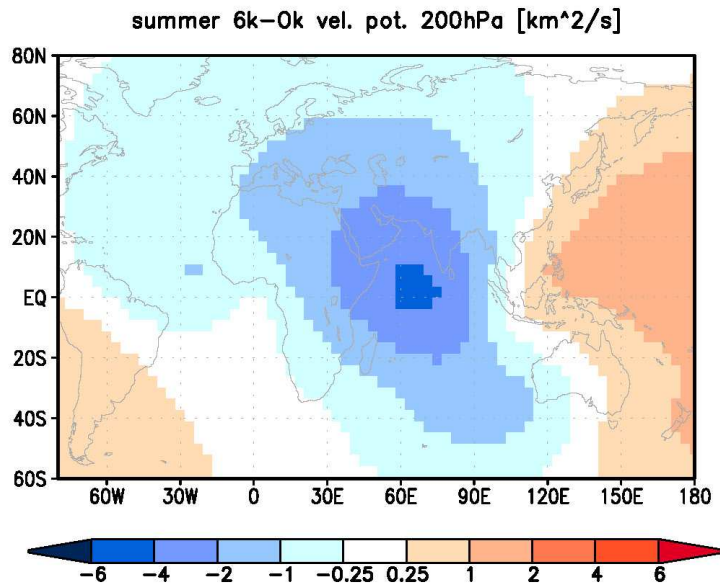


Figure 4.12: Differences in upper-tropospheric velocity potential (200hPa, [km<sup>2</sup>/s]) between mid-Holocene (6k) and present-day (0k) climate, attributed to the ocean-atmosphere interaction and averaged over the summer season. Negative values represent divergence, positive values convergence.

advection from the ocean to the continent might be responsible for the reduction of precipitation in all regions (Figure 4.8, Figure A.7). However, the signal is only robust in INCPIN (-0.04mm/day) and in YANG (-0.14mm/day).

In summer, the pattern of large-scale circulation change due to the interactive ocean offers a much more divergent upper-tropospheric flow above the Arabian Sea and an increased convergence above the Pacific (Figure 4.12). This coincides with a centre of enhanced evaporation in the South Arabian Sea and reduced evaporation in the East China Sea, influencing the precipitation change over the whole continent due to more water availability in the Indian monsoon and diminished water supply to the East Asian monsoon. Thus, IND (+0.68mm/day) and the north coast of the Arabian Sea (including PAK: +0.18mm/day) experience a strong increase of rainfall-rate (Figure 4.8). This oceanic-induced strengthening of the Indian summer monsoon is such as large, that it can overcompensate the direct effect (-0.4mm/day) in India (IND), causing the wetter summer climate in that area in 6k compared to 0k. In all other regions (INCPIN, TP, YANG, NECH), the change in summertime precipitation is not robust. Nevertheless, the interactive ocean tends to weaken the East Asian summer monsoon. Precipitation is particularly reduced above the adjacent ocean (Figure 4.13). However, apart from the reduction of water supply mentioned above, colder than present SSTs in the west Pacific (Figure 4.7) induce a high-pressure anomaly (anticyclone) and a slightly enhanced monsoon flow onto the continent (Figure 4.11). These two mechanisms counteract and might lead to only small changes in the East Asian monsoon region, so that the East Asian summer monsoon is only little affected by the interactive ocean.

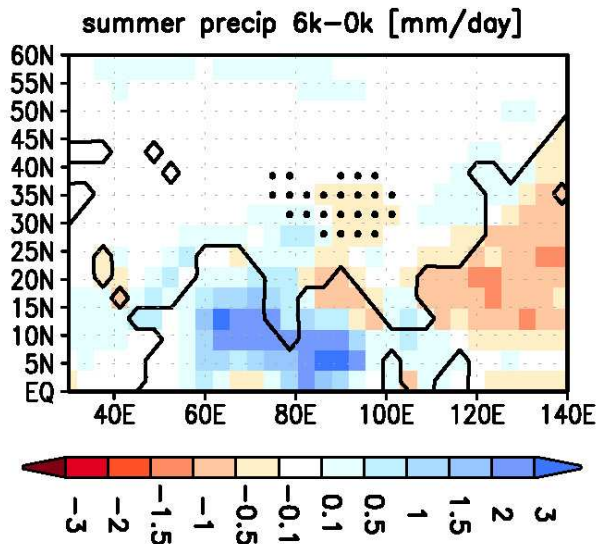


Figure 4.13: Summertime precipitation changes [mm/day], which are attributed to the ocean-atmosphere interaction.

Due to the thermal inertia of the ocean, the sea surface is warmed the most in autumn (Figure 4.7). SSTs are higher in most parts of the adjacent oceans, particularly in the north Arabian Sea. This leads to a warmer lower atmosphere and more evaporation, resulting in more water vapour in the atmosphere. These moist air masses are advected to the land, prolonging the rain period of the Indian summer monsoon. Thus, the most remarkable change occurs in IND (+0.88mm/day, Figure 4.8), where the ocean-atmosphere feedback triples the precipitation increase associated with the direct response of the atmosphere to the insolation change. In PAK, precipitation-rate rises by 0.13mm/day. Like in summer, the East Asian monsoon rainfall-rate is only weakly affected by the interactive ocean and thus not robust.

In winter, the contribution of the interactive ocean to the precipitation change shows a robust signal in all regions, where the direct effect is robust. In PAK (-0.06mm/day) and TP (-0.12mm/day), the ocean-induced precipitation reduction partly compensates the atmospheric response to the insolation change. The atmospheric warming attributed to the ocean likely results in a decrease of cloud cover and precipitation in YANG (-0.11mm/day).

#### 4.4.2.3 Contribution of the dynamic vegetation and synergy

The seasonal precipitation-rates are only little affected by vegetation-atmosphere interactions. Nevertheless, the vegetation-atmosphere feedback (on average) mostly tends to amplify the direct response to the orbital forcing in all seasons except winter (see Figure A.7). As mentioned for temperature, the vegetation-induced precipitation change strongly varies between the different sub-periods and is thus only robust in two sub-regions.

It enhances differences between mid-Holocene and present-day precipitation over PAK in summer (+0.08mm/day) and over IND in autumn (+0.12mm/day). This effect can be attributed to the fact that during mid-Holocene, larger areas are covered by taller

vegetation (shrubs, forest instead of grass and desert) in these regions, which, by their larger leaf area, tend to increase evapotranspiration and, thus, local precipitation.

The contribution of the synergy between the ocean-atmosphere and vegetation-atmosphere feedback to the precipitation change is small and not robust for any region and season.

## 4.5 Summary and discussion of Chapter 4

The impacts of interactive ocean and vegetation on the climate change from mid-Holocene to present-day have been investigated for the Asian monsoon domain by applying the factor separation technique (Stein and Alpert, 1993) on a set of numerical experiments. As the topography in that region is very heterogeneous, different sub-areas are discussed separately. Temperature as well as precipitation changes are considered for all seasons, based on astronomical calendar.

Our analysis reveals, that the ocean-atmosphere feedback significantly influences the temperature and precipitation change between mid-Holocene and present-day, although most of the response can be attributed to the direct effect of the atmosphere. The interactive vegetation and synergy play a minor role in understanding the Asian monsoon climate change.

Averaged over all six sub-regions, the differences between mid-Holocene and present-day seasonal temperatures are given in Figure 4.14a. Following the change in insolation, the Asian monsoon region experiences a colder mid-Holocene climate of approximately -1.32K in spring and a warmer climate by some 1.29K in autumn. On average, the summer temperature is increased by 0.59K in AOV<sub>6k</sub>. This signal, however, is mainly caused by the strong warming in the sub-region NECH. On the contrary, the wintertime temperature

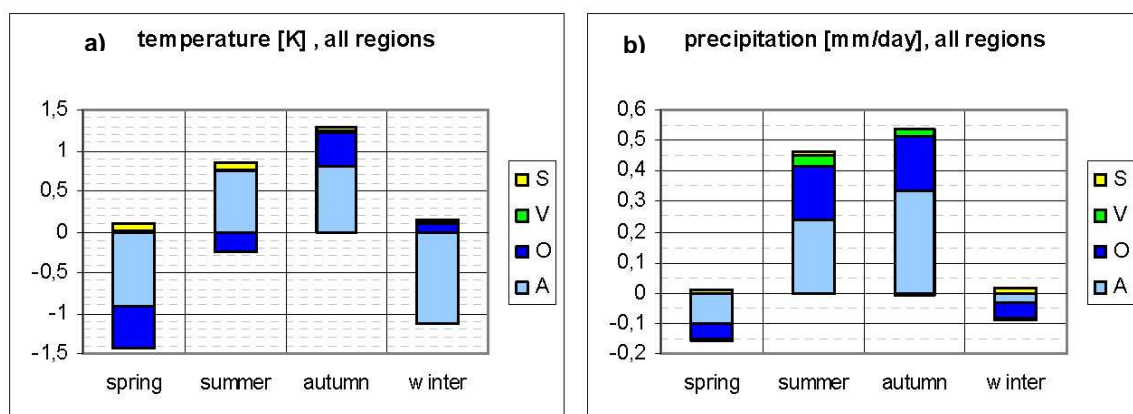


Figure 4.14: Same as Figure 4.5, but averaged over all six regions and periods. Robust as well as not robust contributions of the different factors are taken into account: left panel: temperature [K]; right panel: precipitation [mm/day].

reduction of  $-0.97\text{K}$  (on average) is determined by the colder mid-Holocene winter climate in the tropical regions (IND, INCPIN). Even though the variation of these seasonal temperature changes (i.e. warming in summer and autumn, cooling in winter and spring) is determined by the direct response of the atmosphere, the ocean alters the magnitude of the temperature difference. Due to its larger thermal inertia compared to the atmosphere, the ocean-induced response lags the insolation forcing by one month to one season. Therefore, the ocean-atmosphere feedback leads to an additional warming in autumn by  $0.41\text{K}$  and an additional cooling in spring by  $-0.51\text{K}$ . In summer and winter, the contribution of ocean-atmosphere interaction counteracts the direct effect by  $-0.24\text{K}$  and  $0.09\text{K}$ , respectively. Thus, the interactive ocean shifts the time of strongest warming from summer to autumn, and the strongest cooling from winter to spring. The small contribution of the interactive ocean in winter results from opposing temperature changes in the near-equatorial regions, i. e. cooling in IND and INCPIN, and warming in the other sub-regions.

As the monsoon dynamics mainly depend on the temperature gradient between the ocean and land, the shifted seasonal cycle of the oceanic response significantly affects the monsoon circulation. Due to the oceanic-induced cooling in summer and warming in winter, the ocean modifies the thermal processes in the monsoon system. The Tibetan Plateau is an area, where this mechanism might be particularly interesting. The Tibetan Plateau is a large elevated heat source in summer (March to October) and a weak heat sink in winter, exerting a strong impact on the Asian climate and the regional energy balance (Wu et al., 2007, Liu et al., 2007). By cooling the Plateau in summer and warming it in autumn, the ocean attenuates the magnitude of the heat source at the beginning of the monsoon season, which might affect the climate in the whole region. However, the detailed mechanism behind the feedback between ocean and the Tibetan Plateau is still not fully understood.

The contribution of synergy effect and interactive vegetation to the climate change is large for some simulation periods, but these signals are rarely robust. Robust effects are seen over the northern regions (TP, YANG), mainly due to changes in surface albedo. In the southern regions (IND, PAK, INCPIN), changes in evapotranspiration appear important. On average over all regions and periods, the influence of vegetation-atmosphere-interaction on mid-Holocene - present-day temperature differences are negligibly small. Only the synergy term tends to cause a slight warming from spring to autumn ( $0.06\text{K}$  to  $0.1\text{K}$ ).

Concerning precipitation, the strongest change is the shift and the strengthening of the summer monsoon season, causing a decrease in pre-monsoonal (spring) precipitation and an increased rainfall in summer and autumn between mid-Holocene and present-day climate. Whereas the East Asian monsoon is enhanced, the Indian monsoon flow is rearranged, leading to much more precipitation during mid-Holocene at the western and

northern coast of the Arabian Sea as well as the southern rim of the Tibetan Plateau. As for temperature, the largest precipitation differences between mid-Holocene and present-day climate can be attributed to the direct effect of orbitally induced insolation changes. However, the ocean significantly contributes to the total response. Changed sea surface temperatures in the coupled ocean experiments have a strong influence on evaporation and thus, the moisture supply to the monsoon systems. Furthermore, the ocean-atmosphere interaction modifies the large-scale circulation. The vegetation contributes only slightly to the precipitation change, mainly through the enhancement of evapotranspiration due to the enlargement of area covered by higher vegetation. The synergy has no influence.

Figure 4.14b illustrates the precipitation differences between mid-Holocene and present-day climate on average over all regions. Mid-Holocene summer precipitation-rate is increased by 0.46mm/day. Slightly more than 50% (0.24mm/day) of this change can be attributed to the direct response of the atmosphere. Ocean-atmosphere interaction further amplifies the rainfall by 0.17mm/day. However, this signal is strongly determined by the increase in precipitation over the Indian monsoon region (particularly over IND). The East Asian summer monsoon tends to weaken due to the ocean-atmosphere interaction. Precipitation is reduced, particularly over the ocean. Over land the precipitation associated to the East Asian summer monsoon is only little affected by the ocean-atmosphere interaction. The interactive vegetation further contributes to the enhancement of the summer monsoon by 0.04mm/day, mainly over the Indian monsoon region (PAK and IND).

In autumn, the most of the precipitation differences between mid-Holocene and present-day climate (in total: 0.53mm/day) can be attributed to the direct response of the atmosphere to the insolation change (0.33mm/day). As in summer, the ocean-atmosphere interaction and also the vegetation-atmosphere interaction further enhance the precipitation-rate by +0.18mm/day and 0.02mm/day, respectively.

During mid-Holocene, springtime precipitation is reduced compared to present-day by some -0.14mm/day on average over all regions. Approximately two-third of this difference is caused by the direct response of the atmosphere to the insolation change; one-third can be attributed to ocean-atmosphere interaction. The reduced precipitation-rate in winter (-0.08mm/day) is mostly associated with ocean-atmosphere feedback. The vegetation-atmosphere interaction has on average no influence in both seasons.

Although the ocean-atmosphere feedback appears positive averaged over all domains, our regional analyses reveal a negative feedback in some regions and seasons. The most remarkable example is IND, showing a strongly negative ocean-atmosphere feedback in summer. In that region, the atmosphere-only run suggests less precipitation in 6k compared to present-day. The ocean is able to overcompensate the direct effect, yielding to the wetter

climate in 6k. Whether the ocean-atmosphere feedback can be interpreted as either positive or negative, thus, depends on the spatial averaging (regionally versus entire monsoon region).

Before discussing our model simulations in the context of other studies, we compare our results for the Asian monsoon region with the results of Otto et al. (2009a) for the high northern latitudes.

Otto et al. (2009a) investigated the contribution of vegetation-atmosphere and ocean-atmosphere interactions to the near-surface air temperature change between mid-Holocene and present-day, based on the same set of experiments as in this study. They focused on the region north of 40°N. Despite the very different circulation systems determining the climate in the Asian monsoon region and the northern latitudes, the influence of feedbacks and the direct response of the atmosphere to the orbital forcing are on average similar. Differences between mid-Holocene and present-day temperature in both regions can mostly be attributed to the direct effect of changed insolation, modified by ocean-atmosphere interactions. The summer temperature rise is twice as large in the northern latitudes as in the Asian monsoon region. In autumn, the region north of 40°N experiences a stronger temperature increase (ca. 1.8K) due to the orbital forcing, although the positive insolation change is more pronounced in the tropics. On the one hand, this can be attributed to increased evaporation in the monsoon region, leading to a cooling of the near-surface atmosphere. On the other hand, the pronounced temperature rise north of 40°N reflects the large influence of the ocean-atmosphere feedback on the northern latitude temperature difference between mid-Holocene and present-day. Mainly due to changes in sea ice, the ocean-atmosphere feedback can even change the sign of the response of the system to orbital forcing in the regions north of 40°N: mid-Holocene winter at northern latitudes is warmer than today by approx. 0.3K despite weaker insolation during that season. The vegetation-atmosphere feedback plays a minor role in both regions. The reason for this is currently being investigated. For the Asian monsoon, we tentatively attribute the small effect of vegetation-atmosphere interaction to mid-Holocene – present-day climate difference to the fact that our model yields only small changes between mid-Holocene and present-day vegetation coverage. Although the model captures the main vegetation trend in the Asian region, the simulated change in forest cover is much smaller than found in reconstructions (e.g. Ren, 2007). Therefore, the model presumably underestimates the vegetation-atmosphere interaction. Further studies will have to focus on a detailed comparison of simulated and reconstructed climate using numerical experiments with much higher spatial resolution to capture the effect of strong variation in orography on atmospheric dynamics.

Comparison of our results with previous model studies is difficult, because a factor separation has not yet been applied to mid-Holocene model experiments for the Asian

monsoon region. Furthermore, most studies concentrate on the summer season. If comparable, our results are in line with recent studies. Like most of the models with interactive ocean and vegetation considered in PMIP2 (Paleoclimate Modelling Intercomparison Project, Phase 2, Braconnot et al. 2007b) our model reveals a pronounced summertime cooling in north India (up to 2K) and a warming outside the tropical monsoon region (up to 3K) as response to the orbital forcing. Our model also simulates the increase in precipitation associated with the enhancement of the summer monsoons reported by these studies. Nevertheless, the sign and magnitude of the different feedbacks calculated in our model partly deviate from other studies, particularly concerning precipitation. The atmosphere-only run suggests less summer precipitation in India (IND), the Bay of Bengal as well as the South China Sea and more precipitation on the southern Asian continent compared with the coupled simulations. Whereas this shift in ITCZ is also seen in other model studies above the ocean (Marzin and Braconnot, 2009a; (PMIP1), Braconnot et al., 2007a), a reduction of summer precipitation on land (India) is only detected in a few model simulations (Ohgaito and Abe-Ouchi, 2007 (annual); Li and Harrison, 2008). The spatial distribution as well as the magnitude of the annual/summer precipitation change attributed to the atmospheric response corresponds well with these two studies, although Li and Harrison (2008) suggest a more enhanced summer monsoon in South China.

Concerning the ocean-atmosphere feedback, our results confirm the conclusion that the ocean rather suppresses the direct atmospheric response in large parts of the Asian monsoon region in the summer season (Liu et al. 2004; Ohgaito and Abe-Ouchi, 2007; Li and Harrison 2008, Marzin and Braconnot, 2009b). But our results do not show an overall ocean-induced weakening of the summer monsoon like the simulations in these studies. Large parts of the Indian monsoon region (incl. IND and PAK) experience more precipitation due to the ocean-atmosphere feedback, counteracting the precipitation decrease suggested by the atmosphere-only run (IND). The precipitation in the East Asian monsoon region tends to decrease, particularly above the ocean. On average, the precipitation is enhanced (positive ocean-atmosphere feedback) on the continent, in summer as well as in autumn.

The vegetation-atmosphere interaction can only be compared to other model results with respect to the temperature change. The contribution of interactive vegetation tends to be weaker in our model (smaller than 0.5K in all seasons) than in simulations with prescribed mid-Holocene vegetation (e.g. Diffenbaugh and Sloan, 2002; Zheng et al., 2004). Diffenbaugh and Sloan (2002) suggest temperature change between  $-2\text{K}$  and  $+4\text{K}$  in the Asian monsoon region for summer and spring. The results of Zheng et al. (2004) are in the same order of magnitude ( $0\text{K}$  to  $3\text{K}$  in winter). The spatial distribution of the change is also different to our simulations. In particular, our model does not capture the large vegetation-induced winter warming in China like in Zheng et al. (2004) and proposed by

reconstructions (Yu et al., 2000). This might be a consequence of the underestimated simulated vegetation change for that region. Although our model captures the main vegetation trend, the modelled change in forest cover is much smaller than found in reconstructions (e.g. Ren, 2007). Regarding the coupled AOV-simulations of PMIP2 (Braconnot et al., 2007b), our results are within the range of magnitude of the contribution of vegetation-atmosphere interaction (summer season), but the vegetation-atmosphere feedback strongly varies between the different participating models.

Although our results provide a broad insight into the feedback mechanism, which might be involved in the Holocene Asian monsoon climate change, the magnitude of the feedbacks still requires further discussion. Slightly different boundary conditions (SST and sea-ice) lead to a high variability in the contribution of vegetation-atmosphere feedback and synergy to the overall signal as shown in the five different simulation periods. In most cases, both factors are not robust in any of the regions. In addition, our analyses reveal that, whether a feedback (e.g. ocean-atmosphere feedback) appears positive or negative strongly depends on the spatial averaging and therewith may also depend on the spatial resolution. The results in Chapter 3 suggest that climate model simulations performed in coarse numerical resolutions can represent the large-scale response of the Asian monsoon system to the Holocene insolation forcing. To resolve the regional dynamics, high numerical resolutions have to be used in climate modelling studies for the Asian monsoon region. However, since high resolution simulations performed with coupled ocean-atmosphere-vegetation models need lots of computing power, using coarse numerical resolutions is a good compromise.

### **Implication for the results in Chapter 3:**

Our analysis in Chapter 3 reveals that the high resolution simulation T106\_AV<sub>6k</sub> matches the paleoreconstructions best despite of the missing ocean-atmosphere interactions in this simulation. At this point, we return to the discussion of Chapter 3 and look at the contribution of the ocean-atmosphere interaction to the annual precipitation and temperature signal (Fig. 4.15). According to the coarse resolution model (T31\_AOV), the interactive ocean leads to an enhancement of the temperature signal simulated in T106\_AV and would probably neither improve nor worsen the reproducibility of the reconstructed temperature change in the model. The precipitation is increased in India and decreased in the other parts of the continental Asian monsoon domain by the ocean-atmosphere interaction so that the precipitation signal simulated in T106\_AV is amplified in most of the regions. Including an ocean model, therefore, would probably not change the conclusions gained in Chapter 3.

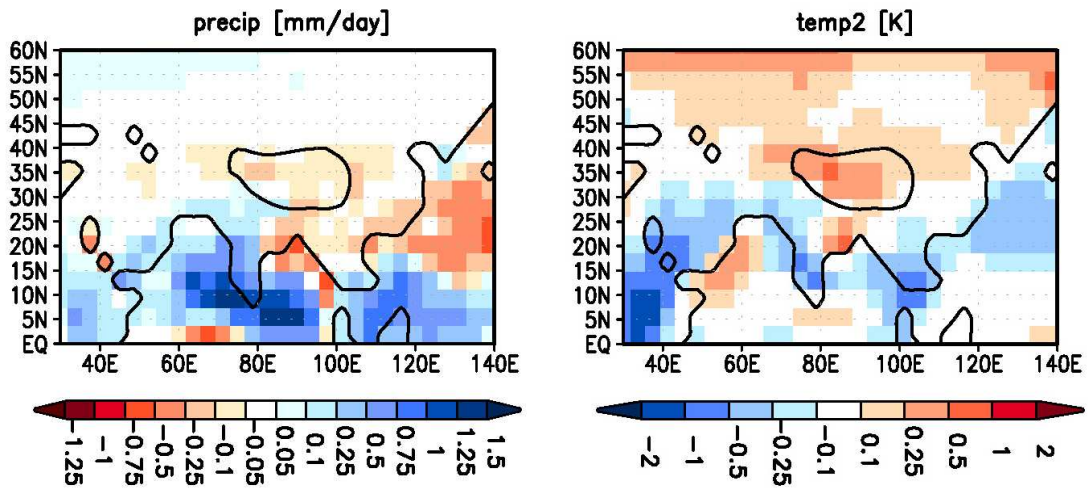


Figure 4.15: Contribution of the atmosphere-ocean interaction to the mid- to late-Holocene annual precipitation and temperature change as simulated by the coupled atmosphere-ocean-vegetation model ECHAM5/JSBACH-MPIOM.

## 5. Comparison of the simulated Holocene vegetation change with pollen-based vegetation reconstructions

### 5.1 Introduction

The Tibetan Plateau covers a region of approx. 2.5 million km<sup>2</sup>. With an average height of more than 4000m above sea level (a.s.l.), it penetrates deep into the troposphere reaching atmospheric levels of less than 500hPa. Due to its large horizontal and vertical extent, the Tibetan Plateau affects the regional as well as the global climate, including the circulation, energy and water cycle (Wu et al., 2007). Besides the mechanical blocking of zonal as well as meridional atmospheric flow (e.g. Wu et al., 2005; Liu Y. et al., 2007), thermal processes on the Tibetan Plateau strongly influence the regional circulation.

Regarding the influence of the land cover of the Tibetan Plateau on climate the following aspects are particularly important:

- Elevated heat source: Acting as a heat source for the atmosphere in spring and summer the Tibetan Plateau plays an important role for the onset and maintenance of the Asian summer monsoon (e.g. Wu and Zhang, 1998; Ye and Wu, 1998; Wu, 2004; Liu Y. et al., 2007).
- Huge air-pump: The large amount of air pumped up in the atmosphere above the Tibetan Plateau due to high convective activity diverges near the tropopause and subsides in North Africa, Central Asia and the Middle East. Thereby, the large-scale subsidence forces and forms dry climates and deserts such as the Sahara, Taklamakan Desert and Dzungar Desert. (Rodwell and Hoskins, 1996; Ye and Wu, 1998; Duan and Wu, 2005).
- Variations in the surface temperature: Recent studies proposed a strong relationship between the heating on the Plateau and the summer monsoon rainfall in East Asia (e.g. Hsu and Liu, 2003; Yanai and Wu, 2006; Zhang et al., 2006; Wang B. et al., 2008). Investigations based on observations as well as climate model sensitivity experiments suggest an enhancement of the moisture transport towards East Asia and increasing precipitation in the subtropical front (Mei-Yu, Baiu and Changma) in years with higher surface temperature on the Tibetan Plateau (Wang B. et al., 2008).
- Accumulation of snow: High-elevation snow accumulation is another important factor by which the Tibetan Plateau exerts influence on the Asian climate. Above-

normal snow cover in winter weakens the land-sea temperature gradient and attenuates the East Asian monsoon in the subsequent summer (Liu Y. et al., 2007).

All these processes depend to a large part on the land cover of the Tibetan Plateau as it modulates the energy balance and the energy transfer between the atmosphere and the land surface (Yasunari, 2007). The albedo of the surface determines the absorbed incoming solar radiation and therewith the strength of diabatic heat fluxes. Changes in the Tibetan Plateau's land cover may thus exert strong influence on the regional and even on the northern hemispheric climate and atmospheric circulation.

Beside the biogeophysical effects of changing albedo, surface roughness and evapotranspiration, land cover changes affect the climate via biogeochemical feedbacks, for example by the emission of carbon into the atmosphere (Claussen et al., 2001). Therefore, it is necessary to get more information about land cover changes on the Tibetan Plateau to understand past climate change in Asia.

So far, reconstructions suggest an increased mid-Holocene forest fraction on the eastern and southern margin of the Plateau compared to the present conditions (Shen et al., 2005; Shen et al., 2006). Enlarged monsoon rainfall and higher summer temperatures due to orbitally-induced insolation changes are seen as the most important forcing mechanisms for the vegetation change (Herzschuh et al., 2010a), but human impact is discussed as an influencing factor as well (Schlütz and Lehmkuhl, 2009). For the central Tibetan Plateau, reconstructions reveal only slight changes in vegetation composition during the Holocene (Tang et al., 2009). Fewer records are available for the western Tibetan Plateau. They indicate wetter climate conditions (Gasse et al., 1991) and more vegetation for the mid-Holocene.

As pollen reconstructions can only illustrate the local vegetation distribution and can only be taken as proxies for climate change, it is important to perform model simulations to identify the mechanism behind the changes. Furthermore, Earth System Models (ESM) have the advantage of calculating area-wide vegetation and climate changes, taking feedback mechanisms into account (Kleinen et al., 2011). Thereby, it is possible to extract the driving parameters, regarding the Holocene climate and vegetation change on the Tibetan Plateau and surrounding monsoonal areas; even more, related changes in the terrestrial carbon storage can be quantified.

Since computing power is limited, long transient experiments in comprehensive Earth system models can only be performed with coarse numerical resolutions. Such an experiment has been conducted by Fischer and Jungclaus (2011) with the model ECHAM5/JSBACH-MPIOM, covering the last 6000 years.

The primary aim of this study is to critically assess the performance of that model with respect to the land cover on the Tibetan Plateau. For this purpose, we compare pollen-

based vegetation reconstructions for different sites on the Plateau with the simulated potential vegetation trend in the surrounding areas. Anthropogenic land use changes are not taken into account by the model. Secondly, we want to identify the specific climatic parameters that caused the past vegetation changes. Thirdly, we quantify the total changes of simulated vegetation carbon storage for the entire Tibetan Plateau.

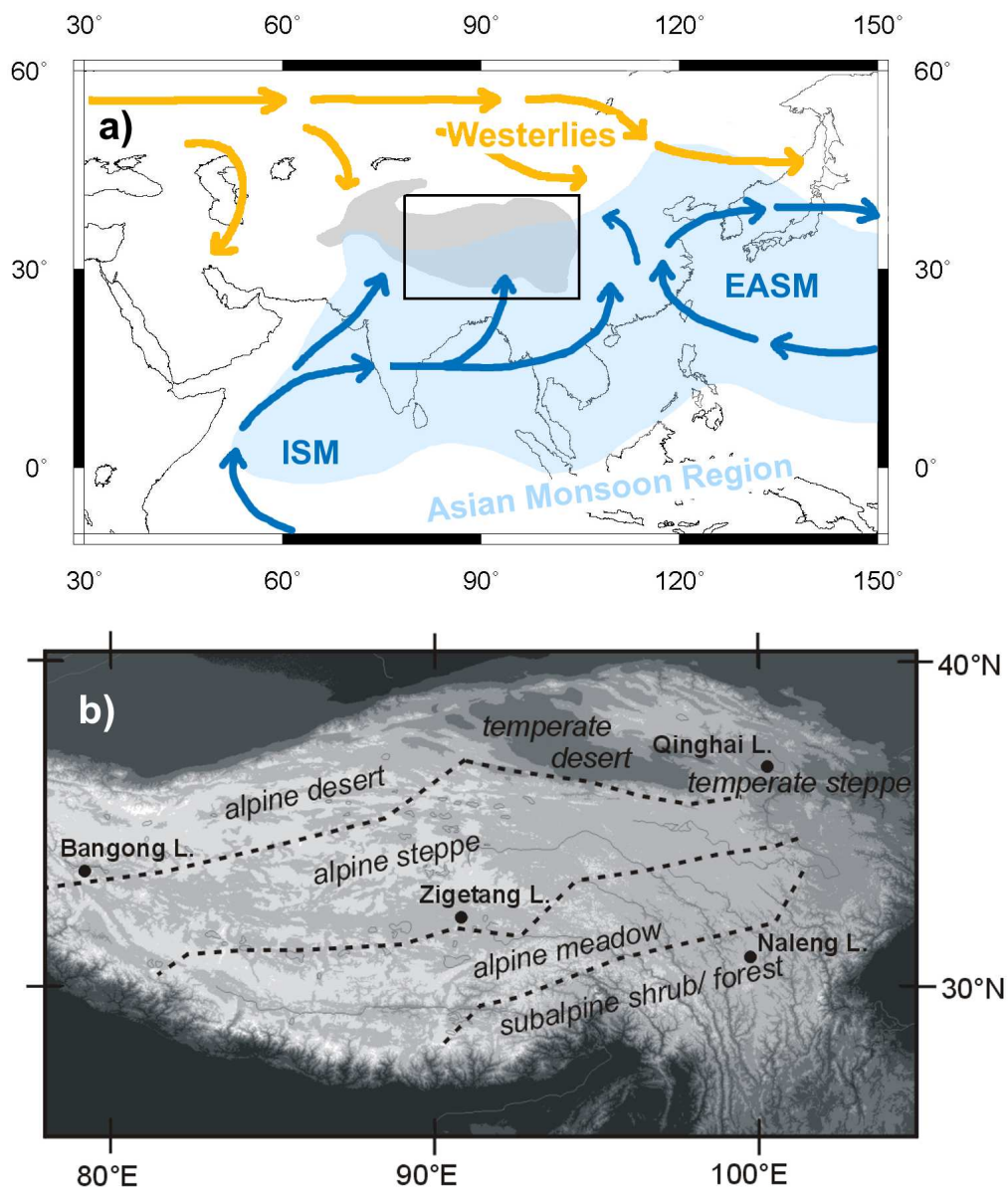


Figure 5.1: a) Sketch of the main atmospheric circulation systems (in 850hPa) affecting the Tibetan Plateau (grey-shaded) during the summer monsoon season, based on observations: Westerly wind circulation (orange), Indian summer monsoon circulation (ISM, blue) and East Asian summer monsoon circulation (EASM, blue). Light blue shaded region marks the Asian monsoon domain; b) shows the area marked as black rectangle in (a) and displays the distribution of the main vegetation types on the Tibetan Plateau (modified from Hou, 2001, by U.Herzschuh) and locations of the different study sites.

## 5.2 Study area

### 5.2.1 The Tibetan Plateau

The Tibetan Plateau covers almost one-sixth of the area in China. Located in a tectonically active region (ca. 80-105°E and 27-37°N), the Plateau exhibits a highly complex orography with steep and huge mountain ranges as well as large elevated plains (cf. Fig. A.2). The Tibetan Plateau penetrates deep into the troposphere. Thus, it shows unique climate conditions with the lowest surface temperature and pressure as well as highest 10-m wind speed compared to areas in the same latitudinal belt (Asnani, 1993).

Following the general decrease in altitude, near-surface air temperature and precipitation increase from the north-western to the south-eastern part of the Plateau. In summer, the Plateau is characterised by near-surface air temperatures up to 19°C in the south-east and ca. 6°C in the north-west (Sun, 1999). Winter temperatures are around 5-10°C in the south-east and -25°C in the north-west (Cui and Graf, 2009). Due to the strong insolation during daytime, near-surface air temperatures experience strong diurnal variations. Surface soil temperature varies up to 50°C (during spring) between day and night (Cui and Graf, 2009).

Annual precipitation ranges from approximately 700mm in the south-eastern part to less than 100mm in the north-western part (Sun, 1999), but precipitation strongly varies in time and space (Ueno et al., 2001). Besides the orography, precipitation distribution on the Tibetan Plateau is strongly determined by the large-scale atmospheric circulation. The southern and eastern parts are affected by the Asian summer monsoon (Figure 5.1a) that provides more than 80% of the annual total (Cui and Graf, 2009). The northern parts are affected by the westerly wind circulation bearing less precipitation.

The diverse climate conditions lead to a unique land cover on the Plateau. Strong temperature and precipitation gradients along the steep mountains offer a very heterogeneous environment for vegetation, but make the located vegetation also highly susceptible to climate change.

The spatial distribution of major vegetation types is described in the Vegetation Atlas of China (Hou, 2001) and summarised in Figure 5.1b. Present-day vegetation along the wet and warm south-eastern and eastern margins of the Tibetan Plateau is dominated by montane conifer and broad-leaved forests. However, loss of natural forest since at least during the past 2000 years and even more intense since the 1950s is attributed to anthropogenic forest clearance as a consequence of the high timber, grazing and agricultural ground demand of a constantly growing population (Studley 1999; Zhang et al. 2000; Dearing et al. 2008; Wischniewski et al., 2011). Only during the last three decades reforestation programs and a logging ban stopped the further forest loss in these areas

(Zhang et al. 2000; Fang et al. 2001). Above the treeline (ca. 3000-4000m), sub-alpine shrubs cover the area, replaced by alpine and high-alpine meadows at higher elevations. The dry north-eastern and central Tibetan Plateau is characterised by temperate and alpine steppe vegetation. Alpine deserts form the landscape at the dry north-central and western Plateau.

### 5.2.2 Study sites for pollen-based vegetation reconstructions

In this study, pollen records from four different lakes are considered, representing different climate and vegetation zones on the Tibetan Plateau (see Figure 5.1). These are Lake Qinghai and Lake Naleng on the north-eastern and south-eastern Tibetan Plateau, respectively, as well as Lake Zigetang on the central and Lake Bangong on the western Tibetan Plateau.

Lake Qinghai (36.55°N, 100.1°E, 3200m a.s.l.) has a surface area of about 4400km<sup>2</sup> and is the largest saline lake in China. Located at the north-eastern Tibetan Plateau and therewith in the fringe area of the Asian monsoon, the climate around the lake is influenced by three planetary-scale circulation systems: The region is not only characterised by the East Asian and Indian monsoon, but also affected by the westerly atmospheric flow (Xu et al., 2007). Thus, changes in climate, in particular the monsoon intensity, probably have a strong impact on the regional vegetation composition. Nowadays, the lake lies in the semi-arid and moderate cold climate zone with mean annual precipitation and temperature reaching approx. 250mm/yr and -0.7°C, respectively (Shen et al., 2005). The nearby climate station (Yeniugou, 99.58°E, 38.42°E, 3320 m a.s.l.) records a mean annual temperature of -2.5°C, a mean July temperature of 10°C and a mean January temperature of -16.3°C.

The vegetation immediately around the lake is characterised by temperate steppes dominated by *Artemisia* and *Poaceae*. The reconstructions used in this study are based on a 795cm long core (QH-2000) from the south-eastern part of the lake. For further description of the study site, material and dating see Shen et al. (2005).

Lake Naleng (31.1°N, 99.75°E, 4200m a.s.l.) is a medium-sized freshwater lake on the south-eastern Tibetan Plateau (area: 1.8km<sup>2</sup>). The pronounced relief and steep elevations in its environment lead to strong climatic and vegetational gradients. The climate around the lake is influenced by the Asian monsoon, yielding 90% of the annual precipitation (ca. 630mm/yr at a near climate station). The mean July temperature at the lake is ca. 7.4°C. Mean annual temperature is approximately 1.6°C (Kramer et al., 2010). Lake Naleng is situated at the upper tree line composed of *Picea*; the (sub-)alpine vegetation is composed of shrubs such as *Potentilla*, *Spiraea*, *Rhododendron* intermixed with *Kobresia* dominated meadows. Due to its location, climate change - especially variability in temperature - is expected to cause strong shifts in regional vegetation. The vegetation trend at this site is

analysed based on the upper part of a 17.8m-long sediment core. Details of the study site, materials and methods are described in Kramer et al. (2010).

Lake Zigetang (32°N, 90.9°E, ca. 4500m a.s.l.) is a large saline lake (surface area ca. 190km<sup>2</sup>) on the high-altitude inner Tibetan Plateau. The regional climate is cold and semi-arid, but still affected by the Indian monsoon circulation. Mean annual precipitation and temperature ranges from about 300-500mm/yr and from -2.6°C to -0.3°C, respectively. According to Naqu climate station (90.02°E; 31.48°N, 4500m a.s.l.), mean July temperature is 9.5°C and mean January temperature is -12°C. The vicinity of Lake Zigetang is covered by alpine steppe (dominated by Poaceae and *Artemisia*), but vegetation turns to alpine *Kobresia* meadows to the east of the lake. Further details are described in Herzschuh et al. (2006).

With a surface area of 604km<sup>2</sup>, Lake Bangong (33.42°N, 79°E, 4200m a.s.l.) is the largest lake on the western Tibetan Plateau. Located in the rain shadow of the Kunlun and Karakorum mountain ranges, climate around the lake is cold and very dry. Temperature ranges from -15.8°C in January to 11.9°C in July and are ca. -1.5°C in the annual mean. Precipitation originates mainly from the Indian monsoon, but does not exceed 70mm/yr (van Campo et al., 1996). Accordingly, montane desert/steppe-desert dominates the area characterised by a sparse vegetation cover. Pollen assemblages used in this study are based on a 12.4m core from the eastern part of the lake. For further information on the material and site see van Campo et al. (1996) and Fontes et al. (1996).

## 5.3 Methods

### 5.3.1 General model setup and experimental design

To estimate the mid- to late-Holocene vegetation change on the Tibetan Plateau a transient numerical experiment was analysed. The simulation was performed by Fischer and Jungclaus (2011) with the comprehensive Earth system model ECHAM5/JSBACH-MPIOM, developed at the Max-Planck-Institute for Meteorology. The model consists of the atmospheric general circulation model ECHAM5 (Roeckner et al., 2003) coupled to the land-surface-scheme JSBACH (Raddatz et al., 2007) and the ocean model MPIOM (Marsland et al., 2003; Jungclaus et al., 2006). JSBACH included the dynamic vegetation module of Brovkin et al. (2009). ECHAM5 ran with 19 vertical levels and a spectral resolution of T31, which corresponds to a latitudinal distance of ca. 3.75°, i.e. a grid-box width of about 354km at 32°N. The ocean-grid had a horizontal resolution of approximately 3° and 40 vertical levels. The models had been tested against observation and reanalysis data proving that they capture the major structure of global and regional climate (cf. Chap.2 and Cui et al. 2006).

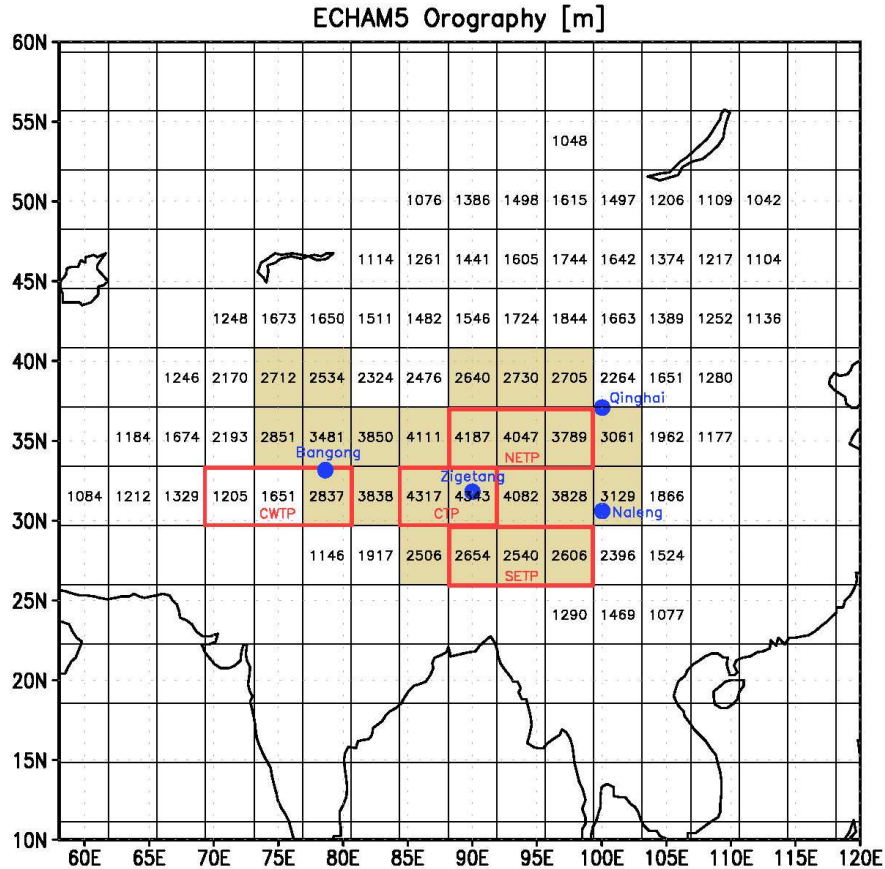


Figure 5.2: ECHAM5 orography (elevation higher than 1000m), model grid (T31) and grid boxes used for determining the averaged vegetation trend in four different regions on the Tibetan Plateau (red boxes). These are the north-eastern Tibetan Plateau (NETP), the south-eastern Tibetan Plateau (SETP), the central Tibetan Plateau (CTP) and the central-western Tibetan Plateau (CWTP). The locations of lakes sampled for vegetation reconstructions are also shown (blue dots). Shaded area marks the regions on the Tibetan Plateau which are elevated above 2500m in the model.

The transient experiment started at mid-Holocene climate conditions: Orbital parameters in the coupled models had been adjusted to the configuration 6000 years before present (henceforth referred to as 6k). Atmospheric composition had been fixed at pre-industrial values with CO<sub>2</sub>-concentration set to 280ppm. Under these boundary conditions, the model was brought to quasi-equilibrium climate state. Afterwards, the orbital configuration was continuously being changed until present-day (0k) conditions were reached. During the entire transient run, atmospheric composition stayed constant. The calculated climate change, thus, can be attributed to orbital forcing alone. Biogeochemical processes have no influence on the climate change.

Due to the coarse model resolution, it was not possible to take the geographically nearest grid-boxes around the lakes for the comparison of model results and reconstructions. Simulated present-day climate differs strongly from observations, since the orography in

the model is underestimated. Instead we use average over two to three grid-boxes in the vicinity of each lake showing an analogue vegetation trend (Figure 5.2). The grid-boxes have been selected by applying the following criteria: a.) The averaged climate in the grid-boxes represents the local climate at the study site more appropriately (e.g. Lake Qinghai, Lake Zigetang); b.) The grid-boxes are located upstream of the study sites with respect to the atmospheric circulation system effecting the site (e.g. Lake Bangong, Lake Naleng, Lake Zigetang).

### 5.3.2 Dynamic vegetation module

The dynamic vegetation module used in this study (Brovkin et al., 2009) distinguishes eight plant-functional types (PFTs), i.e. plants are grouped with regard to their physiology including their leaf phenology type. Trees can be either tropical or extratropical and are further differentiated between evergreen and deciduous trees. The module considers two shrubby vegetation types, namely raingreen shrubs and cold shrubs. The first is limited by moisture; the second represents shrubs limited by temperature. Grass is classified as either C3 or C4 grass.

For each PFT, environmental constraints are defined in the form of temperature thresholds representing their respective bioclimatic tolerance. These thresholds define the area, where establishment of a PFT is possible. They describe cold resistance by the lowest mean temperature of the coldest month ( $T_{c_{min}}$ ), chilling requirements by the maximum mean temperature of the coldest month ( $T_{c_{max}}$ ) and heat requirement for the growth phase. The latter is considered via the summation of temperature over days with temperature higher than 5°C, called growing degree days (GDD5). Cold shrubs are also excluded in regions with warm climate ( $T_{w_{max}}$ ). The values of the limits are listed in Table 5.1 and similar to the limits used in the biosphere model LPJ (Sitch et al., 2003).

For each grid-box of the atmosphere, the land surface is tiled in mosaics, so that several PFTs can be represented in a single grid cell. The fractional cover of each PFT is determined by the balance of their establishment and mortality. The latter is the sum of the mortality by the aging of plants and the disturbance-related mortality (fire and windbreak). The establishment is calculated from the relative differences in annual net primary productivity (NPP) between the PFTs and hence includes the different moisture requirements of the plants. Furthermore, the establishment is weighted by the inverse of the PFT specific lifetime, i.e. plants that live long establish slowly. The establishment of woody PFTs is favoured over grass, so that grass can only establish in the area, which is left after trees and shrubs have established. In the absence of disturbances, woody PFTs thus have an advantage over grasses and the woody PFT with the highest NPP becomes the dominant vegetation-type in the grid-box. Generally, trees have the highest NPP, since they have the largest leaf-area. However, in regions with frequent disturbances or in

unfavourable climate conditions, i.e. bioclimatic conditions near the thresholds, shrubs or even grass might win the competition as they can recover more quickly than trees.

For each grid cell, a non-vegetated area is considered as well, which represents the fraction of seasonally bare soil and permanently bare ground. Their fraction is calculated via the relation of maximum carbon storage in the pool representing living tissues to the carbon actually stored in this pool. This approach is based on the fact that plants need a certain amount of carbon to build their leaves, fine roots, etc., so that they can function properly. If the model calculates a positive NPP for a vegetation type, carbon is filled into this pool while carbon is lost from it proportional to the loss of leaves, which mostly happens in dry or cold seasons/periods. If the filling of the pool is not sufficient for all PFTs, plants cannot grow and the grid-cell is mainly non-vegetated. Simulated changes in vegetation cover thus can be attributed to bioclimatic shifts (i.e. temperature changes), changes in plant productivity (related to precipitation) or changes in the frequency of disturbances. More details about the dynamic vegetation module are described in Brovkin et al. (2009).

No.	landcover classification	phenology type	$T_{c_{min}}$ [°C]	$T_{c_{max}}$ [°C]	$T_{w_{max}}$ [°C]	GDD5 [°C]
1	tropical evergreen trees	raingreen	15.5	-	-	0
2	tropical deciduous trees	raingreen	15.5	-	-	0
3	extratrop. evergreen trees	evergreen	-32.5	18.5	-	350
4	extratrop. deciduous trees	summergreen	-	18.5	-	350
5	raingreen shrubs	raingreen	0	-	-	900
6	cold shrubs	summergreen	-	-2	18	300
7	C3 grass	grasses	-	15	-	0
8	C4 grass	grasses	10	-	-	0

Table 5.1: Bioclimatic limits for the 8 plant functional types (PFTs) used in the coupled model experiment. Listed are phenology type, PFT-specific minimum of coldest monthly mean temperature ( $T_{c_{min}}$ ), PFT-specific maximum of coldest monthly mean temperature ( $T_{c_{max}}$ ), PFT-specific maximum warmest monthly mean temperature ( $T_{w_{max}}$ ) and growing degree days, i.e. temperature sum of days with temperatures exceeding 5°C (GDD5). All temperature values are given in °C.

In this study, PFTs are further aggregated to the three major vegetation types ‘forest’ (containing all trees), ‘shrub’ and ‘grass’. The fourth land cover type ‘desert’ includes the non-vegetated area. To test the significance of the simulated land cover trend, a simple statistical test is used. We assume a significant trend if the absolute differences in mean land cover between the first 500years and the last 500year is greater than two times the

standard deviation of the entire time-series. Detailed results of this test can be seen in the Appendix (Table B.1). According to this test, most land cover trends are significant. If a trend is not significant, this fact is mentioned in the text.

### **5.3.3 Vegetation reconstruction (written by U. Herzschuh)**

The qualitative interpretation of pollen assemblages in terms of past vegetation (Birks and Birks, 1980) can be validated using a quantitative method for pollen-based biome reconstruction (biomisation, Prentice et al., 1996). Based on knowledge of the contemporary biogeography and ecology of modern plants, pollen taxa are assigned to plant functional types (PFTs) and the PFTs are assigned to main vegetation types (biomes). An affinity score for each biome is then calculated according to Prentice et al. (1996). The biome with the highest score dominates in the pollen-source area of the lake, while a relatively lower score indicates less occurrence of a biome in the area. Scores cannot be compared between different records. The pollen taxa-biome matrix (Table B.2) applied in this study is based on the standard biomisation procedure presented by Yu et al. (1998) and their later improved version (Yu et al., 2000). A test of this method with a modern pollen data set of 112 lake sediment-derived pollen spectra from the Tibetan Plateau yielded a correct assignment of 100% of temperate desert sites, 75% of temperate steppe sites, 84% of alpine steppe sites and 79% of alpine meadow sites (Herzschuh et al., 2010a). Patchy forest sites intermixed with alpine shrublands were mostly assigned to temperate or alpine steppes as no shrub biome was considered in this study. Here, we summarized the different biomes so that they fit best to the modelled vegetation types, namely forest, shrub, steppe/meadow and desert. The biome-taxa matrix is based on information on the distribution of the single pollen taxa with respect to vegetation types and biomes presented in Herzschuh et al. (2010b and 2010c). The pollen-based reconstructions describe the vegetation trend qualitatively. The dominant vegetation type and the general trend can be inferred, but no conclusions on vegetation fraction and ratios can be made.

We are aware of differences in the handling of vegetation in the model and in the reconstructions. These differences have historical and technical reasons. Whereas the reconstructed vegetation is usually assigned to plant functional types (PFT) and then to biomes, simulated vegetation is grouped in plant functional types. These or the specific combinations of them then serve as major vegetation types. Nevertheless, we think it is most reasonable to compare pollen-based biomes with model-derived PFT coverages than to directly compare pollen-based PFTs with model-derived PFTs. The advantage of this method is particularly obvious in the case of model-proxy comparisons of deserts or of forested areas. The biome desert, for instance, contains vegetation such as *Ephedra* and Chenopodiaceae that can survive in extremely dry climatic conditions and are therefore representative for a desert environment and reach up to 100% here. In the model, no such

vegetation type exists and the land cover type ‘desert’ is only represented by the non-vegetated area (bare ground). Thus, to compare the pollen-based desert biome to the model bare ground (which also includes only seasonally bare ground) is most reasonable as the same bioclimate is assumed for these vegetations. In forest biomes, pollen-PFT-biome assignment also account for vegetation growing in the understorey such as herbs of Rubiaceae. Thus, vegetation cover can exceed 100% (due to more layers). In the model, vegetation competes for 100% of the grid-box and has to be arranged side by side, herb (Grass PFT) does only out-compete trees due to bioclimatic limitations.

## 5.4 Results

The reconstructed biome trends (forest, shrubland, steppe/meadow, desert) for all sites are illustrated in Figure 5.3. Figure 5.4 shows the corresponding simulated vegetation trend as averages over 20 years which is the highest temporal resolution is occurring in the reconstructions. Thereby, the simulated land cover is divided into forest, shrub and grass fraction as well as non-vegetated area, which is further referred to as desert. Simulated climate and vegetation changes are attributed to orbital forcing alone.

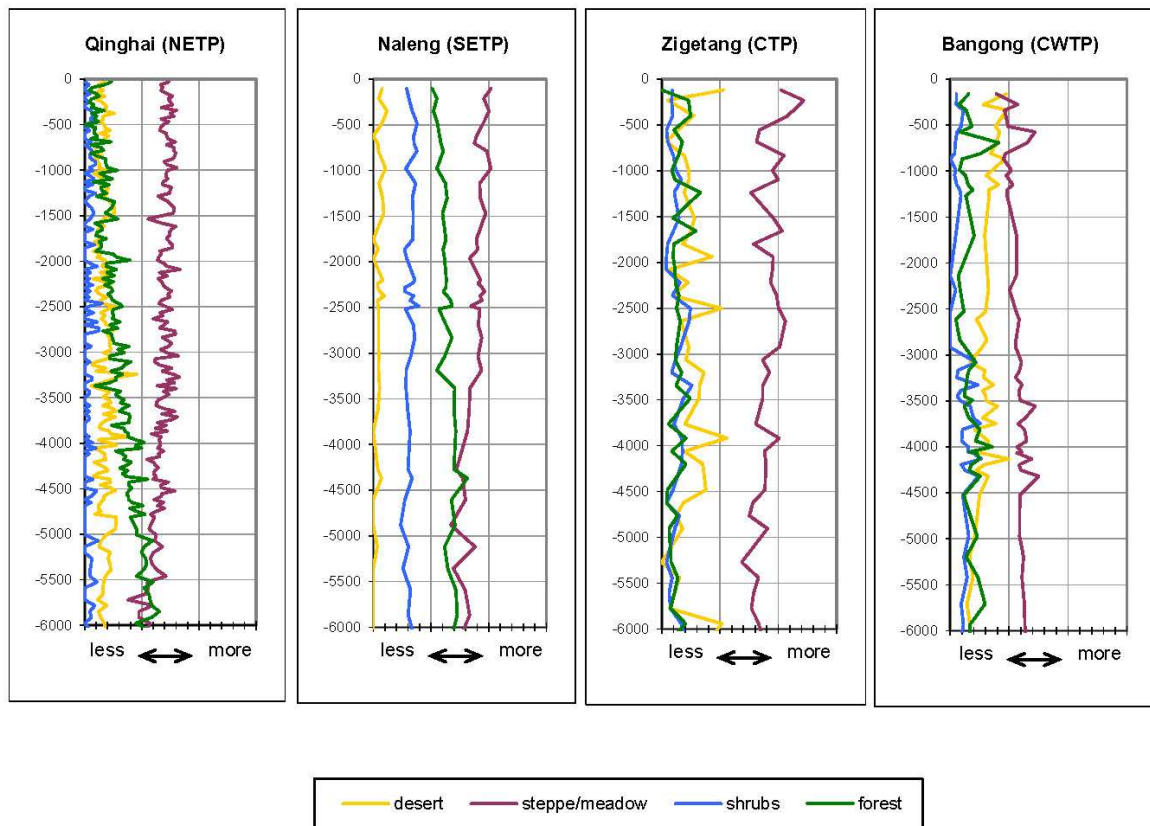


Figure 5.3: Reconstructed vegetation trend from mid-Holocene (6000yrs before present) to present-day, based on four different lake sediment cores on the Tibetan Plateau (in arbitrary units).

The pollen record of Lake Qinghai (north-eastern Tibetan Plateau) reveals a continuous decrease of forest cover since the mid-Holocene (6k) and an expansion of steppe/meadow vegetation. Whereas forests and steppe/meadow dominated the land-cover at 6k, steppe/meadow is the prevalent biome at present-day (0k). Shrub vegetation, as well as desert vegetation, covers only small areas and does not show obvious trends through time. In line with the reconstructions of Qinghai Lake, the simulated vegetation trend on the north-eastern Tibetan Plateau (NETP) shows a continuous forest decline and an expansion of grassland during the last 6000 years. Forest as the dominating land cover type during the mid-Holocene (approx. 38% of the area) is halved until present-day. Grass and shrub fractions increase by 67% and 64%, covering 39% and 19% of the area at 0k, respectively. Thus, grass is the prevalent vegetation simulated and reconstructed for the north-eastern Tibetan Plateau at present-day. The desert fraction slightly decreases from 27% at 6k to 23% at 0k.

The pollen-based vegetation reconstruction from Lake Naleng (south-eastern Tibetan Plateau) suggests a qualitatively similar vegetation trend. During the mid-Holocene, steppe/meadow and forest were the dominant biomes. Around 4.3k, forests started to

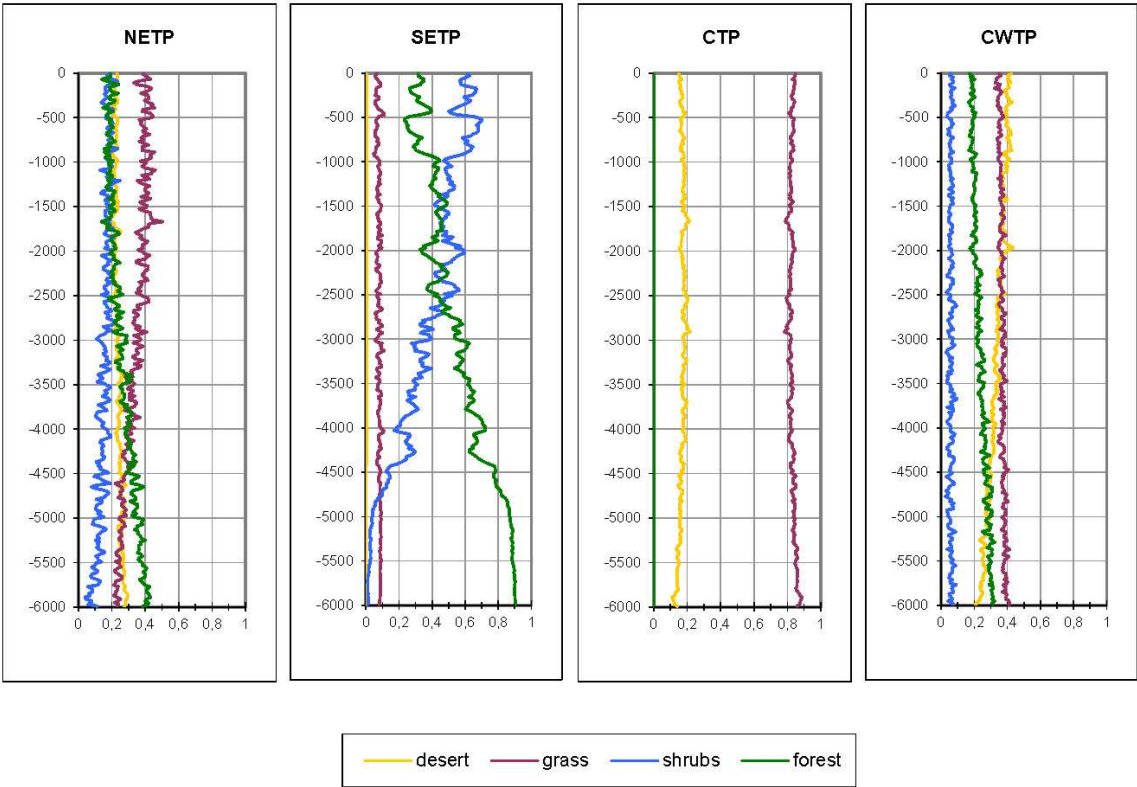


Figure 5.4: Simulated vegetation trend (20yr-mean) from mid-Holocene (6000 years before present) to present-day, averaged for 4 different regions on the Tibetan Plateau: the north-eastern Tibetan Plateau (NETP), the south-eastern Tibetan Plateau (SETP), the central Tibetan Plateau (CTP) and the central-western Tibetan Plateau (CWTP), see Figure 5.2. Values are given in fraction per grid box.

retreat and were replaced by steppes and meadows. Thus, pollen abundances clearly reveal that steppe and meadow vegetation dominate in the area of Lake Naleng for present-day. Desert and shrub vegetation have stayed low constantly since 6k. The simulated mid-Holocene land-cover on the south-eastern Tibetan Plateau (SETP) mainly consists of forest (91%) and to a lesser extent of grass and shrubs (8% and 1%, respectively). This vegetation distribution is constant for nearly 1200 years until shrubs successively replace forest. This decrease of forest fraction agrees with the reconstruction from Lake Naleng, but in the reconstructions steppe/meadow and not shrub fraction increase. A strong fluctuation in the modelled vegetation trend indicates an occasionally recovering tree fraction. At 0k, shrub is the dominant land cover type according to the model (61% of the area), while forests form only 31% of the landscape. Desert (0%) as well as grass fraction stays constant for the whole 6000 years.

Lake Zigetang is situated on the high-altitude central Tibetan Plateau. At 6k as well as 0k, the area is primarily covered by steppe/meadow vegetation. The reconstructed Holocene vegetation change is small, but exhibits a slight increase of steppe/meadow vegetation. The occurrence of desert is highly variable. Shrub and tree pollen taxa occur with low but steady abundances. In contrast to the pollen record, the model simulates no forests and no shrubs on the central Tibetan Plateau (CTP) for the last 6000 years. Like in the reconstructions, grass covers most of the area at 6k (86%) as well as at 0k (85%). The simulated vegetation change is small and not significant. However, grassland is slightly retreating during the first 3000 years (to 80% at 3k) and increasing again afterwards.

The pollen record of Lake Bangong from the western Tibetan Plateau depicts a regional reduction of vegetation during the last 6000 years. Forest, as well as steppe/meadow vegetation, has decreased; desert indicating plants have spread since the mid-Holocene. Whereas steppe was the dominant biome at 6k, pollen concentrations suggest land coverage of desert and steppe in equal parts for present-day. In agreement to the reconstructions from Lake Bangong, the model calculates an overall decrease of vegetated area on the central-western Tibet Plateau (CWTP). Whereas grass (41%) and forest (31%) characterise the landscape during the mid-Holocene, desert (42%) dominates the region at present-day. Simulated forest fraction is nearly halved, desert fraction more than doubled during the last 6000 years. Shrub and grass only decrease by ca. 15%, respectively, but the trend in shrub cover is not significant according to the simple statistical test used in this study.

Overall, the reconstructed and simulated vegetation trends are in agreement, albeit some systematic differences appear. The potential reasons for these differences are discussed in the following section.

## 5.5 Discussion of Chapter 5

### 5.5.1 Potential reasons for disagreements in the simulated and reconstructed vegetation cover

The pollen-based vegetation reconstructions in this study may be influenced by the following factors:

(1) Especially pollen spectra from large lakes such as Qinghai Lake contain a large extra-regional pollen component that increases with lake size (Jacobsen and Bradshaw, 1981) and strongly depends on regional atmospheric conditions (Gehrig and Peeters, 2000). Local pollen production and vegetation composition influence the concentration of long-distance-transported pollen grains as well. Therefore, extra-regional pollen load may vary with time. Since the Tibetan Plateau exhibits a highly heterogeneous, often treeless environment with steep elevations and pronounced vegetation gradients, the problem of extra-regional pollen advection to the lakes is particularly large. The topography of the Tibetan Plateau can form strong anabatic winds transporting pollen from lower vegetation (forest) belts to steppe and desert zones (Markgraf, 1980; Cour et al., 1999; Kramer et al., 2010).

(2) Pollen-productivity and hence its representation in the pollen record depends on the plant species. Most subalpine shrubs, for instance, are poor pollen-producers and thus have a low representation in pollen spectra (van Campo et al., 1996; Herzschuh et al., 2010b). Hence, shrub coverage is most probably underestimated in our biome reconstructions.

(3) Most pollen can only be identified to genus or family level. The assignment of pollen taxa to biomes within the biomisation techniques is therefore a strong simplification of the natural conditions. The most common biomes on the Tibetan Plateau, desert and steppe, share many pollen taxa even though the pollen producing plants belong to different species. Biomisation of fossil pollen assemblages from such non-forested areas often faces the problem of that neighbouring samples were assigned to different biomes despite no shifts in the pollen signal are obvious. This rather reflects ecological noise than a true biome shift because the assignment of the dominant biome is very sensitive to small variations of affinity scores between pairs of closely matched biomes such as desert, steppe or meadow. We face this problem by presenting the affinity score differences between the most important biomes at each site.

The simulated vegetation trend is limited by the following factors:

(1) Due to the coarse numerical resolution (T31L19), the orography is not represented well in the model. This especially applies to the Tibetan Plateau. Whereas its mean elevation

exceeds 4000m in reality (cf. Fig. A.2), orography in the model reaches 4000m at most and only in a few grid-boxes on the central Tibetan Plateau. The Himalaya and the Kunlun Mountains, as well as other mountain ranges, vanish. In reality, the strong spatial variance in orography (e.g. at Lake Naleng) implies a high heterogeneity of regional climate and vegetation, which cannot be captured in the model and may lead to discrepancies between the model results and reconstructions.

(2) Compared to annual mean 2m-temperatures of European Centre for Medium-Range Weather Forecast Reanalysis (ERA40; Simmons and Gibson, 2000), simulated climate is too cold on the central and south-eastern Tibetan Plateau (up to  $-2.8^{\circ}\text{C}$ ) and too warm on the northern Tibetan Plateau (see Figure 5.5). Maximal positive temperature anomalies of up to  $7.2^{\circ}\text{C}$  occur on the north-western Tibetan Plateau. These differences between the model and reanalysis-data may partly arise from a lower (pre-industrial) greenhouse-gas concentration in the model. The comparison of the model output with observations (here: Global Precipitation Climatology Project (GPCP); Adler et al., 2003) also shows that the Asian summer monsoon intensity is overestimated in the central and southern regions of the Tibetan Plateau (see Figure 5.5). Summer (JJA) precipitation anomalies reach values of up to ca. 7.5mm/day. The simulated vegetation depends on certain climate thresholds, e.g. bioclimatic limiting factors. Therefore, biases in the calculated climate may lead to errors in the vegetation distribution and vegetation trend, particularly if the simulated local climate is near these thresholds, where sensitivity of land cover to climate change is expected to be large.

(3) To avoid large climatic biases to observations, vegetation studies are often conducted by prescribing a biases-corrected climate (i.e. sum of simulated climate anomaly and observed mean climate) to a vegetation model instead of using a dynamically coupled atmosphere-ocean-vegetation model (e.g. Wohlfahrt et al. 2008; Miller et al. 2008). This anomaly-approach is particularly useful in climate impact studies but has the drawback of not taking feedbacks between the climate and vegetation into account. Previous climate modelling studies suggest that vegetation and land-surface feedbacks with the atmosphere could have enhanced the orbitally-induced Holocene climate change in monsoon regions (e.g. Claussen und Gayler, 1997; Broström et al., 1998, Diffenbaugh and Sloan, 2002; Levis et al. 2004; Li and Harrison, 2009). In ECHAM5/JSBACH-MPIOM, the overall contribution of the vegetation-atmosphere interaction to the Holocene climate change in the Asian monsoon region is small (Dallmeyer et al., 2010). However, in regions showing a strong land cover change (e.g. in parts of the Tibetan Plateau or the present-day monsoon margin), the Holocene vegetation change has a significant effect on the simulated climate. Therefore, we decided to use a coupled atmosphere-ocean-vegetation model in the current study to account for nonlinearities in the climate system, albeit this method may lead to biases in land cover trend.

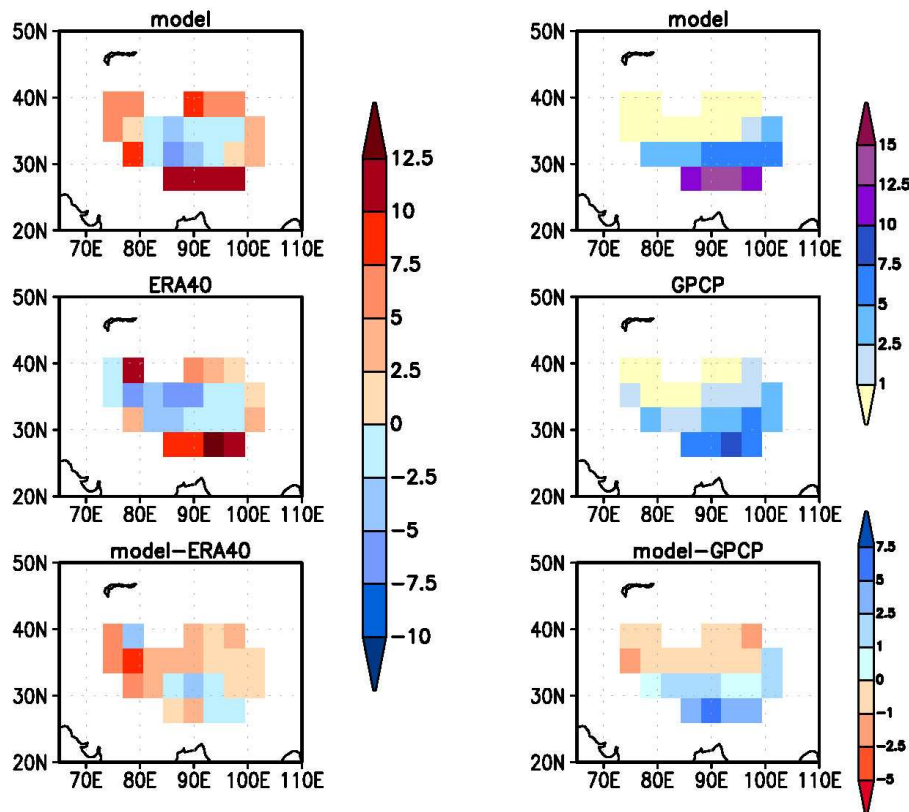


Figure 5.5: Annual mean 2m-temperature in °C (left panel) and summer precipitation in mm/day (right panel) calculated from the last 100 years of our coupled model experiment and a reference dataset. For temperature, results are compared with the reanalysis data ERA40 (Simmons and Gibson, 2000); for precipitation, observational data GPCP (Adler et al., 2003) is used. Shown are also differences between model results and the reference dataset.

(4) Anthropogenic land cover change is another potential source of error as this cannot be depicted with our model configuration, but may be included in the reconstructions. Nomadic people may have influenced the mid-Holocene land-cover on the Tibetan Plateau, at least on lower elevations. The earliest Neolithic settlement on the south-eastern Tibetan Plateau took place at an age between 6.5k and 5.6k (Aldenderfer, 2007). Humans lived on the margin of the north-eastern Tibetan Plateau at least seasonally during the period 9k-5k (Rhode et al. 2007). The expansion of Neolithic cultures coincides well with the forest decline in regions north-east of the Tibetan Plateau (Aldenfelder and Zhang, 2004; Brantingham and Gao, 2006) and in China (e.g. Ren, 2000). To what extent humans influenced the Holocene vegetation change on the Tibetan Plateau is still a matter of discussion (Schlütz & Lehmkuhl, 2009; Herzsuh et al., 2010a).

## 5.5.2 Site-specific discussion of the vegetation change

In the following, the indices 'ann', 'wm' and 'cm' stand for annual, warmest month and coldest month, respectively. The indices '0k' and '6k' denote the simulated present-day and mid-Holocene climate, respectively.

### 5.5.2.1 North-eastern Tibetan Plateau

The simulated present-day climate on the north-eastern Tibetan Plateau (NETP) is dry and cold. Annual mean precipitation ( $p_{ann0k}$ ) and temperature ( $T_{ann0k}$ ) are 230mm/yr and  $-1.8^{\circ}\text{C}$ , respectively (Table 5.2). Thus, the calculated mean climate is in general agreement with observations around Lake Qinghai ( $T_{ann} = -0.7^{\circ}\text{C}$ ,  $p_{ann} = 250\text{mm/yr}$ ). Simulated temperatures range from  $T_{cm0k} = -15.3^{\circ}\text{C}$  in the coldest month to  $T_{wm0k} = 9.3^{\circ}\text{C}$  in the warmest month. Therefore, the only possible woody PFTs are cold shrubs and extratropical forests (cf. Figure C.5). At 6k as well as 0k, the bioclimatic conditions of these PFTs are only partly fulfilled, because the limit for the growing degree days above  $5^{\circ}\text{C}$  is not always reached (Figure 5.6). Due to the warmer summer season during the mid-Holocene ( $T_{wm6k} = 10.6^{\circ}\text{C}$ ) compared to present-day, trees can grow easier at that time. The

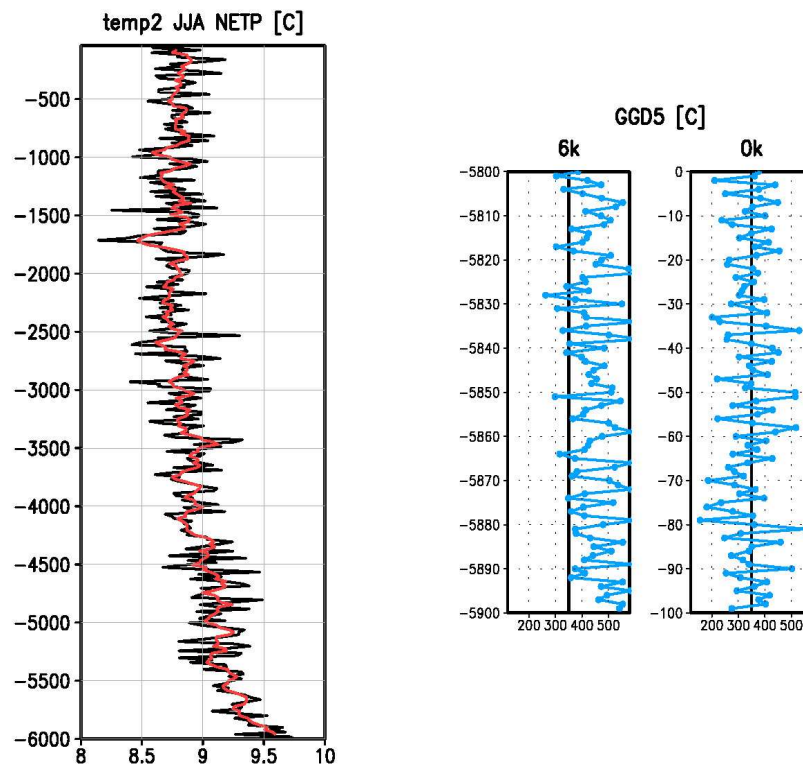


Figure 5.6: Change of the climate factors yielding the land cover change on the north-eastern Tibetan Plateau (NETP), left panel: 20yr-mean summer near-surface air temperature trend [ $^{\circ}\text{C}$ ] from mid-Holocene (-6000yrs) to present-day. The red solid line shows the 100yr-running-mean. Right panel: difference in growing degree days between 100 years of the mid-Holocene (-5900yrs to -5800yrs) and the last 100 years of the simulation period representing present-day. The solid black line marks the GDD5 threshold for extratropical forest of  $350^{\circ}\text{C}$ .

extension of the growth phase, as well as the higher amount of precipitation ( $p_{\text{ann}6k} = 290\text{mm/yr}$ ), provides a more favourable climate for trees. The orbitally-induced gradual cooling towards present-day results in a decline of forest and an increase of grass.

The similarity between the simulated and reconstructed vegetation trend suggests a natural climate change (summer insolation) as the main driving factor for the decreasing forest fraction on the north-eastern Tibetan Plateau. The simulation confirms recent results of a rather minor role of human activity in forming the land cover change in the area (Herzschuh et al., 2010a). However, the model results clearly point out warm season temperatures (GDD5) as the controlling factor, whereas reconstructions identified monsoon intensity related precipitation changes as the primary explanation for the vegetation trend (Herzschuh et al., 2010a). Stable oxygen-isotope measurements performed on ostracod valves suggest a wetter climate during the early-Holocene (9k-6k), a strongly decreasing precipitation trend until 3k and rather stable conditions afterwards (Liu X. et al., 2007).

Site	Location	$H_{\text{real}}$ [m a.s.l.]	$H_{\text{mod}}$ [m a.s.l.]	$p_{\text{ann}}$ [mm/yr]	$p_{\text{ann,mod}}$ [mm/yr]	$t_{\text{ann}}$ [°C]	$t_{\text{ann,mod}}$ [°C]
Qinghai	36.55°N, 100.1°E	3200	4008	250	230	-0.7	-1.8
Naleng	31.1°N, 99.75°E	4200	2600	630	1850	1.6	11.1
Zigetang	32°N, 90,9°E	4500	4330	300-500	743	-2.6 - -0.3	-4.8
Bangong	33.42°N, 79°E	4200	1898	70	250	-1.5	16.5

Table 5.2: Simulated present-day (mod) and observed orographic height (H), annual mean temperature ( $t_{\text{ann}}$ ) and precipitation ( $p_{\text{ann}}$ ) at each site on the Tibetan Plateau.

### 5.5.2.2 South-eastern Tibetan Plateau

Lake Naleng is located at an elevation of 4200m, whereas the mean orography prescribed to the model reaches only 2600m in SETP (Table 5.2). Therefore, the simulated annual temperature and precipitation are highly overestimated ( $p_{\text{ann}0k} = 1850\text{ mm/yr}$ ,  $T_{\text{ann}0k} = 11.1^\circ\text{C}$ ). Bioclimatic conditions ( $T_{\text{cm}0k} = 1.6^\circ\text{C}$ ,  $T_{\text{wm}0k} = 17.3^\circ\text{C}$ ) support growing of raingreen shrubs and extratropical forests as the only possible woody PFTs (Figure C.6).

In this area, the model simulates a higher NPP for raingreen shrubs than for extratropical trees (Figure C.6), so that the preferred land cover type would be shrubs. Due to less winter insolation at 6k, the region experiences a colder winter climate than at present-day

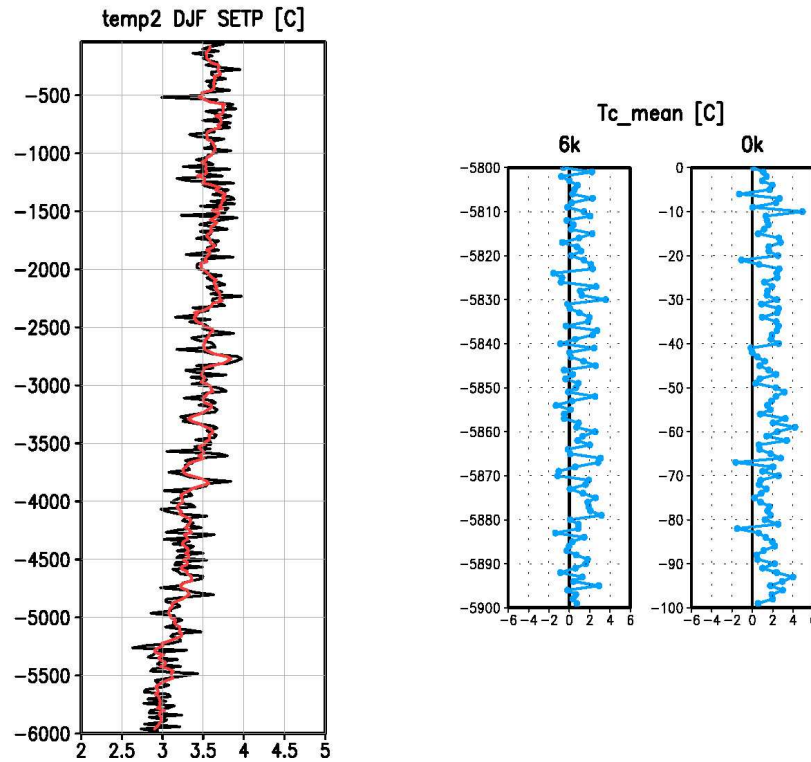


Figure 5.7: Change of the climate factors yielding the land cover change on the south-eastern Tibetan Plateau (SETP), left panel: 20yr-mean winter near-surface air temperature trend [ $^{\circ}\text{C}$ ] from mid-Holocene (-6000yrs) to present-day. Red solid line shows the 100yr-running-mean. Right panel: difference in mean near-surface air temperature of the coldest month between 100 years of the mid-Holocene (-5900yrs to -5800yrs) and the last 100 years of the simulation period representing present-day. Raingreen shrubs are limited by frost events; the solid black line marks the freezing point ( $0^{\circ}\text{C}$ ).

( $T_{\text{cm}6\text{k}} = 0.8^{\circ}\text{C}$ ). Frost events occur regularly (Figure 5.7). Therefore, raingreen shrubs are excluded as mid-Holocene land cover due to less favourable bioclimatic conditions. With increasing winter insolation, the cold season becomes warmer and frost events rare. Given a higher NPP in the model, raingreen shrubs are then able to successively replace the evergreen trees. However, the vegetation cover fluctuates, because frost events still occur with lower frequency.

Whereas the pollen reconstructions show an increase of steppe/meadow towards present-day, the model calculates shrubs as the forests-replacing land cover type. This difference in vegetation trend may partly result from the strong temperature bias of the model. The simulated annual mean temperature in SETP is nearly  $10^{\circ}\text{C}$  higher than observed and well above the freezing point. Given the observed annual mean temperature ( $T_{\text{ann}} = 1.6^{\circ}\text{C}$ ), frost would still limit the occurrence of shrubs and growing of shrubs would probably have been impossible during the entire 6000 years. Simulated present-day land cover would, then, primarily be forest.

Furthermore, human activity cannot be excluded from having an influence on the vegetation trend and modern distribution. Grazing indicators suggest human impact on the environment around Lake Naleng since 3.4k (Kramer et al., 2010). Thus, forest clearance as well as fire activity and grazing may have contributed to the forest decline on the south-eastern Tibetan Plateau (Schlütz & Lehmkuhl, 2009).

Pollen reconstructions assume decreasing summer temperatures as the major controlling climate factor, causing a downward shift of the treeline (Kramer et al., 2010). As Lake Naleng is situated in an area where forests gradually pass into subalpine shrub and alpine meadow, a transition from forest to shrubland during the Holocene would have been possible as well. Since shrub genera in that area, such as *Potentilla*, *Caragana*, *Spiraea*, *Rhododendron*, are poor pollen producers, shrubby vegetation may be underestimated in the vegetation reconstruction from Lake Naleng pollen spectra.

However, winter temperature is the main driving climate factor for the vegetation trend in the model. With regard to the discrepancy in local climate, the simulated vegetation trend should be interpreted in a broader sense: During the mid-Holocene, colder winters provided more unfavourable climatic conditions for frost-sensitive plants than at present-day. With increasing winter temperatures they might have had a chance to establish in spite of the pressure of other competitive, frost-resistant plants.

### 5.5.2.3 Central Tibetan Plateau

The simulated climate on the central Tibetan Plateau is cold and relatively wet. Annual mean precipitation is overestimated by the model (Table 5.2). It reaches 743mm/yr, mainly provided by the Indian summer monsoon. With annual mean temperatures well below freezing point ( $T_{ann0k} = -4.8^{\circ}\text{C}$ ), climate conditions are too cold to allow the establishment of woody PFTs (Figure C.7). Even in the warm season, mean temperatures do not exceed  $4.5^{\circ}\text{C}$ . Therefore, the annual temperature sum is not high enough to exceed the bioclimatic limit of growing degree days needed to get woody vegetation in the model.

These climate conditions have not changed much during the 6000 years of simulation. The calculated vegetation trend seems to follow the mean summer (JJA) temperature (Figure 5.8). Lower temperatures around 3k yield a slight decrease of the grass fraction, indicating warm season temperatures as the controlling climate factor for the vegetation trend.

While the model simulates no forest and shrub on the central Tibetan Plateau, reconstructions for Lake Zigetang reveal at least a low pollen contribution from these vegetation types. These pollen grains represent low-elevation vegetation and have apparently been transported from far regions by the atmospheric wind circulation. This extra-regional pollen component is slightly higher during the late Holocene, when the regional vegetation is characterised by more openness as indicated by the increase ruderal and desert plants such as Brassicaceae.

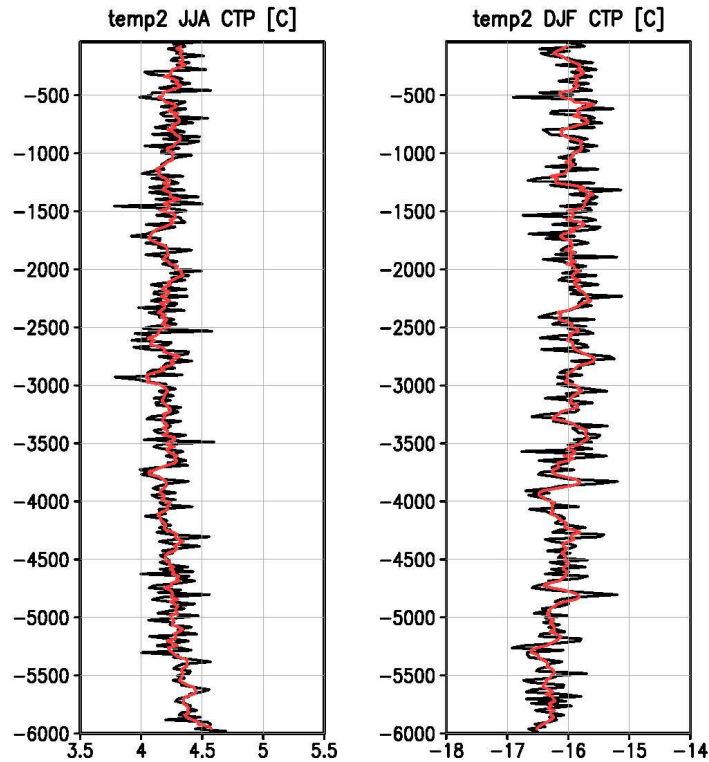


Figure 5.8: Simulated change of summer (JJA) and winter (DJF) 20yr-mean near-surface air temperature [°C] for the last 6000 years on the central Tibetan Plateau (CTP). The red solid line shows the 100yr-running-mean.

Pollen reconstructions suggest a vegetation transition from *Artemisia*-dominated alpine steppe at 6k to *Kobresia*-dominated meadow at 0k (Herzschuh et al., 2006; Herzschuh et al., 2010a) that was interpreted in terms of temperature decrease.

#### 5.5.2.4 Central-western Tibetan Plateau

The simulated vegetation trend agrees well with the reconstructions from Lake Bangong, although the calculated climate highly differs from climate observations in the surrounding of this lake (Table 5.2). Due to the flat orography in the model (mean height <2000m), simulated mean annual temperatures for present-day are 16.5°C instead of the observed -1.5°C. Moreover, the Indian monsoon intensity is slightly overestimated in that region. Annual mean precipitation reaches 250mm/yr (observed: ca. 70mm/yr). Bioclimatic conditions ( $T_{cm0k} = 0.32^{\circ}\text{C}$ ,  $T_{wm0k} = 26.6^{\circ}\text{C}$ ) support growth of extratropical forests and partly of raingreen shrubs (Fig. B8). The latter are hindered by the occasional occurrence of frosts. However, due to its location at the southern margin of the Plateau and due to the low regional pollen productivity, the pollen source area of the lake may comprise large areas of lower elevations and is thus rather similar to the modelled vegetation for that region.

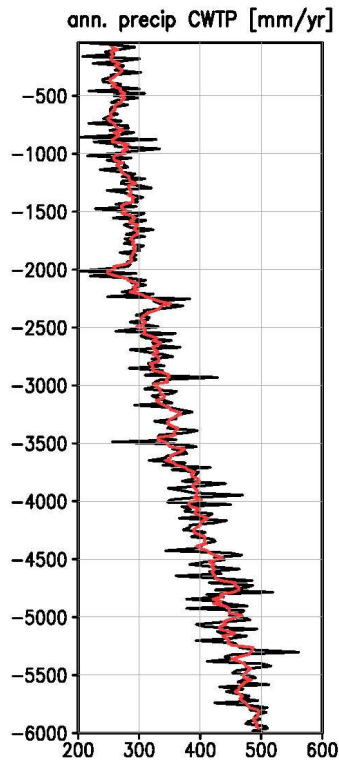


Figure 5.9: Simulated change of 20yr-mean annual precipitation [mm/year] for the last 6000 years on the central-western Tibetan Plateau (CWTP). The red solid line shows the 100yr-running-mean.

Reconstructions as well as the model results identify precipitation - being mainly a function of the Indian monsoon strength - as the main driver for the vegetation change. Calculated annual mean precipitation is halved between 6k ( $p_{\text{ann}6k} = 500\text{mm/yr}$ ) and 0k (see Figure 5.9), resulting in an increase of desert fraction. Proxy data suggests a maximum of moisture availability between 7.2–6.5k and then a trend towards aridity (van Campo et al., 1996). Thus, climate reconstructions and model data both show a decrease of summer monsoon intensity on the western Tibetan Plateau during the last 6000 years.

### 5.5.3 Simulated total vegetation and biomass changes on the Tibetan Plateau

Due to the underestimated orography in the model, the simulated fraction of potential vegetation cover on the Tibetan Plateau is probably overestimated and, therefore, not comparable with the present-day observed, anthropogenic effected distributions. However, as we are not aware of other modelling studies concerning the Holocene land cover change on the Tibetan Plateau, we use our model simulation to assess the total Holocene vegetation and biomass change in this region.

Table 5.3 illustrates the averaged simulated vegetation and biomass change on the Tibetan Plateau, which we ad hoc defined as those grid-boxes exceeding orographic height of 2500m in the model (cf. Figure 5.2). This area has a size of approx. 3.43 million km<sup>2</sup>.

Overall, the simulated forest fraction decreases by nearly one third, i.e. an area of ca. 0.45 million km<sup>2</sup>. Whereas forest covers approx. 41.4% of the Tibetan Plateau at mid-Holocene, only 28.3% area are covered by forests at present-day. Most of the forest has been replaced by shrubs, whose fraction is nearly four times larger at 0k (12.3% of the total area) than at 6k (ca. 3.2% of the total area). The area covered by grass increases from approx. 38.1% at mid-Holocene to 42.3% at present-day. Altogether, a small fraction of the Tibetan Plateau is more vegetated at present-day. Non-vegetated area is reduced from 17.29% at 6k to 17.16% at 0k.

	vegetation			forests			Shrubs			grass		
	6k	0k	6k-0k	6k	0k	6k-0k	6k	0k	6k-0k	6k	0k	6k-0k
area [%]	82.7	82.8	-0.1	41.4	28.3	13.1	3.2	12.3	-9.1	38.1	42.3	-4.1
liv.biom. [gC/m <sup>2</sup> ]	2778.5	2161.8	616.9	2700.8	1627.8	1072.5	49.0	502.6	-453.7	29.3	31.4	-2.1
litt. biom. [gC/m <sup>2</sup> ]	1282.6	990.1	292.5	1139.1	699.2	439.8	26.3	160.0	-133.7	117.3	130.8	-13.6
soil biom. [gC/m <sup>2</sup> ]	14661.5	13634.5	1027.0	9119.3	5576.8	3542.5	597.4	2297.5	-1700.1	4944.5	5760.4	-815.9
tot. biom. [gC/m <sup>2</sup> ]	18722.0	16786.0	1936.0	12958.6	7903.8	5054.8	672.6	2960.1	-2287.5	5091.1	5922.7	-831.6

Table 5.3: Total vegetation and biomass change on the Tibetan Plateau between mid-Holocene (6k) and present-day (0k), averaged over all grid-cells with orography exceeding 2500m in the model (see. Figure 5.2). Listed are the area covered by the vegetation types and by vegetation in total (fraction of grid-cell in %), as well as living biomass, litter biomass, biomass allocated in the soil under the vegetation and total biomass. Biomass is given in gC/m<sup>2</sup>.

This vegetation change results in a relocation of carbon stored in the soil and plants. At mid-Holocene, approx. 2.8kgC/m<sup>2</sup> are stored in the vegetation, particularly in forests (2.7kgC/m<sup>2</sup>). Due to the forest decline from 6k to 0k, more than 1kgC/m<sup>2</sup> living biomass is released. Only half of this biomass loss is compensated by shrubs and, to a small extent, by grass. Therefore, the total living biomass loss on the Tibetan Plateau during the last 6000 years adds up to ca. 0.62kgC/m<sup>2</sup>, on average. The Holocene climate change from 6k to 0k and the associated degradation of vegetation thus lead to a plant carbon loss of nearly one quarter.

The vegetation change on the Tibetan Plateau also strongly affects the total terrestrial biomass, i.e. the biomass stored not only in plants but also in soil and litter. In mid-Holocene, approx. 18.7kgC/m<sup>2</sup> are fixed as terrestrial biomass. The reduction of area covered by forest yield a decrease of terrestrial carbon by more than 5kgC/m<sup>2</sup>. Forest-replacing shrubs and grassland can partly compensate this biomass loss. Nevertheless, the

total terrestrial carbon loss on the Tibetan Plateau between the mid-Holocene and present-day exceeds 1.9kgC/m<sup>2</sup> on average. Projected on the total area of ca. 3.43 million km<sup>2</sup> (in the model), the terrestrial carbon loss adds up to 6.64GtC. These are approx. 7.5% of the simulated global terrestrial biomass loss during the Holocene.

## 5.6 Summary and conclusion of Chapter 5

Pollen-inferred vegetation trends on the Tibetan Plateau since the mid-Holocene were compared to simulated land cover changes, conducted with a coupled atmosphere-ocean-vegetation model with orbital forcing only. As the Tibetan Plateau exhibits diverse environmental and climate conditions, four different pollen records were considered, representing different parts of the Tibetan Plateau. Causes of the vegetation change and consequences for the biomass storage have been investigated.

In general, the simulated and reconstructed vegetation trends are in agreement for most sites but reveal differences with respect to their climatic causes. The results of both methods indicate a degradation of the vegetation, particularly characterised by a strong decrease of forests. Simulated forest fraction is reduced by nearly one-third at present-day. Simulated total biomass on the Tibetan Plateau has decreased by ca. 6.64GtC since the mid-Holocene. In some cases, however, model and reconstructions attribute this vegetation change to different climatic factors, which partly results from the fact that both methods have their deficiencies. On the one hand, reconstructions might be affected by long-distance transports of pollen and the dependence of the pollen-production on the vegetation type and environmental conditions, including climate (Gaillard et al. 2010). Human influence can probably not be neglected either. On the other hand, the coarse resolution of the model and the associated underestimation of the orography lead to discrepancies between the simulated present-day climate and observation.

On the north-eastern Plateau (Lake Qinghai, NETP), the model reveals orbitally-induced cooling of the warm season as the responsible climatic factor for the forest decline. Reconstructions, however, suggest the reduction of summer monsoon precipitation as the limiting factor. The model results might indicate that, so far, the influence of temperature changes on the Tibetan Plateau vegetation has been underestimated as an explanation for the decreasing forest in paleo-reconstructions for monsoon-affected areas.

The vegetation degradation around Lake Naleng (SETP) is probably caused by changes in temperature between mid-Holocene and present-day. According to reconstructions, decreasing summer temperatures lead to a downward shift of the treeline and therefore to less forest vegetation around Lake Naleng (Kramer et al. 2010). The reduction of forest fraction in the model can be attributed to increasing winter temperature. Since the

simulated climate for SETP strongly deviate from observation, this result should be interpreted with caution.

Harsh climatic conditions on the central Tibetan Plateau (Lake Zige tang) during the mid-Holocene as well as present-day lead to only slight vegetation changes in the model and in reconstructions.

The land cover degradation on the central-western Tibetan Plateau (Lake Bangong) can be attributed to a change in precipitation. Since the local climate is dry, the reduction of summer monsoon precipitation from 6k to 0k causes an expansion of deserts and a dieback of vegetation in the model as well as in reconstructions.

Although the spatial resolution of the model is coarse and the experimental set-up is designed to analyse climate and vegetation changes due to orbital forcing alone, the model results agree with the reconstructed vegetation trend on the Tibetan Plateau.

Therefore, reconstructed large-scale land cover change since the mid-Holocene can likely be attributed to natural and not anthropogenic reasons, although humans might still have influenced the vegetation on a local scale strongly. The comprehensive Earth system model used in this study captures the regional climatic reasons for the vegetation change in most instances. Thus, it provides a good tool to understand the long-term vegetation change on the Tibetan Plateau as well as its causes and consequences.

However, the discrepancy between the simulated climate and observations in some parts of the Plateau show that the analysis-options are limited in simulations with coarse spatial resolution. Detailed analyses of important processes such as local changes of the energy balance or atmospheric flow are only possible in experiments with higher numerical resolution, where the complex terrain of the Tibetan Plateau is represented better.



## **6. Sensitivity of the Asian monsoon climate to large-scale forest cover change**

### **6.1 Introduction**

The effects of large scale deforestation and afforestation have often been analysed in climate model studies. In this context, the biogeophysical consequences of tropical rainforest clearance in single regions like Amazonia, tropical Africa or Southeast Asia as well as total tropical deforestation has widely been discussed (e.g. Henderson-Sellers et al., 1993; Polcher and Laval, 1994; Gedney and Valdes, 2000; Werth and Avissar, 2002 and 2005a,b; Findell and Knutson, 2006; Hasler et al., 2009; Snyder, 2010). A few studies also deal with the impact of large-scale extratropical forest cover change on climate (e.g. Bonan et al., 1992; Chalita and Le Treut, 1994; Claussen et al., 2001; Bathiany et al., 2010). Most of these studies agree that tropical forest increases precipitation and cools the local climate compared to lower vegetation, mainly due to an enhanced evaporative cooling. Boreal forests have the opposite effect on temperature since they have a lower albedo than the often snow-covered ground and thus increase the absorption of energy at the surface.

How does climate react to large-scale forest cover changes in the Asian monsoon region? The Asian monsoon region comprises parts of the tropical as well as the temperate climate zone that can even be covered by snow during winter. Due to the heterogeneous orography, including high mountain ranges and parts of the Tibetan Plateau, potential land cover is very diverse. Rainforest grows next to temperate and montane forest; Alpine tundra is located there as well as temperate steppes.

Monsoon circulations are primarily induced by the thermal contrast between the continent and the ocean, generating large scale pressure gradients (Webster et al., 1998). Therefore, monsoon systems have to be seen as coupled interactive atmosphere-ocean-land phenomena (Yasunari, 2007) in which the land surface plays an equally important part as the ocean. Since land cover changes affect the energy and water balance, they may have a direct influence on the monsoon circulation, moisture convergence and precipitation pattern.

The Asian monsoon system is the strongest monsoon system worldwide. Including large parts of China and India, nearly two thirds of the global population live in the region influenced by this monsoon (Clift and Plumb, 2008). Changes in the monsoonal climate are therefore a matter of particular social, economic and environmental interest. In the last decades, the Asian monsoon region experienced large anthropogenic land cover changes. Huge parts of the natural forest in eastern China have been converted into farmland (e.g.

Pongratz et al., 2008). Steppe areas are severely affected by over-grazing and over-farming. Originally vegetated areas in northern China have been overrun by the rapidly expanding deserts. The impact of these land cover change has been analysed in several climate model studies (e.g. Zheng et al., 2002; Fu, 2003; Gao et al., 2007; Zhang and Gao, 2008). They all agree that the vast degradation of the land cover has caused a regional climate change. However, amplitude, sign and distribution of precipitation and temperature change differ and depend on the type of model (regional or global climate model) and the methods for applying the land cover change.

South and East Asia are the homelands of some of the oldest human civilizations. These cultures evolved rapidly and often had advanced agricultural technologies and a well organised urban infrastructure. Particularly the Indus Valley (today's western Pakistan and eastern Afghanistan) and the region around the Yellow River (Fu, 2003; Clift and Plumb, 2008) experienced a long continuing settlement history, starting in the early-Holocene (approx. 7000BC and 6000BC, respectively, Map: Fig. A.1). The linkage between the development or collapse of these cultures and the monsoon climate variability as well as the role early human societies could have played for the Holocene climate and environmental change are of special interest in the context of recent global warming. Some studies relate the decline of diverse major prehistoric cultures to intense long-lasting drought spells embedded in the general decreasing Asian summer monsoon since the early- and mid-Holocene (cf. Clift and Plumb, 2008). On the other hand, human interference via forest clearance can not be excluded as a contributing factor to mid- to late-Holocene land cover and climate change either.

Pollen-based vegetation reconstructions suggest that large parts of Central and Eastern China were much more covered by forest during the mid-Holocene. For instance, Ren (2007) suggested an up to 92% increased forest cover in the middle and lower reaches of the Yellow River for 6k (k = 1000 years before present) compared to today, which strongly declined in the following four millennia. According to Ren (2000), the spatial evolution of forest decline in China correlates well with spreading of cultures out of this area. However, Ren (2000) also remarks that this relation can only be a preliminary conclusion due to the lack of well-dated and well-resolved pollen data.

The steppe-forest boundary in East Asia was shifted north-westward by up to 500km at 6k (Yu et al., 2000). Thus, the area around the present-day East Asian monsoon margin experienced a substantial decrease of vegetation in the course of the Holocene. In eastern Inner Mongolia, pollen assemblages reached the maximum Holocene tree pollen fraction (40-60%) between 8k and 5k. Tree pollen decreased in this region to less than 20% within 2000 years. Also for the nowadays semi-arid north-western Loess Plateau tree pollen dominate the early- to mid-Holocene pollen assemblages, reaching 80% between 8.5k to

6.5k. Afterwards, land cover gradually changed to desert with sparse steppe in this region (Zhao et al., 2009).

Less information is known about the vegetation change in the Indian monsoon margin (e.g. Pakistan and north-western India), but also for this area a vegetation loss during the Holocene is supposed (Singh et al., 1990; Ansari and Vink, 2007; Ivory and Lézine, 2009).

These examples of vegetation reconstructions point to the fact that the vegetated area in the Asian monsoon domain was not only characterised by more forests during mid-Holocene but also expanded further inland.

In a previous study (cf. Chap. 4), we analysed the contributions of the vegetation-atmosphere interaction, the ocean-atmosphere interaction as well as their synergy to the Holocene climate change in the Asian monsoon region by using a comprehensive Earth system model with dynamic vegetation included (Dallmeyer et al., 2010). This study showed a rather small contribution of the simulated vegetation change on Asian monsoon climate. The mid-Holocene to pre-industrial climate change was predominantly caused by the response of the atmospheric circulation to the insolation forcing as well as oceanic feedbacks. The synergy effect was mostly negligible. Presumably, the model underestimated the amplitude of Holocene forest cover changes which could explain the weak vegetation impact. At least compared to the former pollen-based vegetation reconstructions (see above) the simulated vegetation change seemed to be too small.

Since the simulated vegetation change has only revealed a weak effect on climate, we decide to confront the model with a strong forest cover change to assess the maximum effect of large-scale land-cover changes on the climate in the Asian monsoon domain.

For this purpose, we perform idealised sensitivity experiments with either a complete forest cover or a complete grass cover prescribed in the monsoon region. The domain of land cover change is aligned to Holocene vegetation and human development. The resulting climate change is then presented on the basis of precipitation and temperature differences to a control run with present-day potential vegetation.

Secondly, we analyse the remote effect these land cover changes have on precipitation in North Africa and the Middle East. Thirdly, we address the question what information we can deduce from these results regarding the relation of mid-Holocene climate, vegetation and neolithic cultures in the Asian monsoon region.

## **6.2 Model and experiments**

To analyse the influence of large-scale land cover change on the Asian monsoon climate, different sensitivity experiments are performed. In this study, we use the general circulation model ECHAM5 (Roeckner et al., 2003) coupled to the land-surface-scheme

JSBACH (Raddatz et al., 2007). Both models have been developed at the Max-Planck-Institute for Meteorology. ECHAM5 run with 31 vertical levels and a spectral resolution of T63, which corresponds to a grid-box width of  $1.875^\circ$  (i.e. ca. 210 km on a great circle). JSBACH differentiates eight plant-functional types (PFTs). Forests can contain tropical and/or extratropical trees, which are either evergreen or deciduous. Shrubs are distinguished as raingreen shrubs or cold (deciduous) shrubs. Grass is classified as either C3 or C4 grass. The land surface in JSBACH is tiled in mosaics, so that several PFTs can cover one grid cell. Each grid cell also contains non-vegetated area representing the fraction of seasonally bare soil and permanently bare ground (desert).

The global distribution of vegetation in the standard version of JSBACH is based on the potential vegetation map of Ramankutty and Foley (1999) that had been translated into the eight different PFTs of JSBACH. The global distribution of deserts follows the distribution described in the Global Land Cover Characteristics data base of the U.S Geological Survey (Loveland et al., 2000).

PFT	phenology	LAI <sub>max</sub> [m <sup>2</sup> /m <sup>2</sup> ]	$\alpha_{\text{VIS}}$	$\alpha_{\text{NIR}}$	$z_0$ [m]
tropical evergreen forest	raingreen	7	0.03	0.22	2.0
tropical deciduous forest	raingreen	7	0.04	0.23	1.0
extratropical evergreen forest	evergreen	5	0.04	0.22	1.0
extratropical deciduous forest	summergreen	5	0.05	0.25	1.0
raingreen shrubs	raingreen	3	0.05	0.25	0.5
deciduous shrubs	summergreen	2	0.05	0.28	0.5
C3 grass	grass	3	0.08	0.34	0.05
C4 grass	grass	3	0.08	0.34	0.05

Table 6.1: Physical properties and phenology type of each plant functional type, i.e. LAI<sub>max</sub>: maximum value of the leaf area index;  $\alpha_{\text{VIS}}$ : albedo in the visible solar spectrum;  $\alpha_{\text{NIR}}$ : albedo in the near infrared solar spectrum;  $z_0$ : roughness length of vegetation.

For each PFT and also the bare ground, individual physical properties such as albedo or roughness length are defined (Table 6.1). JSBACH calculates dynamically the physical land surface parameters (e.g. albedo or roughness length) in each grid-cell as average of the individual properties of the PFTs and the non-vegetated area, weighted with their respective cover fraction. In the calculation of the albedo, snow-covered soils and snow-covered forest-canopies as well as the masking of snow-covered soils by forests are

additionally accounted for. The soil albedo is prescribed from satellite data and does not change during the simulations. The albedo of leaves depends on the leaf area index that is calculated on the basis of temperature, soil moisture and the net primary production of the PFTs. Concerning phenology, JSBACH differentiates the four types evergreen, raingreen, summergreen and grasses. LAI can not exceed a maximum value specified for each PFT (Table 6.1).

The fluxes of energy, water and momentum between the land and the atmosphere are calculated as described in Roeckner et al. (2003) with the exception that JSBACH uses the aggregated land surface parameter of each grid-cell for the calculation. Surface and atmosphere are coupled implicitly. For further details on the coupling of land-surface schemes (e.g. JSBACH) and general circulation models see Polcher et al., 1998.

The models have been tested against observations and reanalysis data proving that they capture the major structure of global and regional climate (see section 2.3 ).

With regard to the results of our previous study (cf. Dallmeyer et al., 2010), we assume a weak synergy of the vegetation-atmosphere and ocean-atmosphere interactions. To exclude a contribution of changes in ocean parameters to the climate signal, we prescribe pre-industrial sea surface temperatures and sea-ice cover in all simulations. Both have been extracted from a coarse resolution experiment, performed with the comprehensive Earth System Model ECHAM5/JSBACH-MPIOM. This model included the dynamic ocean model MPIOM (Marsland et al., 2003; Jungclaus et al., 2006). Atmospheric composition is kept constant at pre-industrial values; CO<sub>2</sub>-concentration is set to 280ppm.

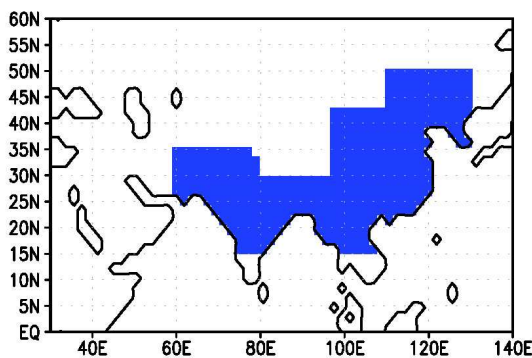


Figure 6.1: Extended Asian monsoon region (shaded). In this region, land cover is changed either to forest or to grass in the afforestation and deforestation experiment, respectively.

Under these boundary conditions, three experiments with differently prescribed land cover in an extended Asian monsoon region (see Figure 6.1) are conducted: These are a control run with standard, potential land cover (CTRL), an experiment with forest in the entire region (FOR) and an experiment with grass cover in the entire region (GRA). Thereby, the region was selected combining the following criteria: We extend the Asian monsoon domain by including areas where previous model

results have suggested a strong increase of vegetation for mid-Holocene orbital conditions to get a representative monsoon domain for the Holocene (cf. Fig. 4.4). Vegetation is not changed in high-elevated areas where the mean orography in the model exceeds 4500m.

Furthermore, the region incorporates areas where humans settled in early- and/or mid-Holocene, i.e. the region includes the Indus Valley, Northeast China and the Chinese provinces Shandong, Hebei, Shanxi, Shaanxi and parts of Gansu and Qinghai.

In the afforestation experiment (FOR), land cover is prescribed as forest in the entire region. In those grid-boxes that have already been forested in the standard land surface map, the ratio between the different tree types is kept constant and the forest sum is scaled to 100% fraction per grid-box. In grid-boxes without forest vegetation in the standard map, forest is prescribed to 50% evergreen and 50% deciduous trees. Trees are prescribed as extratropical or tropical to the north or south of 30°N, respectively.

The same method is applied in the deforestation experiment (GRA). For grid-boxes already containing grass PFTs in the standard map, the ratio between C3 and C4 grass is fixed and

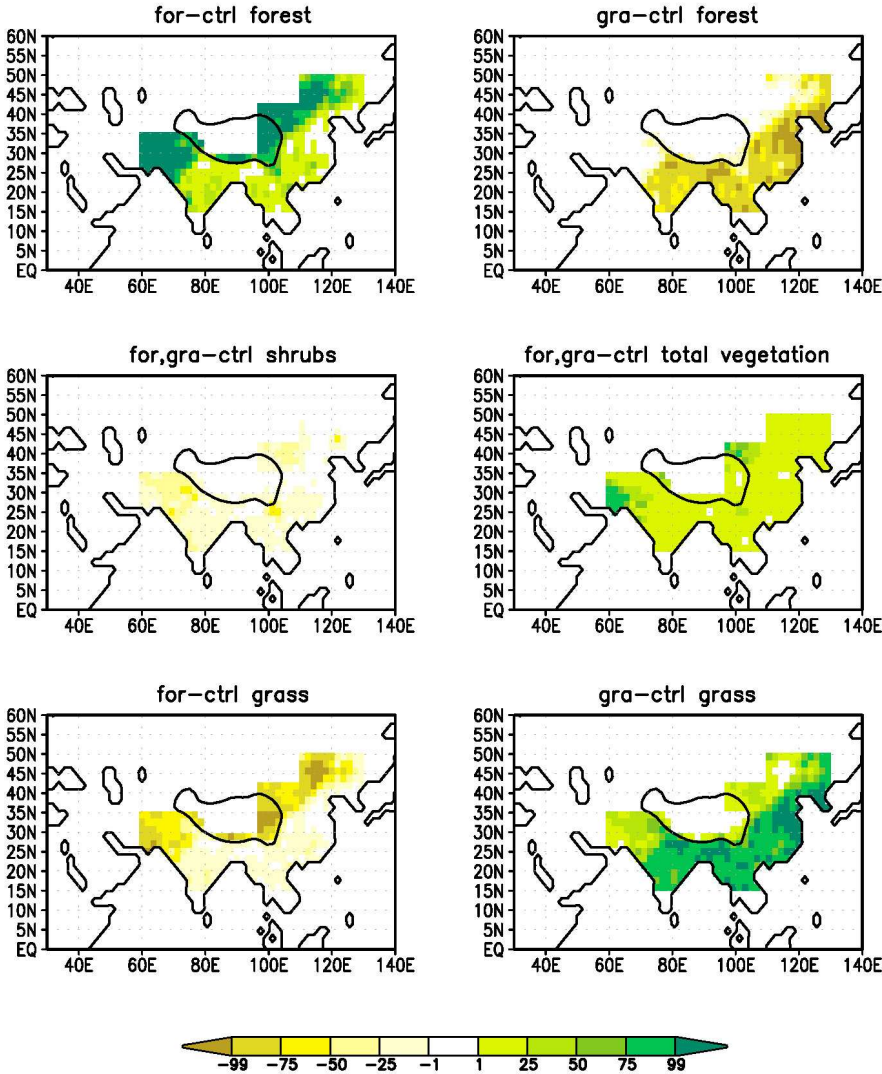


Figure 6.2: Differences in forest, shrubs, grass and total vegetation distribution between the land cover map prescribed in the afforestation experiment (for) or the deforestation experiment (gra) and the control run (ctrl). Values are given in fraction per grid-box.

total grass sum per grid-box is scaled to 100% coverage. Regions not containing grass PFTs in the standard map are covered by 20% C3 and 80% C4 grass south of 30°N and 80% C3 and 20% C4 grass north of 30°N.

The difference between the land cover in the afforestation or deforestation experiment and the control run can be seen in Figure 6.2 for the vegetation types forest, shrubs and grass. The total change of vegetated area as well as the change in fraction covered by shrubs is identical for both experiments.

Each experiment spans 102 years to get significant results despite of the high natural climate variability in the Asian monsoon system. Since carbon cycle dynamics are not included and the vegetation distribution is prescribed, only the first two years of the simulations are considered as spin-up time and excluded from the analysis. The presented plots show results exceeding the 95%-significance level of a standard student's T-Test.

## **6.3 Results**

The period of a reversed upper-tropospheric temperature gradient between 5°N and 30°N is often taken as a definition for the Asian monsoon season (Li and Yanai, 1996; Webster et al., 1998; Ye and Wu, 1998). According to this definition, the length of the monsoon season in our experiments remains unaffected regardless of which land cover is prescribed (not shown). Based on the month of earliest simulated onset and latest simulated withdrawal in the Asian monsoon domain we therefore divide our analyses period into two different seasons. These are the monsoon season (lasting from May to October) and the dry/cold season (lasting from November to April). Furthermore, we concentrate on precipitation and near-surface air temperature as the main parameters describing monsoonal influenced climates. The results presented in this study are based on 100year-means, averaged over the respective season.

### **6.3.1 Effect of land cover change on precipitation**

#### **6.3.1.1 Afforestation experiment**

The significant effect of a prescribed forest cover on seasonal mean precipitation is illustrated in Figure 6.3. The land cover change predominantly has a local and only weak effect on precipitation. Monsoon precipitation is increased particularly on the south-central Tibetan Plateau (up to 0.77mm/day). In north-eastern China (approx. 0.35mm/day) as well as at the monsoon margin zone in Inner Mongolia (approx. 0.17mm/day), precipitation is also enhanced. In contrast, the western Tibetan Plateau receives less precipitation (up to 0.26mm/day) in the afforestation experiment. At the Yangtze delta and parts of the Great Plain of China as well as in South India rainfall is reduced by up to 0.35mm/day and 0.43mm/day, respectively.

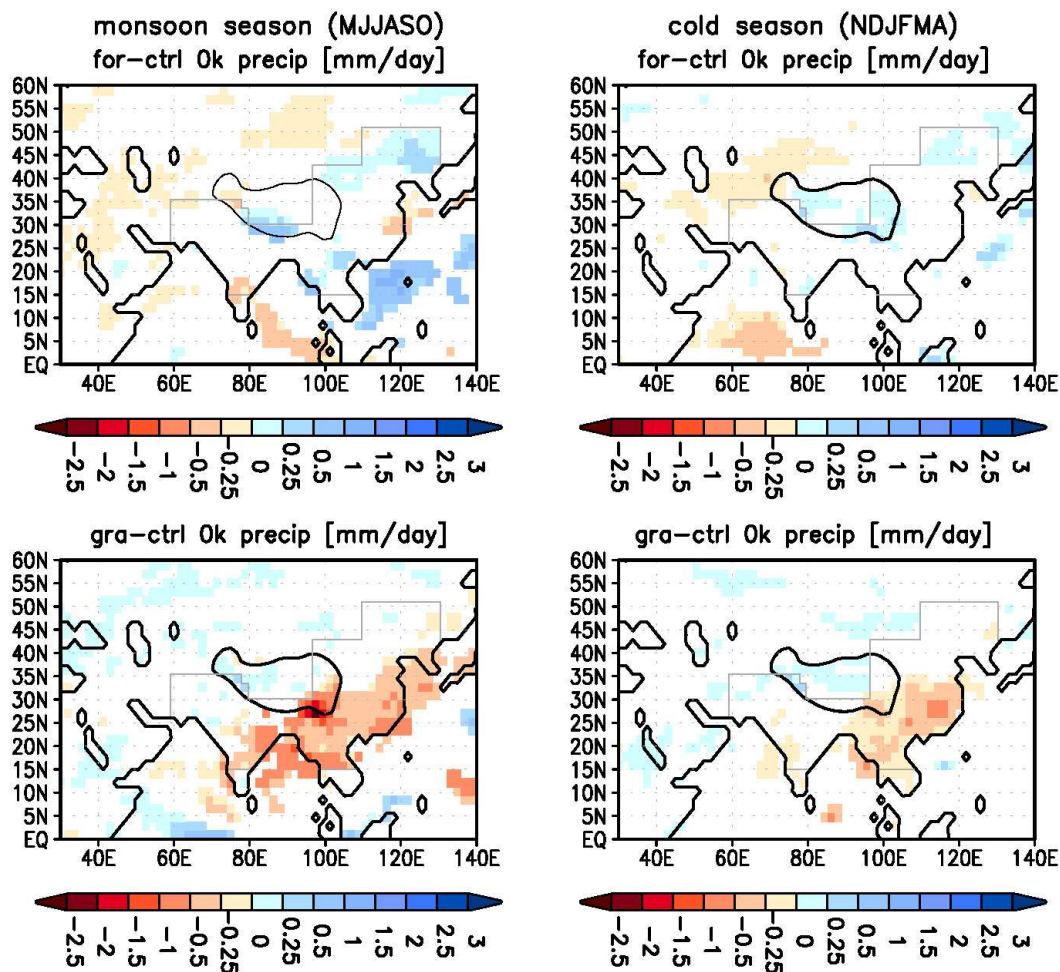


Figure 6.3: Simulated precipitation change between the afforestation (for) or deforestation (gra) experiment and the control run (ctrl), averaged over the monsoon season (left panel) and the dry/cold season (right panel). The monsoon season lasts from May to October, the dry/cold season contains the month from November to April. Values are given in mm/day. Only values exceeding the 95%-significance level (T-test) are shown.

In the dry/cold season, the land cover change causes a significant increase of precipitation on the Tibetan Plateau (ca.0.39mm/day) and in north-eastern China (ca.0.09 mm/day). Less precipitation occurs in the region west and north of the Tian Shan (up to 0.23mm/day).

### 6.3.1.2 Deforestation experiment

Complete grass cover in the Asian monsoon region instead of present-day potential vegetation leads to a decrease in monsoon precipitation in a broad band in South and East Asia, including the Yangtze-Huanghe-plain, Indochina, Bay of Bengal, parts of the Tibetan Plateau and East India (Fig. 6.3). The maximum reduction in monsoon rainfall (2.3mm/day) occurs on the south-eastern edge of the Tibetan Plateau. In contrast, monsoonal precipitation increases slightly, but significantly on the western Tibetan Plateau, reaching 0.26mm/day at most.

In the dry/cold season, the strong precipitation reduction is confined to Eastern China (up to 0.56mm/day) and the Indochinese Peninsula (up to 0.35mm/day). The central and western Tibetan Plateau receives more precipitation, in particular the western Himalaya with up to 0.3mm/day.

### 6.3.2 Effect of land cover change on near-surface air temperature

#### 6.3.2.1 Afforestation experiment

Figure 6.4 shows the significant effect of afforestation on near-surface air temperature. In the monsoon season, the regions north of 30°N that experience a strong afforestation reveal a warmer climate. Temperature increases by up to 0.58K in Inner Mongolia and north-eastern China, by up to 0.4K on the eastern Tibetan Plateau and by up to 0.65K southwest of and on the western Tibetan Plateau. South of 30°N temperatures tend to decrease. The

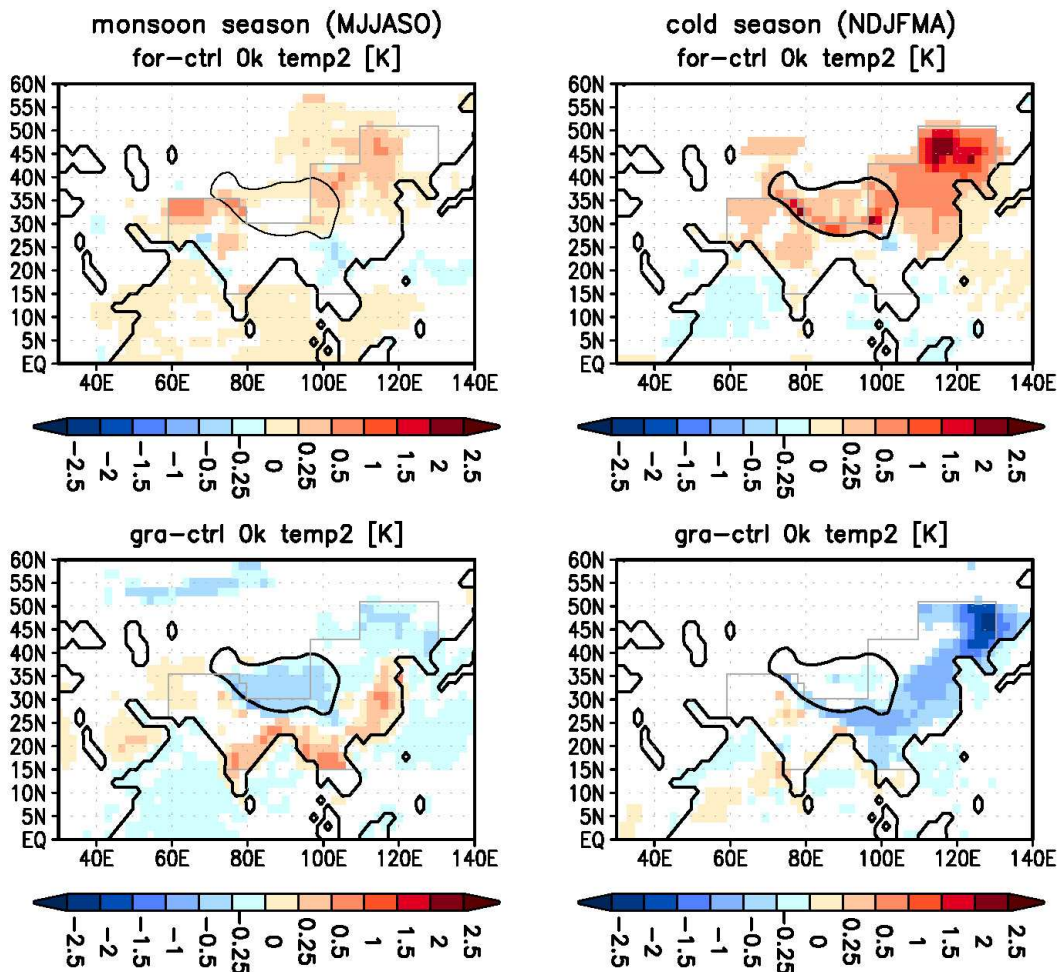


Figure 6.4: Simulated near-surface air temperature (in 2m height) change between the afforestation (for) or deforestation (gra) experiment and the control run (ctrl), averaged over the monsoon season (left panel) and the dry/cold season (right panel). The monsoon season lasts from May to October, the dry/cold season contains the month from November to April. Values are given in K. Only values exceeding the 95%-significance (T-test) are shown.

land cover change leads to significant cooling in some parts of the Indian West coast and southeast of the Tibetan Plateau (up to -0.3K).

In the dry/cold season, 2m-temperature is particularly increased in Northeast China (up to 2.2K) and on the southern flank of the Tibetan Plateau (up to 2.1K). Eastern China, including the eastern Tibetan Plateau, North India, and the region north of the Arabian Sea experience a warmer climate (up to 0.4K). Only at a few grid-boxes southeast of the Tibetan Plateau temperatures slightly decrease by up to -0.25K.

### **6.3.2.2 Deforestation experiment**

In the deforestation experiment, monsoon season temperatures are lower in Northeast China (up to 0.35K), Inner Mongolia (ca. 0.2K) and on the Tibetan Plateau (up to 0.55K) compared to the control run (Figure 6.4). In contrast, the deforested regions south of 25°N experience a warming. Temperatures increase by up to 0.9K in northern Thailand. Higher temperatures are also found in eastern China, particularly at and around the Great Plain (up to 0.6K).

With prescribed grass cover, dry/cold season temperatures are lower in whole eastern China. The cooling is particularly pronounced in regions, which experience a strong deforestation, e.g. the Great Plain (ca. 0.7K). Nevertheless, the strongest temperature decline occurs in Northeast China (up to -2.2K). Climate becomes slightly warmer in the north of India by up to 0.25K. At the deforested southern flank of the Tibetan Plateau, near-surface air temperature decreases (ca. -0.8K).

## **6.4 Discussion of Chapter 6**

The land surface can force the atmosphere via the physical quantities snow cover, soil moisture and vegetation (Yasunari, 2007). In the context of this study, the effect of vegetation change on climate is most important, though vegetation change can also indirectly influence the other parameters. The land cover controls the energy balance at the surface via albedo and roughness length and influences the evapotranspiration. Modifications of the energy fluxes can lead to changes in temperature, pressure field and circulation (Pielke et al., 1998). Modifications of the evaporation due to land cover changes together with circulation changes affect the precipitation distribution. Therefore, we start this chapter with a discussion of the energy and water balance change related to the applied afforestation and deforestation.

## 6.4.1 Change of circulation and water balance

### 6.4.1.1 Afforestation experiment

The Asian monsoon circulation is primarily driven by the seasonal differential heating between the Asian continent and the Indian and Pacific Ocean. During the summer monsoon season, a deep surface heat low covers the region between the Arabian Peninsula and the Chinese East coast with lowest pressure in North India and Pakistan. In consequence of the afforestation, the monsoon trough deepens by up to -120Pa in North India (Figure 6.5c). Therefore, the Indian monsoon is slightly strengthened, which at least contributes to the enhanced precipitation over southern Himalaya.

In North and Northeast China, the precipitation increase coincides with an enhanced cloudiness (up to 3%, Figure 6.5a) and an increased evaporation (up to 0.56mm/day, see Figure 6.5b), probably indicating an enhanced water recycling in that region. The shift in cloud cover from the Great Plain - Japan region to North/Northeast China suggests a shift of the East Asian summer monsoon rain band, i.e. a north-westward extension or shift of

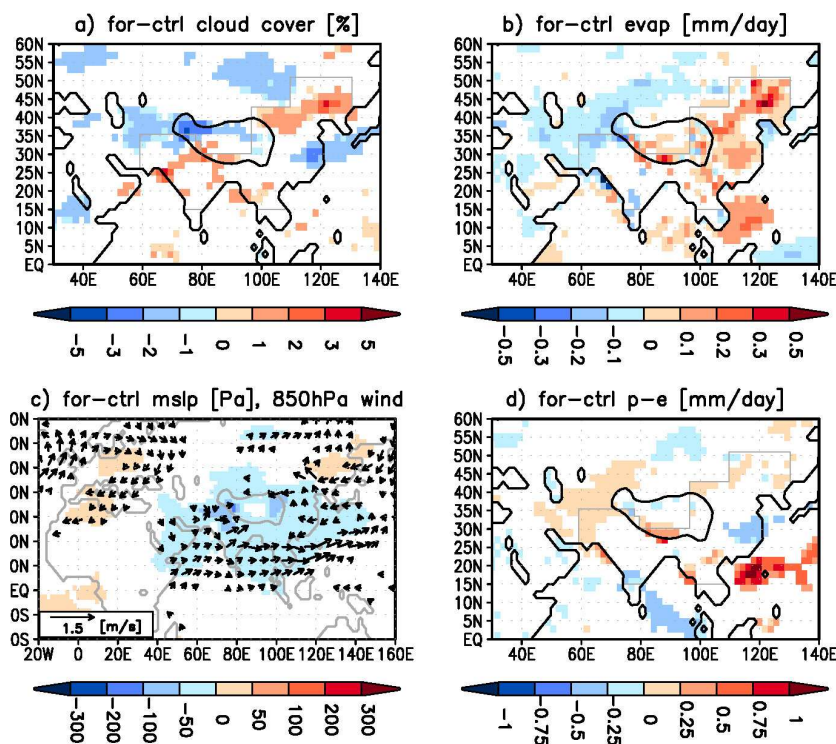


Figure 6.5: Simulated change of different parameters influencing the precipitation change between the afforestation experiment (for) and the control run (ctrl), averaged over the monsoon season. a) total cloud cover in %; b) evaporation in mm/day; c) mean sea level pressure in Pa, shaded, combined with 850hPa wind in m/s, vector; d) precipitation-evaporation in mm/day as approximation of the moisture convergence. Except for the wind-field, only values exceeding the 95%-significance level in a standard student's T-test are shown. Instead, wind-vectors are masked out when their magnitude is smaller than one-tenth of the maximum vector length (here: 0.15 m/s).

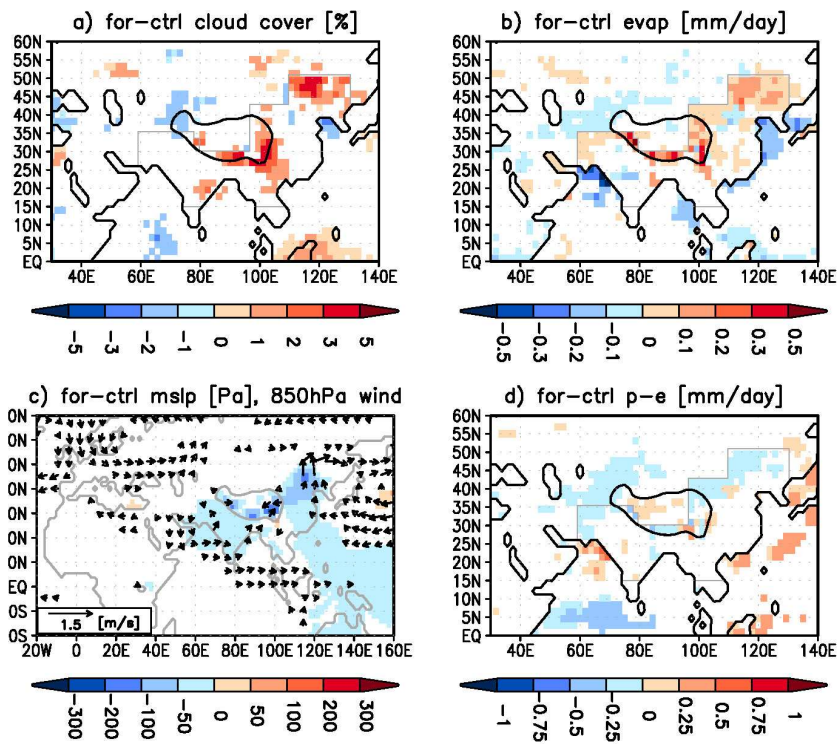


Figure 6.6: Same as Figure 6.5, but for the dry/cold season.

the region influenced by the monsoon. This would also explain the reduction of precipitation at the Great Plain and surroundings. The approximation for the moisture convergence (precipitation-evaporation (p-e), Figure 6.5d) reveals a negative anomaly (i.e., a moisture source) in that region. The extension of the monsoon is consistent with the wind field showing a slight enhancement of the East Asian summer monsoon flow.

During the dry/cold season, the high pressure system in North China is weakened by up to -100Pa (Fig6.6c). Therefore, the strong southward flow in eastern China characterising the East Asian winter monsoon is also weakened. The pressure anomaly induces an anticyclonic wind anomaly with a core over the Yellow Sea which brings warm and wet air-masses to Northeast China. This seems to lead to more clouds and more precipitation in that region.

The increase of precipitation on the Eastern Tibetan Plateau coincides with an enhanced cloudiness (up to 4%) and an increased evaporation (up to 0.38mm/day) as well as a mean sea level low pressure anomaly (up to -220Pa). The latter leads to a wind anomaly from the Bay of Bengal to the continent, probably contributing to the precipitation change.

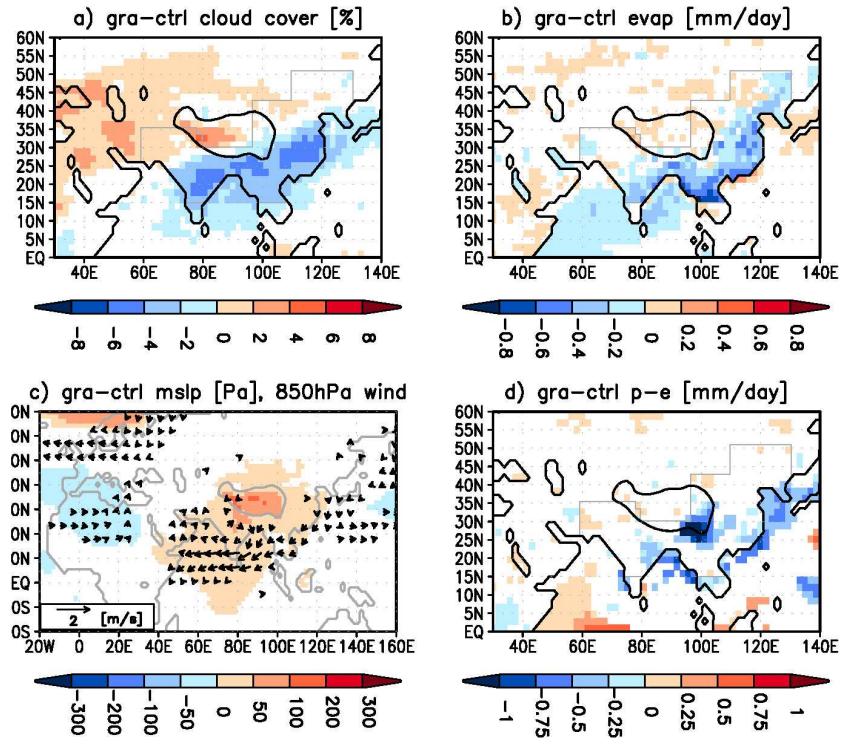


Figure 6.7: Simulated change of different parameters influencing the precipitation change between the deforestation experiment (gra) and the control run (ctrl), averaged over the monsoon season. For further details see Figure 6.5. Limit for wind-magnitude to be shown: 0.2m/s.

#### 6.4.1.2 Deforestation experiment

Deforestation leads to an attenuation of the Indian and East Asian summer monsoon flows (Figure 6.7c). This circulation change is associated with a high pressure anomaly forming in South and Central Asia, in particular on the Tibetan Plateau (up to 110Pa). High pressure anomalies are often related to descending motion and thus indicate less favourable conditions for the formation of precipitation. As a result, monsoon related convection, precipitation and also evaporation in south/south-eastern Asia is reduced (Figure 6.7). Total cloud cover decreases by up to 5%, evaporation decreases by up to 0.78mm/day. In contrast, the increase of precipitation on the western Tibetan Plateau is accompanied by more evaporation (up to 0.3mm/day) and more clouds (up to 4.5%).

During the dry/cold season the moisture flux is more divergent in eastern China than in the control experiment (Figure 6.8). In addition, evaporation rate and cloud cover are reduced by up to 0.52mm/day and up to 4%, respectively. Both indicate a weaker local moisture recycling and weaker moisture convergence being responsible for the precipitation decline in that area. The precipitation increase on the western Tibetan Plateau is associated with more clouds (2%) and moisture convergence.

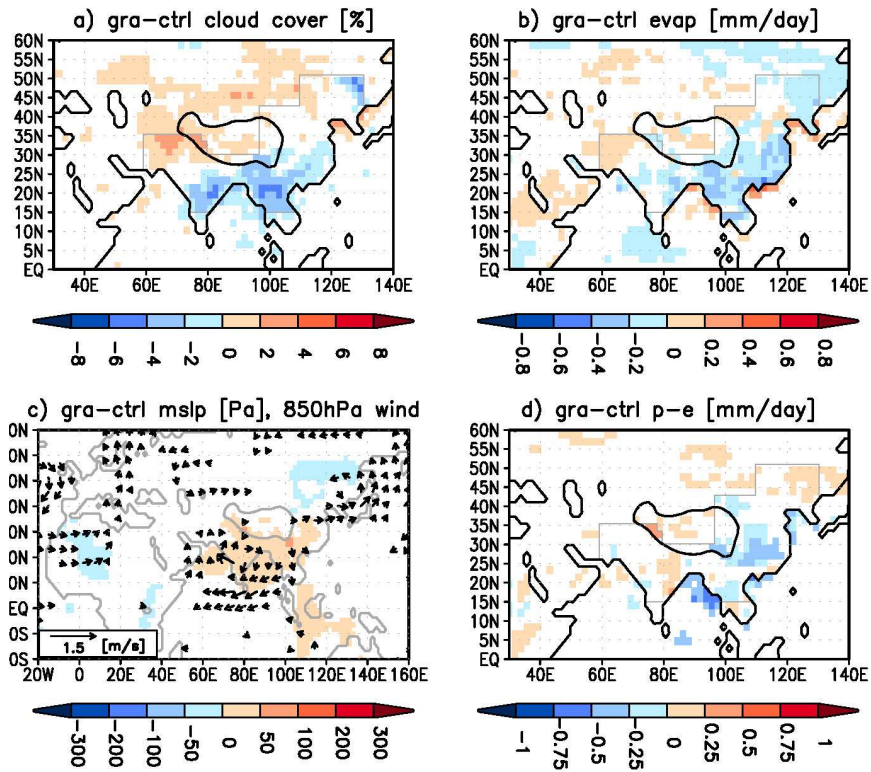


Figure 6.8: Same as Figure 6.7, but for the dry/cold season. Limit for wind-magnitude to be shown: 0.15m/s.

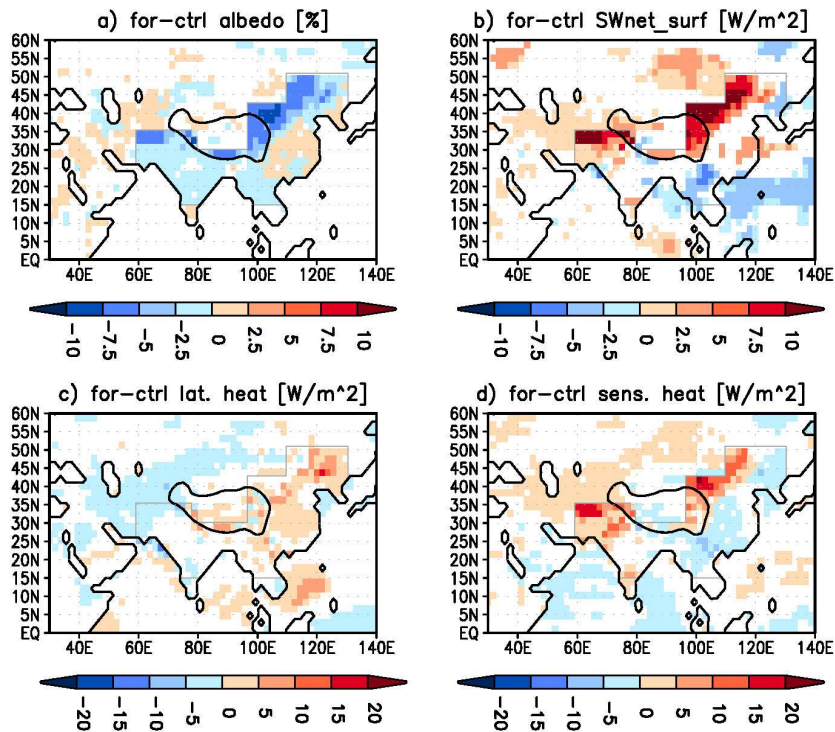


Figure 6.9: Simulated change of different parameters influencing the temperature change between the afforestation experiment (for) and the control run (ctrl), averaged over the monsoon season. a) albedo in %; b) net surface shortwave radiation in  $W/m^2$ ; c) latent heat flux in  $W/m^2$ ; d) sensible heat flux in  $W/m^2$ .

## 6.4.2 Change of albedo and turbulent heat fluxes

### 6.4.2.1 Afforestation experiment

In the monsoon season, afforestation leads to a decrease of albedo by up to 9.5% (Fig. 9a). This results in an increase of the absorbed incoming shortwave radiation, which explains the increase of near-surface air temperature in Northeast China, Inner Mongolia as well as in the region southwest of the Tibetan Plateau. The additional shortwave radiation at the surface is mainly transported to the atmosphere by the sensible heat flux. The region of decreased near-surface temperature southeast of the Tibetan Plateau is associated with a region of less net shortwave radiation at the surface (ca.  $6.5\text{W/m}^2$ ), which is probably induced by more clouds (not significant) and a slight albedo increase in that region. At least partly, the increased evaporation/latent-heat flux (up to  $5\text{W/m}^2$ ) and the decrease of sensible heat flux (up to  $8.5\text{W/m}^2$ ) contribute to lower temperatures in this region due to an increase in evaporative cooling (Figure 6.9).

The strong warming in Northeast China and on the Tibetan Plateau in the dry/cold season is induced by a strong albedo decrease (up to 20% and 35%, respectively, Figure 6.10a) which leads to a strong increase of net shortwave radiation at the surface (up to  $18\text{W/m}^2$  and  $55\text{W/m}^2$ ). These regions are covered by snow in winter, so that the snow-masking effect of the additional forests might contribute to the strong albedo decrease.

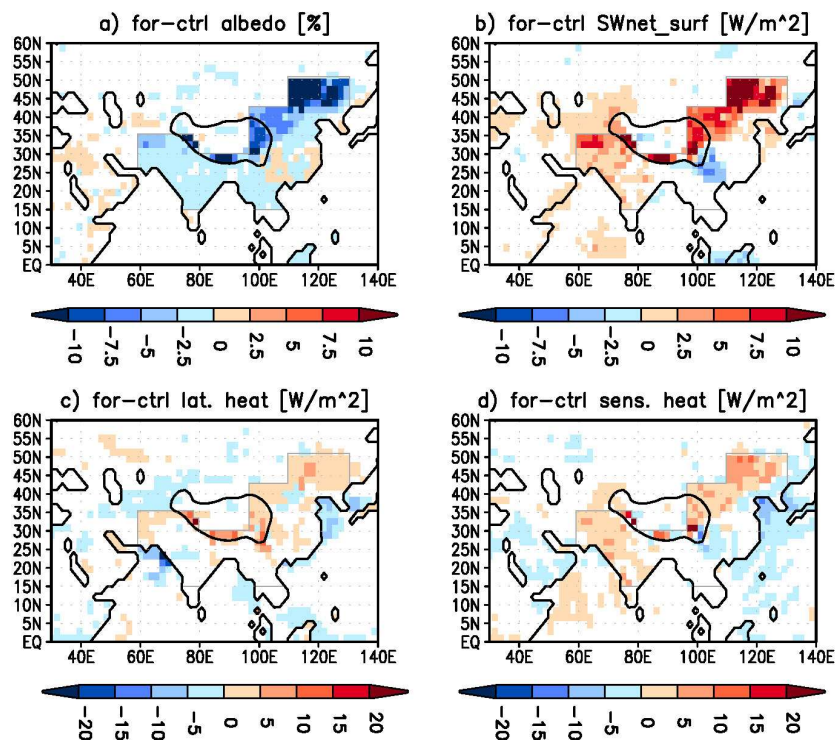


Figure 6.10: Same as Figure 6.9, but for the dry/cold season.

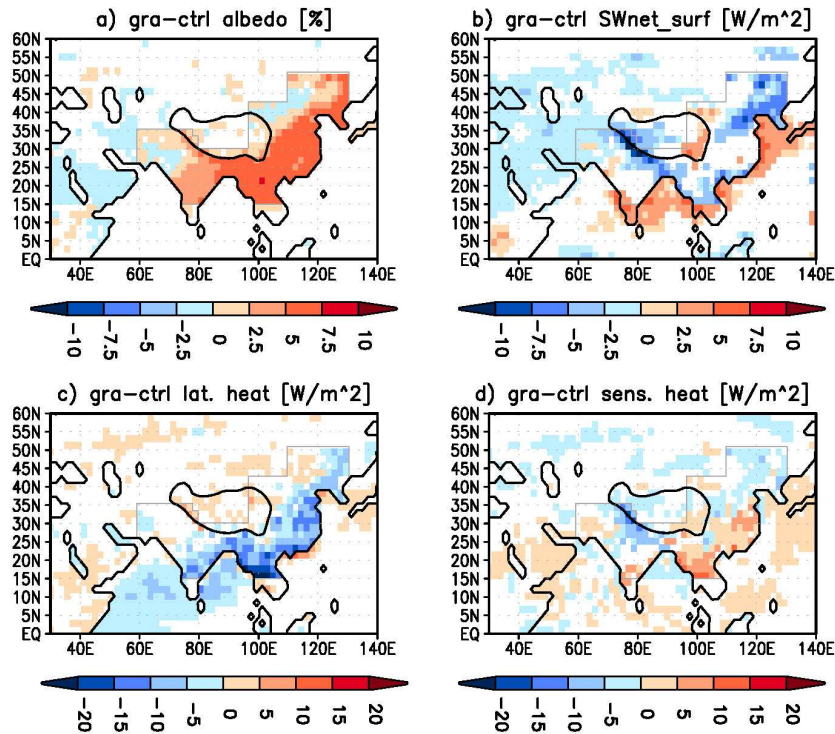


Figure 6.11: Simulated change of different parameters influencing the temperature change between the deforestation experiment (gra) and the control run (ctrl), averaged over the monsoon season. For further details see Figure 6.9.

In the region southeast of the Tibetan Plateau, the temperature decrease coincides with less net shortwave radiation at the surface (up to  $-6\text{W/m}^2$ ), which probably results from an enhanced cloud cover (up to 3 %).

#### 6.4.2.2 Deforestation experiment

The replacement of forest with grass cover in the Asian monsoon domain increases the albedo by up to 8% during the monsoon season (Figure 6.11a). Nevertheless, near-surface air temperatures in Southeast China and the regions south of  $25^\circ\text{N}$  are higher in the deforestation than in the control experiment. This is mainly a consequence of less precipitation/evaporation and less cloud cover in that region (cf. Figure 6.7a,b) which overcompensate the effect of increased albedo on the near-surface temperature.

The lower temperatures on the Tibetan Plateau are induced by less net solar energy at the surface (up to  $-11\text{W/m}^2$ ), mainly due to more clouds (up to 4.5%). Stronger evaporative cooling contributes to the lower temperatures on the western Himalaya. In Northeast China, the temperature decrease results from both, less net shortwave radiation at the surface ( $-6\text{W/m}^2$ ) due to an albedo increase of up to 5% as well as a higher evaporative cooling.

In the dry/cold season, deforestation leads to an up to 25% increase of albedo in the eastern part of Northeast China (Figure 6.12), which results in less net shortwave radiation at the surface (up to  $-20\text{W/m}^2$ ). This part of China is usually covered by more snow than the other parts of the Asian monsoon domain. Therefore, the lack of snow-masking by trees as well as a possibly enhanced snow-albedo feedback in the deforestation experiment may play an important role in decreasing the near-surface air temperature in this region.

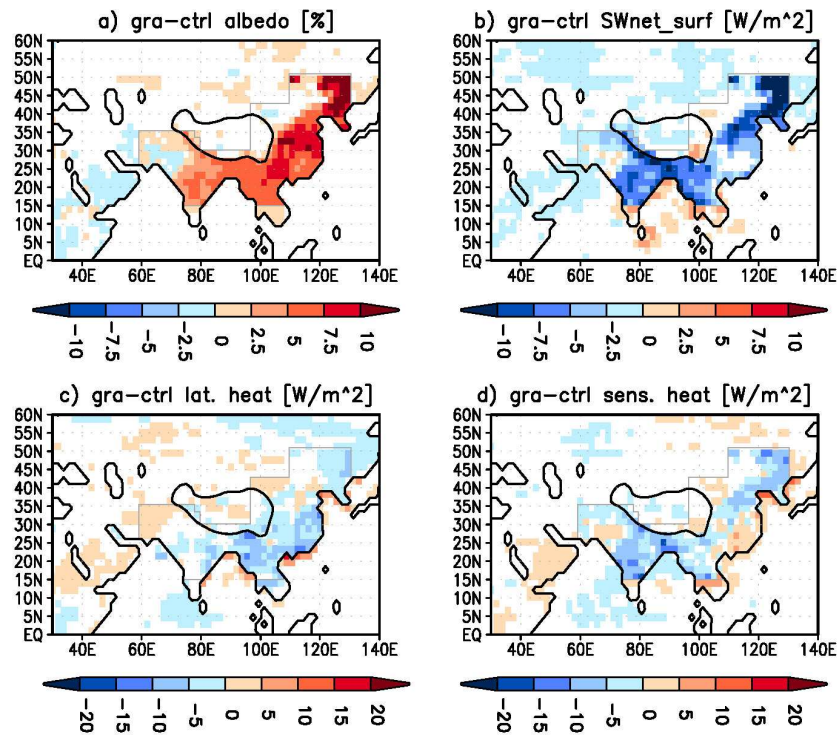


Figure 6.12: Same as Figure 6.11, but for the dry/cold season.

### 6.4.3 Comparison to other model studies

The experimental design and research questions of our study and previous studies that analyse land cover changes in the Asian monsoon region (and parts of it) strongly differ. While previous studies mainly focus on the impact of recent anthropogenic land use change on the regional climate in China our study assesses the maximum effect of large-scale forest cover change on the climate in the entire Asian monsoon domain. Our study does not aim to represent the actual land cover change of the past decades. It is a sensitivity study on the general effect of large-scale deforestation and afforestation in the Asian monsoon region on climate. Furthermore, in most of the previous studies, regional climate models were used. The Asian monsoon system is very complex and involves large-scale circulation systems which strongly determine the precipitation distribution. Regional climate models cannot capture the impact of vegetation changes on the large-scale

circulation and, thus, may not capture the entire effect of vegetation on the regional climate change.

So far, no other publications exist prescribing complete forest or grass cover in the Asian monsoon domain, but our results show similar climate signals received in previous studies performing land cover change experiments. Like in studies with tropical deforestation, precipitation in our simulation decreases when grass cover is prescribed instead of potential present-day vegetation (cf. e.g. Werth and Avissar, 2005a). These studies also report that less forest cover in tropical regions leads to a warmer local climate (c.f. e.g. Polcher and Laval, 1994). Increased near-surface air temperatures are also simulated in our deforestation experiment in the regions with a rather tropical climate, i.e. the region ca. south of approx. 26°N and Southeast China, in the monsoon season. Outside of this area, temperature decreases as a consequence of forest loss. This response is in line with previous studies of extratropical deforestation (Bonan, 2008). The results from our afforestation experiment reveal a similar pattern of precipitation change as model studies which analyse the effect of present-day land use change in China. For instances, Gao et al. (2007) have compared results from simulations with potential vegetation cover and observed land cover in China by using a regional climate model. Their results show that the vegetation conversion from forest to farmland reduces summer precipitation in northern and western China and enhance precipitation in Southeast China. Similar results were deduced by Zheng et al. (2002) by prescribing simultaneous vegetation degradation in the northern Chinese prairies and the southern evergreen forests. Furthermore, precipitation increases at the Indian East coast. The forest loss between our afforestation experiment and the control run leads to a similar precipitation change in the monsoon season.

#### **6.4.4 Remote effect on precipitation in North Africa and the Middle East**

Rodwell and Hoskins (1996) showed in an idealised model study that Asian monsoon related diabatic heating can induce descent in south-western Asia, the Arabian Peninsula and northern Africa via the initiation of Rossby-waves. Other studies emphasise the important role of diabatic heating on the Tibetan Plateau by forming desert climate in North Africa, Central Asia and the Middle East (e.g. Ye and Wu, 1998; Duan and Wu, 2005). As a consequence of this link, land cover change in the Asian monsoon domain may affect the climate in these regions as it has a strong influence on the energy balance. We address the possible remote effect of land cover change by analysing precipitation change in the monsoon season.

Figure 6.3 already reveals that the land cover change prescribed in this model study has predominantly a local and only weak influence on precipitation regarding the change of absolute precipitation amount. But, when looking at the relative precipitation change the

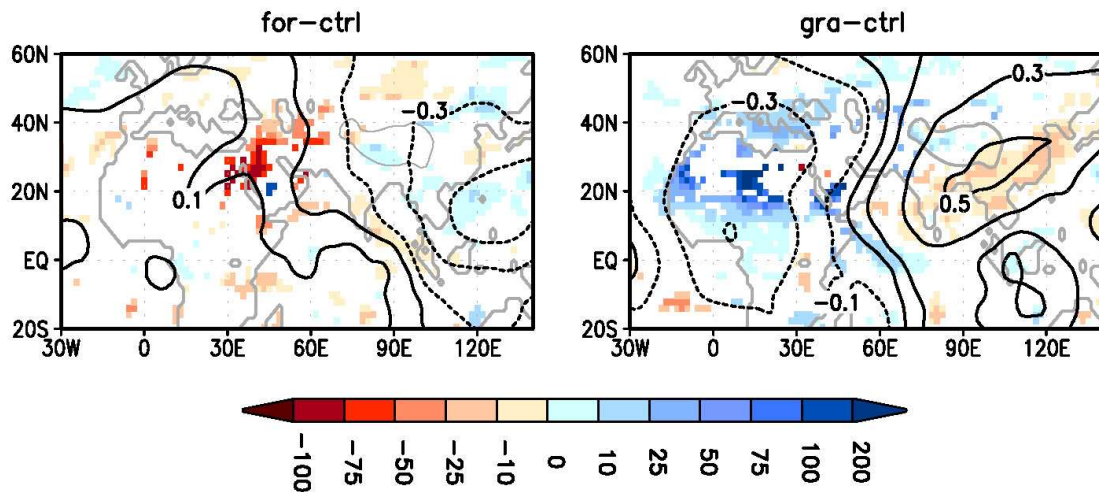


Figure 6.13: Simulated change in monsoon season precipitation weighted by the precipitation of the control run in % (shaded) and simulated change in upper-tropospheric velocity potential in  $\text{km}^2/\text{s}$  (contour). Left panel: afforestation experiment (for) - control run (ctrl); right panel: deforestation experiment (gra) - control run (ctrl). Values are averaged over the monsoon season. Precipitation differences are only shown if they exceed the 95%-significance level in a standard student's T-test.

anomaly can be very large. Figure 6.13 illustrates the change in monsoon season precipitation rate weighted by the current (ctrl) precipitation rate. Afforestation has a strong influence on precipitation in North Arabia, East Egypt and the region around the Southern Caspian Sea. Precipitation is more than halved in a large area. In many places, precipitation even decreases by 80-100%. The upper-tropospheric velocity-potential anomaly suggests that this change results from an increase in upper-level wind convergence, enhancing the descending motion and suppressing convective precipitation. In contrast, no significant large-area precipitation change occurs in the North African monsoon region and the Sahara.

Deforestation in the Asian monsoon region leads to a significant increase of precipitation in large parts of North Africa. In the Sahel zone precipitation amount rises by more than 10%, in the eastern Sahel even by more than 50%. The west coastal regions receive more than 25% more precipitation. In the central Sahara precipitation is more than doubled. Besides, precipitation rate is increased in the north-eastern Mediterranean by 20%-30%. Figure 6.7 shows that the deforestation leads to a low-pressure anomaly of up to 33Pa in Northern Africa. Therefore, the heat low in the Sahara is expanded and deepened. This induces an enhanced low-level flow from the ocean to the continent, bringing more moisture to the Sahara and Sahel. Furthermore, a reduced convergence in the upper troposphere above Africa and the Mediterranean (Figure 6.13) facilitate the formation of deep convection and precipitation.

#### **6.4.5 Effect of idealised forest-cover change on mid-Holocene climate**

During mid-Holocene, large parts of the Asian monsoon domain were covered by more forest and the forested and vegetated region expanded further inland compared to present-day (e.g. Yu et al., 2000; Ren and Beug, 2002; Ren, 2007; Herzschuh et al., 2010a). Pollen-based vegetation reconstructions reveal broad land-cover degradation since that period (e.g. Zhao et al. 2009). These changes are often related to the decrease in Asian monsoon strength (e.g. Fleitmann, 2003; Wang YJ. et al., 2005; Maher, 2008) entailing shifts in precipitation pattern.

However, early human forest clearance might also have impacted the mid- to late-Holocene climate and land cover change. Conversely, climate and land cover change could strongly have influenced the development and decline of different prehistoric cultures in the Asian monsoon domain (cf. Fu, 2003; Clift and Plumb, 2008). The linkage between mid-Holocene climate, vegetation and human dynamics in the Asian monsoon region is therefore a scientific question worth to investigate.

As the Asian topography is very complex, the relatively sparse-distributed reconstructions cannot necessarily represent the land cover in the entire region. Numerical experiments, for example conducted with the comprehensive Earth system model ECHAM5/JSBACH-MPIOM support the increase of vegetation and forest in the Asian monsoon domain under 6k climate conditions (Dallmeyer et al., 2010 and Fig. 4.4). But, compared to the available pollen records, the magnitude of Holocene vegetation change in these simulations seems to be underestimated. A complete picture of the mid-Holocene land cover in the Asian monsoon region and its change during the following millennia thus cannot be derived yet, neither from reconstructions nor from previous model-results.

To assess the biogeophysical impact of Holocene land cover change on the Asian monsoon climate we therefore chose an idealised approach: We assume that during mid-Holocene, the entire Asian monsoon domain was covered by forest and that mid- to late-Holocene climate change as well as early human forest clearance have altered the vegetation up to its present-day potential distribution. In other words, we repeat the afforestation and control experiment with the same boundary conditions with the exception that we prescribed mid-Holocene (6k = 6000yrs before present) insolation (FOR6k and CTRL6k). The biogeophysical effect of the idealised Holocene land cover change is then defined as the difference between the experiments 'FOR6k' and 'CTRL6k'.

Figure 6.14a depicts the summer monsoon related precipitation difference between the afforestation and control experiment under 6k-orbital conditions. Overall, the amplitude of monsoon precipitation change is similar as for 0k-orbit (cf. Fig 6.3, upper left panel), but the pattern of change is different. Afforestation has the same effect on precipitation at the south-central Tibetan Plateau (increase), the western Tibetan Plateau (decrease) and in

Northeast China (increase), regardless which orbit is prescribed. However, under 6k-orbital conditions, afforestation leads to more instead of less precipitation in south-eastern China (up to 0.2mm/day) and significantly more precipitation in north-western India (up to 0.25mm/day). Most striking is that precipitation is significantly increased by up to 0.45mm/day in the Shaanxi - Shandong region, where the prehistoric cultures settled.

To better visualise the different effect of afforestation under 6k- and 0k-orbital conditions, Figure 6.14b illustrates the difference of the afforestation-induced precipitation anomalies (6k-0k). It emphasises that afforestation leads to more precipitation in south- and central-

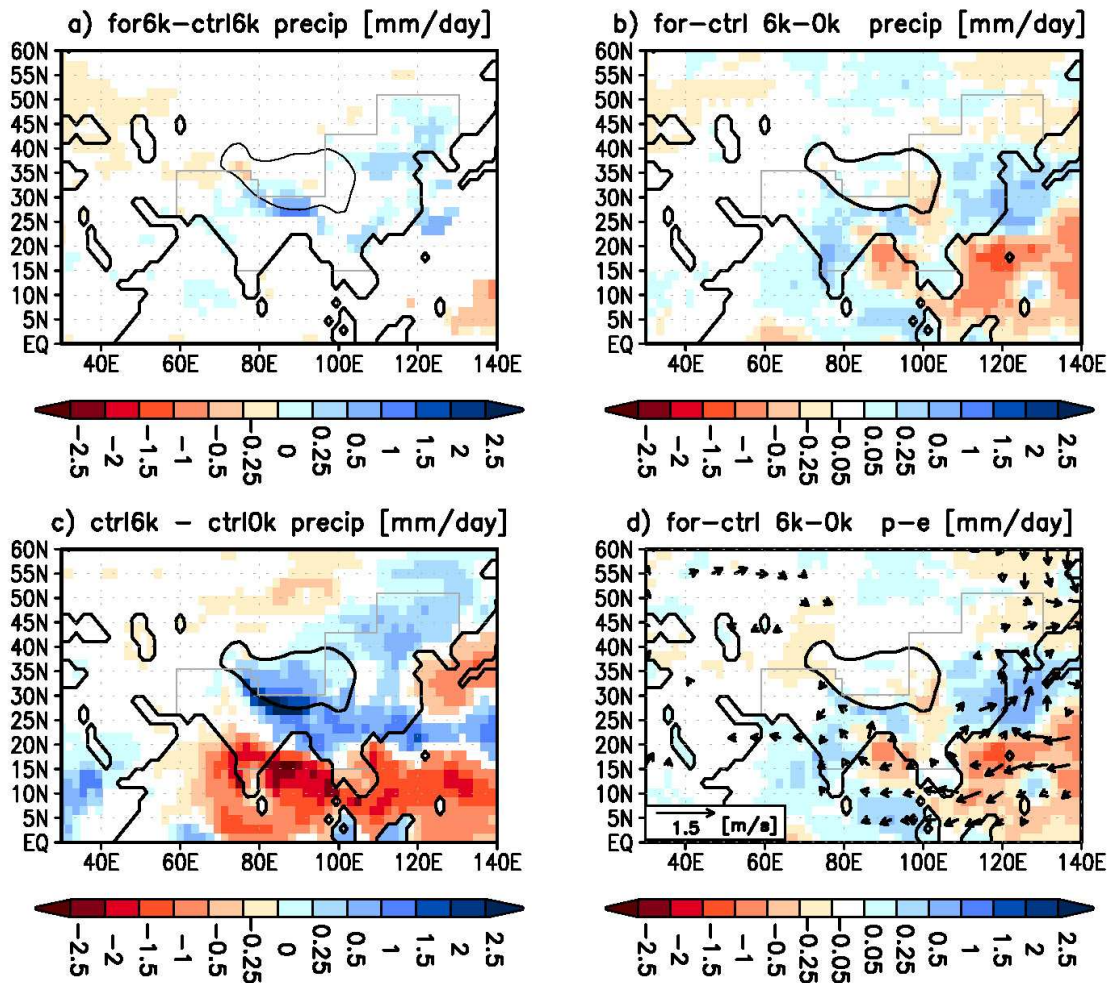


Figure 6.14: Simulated precipitation change [mm/day] between different experiments, averaged over the monsoon season: a) significant (95%, T-test) difference between the afforestation experiment (for) and the control run (ctrl) under mid-Holocene orbital conditions. b) difference of the afforestation-induced climate signal (for-ctrl) between the simulations with mid-Holocene (6k) and present-day (0k) orbital condition. c) significant (95%, T-test) difference between the control run with mid-Holocene orbit and the control run with present-day orbit prescribed. d) moisture convergence [mm/day] between for-ctrl under 6k-orbit and for-ctrl under 0k-orbit combined with the difference in 850hPa-wind [m/s]. Wind vectors with a magnitude of less than 0.15m/s are not shown. Please note that the figures on the right panel do not only show significant values.

eastern China as well as in India when mid-Holocene instead of present-day orbit is prescribed. These differences in the precipitation signal can be related to a change in circulation and moisture convergence (Figure 6.14d). With prescribed 6k-orbit, afforestation leads to a stronger monsoon flow anomaly onto the continent than under 0k-orbital conditions. Therefore, more moisture is transported from the Pacific Ocean and Bay of Bengal to East China and India.

Figure 6.14c shows the monsoon precipitation difference associated with the pure orbital forcing. Compared to this signal, the effect of afforestation on monsoon precipitation is weak. However, in the region with prehistoric settlement in eastern China, the precipitation change due to afforestation (6k) is approx. half as large as the change induced by the orbital forcing. Averaged over the region of approx. 99°E-120°E and 28°N-42°N, afforestation leads to a precipitation increase of 0.14mm/day. The orbital forcing results in 0.25mm/day additional precipitation.

According to our model results, large-scale Holocene forest decline, regardless, whether it has been climate- or human-induced, could thus strongly have contributed to the decrease in summer monsoon precipitation reconstructed for the East Asian monsoon region (e.g. Wang YJ. et al., 2005). However, the magnitude of the assumed forest loss in our study is intentionally exaggerated. The resulting climate signal can only be interpreted as a maximum effect. In comparison with the strong orbitally-induced climate signal, prehistoric deforestation might have been of no consequence. Nevertheless, according to our model results, one can not exclude that decreasing forest cover in the Asian monsoon region during the Holocene could have generated an additional environmental pressure on the Asian human civilisations by further reducing water availability.

## **6.5 Summary and conclusion of Chapter 6**

This study highlights the effect large-scale land cover change in the Asian monsoon domain could have on the regional and remote climate. By applying the general circulation model ECHAM5/JSBACH a set of numerical experiments has been performed with either complete forest cover or complete grass cover or potential present-day vegetation prescribed. Our analyses address the following questions: How do afforestation and deforestation influence the local climate? How large is the remote effect on precipitation in North Africa and the Middle East? Could early- and mid-Holocene land cover changes have contributed to the decreasing Asian monsoon precipitation known from reconstructions?

a.) Local effect:

- The impact of land cover change on local precipitation is most pronounced in the monsoon season. During this time, deforestation leads to a broad reduction of precipitation in the Asian monsoon domain. In contrast, the change of precipitation resulting from afforestation is arranged in an alternating pattern: rainfall is decreased in South India and the Great Plain of China, while it is increased in south-eastern China, the southern part of the Tibetan Plateau and Northeast China.
- The precipitation signal can partly be related to changes in humidity and moisture convergence and is partly induced by a modification of the low level circulation and vertical motion.
- The impact of land cover change on local near-surface air temperatures is most pronounced in the dry/cold season. During this time, deforestation leads to a cooling and afforestation to a warming of the climate in most parts of the Asian monsoon domain. In the monsoon season, the signal is of similar shape in the regions with a rather temperate or cool climate, i.e. the northern parts. In the southern parts where climate is tropical, afforestation (deforestation) leads to a temperature decrease (increase) resulting from an enhanced (reduced) evaporative cooling.
- Most of the temperature signal can be explained directly by the change in surface albedo due to the land cover change and the accompanied alteration of the surface energy balance.

b.) Remote effect:

- Changes in the Asian monsoon system can affect the climate in North Africa and the Middle East via the modification of the large-scale circulation. In our experiments, the remote effect of land cover change in the Asian monsoon domain on the precipitation pattern in these regions is strong with respect to the relative precipitation amount.
- According to our simulations, deforestation in the Asian monsoon domain significantly increases precipitation in most parts of North Africa. In some parts of the Sahara, rainfall is even doubled.
- Afforestation has no significant influence on African climate, but reduces precipitation in northern Arabia by up to 100%. That means, large-scale afforestation in monsoonal Asia could lead to a complete cessation of summer rainfall in northern Arabia.

c.) Role of Holocene land-cover change:

- The amplitude of the climate signal induced by afforestation does not change when prescribing mid-Holocene instead of present-day orbital conditions, but the pattern shifts, showing more precipitation in the region along the Yellow River.
- Compared to the climate change related to the orbital forcing, the overall climate signal induced by the land cover change is small in our model experiments. However, in the settlement area of East Asian prehistoric societies (mainly along the Yellow River) the precipitation change associated with the afforestation is half as large as the orbitally-induced precipitation change. In other words: under the assumption that the entire Asian monsoon region was covered by forest in early- and mid-Holocene, the loss of forest to the present-day potential land cover is responsible for more than one-third of the total mid- to late Holocene precipitation change in the settlement area of the major East Asian neolithic civilisations.
- The here prescribed complete forest cover is definitely an exaggerated representation of the mid-Holocene land cover in the Asian monsoon region. Therefore, the amplitude of the climate signal is probably too high.
- Our model results show that large-scale forest decline in East and South Asia leads to heavy losses in regional precipitation. One can not exclude that climate- or human-induced land cover changes have contributed to the decline of major prehistoric civilisations by amplifying the general orbital-induced attenuating Asian summer monsoon.

## 7. Summary and Conclusion

### 7.1 Summary and Conclusion

This study provides a detailed analysis of the mid- to late Holocene climate and vegetation change in the Asian monsoon region. The performance of the state-of-the-art general circulation model ECHAM5/JSBACH(-MPIOM) is evaluated in several model setups against present-day observations and reanalyses of the Asian monsoon climate (Chapter 2). We compare results of high resolution climate model simulations with a standardised and synchronised set of mid-Holocene climate reconstructions. We investigate in depth the changes in the monsoon characteristics and the mechanisms behind the Holocene precipitation changes (Chapter 3). The total climate response to the orbitally-induced insolation difference between the mid-Holocene and present-day is separated into the direct response of the atmosphere and the pure contribution of ocean-atmosphere and vegetation atmosphere interactions as well as their synergy. Herewith, the role of vegetation and ocean feedbacks in the Holocene Asian monsoon climate change are derived for the first time in a consistent set of climate model simulations (Chapter 4). To assess the performance of the model with respect to the Holocene land cover change, pollen-based vegetation reconstructions for different climate regions on the Tibetan Plateau are compared with the simulated land cover trend derived from a 6000yr-long transient simulation (Chapter 5). Furthermore, the effect of large-scale forest cover changes in the Asian monsoon domain on regional and global climate is investigated for the mid-Holocene and present-day (Chapter 6).

To conclude this study, we take up our research questions (Q) again and summarise the main findings:

#### **a.) Reproducibility of the present-day Asian monsoon climate (QI, QII):**

The general circulation model ECHAM5/JSBACH is able to capture the pattern of mean climate state in the Asian monsoon domain and can reproduce the major characteristics of the seasonal monsoon cycle. The model shows less skill in simulating the observed magnitude of temperature and precipitation and reveals a large rainfall deficit in the African and Indian monsoon domain in simulations with high numerical resolutions. Precipitation is better reproduced in coarse resolutions, but this is caused by a stronger numerical diffusion in coarse vertical resolutions (Roekner et al., 2006) and therefore only an artificial effect. The near-surface air temperature and monsoon dynamics are better represented in model setups with a high horizontal and vertical resolution since the regional topography is better resolved. The method of prescribing sea surface temperatures derived from coupled model simulations leads to additional biases in the model, but

influences particularly the precipitation distribution above the ocean. Therefore, this method has no negative consequences for the conclusions drawn in this thesis.

**b.) Mean climate differences and fundamental processes of the climate change between mid-Holocene and present-day (QIII-QV):**

As response to the mid-Holocene insolation forcing, the model simulates a warmer climate north of 20°N and a cooler climate south of 20°N. The summer monsoon is enhanced and prolonged in most parts of the Asian monsoon domain. Thus, ECHAM5/JSBACH shows a similar tendency of mid-Holocene to present-day climate change as other climate models. The comparison of the model results and climate reconstructions reveals the added value of using high numerical resolution in climate simulations for the Asian monsoon domain. The reconstructions suggest a regionally inhomogeneous Holocene moisture change with wetter mid-Holocene climate in the Indian monsoon domain and a spatially varying signal in the East Asian monsoon region. In the high resolution simulation, the model is able to reproduce this complex response to the insolation forcing and the results are more consistent with the reconstructions than other simulations, e.g. the simulations performed within the Paleoclimate Modelling Intercomparison Project (Braconnot et al., 2007a).

The reconstructions and the model results reveal differences in the response of the Indian and East Asian monsoon to the insolation forcing. This can be related to the different character of the monsoon systems determined by a meridional thermal gradient in case of the Indian monsoon and a zonal thermal gradient in case of the East Asian monsoon. In addition, the East Asian monsoon domain is strongly affected by the mid-latitude westerly wind circulation that leads to a different seasonal precipitation cycle compared to the Indian monsoon. Therefore, the behaviour of the monsoon systems is different. The increased annual precipitation change in the Indian monsoon region during the Holocene is determined solely by the intensification of the summer monsoon. In the East Asian monsoon domain, the sign of the annual precipitation change depends on the balance of decreased pre-monsoon precipitation and increased monsoon precipitation. This study shows the importance to extend the analysis period of mid-Holocene monsoon climate change to other seasons. So far, most studies confine their investigation to the summer season (e.g. Wang T. et al., 2010).

**c.) Role of ocean-atmosphere and vegetation-atmosphere feedbacks (QVI):**

Most of the Holocene climate change can be related to the direct atmospheric response to the insolation forcing, but the ocean-atmosphere interaction strongly modifies the signal. Due to the larger heat capacity of the ocean, the oceanic temperature response lags the insolation forcing and leads to a cooling of the climate in spring and summer and a warming of the climate in autumn and winter. Thereby, the ocean-atmosphere interaction shifts the magnitude of the seasonal signal imposed by the insolation forcing, i.e. the

strongest temperature change in the Asian monsoon region occurs in autumn and spring and not in summer and winter.

Regarding precipitation, the ocean-atmosphere interaction, on average, amplifies the atmospheric response to the insolation forcing. Regionally, e.g. in India, the model simulates a negative feedback. The pure contribution of the ocean-atmosphere interaction leads to a wetter Holocene climate in the Indian monsoon region and a rather drier climate in the East Asian monsoon region. Differences in the behaviour of the East Asian and Indian monsoon, thus, are also visible in the interaction of the atmosphere with the ocean.

The averaged contribution of the pure vegetation-atmosphere interaction is small with respect to the Holocene Asian monsoon temperature and precipitation changes. However, the simulated vegetation change in the Asian monsoon domain is also small and seems to be underestimated compared to reconstructions. In regions showing strong land cover changes like in the margins of the present-day Asian monsoon domain, the vegetation-atmosphere interaction significantly affects the climate.

**d.) Land cover change on the Tibetan Plateau (QVII,QVIII):**

The reconstructed and simulated land cover trends are qualitatively in agreement at most of the here considered sites on the Tibetan Plateau. Both show a strong degradation of the vegetation since the mid-Holocene that is particularly expressed in a reduction of forested area (decrease by 30% in the model). The resemblance of the simulated and reconstructed trend suggests a naturally and not anthropogenically induced mid- to late-Holocene land cover change on the Plateau. Besides changes in monsoonal precipitation, the model identifies variations in seasonal temperatures as the major mechanisms driving the Holocene vegetation trend. Temperature changes had, so far, rarely been considered as explanation for vegetation changes in regions affected by the Asian summer monsoon.

This study shows that ECHAM5/JSBACH is able to capture long-term vegetation trends. The reproducibility of the reconstructed trend and the analysis options of the model results, however, are limited by the coarse numerical resolution of the model simulation that leads to strong climatic biases in such an orographically complex area as the Tibetan Plateau. The vegetation on the Plateau is often living in climates near the limit of their bioclimatic range. Therefore, biases in the simulated climate can lead to large discrepancies between the model results and reconstructions regarding the kind of vegetation. The dependence of the simulated vegetation on fixed bioclimatic threshold makes the simulated vegetation on the Tibetan Plateau highly sensitive to even small climate changes. As the Asian monsoon climate is very complex, the vegetation change on the Tibetan Plateau is not representative for the entire monsoon domain. For a complete test of the simulated vegetation change, a detailed comparison of the model results and consistent vegetation reconstructions covering the entire Asian monsoon region is needed.

**e.) Climate response to large-scale forest cover changes and implications for the relation between Holocene climate, vegetation and neolithic cultures (QIX-XI):**

This study reveals that large-scale land cover degradation in the Asian monsoon domain can lead to a substantial decrease in regional precipitation and induces rainfall changes even in remote areas. According to current estimates of the magnitude of the Holocene vegetation change in the Asian monsoon region, the Holocene vegetation change, however, seems to have only a weak influence on the large-scale monsoon system and precipitation distribution. Our model reveals on the large-scale a much weaker precipitation change in response to the idealised forest decrease than in response to the orbital forcing. However, on regional scale, some areas exhibit a strong sensitivity to the forest cover change. This idealised experiment, thus, confirms the previous results of a locally strong vegetation feedback derived in Chapter 4. In the region along the Yellow river, for instance, the precipitation decrease related to the forest decline is half as large as the orbitally-induced precipitation decrease. This region was the settlement area of the major neolithic cultures in East Asia. According to our model simulation, one can not exclude an impact of natural or anthropogenic land cover changes on the Holocene climate development. One furthermore can not exclude that large-scale Holocene land cover changes have contributed to the decline of major Asian neolithic civilisation by further amplifying the decreasing precipitation trend in the settlement area known from reconstructions.

## **7.2 Outlook**

**Improvement of the model:** Our results show the added value of using high numerical resolutions in climate modelling studies for the Asian monsoon domain. Compared to observations, however, the model calculates much too little precipitation in the African and Indian monsoon domain in high resolution simulations. As the model shows a good skill in simulating the large-scale monsoon circulation, this rainfall deficit could be related to deficiencies in the model parameterisation. To further improve the model, the representation of the Asian monsoon climate in the model should be tested e.g. with respect to different cloud parameterisations and convection schemes. Furthermore, the comparison of the simulated and reconstructed mid-to late-Holocene temperature signal suggests an overestimation of the evaporative cooling in the model that may result from a too strong evaporation in the tropics. This should also be tested in sensitivity studies.

**Analysis of the Holocene climate variability of the East Asian and Indian monsoon:** The climate reconstructions of Wang et al. (2010) and our climate modelling results reveal regional dissimilarities in the climatic response to the mid-Holocene insolation forcing that indicate a different character of the Indian and East Asian monsoon system. An out-of-phase temporal development of these two sub-systems of the Asian monsoon has also been

suggested in previous paleo-reconstruction studies (e.g. An et al, 2000; He et al., 2004; Maher, 2008) identifying different timing of the maximum precipitation response to the Holocene insolation forcing. The annual precipitation trend in the last decades reveals a large spatial inhomogeneity (Ding et al., 2007; Trenberth et al., 2007). The East Asian summer monsoon circulation seems to weaken, thereby leading to a dipole change in precipitation with decreasing trend in North China and increasing trend in South China. The Indian summer monsoon precipitation shows no trend on a large-scale in the last century (Goswami et al. 2006). Locally increasing and decreasing trends are observed (Ghosh et al., 2009). However, the time interval used for the calculation strongly affects the sign of the calculated trend as the Asian monsoon exhibits a strong interdecadal variability (Webster et al., 1998; Wang B., 2006). The mechanisms causing the different behaviour of the Asian monsoon are not yet understood. A detailed spatial and temporal analysis of the Holocene monsoon variability (e.g. in transient climate simulations) and its relationship to other large-scale climate phenomena such as other monsoon systems, the El Nino Southern Oscillation, the Indian Ocean Dipole or the North Atlantic Oscillation during the Holocene will improve the understanding of teleconnections and the Asian monsoon variability. Such a study will give new insight into the mechanisms leading to the asynchronous response of the different Asian monsoon sub-systems to external forcings and will shed light on the processes characterising the inter- and counteraction of the monsoon sub-systems. This will also help to improve the future climate projections in the Asian monsoon domain.

**Detailed spatial comparison with Holocene vegetation reconstructions:** To represent the Holocene vegetation change in such a topographically complex area as the Asian monsoon region, well-dated and standardised high-quality pollen records are needed for as many sites as possible. So far, the pollen-based vegetation reconstructions in the Asian monsoon region are scarce and lack a consistent quality- and age-control. Therefore, a complete picture of the mid-Holocene vegetation distribution and its temporal variation cannot be provided by reconstructions yet. In a current project, all available fossil pollen records for monsoonal central Asia are collected, revised and synchronised (Herzschuh, personal communication). Maps with vegetation distributions at different time-slices (500-year interval) covering the last 18000 years will be available soon and can be compared to results of coupled atmosphere-ocean-vegetation models. With this dataset, the performance of the dynamic vegetation module in ECHAM5/JSBACH can be assessed in detail for the Asian monsoon region. Furthermore, it will be worth to repeat the idealised sensitivity study on large-scale forest cover changes with prescribed realistic (i.e. reconstructed) Holocene vegetation change to derive the magnitude of the vegetation-induced climate change and to strengthen our conclusions.

**Investigation of biogeochemical feedbacks resulting from land cover changes:** In the current study, we focus on the biogeophysical effect of land cover changes. Besides, land cover changes also affect the climate via a modification of the biogeochemical fluxes between the land and the atmosphere such as the release or uptake of CO<sub>2</sub> that, in turn, has an impact on the atmospheric CO<sub>2</sub>-concentration and hence on the global climate (e.g. Claussen et al., 2001). The strength and relative role of the biogeochemical and biogeophysical feedbacks is currently debated and investigated. Both can be positive or negative depending on region and time-scale (Claussen, 2009 and references therein) and climate changes amplified by the one feedback can be compensated by the other. To investigate the contribution of the ‘full’ atmosphere-vegetation interaction to the Holocene climate change in the Asian monsoon region both feedbacks should be accounted for in future studies. In this context, the influence of early human land use change on atmospheric greenhouse gas concentration is also discussed (e.g. Ruddiman, 2003, 2007, Ruddiman and Ellis, 2009, Varvus et al., 2008; Stocker et al., 2011). Early human societies in China could have played a decisive role in altering atmospheric methane concentration by irrigated rice farming, for instance (Ruddiman et al., 2008).

## Bibliography

- Adler, R.F., Huffman, G.J., Chang, A., Ferraro, R., Xie, P., Janowiak, J., Rudolf, B., et.al.: The Version 2 Global Precipitation Climatology Project (GPCP) Monthly Precipitation Analysis (1979-Present). *J. Hydrometeor.*, 4,1147-1167, 2003.
- Aldenderfer, M.S.: Modeling the Neolithic on the Tibetan Plateau. In: Madsen, D.B., 3, Chen, F., Gao, X. (eds.), Late Quaternary climate change and human adaption in arid China. *Developments in Quaternary Science*. 151-166, 2007.
- Aldenderfer, M., and Zhang, Y.: The prehistory of the Tibetan Plateau to the seventh century A.D.: perspectives and research from China and the West since 1950. *J. World Prehist.*, 18, 1–55, 2004.
- An, Z., Porter, S.C., Kutzbach, J.E., Wu, X., Wang, S., Liu, X., Li, X., and Zhou, W.: Asynchronous Holocene optimum of the East Asian monsoon. *Quat. Sci. Rev.*, 19, 743-762, 2000.
- Ansari, M., and Vink, A.: Vegetation history and palaeoclimate of the past 30 kyr in Pakistan as inferred from the palynology of continental margin sediments off the Indus Delta. *Rev. Paleobot. Palynol*, 145, 201–216, 2007.
- Asnani, G.C.: Tropical meteorology. Published by G.C. Asnani, c/o Indian Institute of Tropical Meteorology, Noble Printers, Pashan, Pune-411008, India, pp 1202 (2vols.), 1993.
- Bathiany, S., Claussen, M., Brovkin, V., Raddatz, T., and Gayler, V.: Combined biogeophysical and biogeochemical effects of large-scale forest cover changes in the MPI earth system model. *Biogeosciences*, 7 (5), 1383-1399, 2010.
- Berger, A.: Long-term variations of daily insolation and Quaternary climate changes. *J. Atmos. Sci.*, 35, 12, 2362-2367, 1978.
- Birks, H.J.B., and Birks, H.H.: *Quaternary Palaeoecology*. Edward Arnold, 1980.
- Bonan, G. B.: Forests and climate change: Forcings, feedbacks, and the climate benefits of forests. *Science*, 320, 1444-1449, 2008.
- Bonan, G. B., Pollard, D., and Thompson, S.L.: Effects of boreal forest vegetation on global climate. *Nature*, 359, 716-718, 1992.

- Boo, K.-O, Martin, G., Sellar, A., Senior, C., and Byun, Y.-H.: Evaluating the East Asian monsoon simulation in climate models. *J. Geophys. Res.*, 116, D01109, doi:10.1029/2010JD014737, 2011.
- Braconnot, P., Marti, O., Joussaume, S., and Leclainche, Y.: Ocean feedback in response to 6kyr BP insolation. *J. Climate*, 13, 1537-1553, 2000.
- Braconnot, P., Otto-Bliesner, B., Harrison, S., Joussaume, S., Peterchmitt, J.-Y., Abe-Ouchi, A., Crucifix, M., Driesschaert, E., Fichet, Th., Hewitt, C. D., Kageyama, M., Kitoh, A., Lañé, A., Loutre, M.-F., Marti, O., Merkel, U., Ramstein, G., Valdes, P., Weber, S. L., Yu, Y., and Zhao, Y.: Results of PMIP2 coupled simulations of the Mid-Holocene and Last Glacial Maximum – Part 1: experiments and large-scale features. *Clim. Past*, 3, 261-277, 2007a.
- Braconnot, P., Otto-Bliesner, B., Harrison, S., Joussaume, S., Peterchmitt, J.-Y., Abe-Ouchi, A., Crucifix, M., Driesschaert, E., Fichet, Th., Hewitt, C. D., Kageyama, M., Kitoh, A., Loutre, M.-F., Marti, O., Merkel, U., Ramstein, G., Valdes, P., Weber, L., Yu, Y., and Zhao, Y.: Results of PMIP2 coupled simulations of the Mid-Holocene and Last Glacial Maximum – Part 2: feedbacks with emphasis on the location of the ITCZ and mid- and high latitudes heat budget. *Clim. Past*, 3, 279-296, 2007b.
- Brantingham, P.J., and Gao, X.: Peopling of the northern Tibetan Plateau. *World Archaeol.*, 38, 387–414, 2006.
- Broccoli, A.J., and Manabe, S.: The effects of orography on mid-latitude northern hemisphere dry climates. *J. Climate*, 5, 1181–1201, 1992.
- Broström, A., Coe, M., Harrison, S.P., Gallimore, R., Kutzbach, J.E., Foley, J.A., Prentice, I.C., and Behling, P.: Land surface feedbacks and palaeomonsoons in northern Africa. *Geophys. Res. Lett.*, 25, 19, 3615-3618, 1998.
- Brovkin, V., Raddatz, T., Reick, C.H., Claussen, M., and Gayler, V.: Global biogeophysical interactions between forest and climate. *Geophys. Res. Lett.*, 36, L07405, doi:10.1029/2009GL037543, 2009.
- Bush, A.B.G.: Modelling of late Quaternary climate over Asia: a synthesis, *Boreas*, 33, 155–163, 2004.
- Chalita, S. and Le Treut, H.: The albedo of temperate and boreal forest and the Northern Hemisphere climate: a sensitivity experiment using the LMD GCM. *Climate Dynamics*, 10, 231-240, 1994.
- Claussen, M.: Modelling bio-geophysical feedback in the African and Indian monsoon region. *Clim. Dyn.*, 13, 247-257, 1997.

- Claussen, M.: Late Quaternary vegetation-climate feedbacks, *Clim. Past*, 5, 203-216, 2009.
- Claussen, M. and Gayler, V.: The greening of Sahara during the mid-Holocene: Results of an interactive atmosphere - biome model. *Global Ecol. Biogeogr.*, 6, 369-377, 1997.
- Claussen, M., Brovkin, V., and Ganopolski, A.: Biogeophysical versus biogeochemical feedbacks of large-scale land cover change. *Geophys. Res. Lett.*, 28, 6, 1011-1014, 2001.
- Clift, P. D., and Plumb, R.A.: *The Asian monsoon: causes, history and effects*. Cambridge Univ. Press, Cambridge, 270 p., 2008.
- Cour, P., Zheng, Z., Duzer, D., Calleja, M., and Yao, Z.: Vegetational and climatic significance of modern pollen rain in northwestern Tibet, *Rev. Palaeobot. Palyno.*, 104, 183-204, 1999.
- Cui, X., and Graf, H.F.: Recent land cover changes on the Tibetan Plateau: a review. *Climate Change*, 94, 47-61, 2009.
- Cui, X., Graf, H.F., Langmann, B., Chen, W., and Huang, R.: Climate impacts of anthropogenic land use changes on the Tibetan Plateau. *Global Planet. Change*, 54, 33-56, 2006.
- Dallmeyer, A., and Claussen, M.: The influence of land cover change in the Asian monsoon region on present-day and mid-Holocene climate. *Biogeosciences*, 8, 1499-1519, 2011.
- Dallmeyer, A., Claussen, M., and Otto, J.: Contribution of oceanic and vegetation feedbacks to Holocene climate change in monsoonal Asia. *Clim. Past*, 6, 195-218, 2010.
- Dallmeyer, A., Claussen, M., Herzsuh, U., and Fischer, N.: Holocene vegetation and biomass changes on the Tibetan Plateau – a model-pollen data comparison. *Clim. Past*, 7, 881-901, 2011)
- Dearing, J.A., Jones, R.T., Shen, J., Yang, X., Boyle J.F., Foster, G.C., Crook D.S., and Elvin, M.J.D.: Using multiple archives to understand past and present climate–human–environment interactions: the lake Erhai catchment, Yunnan Province, China. *J. Paleolimnol.*, 40, 3–31, 2008.
- Diffenbaugh, N.S., and Sloan, L.C.: Global climate sensitivity to land surface change: The mid Holocene revisited. *Geophys. Res. Lett.*, 29, 10, 1476, 2002.
- Ding, Y. H.: The variability of the Asian summer monsoon. *J. Meteor. Soc. Japan*, 85, 21–54, 2007.

- Ding, Y. H., and Chan, J.C.L.: The East Asian summer monsoon: an overview. *Meteorol. Atmos. Phys.*, 89,117–142, 2005.
- Ding, Y.H., Ren, G., Zhao, Z., Xu, Y., Luo, Y., Li, Q., and Zhang, J.: Detection, causes and projection of climate change over China: An overview of recent progress. *Adv. Atmos. Sci.* 24, 954-971, 2007.
- Duan, A., and Wu, G.X.: Role of the Tibetan Plateau thermal forcing in the summer climate pattern over subtropical Asia. *Clim. Dynam.*, 24, 793-807, 2005.
- Fang, J., Chen, A., Peng, C., Zhao, S., Ci, L.: Changes in forest biomass carbon storage in China between 1949 and 1998. *Science*, 292, 2320, 2001.
- Findell, K. L., Knutson, T.R., and Milly, P.C.D.: Weak simulated extratropical responses to complete tropical deforestation. *J. Climate*, 19, 2835–2850, 2006.
- Fischer, N., and Jungclauss, J.H.: Evolution of the seasonal temperature cycle in a transient Holocene simulation: orbital forcing and sea-ice. *Clim. Past Discuss.*, 7, 463-483, 2011.
- Fleitmann, D., Burns, S.J., Mudelsee, M., Neff, U., Kramers, J., Mangini, A., and Matter, A.: Holocene forcing of the Indian monsoon recorded in a stalagmite from Southern Oman, *Science*, 300 , pp. 1737–1739, 2003.
- Fontes, J., Gasse, F., and Gibert, E.: Holocene environmental changes in Lake Bangong basin (Western Tibet). Part 1: Chronology and stable isotopes of carbonates of a Holocene lacustrine core. *Palaeogeogr. Palaeoclimatol.*, 120 (1-2), 25-47, 1996.
- Fu, C.: Potential impacts of human-induced land cover change on East Asia monsoon. *Global and Planetary Change*, 37, 219-229, 2003.
- Gaillard, M.-J., Sugita, S., Mazier, F., Trondman, A.-K., Broström, A., Hickler, T., Kaplan, J. O., Kjellström, E., Kokfelt, U., Kuneš, P., Lemmen, C., Miller, P., Olofsson, J., Poska, A., Rundgren, M., Smith, B., Strandberg, G., Fyfe, R., Nielsen, A. B., Alenius, T., Balakauskas, L., Barnekow, L., Birks, H. J. B., Bjune, A., Björkman, L., Giesecke, T., Hjelle, K., Kalnina, L., Kangur, M., van der Knaap, W. O., Koff, T., Lagerås, P., Latałowa, M., Leydet, M., Lechterbeck, J., Lindbladh, M., Odgaard, B., Peglar, S., Segerström, U., von Stedingk, H., and Seppä, H.: Holocene land-cover reconstructions for studies on land cover-climate feedbacks, *Clim. Past*, 6, 483-499, 2010.
- Gao, X. J., Zhang, D. F., Chen, Z.X., Pal, J. S., and Giorgi, F.: Land use effects on climate in China as simulated by a regional climate model. *Science in China Series D: Earth Sciences*, 50 (4), 620-628, 2007.

- Gasse, F., Arnold, M., Fontes, J.Ch., Fort, M., Gibert, E., Huc, A., Bingyan, Li, Yuanfang, Li, Qing, Liu, Mélières, F., Van Campo, E., Fubao, Wang, and Qingsong, Zhang: A 13,000yr climate record from Western Tibet. *Nature*, 353, 742-745, doi:10.1038/353742a0, 1991.
- Ge, Q., Wang, S., Wen, Y., Shen, C., and Hao, Z.: Temperature and precipitation changes in China during the Holocene. *Adv. Atmos. Sci.*, 24, 6, 1024-1036, 2007.
- Gedney, N., and Valdes, P.J.: The effect of Amazonian deforestation on the Northern Hemisphere circulation and climate. *Geophys. Res. Lett.*, 27, 3053–3056, 2000.
- Gehrig, R., and Peeters, A.G.: Pollen distribution at elevations above 1000 m in Switzerland. *Aerobiologia*, 16, 69–74, 2000.
- Ghosh, S., Luniya, V, and Gupta: Trend analysis of Indian summer monsoon rainfall at different spatial scales. *Atmos. Sci Lett.*, 10, 4, 285-290, doi: 10.1002/asl.235, 2009.
- Goswami, B.N., Venugopal, V., Sengupta, D., et al.: Increasing trend of extreme rain events over India in a warming environment. *Science*, 314, doi: 10.1126/science.1132027, 2006.
- Hales, K., Neelin, J.D., and Zeng, N.: Interaction of Vegetation and Atmospheric dynamical mechanisms in the mid-Holocene African monsoon. *J. Climate*, 19, 4105-4120, 2006.
- Harrison, S. P., Jolly, D., Laarif, F., Abe-Ouchi, A., Dong, B., Herterich, K., Hewitt, C., Joussaume, S., Kutzbach, J.E., Mitchel, J., De Noblet, N., and Valdes, P.: Intercomparison of simulated global vegetation distributions in response to 6kyr BP orbital forcing. *J. Climate*, 11, 2721-2742, 1998.
- Hasler, N., Werth, D., and Avissar, R.: Effects of tropical deforestation on global hydroclimate: A multimodel ensemble analysis. *J. Climate*, 22, 1124–1141, 2009.
- He, J., Ju, J., Wen, Z., Lü, J., and Jin, Q.: A review of recent advances in Research on Asian monsoon in China. *Adv. Atmos. Sci.*, 24, 6, 972-992, 2007.
- He, Y., Theakstone, W.H., Zhang, Z.L., Zhang, D., Yao, T.D., Chen, T., Shen, Y.P., and Pan, H.X.: Asynchronous Holocene climate change across China, *Quatern. Res.*, 61, 52–63, 2004.
- Henderson-Sellers, A., Dickinson, R. E. , Durbidge, T. B., Kennedy, P. J., McGuffie, K., and Pitman, A. J.: Tropical deforestation: Modeling local-scale to regional-scale climate change. *J. Geophys. Res.*, 98 (D4), 7289–7315, 1993.

- Herzschuh, U., Winter, K., Wünnemann, B., and Li, S.: A general cooling trend on the central Tibetan Plateau throughout the Holocene recorded by the Lake Zigetang pollen spectra. *Quat. Int.*, 154-155, 113-121, 2006.
- Herzschuh, U., Kramer, A., Mischke, S., and Zhang, C.: Quantitative climate and vegetation trends since the late glacial on the northeastern Tibetan Plateau deduced from Koucha Lake pollen spectra. *Quat. Res.*, 71, 162-171, 2009.
- Herzschuh, U., Birks, J.: Evaluating the indicator value of Tibetan pollen taxa for modern vegetation and climate. *Rev. Palaeobot. Palyno*, 160, 197-208, 2010b.
- Herzschuh, U., Birks, H.J.B., Mischke, S., Zhang, C., and Böhner, J.: A modern pollen-climate calibration set based on lake sediments from the Tibetan Plateau and its application to a Late Quaternary pollen record from the Qilian Mountains. *J. Biogeogr.*, 37, 752-766, 2010c.
- Herzschuh, U., Birks, H.J.B., Ni, J., Zhao, Y., Liu, H., Liu, X., and Grosse, G.: Holocene land-cover changes on the Tibetan Plateau. *The Holocene*, 20, 91-104, 2010a.
- Hewitt, C.D., and Mitchell, J.F.B.: A fully-coupled GCM simulation of the climate of the mid-Holocene. *Geophys. Res. Lett.*, 25, 361-364, 1998.
- Hou, X. (chief ed.): *Vegetation atlas of China*. Science Press, Beijing, 2001.
- Hsu, H.-H., and Liu, X.: Relationship between the Tibetan Plateau heating and East Asian summer monsoon rainfall. *Geophys. Res. Lett.*, 30(20), 2066, doi:10.1029/2003GL017909, 2003.
- Irizarry-Ortiz, M., Wang G., and Elthair, E.A.B.: Role of the biosphere in the mid-Holocene climate of West Africa, *J. Geophys. Res.*, 108 (D2), 4042, 2003.
- Ivory, S., and Lézine, A.-M.: Climate Environmental change at the end of the Holocene Humid Period: a pollen record off Pakistan. *C. R. Geoscience*, 341, 760–769, 2009.
- Jacobson, G.L. Jr., and Bradshaw, R.H.W.: The selection of sites for paleovegetational studies. *Quat. Res.*, 16, 80-96, 1981.
- Jolly, D., Prentice, I.C., Bonnefille, R., Ballouche, A., Bengo, M., Brenac, P., Buchet, G., Burney, D., Cazet, J.P., Cheddadi, R., Ectorh, T., Elenga, H., Elmoutaki, S., Guiot, J., Laarif, F., Lamb, H., Lézine, A.M., Maley, J., Mbenza, M., Peyron, O., Reille, M., Reynaud-Farrera, I., Riollet, G., Ritchie, J.C., Roche, E., Scott, L., Ssemmanda, I., Straka, H., Umer, M., Van Campo, E., Vilimumbalo, S., Vincens, A., and Waller, M.: Biome reconstruction from pollen and plant macrofossil data for Africa and the Arabian peninsula at 0 and 6000 years. *J. Biogeogr.*, 25, 6, 1007–1027, 1998.

- Joussaume, S., and Braconnot, P.: Sensitivity of paleoclimate simulation results to season definitions. *J. Geophys. Res.*, 102 (D2), 1943-1956, 1997.
- Joussaume, S., Taylor, K.E., Braconnot, P., Mitchell, J.F.B., Kutzbach, J.E., Harrison, S.P., Prentice, I.C., Broccoli, A.J., Abe-Ouchi, A., Bartlein, P.J., Bonfiels, C., Dong, B., Guiot, J., Herterich, K., Hewit, C.D., Jolly, D., Kim, J.W., Kislov, A., Kitoh, A., Loutre, M.F., Masson, V., McAvaney, B., McFarlane, N., deNoblet, N., Peltier, W.R., Peterschmitt, J.Y., Pollard, D., Rind, D., Royer, J.F., Schlesinger, M.E., Syktus, J., Thompson, S., Valdes, P., Vettoretti, G., Webb, R.S., and Wyputta, U.: Monsoon changes for 6000 years ago: Results of 18 simulations from the Paleoclimate Modeling Intercomparison Project (PMIP). *Geophys. Res. Lett.*, 26 (7), 859-862, 1999.
- Jungclauss, J. H., Botzet, M., Haak, H., Keenlyside, N., Luo, J.-J., Latif, M., Marotzke, J., Mikolajewicz, U., and Roeckner, E.: Ocean circulation and tropical variability in the coupled model ECHAM5/MPI-OM. *J. Climate* 19, 3952-3972, 2006.
- Kalnay, E., Kanamitsu, M.; Kistler, R., Collins, W., Deaven, D., Gandin, L., Iredell, M., Saha, S., White, G., Woollen, J., Zhu, Y., Chelliah, M., Ebisuzaki, W., Higgins, W., Janowiak, J., Mo, K.C., Ropelewski, C., Wang, J., Leetmaa, A., Reynolds, R., Jenne, R., Joseph, D.: The NCEP/NCAR 40-year reanalysis project, *Bull. Amer. Meteor. Soc.*, 77, 437-470, 1996.
- Kang, I.S, Jin, K., Lau, K.-M., Shukla, J. et al: Intercomparison of atmospheric GCM simulated anomalies associated with the 1997/98 El Nino. *J. Climate*, 15, 2791–2805, 2002
- Kang, S., Xu, Y., You, Q., Flügel, W.-A., Pepin, N., and Yao, T.: Review of climate and cryospheric change in the Tibetan Plateau. *Environ. Res. Lett.*, 5, 015101, 8pp, doi:10.1088/1748-9326/5/1/015101, 2010.
- Kleinen, T., Tarasov, P., Brovkin, V., Andreev, A., and Stebich, M.: Comparison of modeled and reconstructed changes in forest cover through the past 8000 years: Eurasian perspective. *The Holocene*, doi: 10.1177/0959683610386980, 2011.
- Kohfeld, K.E., and Harrison, S.P.: How well can we simulate past climates? Evaluating the models using global palaeo-environmental data sets. *Quat. Sci. Rev.*, 19, 321-346, 2000.
- Kramer, A., Herzschuh, U., Mischke, S., and Zhang, C.: Holocene treeline shifts and monsoon variability in the Hengduan Mountains (southeastern Tibetan Plateau), implications from palynological investigations. *Palaeogeogr. Palaeoclimatol.*, 286, 1-2, 23-41, 2010.
- Kutzbach, J.E., and Liu, Z.: Oceanic feedback on the western African monsoon at 6000 BP. *Science*, 278, 440-443, 1997.

- Kutzbach, J.E., and Otto-Bliesner: The sensitivity of the African-Asian monsoonal climate to orbital parameter changes for 9000 yr BP in a low-resolution general circulation model. *J. Atmos. Sci.*, 39, 1177-1188, 1982.
- Lau, K.-M., Kim, K.-M., and Yang, S.: Dynamical and boundary forcing characteristics of regional components of the Asian summer monsoon. *J. Climate*, 13, 2461-2482, 2000.
- Levis, S., Bonan, G.B., and Bonfils, C., 2004: Soil feedback drives the mid-Holocene North African monsoon northward in fully coupled CCSM2 simulations with a dynamic vegetation model. *Clim. Dynam.*, 23, 791-802, 2004.
- Li, C., and Yanai, M.: The onset and interannual variability of the Asian summer monsoon in relation to land-sea thermal contrast. *J. Clim.*, 9, 358-375, 1996.
- Li, Y., and Harrison, S.: Simulations of the impact of orbital forcing and ocean on the Asian summer monsoon during the Holocene. *Global and Planetary Change*, 60, 505-522, 2008.
- Li, Y., Harrison, S., Zhao, P., and Ju, J.: Simulations of the impact of dynamic vegetation on interannual and interdecadal variability of Asian summer monsoon with modern and mid-Holocene orbital forcings. *Global Planet. Change*, 66, 3/4, 235-252, 2009.
- Liu, X., Shen, J., Wang, S., Wang, Y., and Liu, W.: Southwest monsoon changes indicated by oxygen isotope of ostracode shells from sediments in Qinghai Lake since the late Glacial. *Chinese Sci. Bull.*, 52, 539-544, 2007.
- Liu, Y. M., Bao, Q., Duan, A. M., Qian, Z.A., and Wu, G. X., 2007: Recent progress in the impact of the Tibetan Plateau on climate in China. *Adv. Atmos. Sci.*, 24, 1060-1076, 2007.
- Liu, Z., Harrison, S.P., Kutzbach, J.E., and Otto-Bliesner, B.: Global monsoons in the mid-Holocene and oceanic feedback. *Clim. Dyn.*, 22, 157-182, 2004.
- Loveland, T.R., Reed, B.C., Brown, J.F., Ohlen, D.O., Zhu, Z., Yang, L., and Merchant, J.W.: Development of a global land cover characteristics database and IGBP DISCover from 1 km AVHRR data. *Int. J. Remote Sensing*, 21, 1303-1330, 2000.
- Maher, B.A.: Holocene variability of the East Asian summer monsoon from Chinese cave records: a re-assessment. *The Holocene*, 18, 6, 861-866, 2008.
- Maher, B.A., and Hu, M.: A high-resolution record of Holocene rainfall variations from the western Chinese Loess Plateau: antiphase behaviour of the African/Indian and East Asian summer monsoons. *The Holocene* 16, 309-319, 2006.
- Markgraf, V.: Pollen dispersal in a mountain area. *Grana*, 19, 127-146, 1980.

- Marsland, S. J., Haak, H., Jungclaus, J. H., Latif, M., and Roske, F.: The Max-Planck-Institute global ocean/sea ice model with orthogonal curvilinear coordinates. *Ocean Modell.*, 5, 91-127, 2003.
- Marzin, C., and Braconnot, P.: Variations of Indian and African monsoons induced by insolation changes at 6 and 9.5 kyr BP. *Clim. Dyn.* 33(2-3): 215, 2009a.
- Marzin, C., and Braconnot, P.: The role of the ocean feedback on Asian and African monsoon variations at 6 kyr and 9.5 kyr BP. *Comptes Rendus Geoscience*, 341, 8-9, 643-655, 2009b.
- Miller, P. A., Giesecke, T., Hickler, T., Bradshaw, R. H. W., Smith, B., Seppä, H., Valdes, P. J., and Sykes, M. T.: Exploring climatic and biotic controls on Holocene vegetation change in Fennoscandia. *J. Ecol.*, 96: 247–259. doi: 10.1111/j.1365-2745.2007.01342.x, 2008.
- Mitchell, T.D, Jones, P.D.: An improved method of constructing a database of monthly climate observations and associated high-resolution grids. *International Journal of Climatology*, 25, 6, 693-712, 2005.
- Ohgaito, R., and Abe-Ouchi, A.: The role of ocean thermodynamics and dynamics in Asian summer monsoon changes during the mid-Holocene. *Clim. Dyn.*, 29, 39-50, 2007.
- Otto, J., Raddatz, T., Claussen, M., Brovkin, V., and Gayler, V.: Separation of atmosphere-ocean-vegetation feedbacks and synergies for mid-Holocene climate. *Geophys. Res. Lett.*, 36, L09701, 2009a.
- Otto, J., Raddatz, T., and Claussen, M.: Climate variability-induced uncertainty in mid-Holocene atmosphere-ocean-vegetation feedbacks. *Geophys. Res. Lett.*, 36, 23, doi:10.1029/2009GL041457, in press, 2009b.
- Otto, J., Raddatz, T., and Claussen, M.: Strength of forest-albedo feedback in mid-Holocene climate simulations, *Clim. Past Discuss.*, 7, 809-840, 2011.
- Pielke, R. A., Avissar, R., Raupach, M., Dolman, A. J., Zeng, X. B., and Denning, A. S.: Interactions between the atmosphere and terrestrial ecosystems: influence on weather and climate. *Glob. Change Biol.*, 4, 461–475, 1998.
- Polcher, J., and Laval, K.: The impact of African and Amazonian deforestation on tropical climate. *Journal of Hydrology*, 155, 389-405, 1994.
- Polcher J, McAvaney, B., Viterbo, P., Baertner, M-A., Hahmann, A., Mahfouf, J-F., Noilhan, J., Phillips, T., Pitman, A., Schlosser, C.A., Schulz, J-P., Timbal, B.,

- Verseghy, D., Xue, Y.: A proposal for a general interface between land surface schemes and general circulation models. *Global and Planetary Change* 19, 261–276, 1998.
- Pongratz, J., Reick, C., Raddatz, T., and Claussen, M.: A reconstruction of global agricultural areas and land cover for the last millennium. *Global Biogeochem. Cycles*, 22, GB3018, doi:10.1029/2007GB003153, 2008.
- Pope, V.D., Pamment, J.A., Jackson, D.R., and Slingo, A.: The representation of water vapor and its dependence on vertical resolution in the Hadley Centre climate model. *J. Climate*, 14, 3065-3085, 2001.
- Prentice, I.C., Guiot, J., Huntley, B., Jolly, D., and Cheddadi, R.: Reconstructing biomes from palaeological data: a general method and its application to European pollen data at 0 and 6 ka. *Clim. Dynam.*, 12, 185–94, 1996.
- Raddatz, T.J., Reick, C.H., Knorr, W., Kattge, J., Roeckner, E., Schnur, R., Schnitzler, K.-G., Wetzell, P., and Jungclaus, J.: Will the tropical land biosphere dominate the climate-carbon cycle feedback during the twenty-first century? *Clim. Dynam.*, 29, 565-574, 2007.
- Ramankutty, N., and Foley, J.A.: Estimating historical changes in global land cover: croplands from 1700 to 1992. *Global Biogeochem. Cy.*, 13(4), 997-1027, 1999.
- Ren, G.: Decline of the mid- to late Holocene forests in China: climatic change or human impact?. *J. Quaternary Sci.*, 15(3), 273-281, 2000.
- Ren, G.: Changes in forest cover in China during the Holocene. *Veget. Hist. Archaeobot.*, 16, 119-126, 2007.
- Ren, G., and Beug, H-J.: Mapping Holocene pollen data and vegetation of China. *Quat. Sci. Rev.*, 21, 1395-1422, 2002.
- Rhode, D., Zhang, H.Y., Madsen, D.B., Xing, G., Brantingham, R.J., Ma, H.Z., and Olsen, J.W.: Epipaleolithic/early Neolithic settlements at Qinghai Lake, western China. *J. Archaeol. Sci.*, 34, 600-612, 2007.
- Rodwell, M., and Hoskins B.: Monsoons and the dynamics of deserts. *Quart. J. Roy. Meteor. Soc.*, 122, 1385-1404, 1996.
- Roeckner, E., Bäuml, G., Bonaventura, L., Brokopf, R., Esch, M., Giorgetta, M., Hagemann, S., Kirchner, I., Kornbluh, L., Manzini, E., Rhodin, A., Schlese, U., Schultzweida, U., and Tompkins, A.: The atmospheric general circulation model ECHAM5. Part I: Model description. Max-Planck-Inst. f. Meteor., Report No. 349, Hamburg, 2003.

- Roeckner, E., Brokopf, R., Esch, M., Giorgetta, M., Hagemann, S., Kornbluh, L., Manzini, E., Schlese, U., and Schulzweida, U.: Sensitivity of simulated climate to horizontal and vertical resolution in the ECHAM5 atmosphere model. *J. Climate*, 19, 3771-3791, 2006.
- Ruddiman, W.F: The anthropogenic greenhouse era began thousands of years ago. *Clim. Change*, 61, 3, 261-193, doi:10.1023/B:CLIM.0000004577.17928.fa, 2003.
- Ruddiman, W.F: The early anthropogenic hypothesis: Challenges and responses, *Rev. Geophys.*, 45, 3, RG4001, doi:10.1029/2006RG000207, 2007.
- Ruddiman, W.F., and Ellis, E.C.: Effect of per-capita land use changes on Holocene forest clearance and CO<sub>2</sub> emissions. *Quatern. Sci. Rev.*, 28, 27-28, 3011-3015, 2009.
- Ruddiman, W.F., Guo, Z., Zhou, X. et al.: Early rice farming and anomalous methane trends. *Quatern. Sci. Rev.*, 27,13-14,1291-1295, doi: 10.1016/j.quascirev.2008.03.007, 2008.
- Sato, T.: Influences of subtropical jet and Tibetan Plateau on precipitation pattern in Asia: insights from regional climate modelling. *Quatern. Int.*, 194,148–158, 2009.
- Schlütz, F., and Lehmkuhl, F.: Holocene climatic change and the nomadic Anthropocene in Eastern Tibet: palynological and geomorphological results from the Niabooyeze Mountains. *Quat. Sci. Rev.*, doi: 10.1016/j.quascirev.2009.01.009, 2009.
- Shen, J., Liu, X., Wang, S., and Ryo, M.: Paleoclimatic changes in the Qinghai Lake area during the last 18.000 years. *Quat. Int.*, 136, 131-140, 2005.
- Shen, J., Jones, R.T., and Yang, X.: The Holocene vegetation history of Lake Erhai, Yunnan Province southwestern China: the role of climate and human forcings. *The Holocene*, 16, 265-276, 2006.
- Shi, Y., Kong, Z., Wang, S., Tang, L., Wang, F., Yao, T., Zhao, X., Zhang, P., and Shi, S.: Mid-holocene climates and environments in China. *Global Planet. Change*, 7, 1-3, 219-233, 1993.
- Simmons, A. J. and Gibson, J. K.: The ERA-40 Project Plan, ERA-40 Project Report Series No. 1 ECMWF. Shinfield Park, Reading, UK, 63 pp., 2000.
- Singh, G., Wasson, R.J., and Agrawal, D.P.: Vegetational and seasonal climate changes since the last full glacial in the Thar Desert, northwestern India. *Rev. Paleobot. Palynol.* 64, pp. 351–358, 1990.
- Sitch, S., Smith, B., Prentice, I.C., Arneth, A., Bondeau, A., Cramer, W., Kaplan, J. O., Levis, S., Lucht, W., Sykes, M. T., Thonicke, K., and Venevsky, S.: Evaluation of

- ecosystem dynamics, plant geography and terrestrial carbon cycling in the LPJ dynamic global vegetation model. *Glob. Change Biol.*, 9, 161-185, 2003.
- Sivakumar, M. V. K., Brunini, O., and Das, H. P.: Impacts of present and future climate variability on agriculture and forestry in the arid and semi-arid tropics. *Clim. Change*, 70, 31–72, 2005.
- Snyder, P.K.: The influence of tropical deforestation on the Northern Hemisphere climate by atmospheric teleconnections. *Earth Interact.*, 14, 1-34, doi:10.1175/2010EI280.1, 2010.
- Stein, U., and Alpert, P.: Factor separation in numerical simulations. *J. Atmos. Sci.*, 50, 2107-2115, 1993.
- Stocker, B.D., Strassmann, K., and Joos, F.: Sensitivity of Holocene atmospheric CO<sub>2</sub> and the modern carbon budget to early human land use: analyses with a process-based model. *Biogeosciences*, 8, 1, 69-88, 2011.
- Studley, J.: Forests and environmental degradation in SW China. *Int. For. Rev.*, 1, 260-265, 1999.
- Sun, H. (chief editor): The national physical atlas of China. China Cartographic Publishing House, 230pp., 1999.
- Tang, L., Shen, C., Liu, K., and Overpeck, J.T.: New high resolution pollen records from two lakes in Xizang (Tibet). *Acta Botanica Sinica*, 41, 896-902, 1999.
- Tang, L. Y., Shen, C. M., Li, C. H., et al.: Pollen-inferred vegetation and environmental changes in the central Tibetan Plateau since 8200 yr BP, *Sci China Ser D-Earth Sci.*, 52(8), 1104-1114, doi: 10.1007/s11430-009-0080-5, 2009.
- Texier, D., de Noblet, N., and Braconnot, P.: Sensitivity of the African and Asian monsoons to mid-Holocene insolation and data-inferred surface changes. *J. Climate*, 13, 164-181, 2000.
- Trenberth, K.E., Jones, P.D., Ambenje, P., Bojariu, R., Easterling, D., Klein Tank, A., Parker, D., Rahimzadeh, F., Renwick, J.A., Rusticucci, M., Soden, B., and Zhai, P.: Observations: Surface and Atmospheric Climate Change. In: *Climate Change 2007: The Physical Science Basis. Contribution of Working Group I to the Fourth Assessment Report of the Intergovernmental Panel on Climate Change* [Solomon, S., D. Qin, M. Manning, Z. Chen, M. Marquis, K.B. Averyt, M. Tignor and H.L. Miller (eds.)]. Cambridge University Press, Cambridge, United Kingdom and New York, NY, USA, 2007.

- Ueno, K., Fujii, H., Yamada, H., and Liu, L.: Weak and frequent monsoon precipitation over the Tibetan Plateau. *J. Meteorol. Soc. Jpn*, 79 (1B), 419-434, 2001.
- Vamborg, F.S.E.: Vegetation - albedo - precipitation interactions in North Africa during the Holocene. PhD-Thesis, *Berichte zur Erdsystemforschung*, 94, Max-Planck-Institute for Meteorology, Hamburg, 2011.
- Van Campo, E., Cour, P., and Sixuan, H.: Holocene environmental changes in Bangong Co basin (Western Tibet). Part 2: The pollen record. *Palaeogeogr. Palaeoclimatol.*, 120 (1-2), 49-63, 1996.
- Vavrus, S, Ruddiman, W.F, and Kutzbach, J.E: Climate model tests of the anthropogenic influence on greenhouse-induced climate change: the role of early human agriculture, industrialization, and vegetation feedbacks, *Quatern. Sci Rev.*, 27, 13-14, 1410-1425, doi: 10.1016/j.quascirev.2008.04.011, 2008.
- Voss, R., and Mikolajewicz, U.: The climate of 6000 years BP in near-equilibrium simulations with a coupled AOGCM. *Geophys. Res. Lett.*, 28, 11, 2213-2216, 2001.
- Wang, B. (Ed.): *The Asian Monsoon*. Springer/Praxis Publishing Co., Berlin, Heidelberg, New York, pp787, 2006.
- Wang, B., and LinHo: Rainy season of the Asian-Pacific summer monsoon. *J. Climate*, 15, 386–398, 2001.
- Wang, B., Wu, R., Lau, and K.-M.: Interannual variability of the Asian summer monsoon: Contrasts between the Indian and the Western North Pacific-East Asian Monsoon. *J. Climate*, 14, 4073-4090, 2001.
- Wang, B., Bao, Q., Hoskins, B., Wu, G.X., and Liu, Y.: Tibetan Plateau warming and precipitation changes in East Asia. *Geophys. Res. Lett.*, 35, 14, doi:10.1029/2008GL034330, 2008.
- Wang, H.-J.: Role of vegetation and soil in the Holocene megathermal climate over China. *Journal of Geophysical Research*, 104, D8, 9361-9367, 1999.
- Wang, T., Wang, H. J., and Jiang, D. B.: Mid-Holocene East Asian summer climate as simulated by the PMIP2 models, *Palaeogeogr. Palaeoclimatol. Palaeoecol.*, 288, 93–102, 2010.
- Wang YB., Liu, XQ. , and Herzschuh, U.: Asynchronous evolution of the Indian and East Asian Summer Monsoon indicated by Holocene moisture patterns in monsoonal central Asia. *Earth-Sci. Rev.*, 103, 3-4, 135-153, doi: 10.1016/j.earscirev.2010.09.004, 2010.

- Wang, Y. J., Cheng, H., Edwards, R.L., He, Y.Q., Kong, X.G., An, Z.S., Wu, J.Y., Kelly, M.J., Dykoski, C.A., and Li, X.D.: The Holocene Asian monsoon: Links to solar changes and North Atlantic climate. *Science*, 308, 854-857, 2005.
- Webster, P.J., Magaña, V.O., Palmer, T.N., Shukla, J., Tomas, R.A., Yanai, M., and Yasunari, T.: Monsoons: Processes, predictability, and the prospects for prediction. *J. Geophys. Res.*, 103 (C7), 14451-14510, 1998.
- Wei, J., and Wang, H.: A possible role of solar radiation and ocean in the mid-Holocene East Asian monsoon Climate. *Adv. Atmos. Sci.*, 21, 1, 1-12, 2004.
- Werth, D., and Avissar, R.: The local and global effects of Amazonian deforestation. *J. Geophys. Res.*, 107, 8087, doi:10.1029/2001JD000717, 2002.
- Werth, D., and Avissar, R.: The local and global effects of Southeast Asian deforestation. *Geophys. Res. Lett.*, 32, L20702, doi: 10.1029/2005GL022970, 2005a.
- Werth, D., and Avissar, R.: The local and global effects of African deforestation. *Geophys. Res. Lett.*, 32, L12704, doi:10.1029/2005GL022969, 2005b.
- Winkler, M. G., and Wang, P. K.: The late-Quaternary vegetation and climate of China. In Wright, H. E., Kutzbach, J. E., Webb III, T., Ruddiman, W. F., Street-Perrott, F. A., Bartlein, P. J. (eds). *Global Climate since the Last Glacial Maximum*, University of Minnesota Press, Minneapolis, 221– 264, 1993.
- Wischniewski, J., Mischke, S., Wang, Y., and Herzschuh, U.: Reconstructing climate variability on the northeastern Tibetan Plateau since the last Lateglacial – a multi-proxy, dual-site approach comparing terrestrial and aquatic signals. *Quat. Sci. Rev.*, 30, 1-2, 82-97, 2011.
- Wohlfahrt, J., Harrison, S.P., Braconnot, P., Hewitt, C.D., Kitoh, A., Mikolajewicz, U., Otto-Bliesner, B.L., and Weber, S.L.: Evaluation of coupled ocean-atmosphere simulations of the mid-Holocene using palaeovegetation data from the northern hemisphere extratropics. *Clim. Dynam.*, 31, 871-890, doi:10.1007/s00382-008-0415-5, 2008.
- Wu, G.X.: Recent advances in Qinghai-Xizhang-Plateau climate dynamic research. *Quarterly Science*, 24(1), 1-9, 2004. (in Chinese).
- Wu, G.X., and Zhang, Y.S.: Tibetan Plateau forcing and the timing of the monsoon onset over South Asia and the South China Sea. *Mon. Wea. Rev.*, 126, 913-927, 1998.

- Wu, G.X., Wang, J., Liu, X., and Liu, Y.M.: Numerical modelling of the influence of Eurasian orography on the atmospheric circulation in different seasons. *Acta Meteorol. Sin.*, 63 (5), 603-612, 2005. (in Chinese).
- Wu, G.X., Liu, Y.M., Wang, T.M., Wan, R., Liu, X., Li, W., Wang, Z., Zhang, Q., Duan, A., and Liang, X.: The influence of the mechanical and thermal forcing of the Tibetan plateau on the Asian climate. *J. Hydrometeorol.*, 8, 770-789, 2007.
- Xie, P., and Arkin, P.A.: Global precipitation: A 17-year monthly analysis based on gauge observations, satellite estimates, and numerical model outputs. *Bull. Amer. Meteor. Soc.*, 78, 2539 – 2558, 1997.
- Xu, H., Hou, Z.H., Ai, L. and Tan, L.C.: Precipitation at Lake Qinghai, NE Qinghai-Tibet Plateau, and its relation to Asian summer monsoons on decadal/ interdecadal scales during the past 500 years. *Palaeogeogr. Palaeoclimatol.*, 254, 541-549, 2007.
- Yanai, M., and Wu, G.X.: Effects of the Tibetan Plateau. *The Asian Monsoon*, B. Wang, Ed., Springer, 513-549, 2006.
- Yasunari, T.: Role of Land-Atmosphere Interaction on Asian Monsoon Climate. *J. Meteorol. Soc. Jpn.*, 85B, 55-75, 2007.
- Yasunari, T., Saito, K., and Takata, K.: Relative roles of large-scale orography and land surface processes in the global hydroclimate. Part 1: Impacts on monsoon systems and the Tropics. *Journal of Hydrometeorology*, 7, 626-641, 2006.
- Ye, D.Z., and Wu, G.X.: The role of the heat source of the Tibetan Plateau in the general circulation. *Meteorol. Atmos. Phys.*, 67, 181-198, 1998.
- Yihui, D., and Zunya, W.: A study of rainy seasons in China. *Meteorol. Atmos. Phys.*, 100, 1-4, 121-138, doi: 10.1007/s00703-008-0299-2, 2008.
- Yu, G., Prentice, I.C., Harrison, S.P., and Sun, X.: Pollen-based biome reconstruction for China at 0 and 6000 years. *J. Biogeogr.*, 25, 1055–69, 1998.
- Yu, G., Chen, X., Ni, J., Cheddadi, R., Guiot, J., Han, H., Harrison, S.P., Huang, C., Ke, M., Kong, Z., Li, S., Li, W., Liew, P., Liu, G., Liu, J., Liu, Q., Liu, K.-B., Prentice, I.C., Qui, W., Ren, G., Song, C., Sugita, S., Sun, X., Tang, L., Van Campo, E., Xia, Y., Xu, Q., Yan, S., Yang, X., Zhao, J., and Zheng, Z.: Palaeovegetation of China: a pollen date-based synthesis for the mid-Holocene and last glacial maximum. *J. Biogeogr.*, 27, 635–664, 2000.
- Zhang, H. Q., and Gao X.J.: On the atmospheric dynamical response to land-use change in East Asian monsoon region. *Clim. Dyn.*, 33, 409-426, 2008.

- Zhang, P., Shao, G., Zhao, G., Le Master, D., Parker, G., Dunning, Jr. J., and Li, Q.: Ecology: China's forest policy for the 21st century. *Science*, 288, 2135, 2000.
- Zhang, Q. Y., Jin, Z.H., and Peng, J.B.: The relationship between convection over the Tibetan Plateau and circulation over East Asia. *Chinese J. Atmos. Sci.*, 30, 802-812, 2006, (in Chinese).
- Zhao, Y., Yu, Z., and Chen, F.: Spatial and temporal patterns of Holocene vegetation and climate changes in arid and semi-arid China. *Quat. Int.*, 194, 6-18, 2009.
- Zheng, Y.Q., Yu, G., Qian, Y. F., Miao, M., Zeng, X.M., and Liu, H.Q.: Simulations of regional climatic effects of vegetation change in China. *Q.J.R. Meteorol. Soc.*, 128, 2089-2114, 2002.
- Zheng, Y.Q., Yu, G., Wang, S.M., Xue, B., Zhuo, D.Q., Zeng, X.M., Liu, H.Q.: Simulation of paleoclimate over East Asia at 6ka BP and 21ka BP by regional climate model. *Clim. Dyn.*, 23, 513-529, 2004.
- Zhou, T., Wu, B., Scaife, A.A., Brönnimann, S., Cherchi, A., Fereday, D., Fischer, A.M., Folland, C.K., Jin, K.E., Kinter, J., Knight, J.R., Kucharski, F., Kusunoki, S., Lau, N.-C., Li, L., Nath, M.J., Nakaegawa, T., Navarra, A., Pegion, P., Rozanov, E., Schubert, S., Sporyshev, P., Voldoire, A., Wen, X., Yoon, J.H., Zeng, N.: The CLIVAR C20C Project: Which components of the Asian-Australian Monsoon variability are forced and reproducible?. *Clim. Dyn.*, 33 (7-8), 1051-1068, doi:10.1007/s00382-008-0501-8, 2009.

## Appendix A: Additional figures

### A.I Maps of Central and Eastern Asia

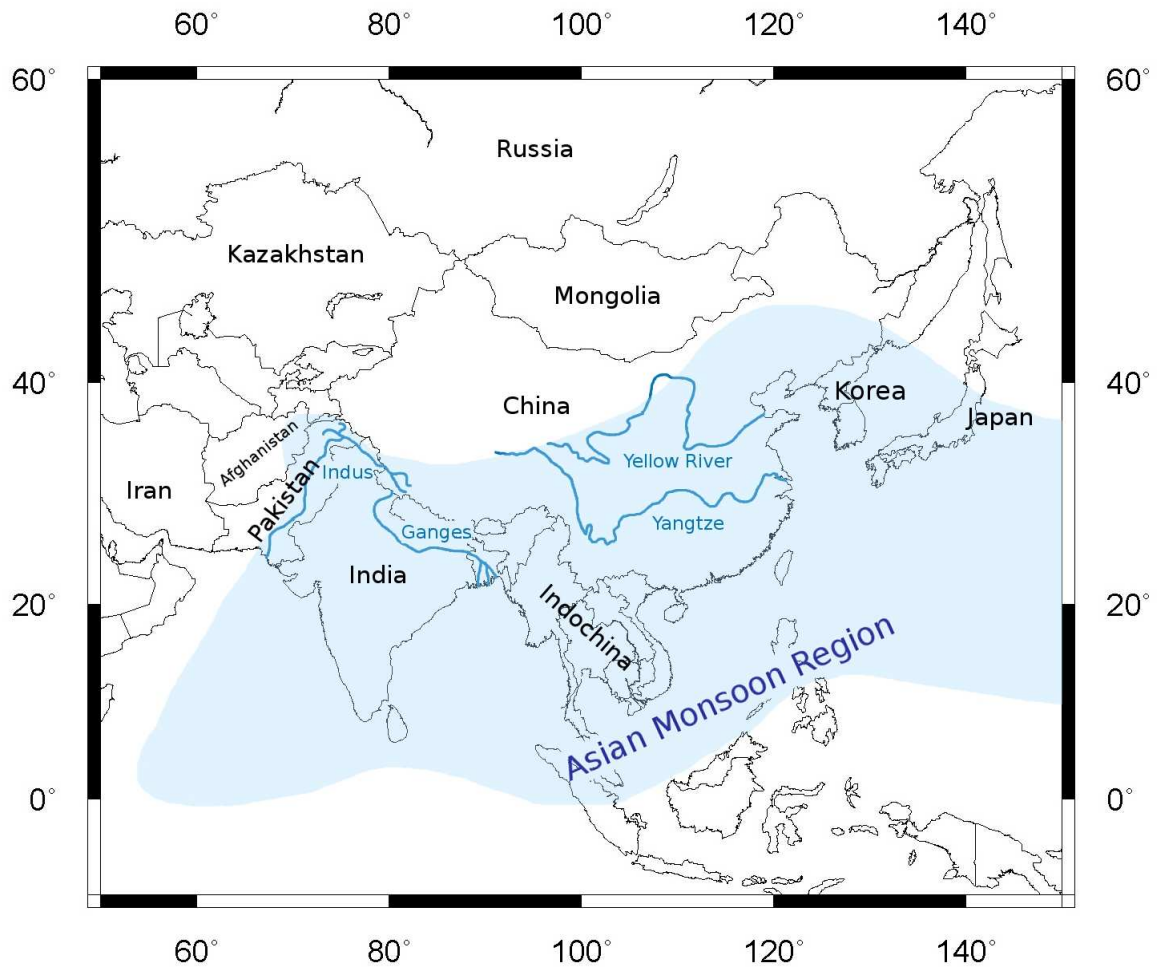


Figure A.1: The Asian monsoon region, only some rivers are shown.

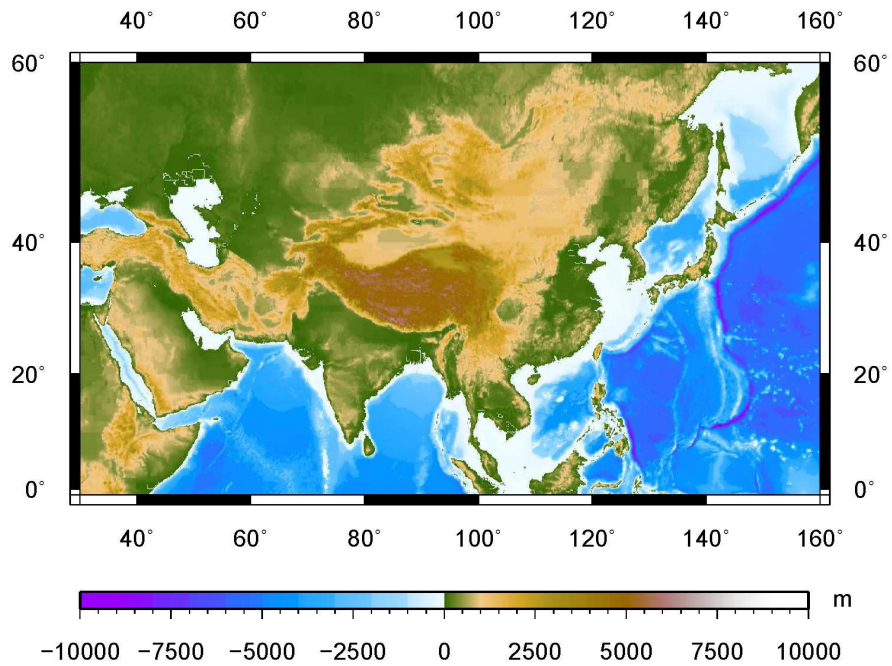


Figure A.2: Land and sea-floor elevation, based on ETOPO5 (Data Announcement 88-MGG-02: Digital relief of the Surface of the Earth. NOAA, National Geophysical Data Center, Boulder, Colorado, 1988).

## A.II Main features of the Asian monsoon climate

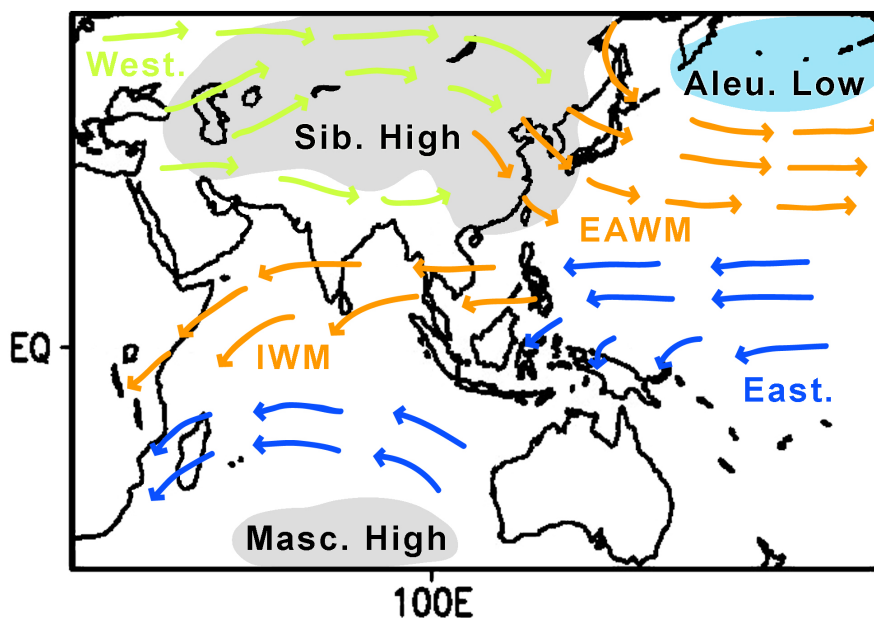


Figure A.3: Sketch of the main mean sea-level pressure and circulation systems (850hPa) affecting the Asian monsoon region during winter, i.e. the Aleutian Low (blue), the Mascarene High and the Siberian High (grey), the mid-latitude Westerlies (green), the equatorial Easterlies, the Indian winter monsoon (orange, IWM) and the East Asian winter monsoon (orange, EAWM).

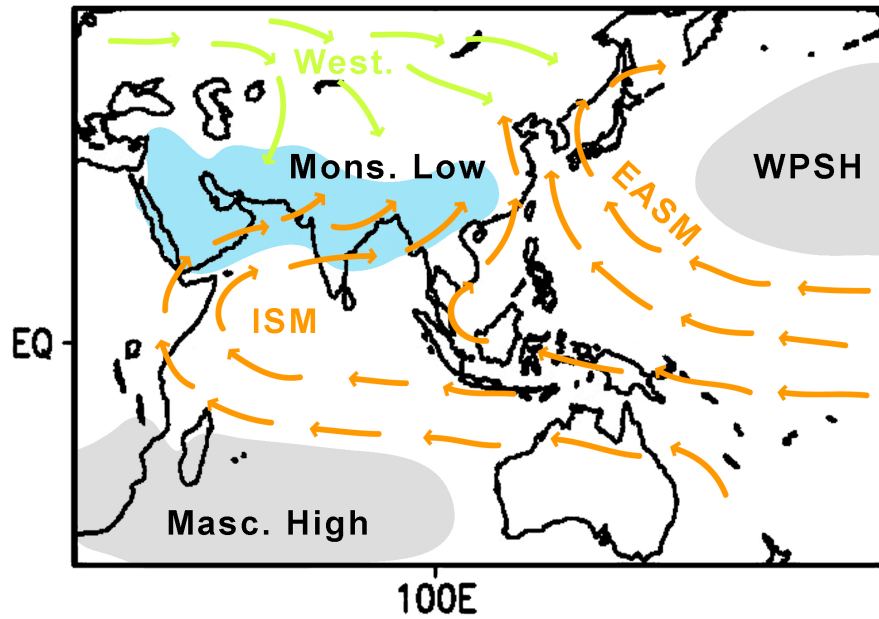


Figure A.4: Sketch of the main mean sea-level pressure and circulation systems (850hPa) affecting the Asian monsoon region during summer, i.e. the Western Pacific Subtropical High (grey), the Mascarene High (grey) and the Monsoon trough (blue), the Westerlies (green), the Indian summer monsoon (orange, ISM) and the East Asian summer monsoon (orange, EASM).

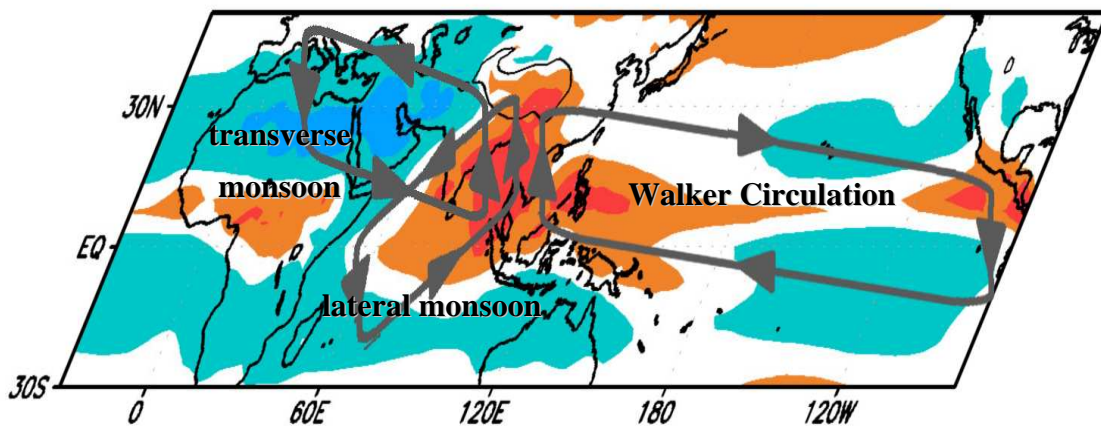


Figure A.5: The Asian monsoon in its planetary context. Synthesis of the boreal summer divergent wind circulation, heat sinks (bluish colour) and heat sources (redish) for the atmosphere based on NCEP reanalysis outgoing longwave radiation (1979-1995, Kalnay et al., 1996); more redish = stronger heat source, more bluish = stronger heat sink. (Modified from Webster et al. 1998)

### A.III Detailed overview on the factors contributing to the mid-to late-Holocene climate change

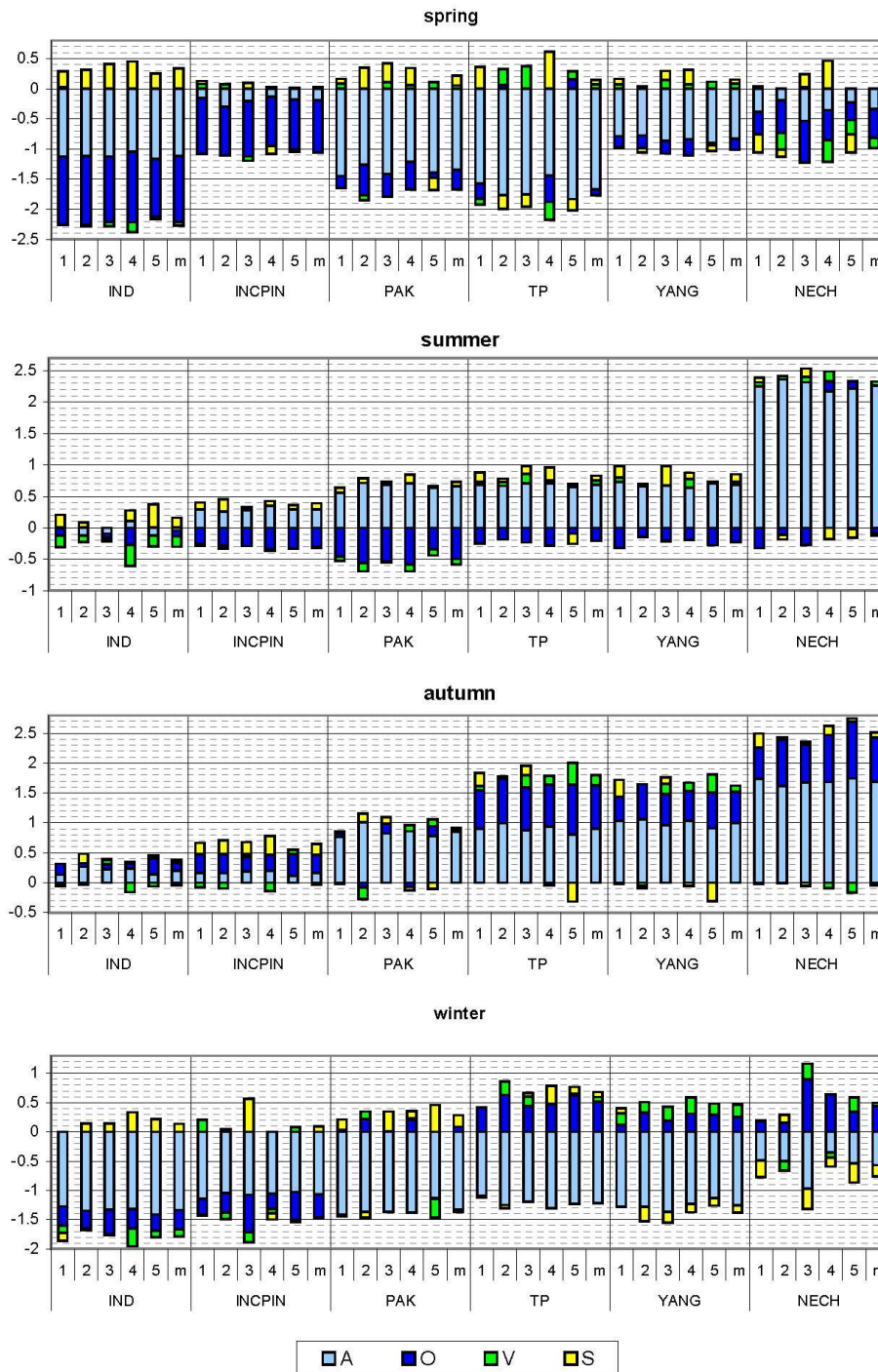


Figure A.6: Factors contributing to the seasonal temperature change [K] between mid-Holocene and present-day climate for six regions in the area of the Asian monsoon. Depicted are seasonal averages for all 120-year periods as well as the 600-year mean. Light blue: atmosphere-only run (direct response of atmospheric dynamics (A) to changes in insolation). Dark blue: contribution of ocean-atmosphere-interaction (O). Green: contribution of vegetation-atmosphere interaction (V). Yellow: contribution of the synergy (S) between atmosphere - ocean and atmosphere - vegetation interactions. Please note the change in scales.

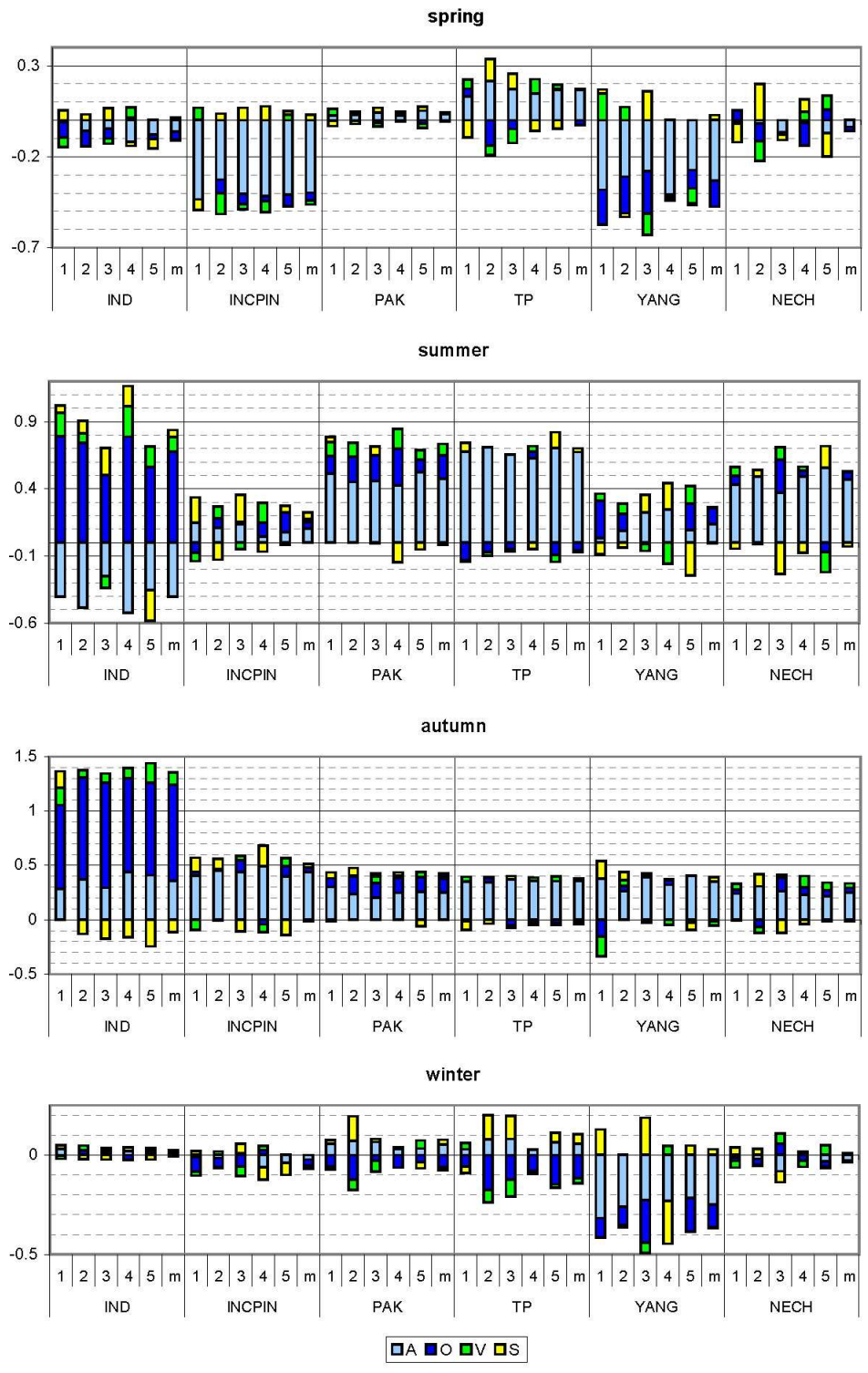


Figure A.7: Same as Figure A.6, but for precipitation [mm/day]. Please note the different scales.

**A.IV Simulated summer circulation in an ECHAM5 (atmosphere-only) run**

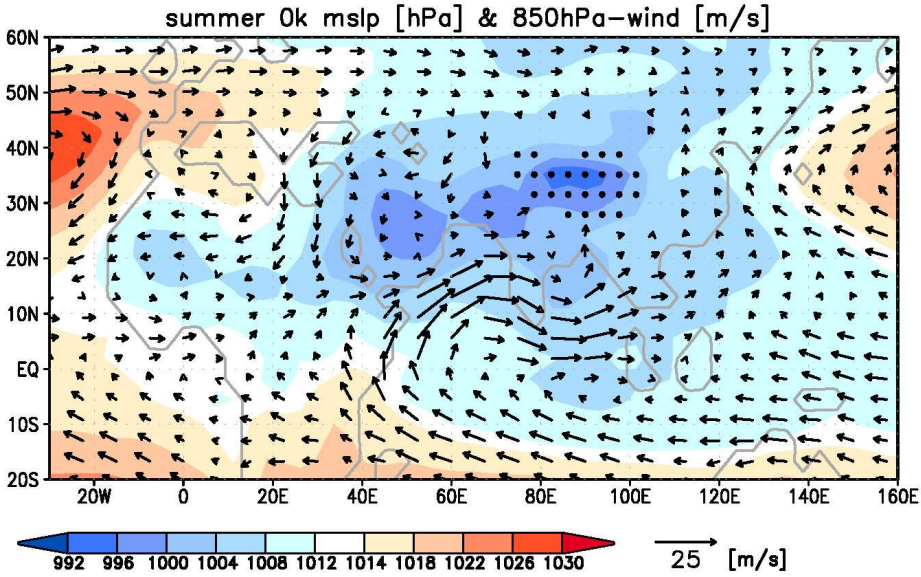


Figure A.8: Summer mean sea level pressure (shaded, [hPa]) and wind in 850hPa (vector, [m/s]) as simulated by the atmosphere-only run for present-day orbital conditions.

## Appendix B: Additional tables

### B.I Significance-test of the simulated vegetation trend

To test the significance of the simulated vegetation trends, we applied a simple statistical test: We calculated the standard deviation of the time-series ( $\sigma$ ) and the difference between the mean value of the first 500years and the last 500years of the time-series ( $\Delta\text{cov\_frac}$ ). We assume a significant land cover trend, if  $|\Delta\text{cov\_frac}| > 2*\sigma$ .

Results of this test can be seen in Table B.1. According to this test, the simulated land cover trend on the north-eastern Tibetan Plateau is significant. For the south-eastern Tibetan Plateau, only the simulated grass cover shows a non-significant trend. The simulated land cover change on the central Tibetan Plateau has no trend. On the central-western Tibetan Plateau the shrub cover trend is not significant, but the desert, grass and forest fraction show a significant trend.

	North Eastern Tibetan Plateau				South Eastern Tibetan Plateau			
	desert	grass	shrubs	forest	desert	grass	shrubs	forest
$2*\sigma$	0.040	0.132	0.073	0.148	0.003	0.024	0.420	0.410
$\Delta\text{cov\_frac}$	-0.052	0.175	0.087	-0.210	0.004	-0.014	0.585	-0.575

	Central Tibetan Plateau				Central Western Tibetan Plateau			
	desert	grass	shrubs	forest	desert	grass	shrubs	forest
$2*\sigma$	0.034	0.034	0.000	0.000	0.106	0.033	0.026	0.084
$\Delta\text{cov\_frac}$	0.028	-0.028	0.000	0.000	0.156	-0.038	-0.003	-0.115

Table B.1: Simple statistical significance test of the simulated land cover trend at each area on the Tibetan Plateau.  $\sigma$ : standard deviation of the entire time-serie,  $\Delta\text{cov\_frac}$ : difference between the mean land cover of the first 500years and last 500years of the time-serie.

## B.II Assignment of the pollen-taxa to the major vegetation types in the model

	forest	shrub	steppe/meadow	desert
<i>Alnus</i>	1	0	0	0
<i>Betula</i>	1	0	0	0
<i>Juniperus</i>	1	0	0	0
<i>Picea</i>	1	0	0	0
<i>Pinus</i>	1	0	0	0
<i>Quercus</i>	1	1	0	0
<i>Salix</i>	1	1	0	0
<i>Thalictrum</i>	1	1	0	0
Rubiaceae	1	1	1	0
<i>Berberis</i>	0	1	0	0
<i>Hippophaë</i>	0	1	0	0
<i>Rhododendron</i>	0	1	0	0
Fabaceae	0	1	0	0
<i>Potentilla</i> type	0	1	0	0
Spiraea	0	1	0	0
Apiaceae	0	0	1	0
<i>Bupleurum</i> type	0	0	1	0
<i>Artemisia</i>	0	0	1	0
Chichorioideae	0	0	1	0
Crassulaceae	0	0	1	0
Cyperaceae	0	0	1	0
Gentianaceae	0	0	1	0
Lamiaceae	0	0	1	0
Liliaceae	0	0	1	0
Poaceae	0	0	1	0
<i>Rumex/Rheum</i>	0	0	1	0
<i>Polygonum bistorta</i> type	0	0	1	0
<i>Aconitum</i>	0	0	1	0
<i>Ranunculus acris</i> type	0	0	1	0
<i>Trollius</i> type	0	0	1	0
<i>Stellera</i>	0	0	1	0
<i>Anthemis</i> type	0	0	1	1
<i>Aster</i> type	0	0	1	1
Saussurea	0	0	1	1
Papaveraceae	0	0	1	1
Brassicaceae	0	0	0	1
Caryophyllaceae	0	0	0	1
Chenopodiaceae	0	0	0	1
<i>Ephedra distachya</i> type	0	0	0	1
<i>Ephedra fragilia</i> type	0	0	0	1
<i>Calligonum</i>	0	0	0	1
<i>Tamarix</i>	0	0	0	1
<i>Nitraria</i>	0	0	0	1

Table B.2: Assignment of the pollen-taxa to the major vegetation types in the model, this table was prepared by U.Herzschuh.

## Appendix C: Summary of the simulated climate and land cover change on the Tibetan Plateau

The simulated change in summer and winter temperature as well as the change in annual precipitation at each site of the Tibetan Plateau is shown in Fig. C.1-C.4. In all regions, the model calculates a decreasing Holocene precipitation trend that is probably related to the general weakening of the Asian summer monsoon since the early- and mid-Holocene reported also in vegetation-independent reconstructions such as cave records (e.g. Fleitmann, 2003; Wang et al. 2005; or Maher, 2008). Due to the increasing solar radiation on the northern hemisphere in winter, the simulated near-surface air temperature increases from mid-Holocene to present-day at all sites. Summer temperatures show a decreasing Holocene trend on the north-eastern Tibetan Plateau and an increasing trend on the south-eastern and central-western Tibetan Plateau. The differences in temperature trend can probably be attributed to the decreasing precipitation and the accompanying decrease in evaporative cooling at the latter sites that counteracts the temperature-decline resulting from the decreasing solar insolation from mid-Holocene to present-day in the summer season of the northern hemisphere.

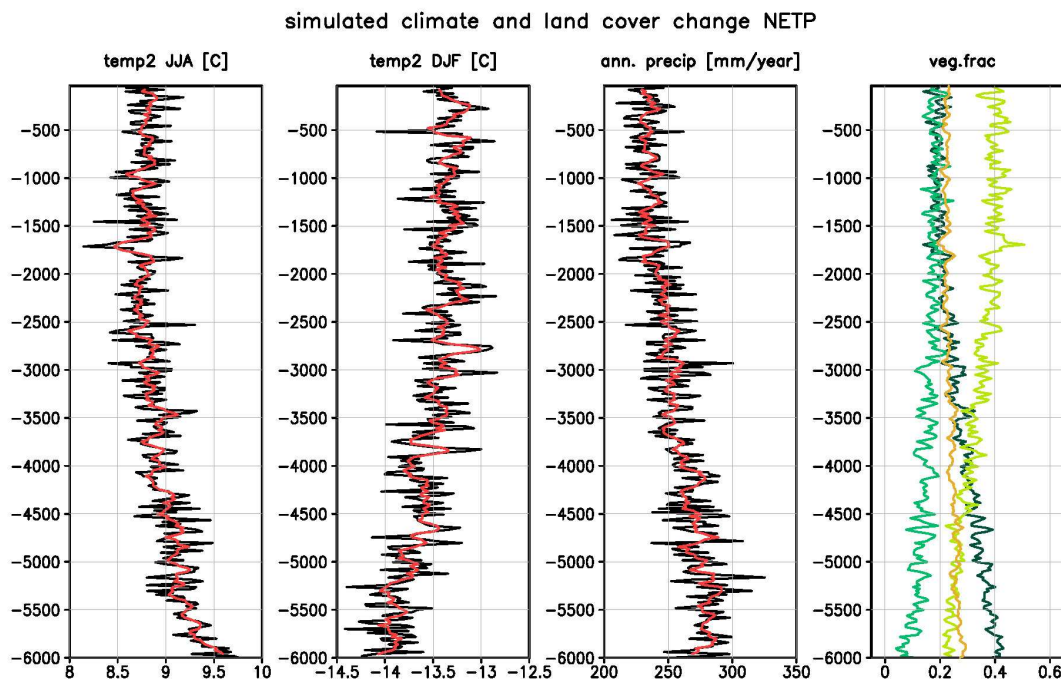


Figure C.1: Simulated change in summer (JJA) and winter (DJF) temperature [°C], annual precipitation [mm/year] and land cover [fraction per grid-box] on the north-eastern Tibetan Plateau (NETP). Values are averaged over 20 years, covering the last 6000 years from mid-Holocene to present-day. The red solid line shows the 100yr-running-mean. Land cover is divided into forest (dark green), shrubs (green), grass (light green) and non-vegetated area (orange).

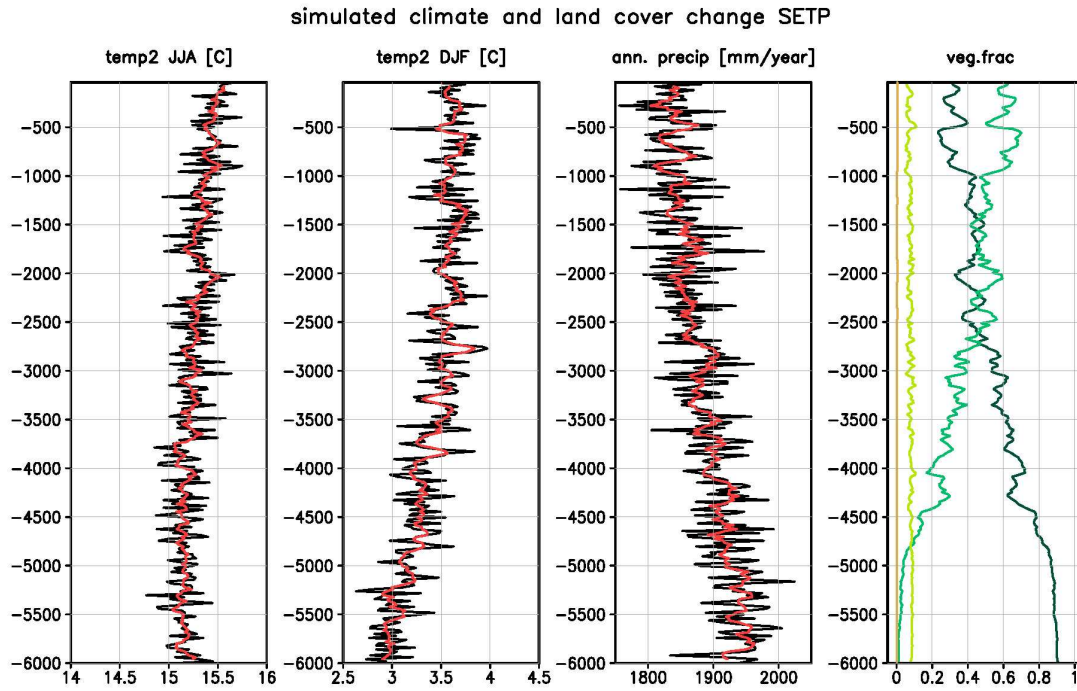


Figure C.2: Same as Figure C.1, but for the south-eastern Tibetan Plateau (SETP).

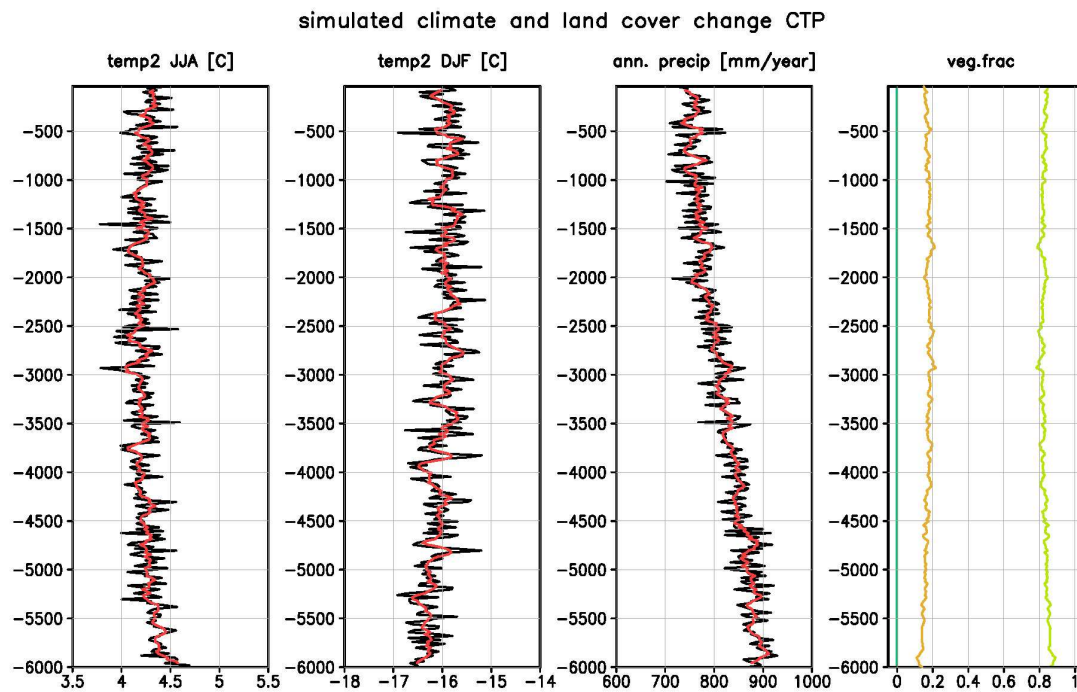


Figure C.3: Same as Figure C.1, but for the central Tibetan Plateau (CTP).

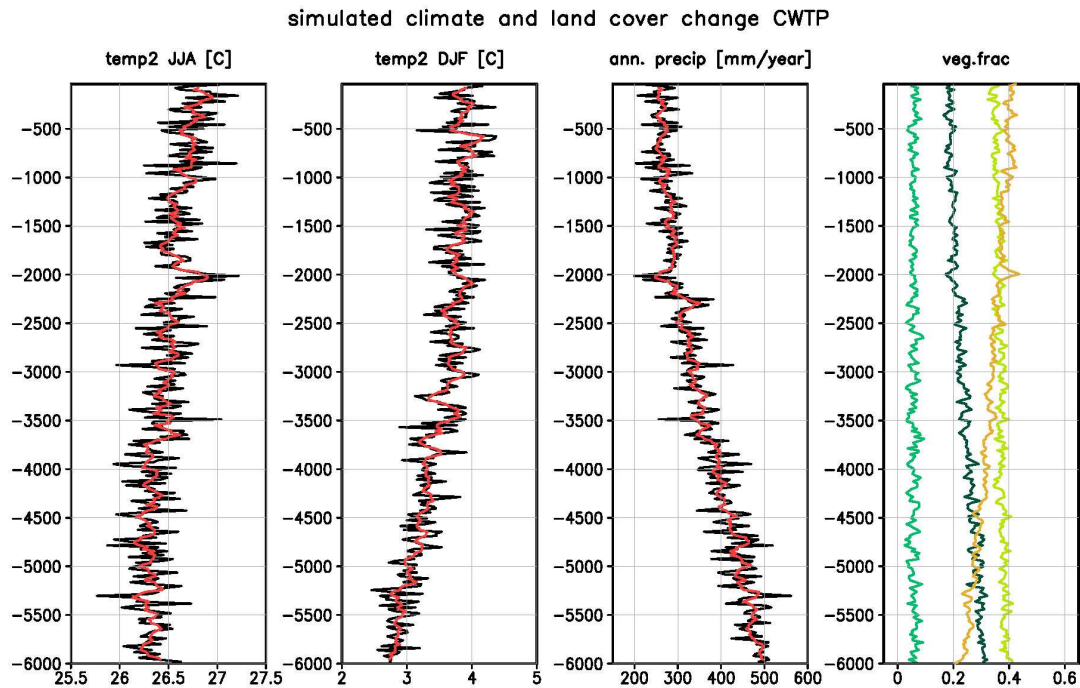


Figure C.4: Same as Figure C.1, but for the central-western Tibetan Plateau (CWTP).

The simulated change in the bioclimatic relevant parameters and the net primary productivity (NPP) is displayed in Fig. C.5-C.8. The bioclimate and NPP determine the distribution of the different plant functional types (PFTs) in the model. Whereas the bioclimate defines the grid-boxes where the PFTs can grow, the NPP controls the competition of the woody PFTs. In a favourable bioclimate, the woody PFT with the highest NPP is the dominant vegetation-type in the grid-box. The bioclimate indicator in Fig. C.5-C.8 quantifies how suitable the simulated climate in the different region on the Tibetan Plateau is. On the north-eastern Tibetan Plateau bioclimatic conditions allow the growing of extratropical trees, cold shrubs and C3 grass only. For these PFTs, the bioclimate is more favourable during mid-Holocene than at present-day. This is related to the bioclimatic limit of growing degree days that is not permanently exceeded any more in the colder present-day climate on the north-eastern Tibetan Plateau. On the south-eastern Tibetan Plateau, simulated bioclimatic conditions are perfect for the growing of extratropical trees and C3 grass during mid-Holocene as well as present-day. For raingreen shrubs, the bioclimatic conditions become more favourable in the course of the Holocene, since frost-events occur less often at present-day than at mid-Holocene ( $T_{c_{min}}$ ). The simulated climate on the central Tibetan Plateau is too cold to allow the establishment of woody PFTs in the model. C3 grass is the only PFT that can survive. On the central-western Tibetan Plateau, the growing of extratropical trees and C3 grass is not limited by the simulated bioclimate during the entire simulation. The establishment of shrubs is partly limited by frost. The decreasing precipitation leads to a halving of the simulated NPP from mid-Holocene to present-day.

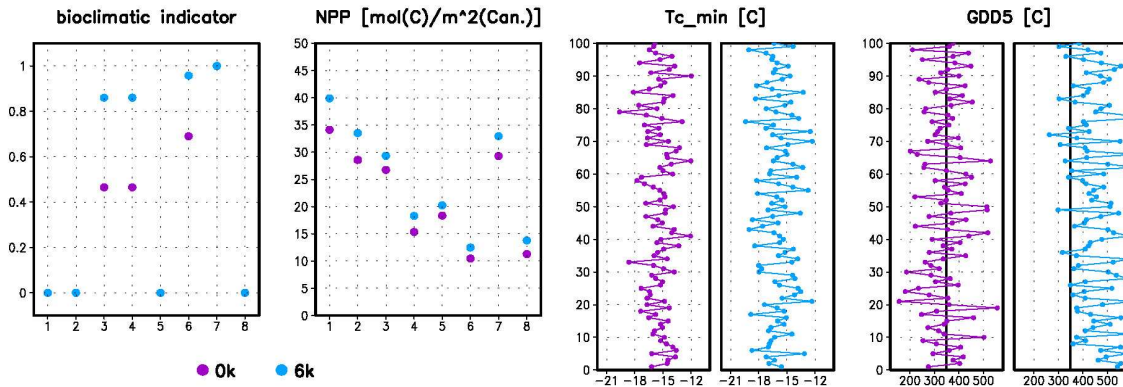


Figure C.5: Simulated change in bioclimatic conditions and the net primary productivity (NPP) on the north-eastern Tibetan Plateau for all simulated plant functional types (PFT, see Tab. 5.1). These are: tropical evergreen trees (1), tropical deciduous trees (2), extratropical evergreen trees (3), extratropical deciduous trees (4), raingreen shrubs (5), cold shrubs (6), C3 grass (7) and C4 grass (8). The bioclimatic indicator ranges from 0 (climate unfavourable) to 1 (climate favourable) and indicates if the bioclimatic conditions allow the establishment of the PFT. The lowest mean temperature of the coldest month ( $T_{c_{min}}$ ) and the growing degree days (GDD5) are based on the first and last 100years of the transient simulation, representing the mid-Holocene and present-day climate, respectively. Black lines mark the nearest threshold (here: GDD5=350, limit for extratropical trees).

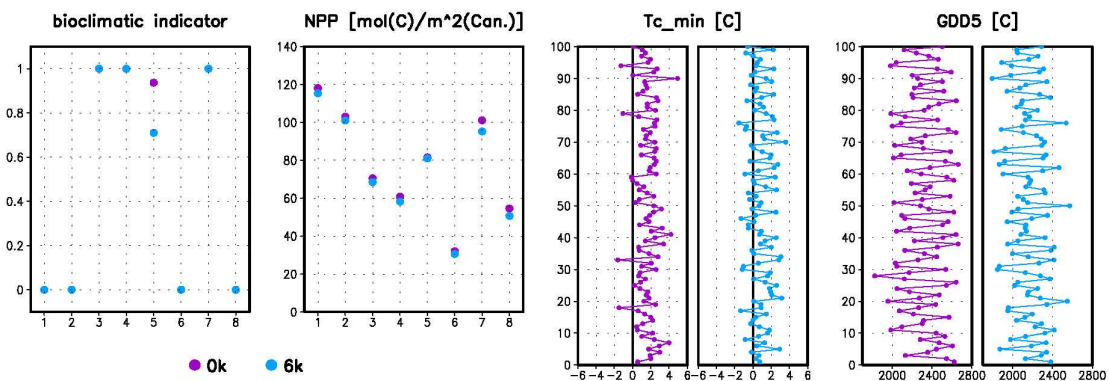


Figure C.6: Same as Figure C.5, but for the south-eastern Tibetan Plateau.

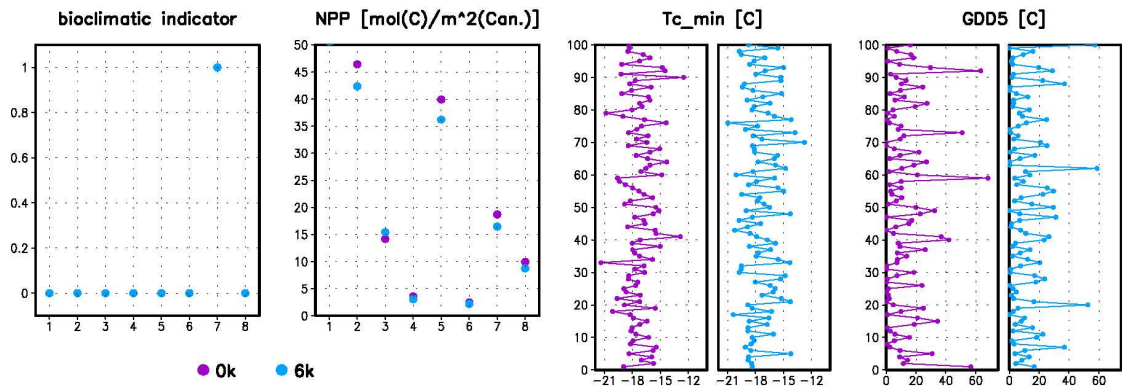


Figure C.7: Same as Figure C.5, but for the central Tibetan Plateau.

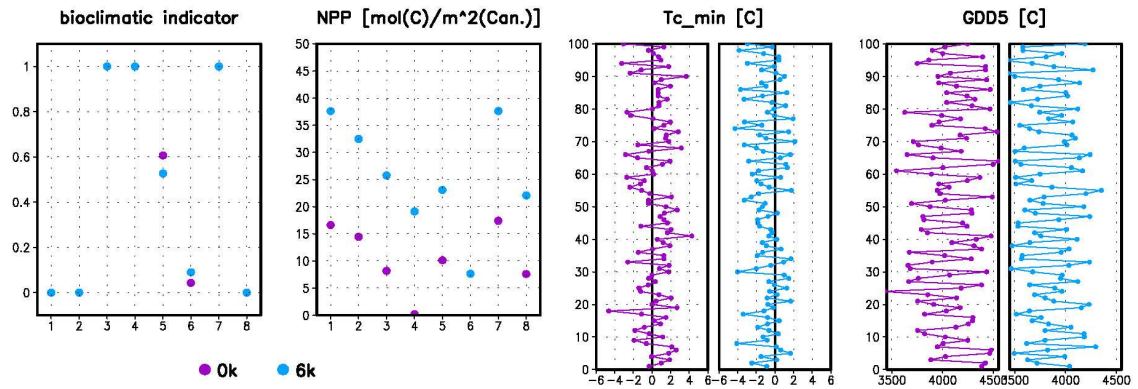


Figure C.8: Same as Figure C.5, but for the central-western Tibetan Plateau.



## Acknowledgements

I would like to acknowledge all people who supported the creation of this thesis. In the first place, I want to thank my supervisor Martin Claussen for his scientific advises and guidance, for his time, his interest and the continuous support throughout the last years. He gave me the opportunity to work on this thesis in the inspiring working environment of the Max-Planck-Institute for Meteorology. I gratefully acknowledge Thomas Raddatz for fruitful discussions and the patience to answer all my technical and scientific questions. I would also like to express my gratitude to Victor Brovkin and Thomas Kleinen for their helpful advises and comments, particularly on writing scientific texts.

Special thanks to Ulrike Herzschuh for providing climate and vegetation reconstructions and the many helpful discussions. Her continuous interest on my work was very encouraging. Many thanks also to Nils Fischer, Juliane Otto and Freja Vamborg, who provided me with model data for interesting studies.

I thank Veronika Gayler and Reiner Schnur for the technical support associated with global climate modelling and the help whenever my computer had his special moments. In this regard, I also want to thank CIS for permanent technical assistance and their voluntary help in cleaning up my hard disk.

I very much enjoyed being part of the vegetation modelling groups that always provided a friendly and inspiring working atmosphere. Thanks to all my Land-colleagues, especially to my office mates/neighbours Freja Vamborg, Tim Brücher, Juliane Otto and Daniela Kracher, as well as to the other 17<sup>th</sup>-floor-PhD-students. Special thanks to Sebastian Bathiany for interesting discussions on music and other topics, very helpful technical and scientific comments and particularly for proof-reading all my texts. Many thanks also to Kerstin Haberkorn and Stefan Polanski, who accompanied me on many official trips. They were always very helpful and pleasant companions.

With respect to the manuscripts included in this paper, I would like to acknowledge Andrej Ganopolski, Oliver Timm and the anonymous reviewer for constructive comments improving the manuscripts. I also thank Yongbo Wang, E. van Campo, X. Liu, A. Kramer and PMIP for providing data. Financial support for this thesis was provided by the priority program INTERDYNAMIK of the German Research Foundation (DFG).

On a more personal level, I want to thank my former fellow students that kept my interest on meteorology alive and provided not only an entertaining but also an instructive and productive studying atmosphere. Without them, learning physics and maths would not have been half the fun. Last but not least, I want to thank Björn and my family. Many thanks to my parents for their material and non-material support, including many recreative weekends at home.

